Universidade de Aveiro Departamento de Química
2017

Lucía Fernández Fernández

Degradação de 17β-estradiol em meio aquoso por processos de fotossensibilização e biodegradação

Degradation of 17β-estradiol in water media by photosensitized and biodegradation processes

Universidade de Aveiro Departamento de Química
2017

Lucía Fernández Fernández

Degradação de 17β-estradiol em meio aquoso por processos de fotossensibilização e biodegradação

Degradation of 17β-estradiol in water media by photosensitized and biodegradation processes

Doctoral thesis submitted to the Universidade de Aveiro to fulfill the requirements to obtain the degree of Doctor of Chemistry from Universidade de Aveiro. This doctoral thesis was prepared under the supervision of Doctor João Paulo Costa Tomé, Associate Professor at Centro de Química Estrutural, Instituto Superior Técnico, Universidade de Lisboa; Doctor Maria Ângela Sousa Dias Alves Cunha, Assistant Professor at the Department of Biology, Universidade de Aveiro; and Doctor Valdemar Inocêncio Esteves, Assistant Professor at the Department of Chemistry, Universidade de Aveiro.

Cofinanciado por:
COMPETE 2020 PORTUGAL 2020
FCT Fundação para a Ciência e a Tecnologia
MINISTÉRIO DA CIÊNCIA, TECNOLOGIA E ENSINO SUPERIOR
Governo da República Portuguesa
UNIÃO EUROPEIA Fundo Europeu de Desenvolvimento Regional

Financial support came from FCT/MEC to QOPNA (FCT UID/QUI/00062/2013), CESAM (FCT UID/MAR/LA0017/2013), CICECO (FCT UID/CTM/50011/2013) and CQE (FCT UID/QUI/0100/ 2013) research units, through national funds, and where applicable cofinanced by the FEDER, within the PT2020 Partnership Agreement. This work was also supported by the Seventh Framework Programme (FP7-People-2012-ITN, SO2S project with grant agreement number: 316975).

Dedico esta tesis a mis padres, a mi hermana y a mi sobrino.

o júri

presidente

Prof. Dr. Fernando Joaquim Fernandes Tavares Rocha
Cathedratic Professor - Department of Geosciences - Universidade de Aveiro

Dr. Maria de Fátima Costa Guedes da Silva
Associate Professor with Aggregation - Department of Chemical Engineering - Instituto Superior Técnico – Universidade de Lisboa

Dr. Anthony Joseph Burke
Assistant Professor with Aggregation - Department of Chemistry – Universidade de Évora

Dr. Adelaide Almeida
Associate Professor with Aggregation - Department of Biology - Universidade de Aveiro

Dr. Maria Eduarda Bastos Henriques dos Santos
Assistant Professor - Department of Chemistry - Universidade de Aveiro

Dr. Rudolf Josef Schneider
Head of Division - BAM Federal Institute for Materials Research and Testing, Berlin, Germany

Dr. Kevin Huvaere
Principal Researcher (Chief Scientist), EcoSynth, Ostend, Belgium

Dr. João Paulo Costa Tomé (supervisor)
Associate Professor – Department of Chemical Engineering – Instituto Superior Técnico - Universidade de Lisboa

agradecimentos

acknowledgments

I would like to express my sincere acknowledgment to my main supervisor, Dr. João Tomé, for giving me the opportunity to join this adventure, encouraging my research and making me grow as scientist. Thank you for all the support, motivation and knowledge. This has been hard, but also fun.

I would like to thank my co-supervisors, Dr. Ângela Cunha and Dr. Valdemar Esteves, for their continuous help and inspiration, insightful expertise and enthusiasm.

My true acknowledgment also goes to Dr. Rudolf J. Schneider, who provided me the opportunity to join his team at the Federal Institute for Materials Research and Testing, in Berlin, for nine months. Thank you for all the access to the amazing laboratory and research facilities, for your friendliness and for your dedication.

I would like to thank Dr. Kevin Huvaere, for hosting me at EcoSynth, in Ostend, for just one month, but probably one of the most fruitful period within this work. Thank you for all the care and dedication during my stay, and for your wise advices.

I would especially like to thank all technicians from QOPNA and BAM, because their indispensable work has been essential in achieving my goals. Thank you for your availability and knowledge.

A big acknowledgment goes to my labmates in Aveiro, for all the help and stimulating discussions, and above all, for all the fun and affection. I thank to Antonio Louvado, who helped me a lot in the area of microbiology. I would also like to thank all my colleagues in BAM. In particular, I am especially grateful to Holger Hoffmann and Gabriela Alfaro Espinoza, for all their help and kindness in every moment.

I thank my colleagues from the SO_2S project, for all the motivation and nice times we spent. Especial acknowledgments go to Wioleta Borzęcka, Margarida Carvalho and Mafalda Bispo, because it was really nice to travel together a part of this trip.

I would like to thank to Sara Pena, Paula G. Cochón and Noemi Fernández, for all their inspiration, friendship and love.

A big acknowledgment goes to my partner and my love, Xose Lois.

Gracias infinitas a mi familia, especialmente a mis padres, por su apoyo incondicional y por todo su amor. Gracias a mi hermana por creer en mí. Y a Nico, por la magia y su ternura.

palavras-chave

Tratamento de águas, desinfecção de águas, poluentes orgânicos, 17β-estradiol, fotodegradação, porfirina, ftalocianina, nanopartículas magnéticas, modo de fluxo, biodegradação.

resumo

Novos métodos de tratamento de água são requeridos como um resultado a partir da crescente sensibilização para a redução do impacto da poluição no ambiente. As principais vias para a destruição de compostos tóxicos em água são os processos de biodegradação e fotodegradação. A degradação biológica de um composto químico refere-se à eliminação do poluente pela actividade metabólica de microrganismos. A fotodegradação é um mecanismo eficiente para degradar simultaneamente diferentes tipos de compostos orgânicos. No entanto, a fotodegradação pode implicar custos elevados relacionados com a produção dos fotocatalisadores e o consumo energético. Na perspectiva de abordagens sustentáveis para o tratamento da água, sugere-se a combinação de tratamentos de fotodegradação e biológicos.

Os compostos disruptores endócrinos (CDEs) são considerados pela investigação como uma prioridade elevada, pois são uma fonte de potencial adverso para efeitos de saúde ecológica nas águas ambientais. O 17β-estradiol (E2), um recalcitrante CDE, foi seleccionado como poluente alvo neste trabalho.

Nesta dissertação descreve-se a preparação e a avaliação fotocatalítica de novos materiais híbridos à base de nanopartículas de magnetita decoradas com porfirinas ou ftalocianinas. Este estudo apresenta a aplicação destes fotocatalisadores em modos batch e de fluxo, bem como a sua utilização em águas residuais reais para remoção de diferentes poluentes orgânicos. Adicionalmente, modificações ligeiras destes materiais permitem a sua utilização como agentes antimicrobianos para fins de desinfecção da água contra bactérias patogénicas.

O rastreio de estirpes bacterianas capazes de metabolizar o E2 como poluente orgânico alvo em águas provocou a descoberta de utilizações relevantes da estirpe bacteriana Bacillus licheniformis, isolada previamente a partir de sedimentos de profundidade do mar no Golfo de Cádiz. Bacillus licheniformis apresenta uma grande versatilidade em aplicações de remediação de água, sendo capaz de remover diferentes estrogênios em concentrações relevantes ($ng \cdot L^{-1}$) em águas residuais. Finalmente, o estudo de uma abordagem combinada para o tratamento de águas foi focado na capacidade de Bacillus licheniformis para tratar a água, a partir da qual foi previamente e parcialmente foto-tratada pela ação de um material híbrido, sob irradiação de luz branca.

keywords

Water treatment, water disinfection, organic pollutants, 17β-estradiol, photodegradation, porphyrin, phthalocyanine, magnetic nanoparticles, flow mode, biodegradation.

abstract

New methods for water treatment are required as a result from an increasing awareness in the reduction of the pollution impact in the environment. The main routes for destroying toxic compounds in water are biodegradation and photodegradation processes. Biological degradation of a chemical refers to the elimination of the pollutant by the metabolic activity of microorganisms. Photodegradation is an efficient mechanism for simultaneously degrade different types of organic compounds. However, photodegradation may imply high costs related to the photocatalysts' production and energetic consumption. In the perspective of sustainable approaches for water treatment, the combination of photo- and biological treatments are proposed.

Endocrine disrupting compounds (EDCs) are considered as high research priority being a source of potential adverse ecological health effects in environmental waters. 17β-estradiol (E2), a recalcitrant EDC, was selected as target pollutant in this work.

In this dissertation, the preparation and photocatalytic evaluation of new hybrid materials based on magnetite nanoparticles decorated with porphyrins or phthalocyanines are described. This study presents the application of these photocatalysts in both batch and flow modes, as well as their use in real wastewaters for the removal of different organic pollutants. In addition, slight modifications of these materials allow their utilization as antimicrobial agents for water disinfection purposes, against pathogenic bacteria.

The screening of bacterial strains able to metabolize E2 as target organic pollutant in water caused the finding of relevant uses of the bacterial strain Bacillus licheniformis, previously isolated from deep sea sediments in the Gulf of Cádiz. Bacillus licheniformis displays great versatility in water remediation applications, being able to remove different estrogens in relevant concentrations ($ng \cdot L^{-1}$) in wastewaters. Finally, the study of a combined approach for water treatment was focused on the ability of Bacillus licheniformis to treat water, which previously was partially photo-treated by the action of a hybrid material, under white light irradiation.

TABLE OF CONTENTS

List of figures

List of tables

Abbreviations

Amp	Ampicillin
ANOVA	Analysis of variance
AOP	Advanced oxidation process
APTES	(3-Aminopropyl) triethoxysilane
BET	Brunauer–Emmett–Teller
BF_3	Boron trifluoride etherate
BJH	Barrett, Joyner, and Halenda
BLAST	Basic Local Alignment Search Tool
br	Broad signal
BSA	Bovine serum albumin
BOD_5	Five-day biochemical oxygen demand
ca.	Circa
CBZ	Carbamazepine
CE	Collision energy
CET	Cetirizine dihydrochloride
CFU	Colony-forming units
Cm	Chloramphenicol
COD	Chemical oxygen demand
CTAB	Cetyl trimethylammonium bromide
CXP	Collision cell exit potential
d	Doublet
DBN	Diazabicyclo(4.3.0)non-5-ene
DBP	Disinfection by-product
dd	Doublet of doublets
ddd	Doublet of doublet of doublets
DDQ	2,3-Dichloro-5,6-dicyanobenzoquinone
DEA	Diethylamine
DLS	Dynamic light scattering
DMAE	Dimethylethanolamine
DMF	Dimethylformamide
DMSO	Dimethyl sulfoxide
DNA	Deoxyribonucleic acid
DP	Declustering potential
DPBF	Diphenylisobenzofuran
dt	Doublet of triplets
E. coli	*Escherichia coli*
E0	Estratetraenol
E1	Estrone
E2	17β-Estradiol
E3	Estriol
EDC	Endocrine disrupting compound
EDTA	Ethylenediaminetetraacetic acid
EE2	17α-Ethinylestradiol
EP	Entrance potential
ESI	Electrospray ionization
GS1	Nebulizer gas

GS2	Turbo gas
HMDS	Hexamethyldisilazane
HPLC	High-performance liquid chromatography
IC	Inorganic carbon
ISC	Intersystem crossing
IUPAC	International Union of Pure and Applied Chemistry
LB	Luria Bertani
LOD	Limit of detection
LOQ	Limit of quantification
LED	Light-emitting diode
m	Multiplet
MALDI	Matrix-assisted laser desorption/ionization
MeEE2	3-Methyl ether of ethinylestradiol
MNP	Magnetic nanoparticle
MO	Methyl orange
MPc	Metallophthalocyanine
MPor	Metalloporphyrin
MS	Mass spectrometry
n.a.	Not analysed
N/A	Not applicable
n.d.	Not detected
NAS	Nitrifying activated sludge
NMR	Nuclear magnetic resonance spectroscopy
NP^{+}-PS	Cationic nanoparticles-photosensitizer
NP-PS	Nanoparticles-Photosensitizer
OAP	Octalkylporphyrin
OD	Optical density
***o*-DCB**	*o*-Dichlorobenzene
OG	Orange G
PBS	Phosphate buffer saline
PBS_N	Phosphate buffer saline with a nitrogen source
Pc	Phthalocyanine
PCR	Polymerase chain reaction
PDI	Photodynamic inactivation of microorganisms
Por	Porphyrin
PS	Photosensitizer
PVDF	Polyvinylidene fluoride
q	Quartet
RDP	Ribosomal database project
RLU	Relative light units
ROS	Reactive oxygen species
rRNA	Ribosomal ribonucleic acid
rt	Room temperature
s	Singlet
SDS	Sodium dodecyl sulfate
SMX	Sulfamethoxazol
SPE	Solid-phase extraction
SRM	Selected reaction monitoring mode

STP	Sewage treatment plant
SWNT	Single-walled carbon nanotube
t	Triplet
TC	Total carbon
td	Triplet of doublets
TEM	Transmission electron microscopy
TIC	Total ion current
TLC	Thin-layer chromatography
TMS	Tetramethylsilane
TOC	Total organic carbon
TOF	Time-of-flight
TSA	Tryptic soy agar
TSB	Tryptic soy broth
UV-vis	Ultraviolet–visible spectroscopy
WWTP	Wastewater treatment plant
XRD	X-ray diffraction crystallography

Symbols

ø	Diameter
δ	Chemical shift
ε	Molecular absorption coefficient
λ	Wavelength
$^{3}\Sigma$	Triplet oxygen
$HO^{\bullet}$	Hydroxyl radical
J	Coupling constant
k	Kinetic rate constant
K_{ow}	Octanol-water partition coefficient
m/z	Mass to charge ratio
n	Number of data
$^{1}O_2$ or $^{1}\Delta$	Singlet oxygen
$O_2^{-\bullet}$	Superoxide anion radical
pKa	Acid dissociation constant
$R^{\bullet}$	Radical
$ROO^{\bullet}$	Peroxyl radical
r	Correlation coefficient
S_1	Singlet state
S_1^*	Singlet excited state
S_o	Singlet ground state
T_1^*	Triplet excited state
$t_{1/2}$	Half-life

Lucía Fernández
Universidade de Aveiro, 2017

CHAPTER 1

INTRODUCTION

Fernández, L., Esteves, V.I., Cunha, Â., Schneider, R.J., Tomé, J.P.C., Photodegradation of organic pollutants in water by immobilized porphyrins and phthalocyanines. *J. Porphyrins Phthalocyanines*. **2016**, 20, 150-166

Summary

The main routes for destroying toxic compounds in water are biodegradation and photodegradation processes. Photodegradation is an important mechanism for degrading aromatic hydrocarbons, chlorinated aromatic hydrocarbons, chlorinated phenols and many pesticides. In photolysis, a photosensitizer absorbs light and transfers the energy to the dissolved oxygen or another substrate in the medium to generate reactive oxygen species (ROS), such as singlet oxygen and radicals, which are the responsible species for the degradation of the target compounds.

Photosensitized processes in presence of porphyrins (Pors) and phthalocyanines (Pcs) can be very suitable, due to their ability to absorb several wavelengths in the UV-Vis range and generate ROS at high rates. The use of magnetic supports for the dispersion of Pors and Pcs in water can facilitate its recovery just by applying a magnetic field, thus allowing their reuse on further photocatalytic cycles. In addition, the versatility of these photomaterials allows their use in the photoinactivation of microorganisms, for water disinfection purposes.

The possibility of combining photodegradation processes with biological treatments is desirable to make the water treatment more cost effective. Biological degradation of a chemical refers to the elimination of the pollutant by the metabolic activity of living organisms, usually microorganisms such as bacteria.

The present work envisages the elimination of endocrine disruptor compounds, such as 17β-estradiol, estrone, estriol, or 17α-ethinylestradiol, in the context of water treatment applications.

1.1. Overview: General considerations about water pollution

Water is essential to all forms of life and a fundamental player in environmental health and management. Consequently, the presence of organic pollutants in waste and surface waters represents a major risk for ecosystem sustainability and human health. Environmental recovery and protection are key issues within the current chemical research. New methods for water treatment are required for the implementation of strict regulations, such as the European Water Framework Directive, 2008/105/EC,[1] which results of an increasing awareness of the need to reduce the impact of pollution in the environment. In line with this, green chemistry approaches have been proposed for the development of alternative sustainable technologies, favouring the design of processes that minimize the energetic requirements and the use of hazardous products, while maximizing global efficiency and reuse of materials.

Various types of organic pollutants, such as pesticides, petroleum hydrocarbons, phenols, plasticizers, chlorinated biphenyls, detergents, or pharmaceuticals, among others, have been found in different water bodies.[2] Special attention relies on pharmaceuticals, which are a large and varied class of compounds with diverse properties and applications. In the European Union there are more than 3000 active substances currently available in the market.[3] In 1960s and 1970s, some studies reported the incomplete removal at wastewater treatment plants (WWTPs) of certain pharmaceuticals, which consequently were discharged into environmental waters.[4] This problem captured the attention of researchers during 1990s,[5] with the development of analytical techniques able to determine compound concentrations in the range of a few nanograms per litre.[6]

The main origins of pharmaceuticals reaching the environment come from patient use in residential areas, discharges from hospitals and other clinical centres which are connected to the sewerage system, and, in some cases, wastewaters from pharmaceutical manufacturing.[7] In addition, veterinary pharmaceuticals can be introduced into the environment from farms and aquaculture. Other pharmaceuticals may be introduced in agricultural land *via* the application of biosolids to fields.[8] There are two main pathways to release pharmaceuticals into the environment:

- **Ordinary use of pharmaceuticals**. After the uptake of a medicine, a proportion of the active substance passes through the body unchanged.[9] The quantity excreted depends on the kind of medicine and the person being treated for a medical issue. This travels by the sewage system to a WWTP, where can be fully or partially

removed by the treatment process before the effluent is finally discharged into receiving waters.[10]

- **Disposal of unused and expired pharmaceuticals**. Drugs disposed in this way are in an unmodified form and may therefore contribute disproportionately to environmental contamination.[11]

Endocrine disrupting compounds (EDCs) are one of the highest research priorities as sources of potential adverse ecological health effects. Despite the low levels of many pharmaceuticals found in the environment, hormonally active chemicals can affect organisms even at low concentrations ranging $ng \cdot L^{-1}$. In 2002, the World Health Organization defined an EDC as *an exogenous substance or mixture that alters function(s) of the endocrine system and consequently causes adverse health effects in an intact organism, or its progeny, or (sub) populations.*[12]

According to the classification developed by the European Commission in 1999,[13] there are two classes of substances which can cause endocrine disruption:

- **Natural hormones**, including estrogens, progesterone and testosterone, which are found naturally in the body of humans and animals, and phytoestrogens, which are substances contained in some plants and may display estrogen-like activity when ingested.
- **Man-made substances**, which include:

  – Synthetically-produced hormones, including those hormones which are alike to natural hormones, such as oral contraceptives, hormone replacement therapy and some animal feed additives. They have been designed purposely to modulate and interfere with the endocrine system.

  – Man-made chemicals designed for use in industry, such as in some industrial cleaning agents; in agriculture, such as in some pesticides; and in consumer goods, such as in some plastic additives. This category also includes chemicals produced as by-products of industrial processes, such as dioxins, which are suspected of interfering with the endocrine systems of humans and wildlife.

Hormones act at extremely low concentrations, being present in plasma at typical concentrations of 1-10 $ng \cdot mL^{-1}$. Hormones act through high affinity intracellular receptors, forming complexes that can increase or decrease transcription of specific genes (Fig. 1.1),

thus very low concentrations of hormone can bind to the receptor population and initiate important biological effects.[14]

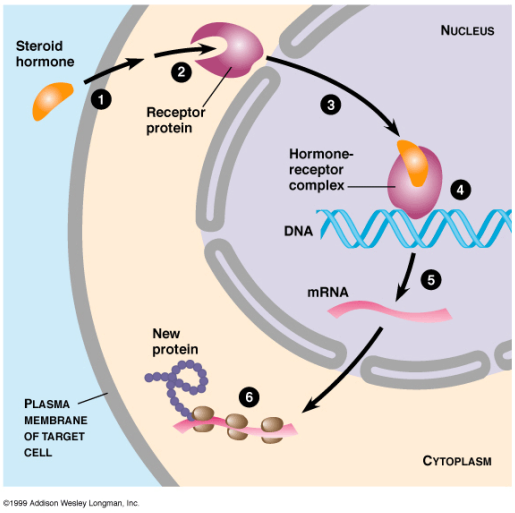

Figure 1.1. Mechanism of action for a steroid hormone.[15]

Natural estrogens, estrone (E1), 17ß-estradiol (E2), and estriol (E3), and synthetic estrogens, as the contraceptive 17α-ethinylestradiol (EE2) and 3-methyl ether of ethinylestradiol (MeEE2), used as the active ingredient in birth control pills and in other drugs administered during menopause, appear to be the most probable cause of endocrine disruption effects observed in wild fish.[16] In addition to the natural origin of E2, the European Medicines Agency has approved the use of E2 as a pharmaceutical indicated to treat some symptoms of menopause, prevent osteoporosis in postmenopausal women, treat dysmenorrhea and prevent pregnancy, replace estrogen levels in women with ovarian failure or other conditions that cause a lack of natural estrogen in the body, and sometimes is used as part of cancer treatment in women and men.

There is a growing body of scientific research which indicates that EDCs in the environment may interfere with the normal function of the endocrine system of humans and wildlife by mimicking and antagonizing the effect of endogenous hormones, disrupting the synthesis and metabolism of endogenous hormones, or disturbing the synthesis of the specific hormone receptors.[17]

Estrogens are steroids constituted by 18 carbon atoms, which are distributed in three hexagonal and one pentagonal rings. The different positions of hydroxyl groups in the cyclopentane-phenanthrene nucleus differentiate these molecules. In synthetic estrogens, the addition of ethynyl and methyl groups to E2 forms, respectively, EE2 and MeEE2, which are the molecules used in the formulation of the contraceptive pill (Fig. 1.2).[18]

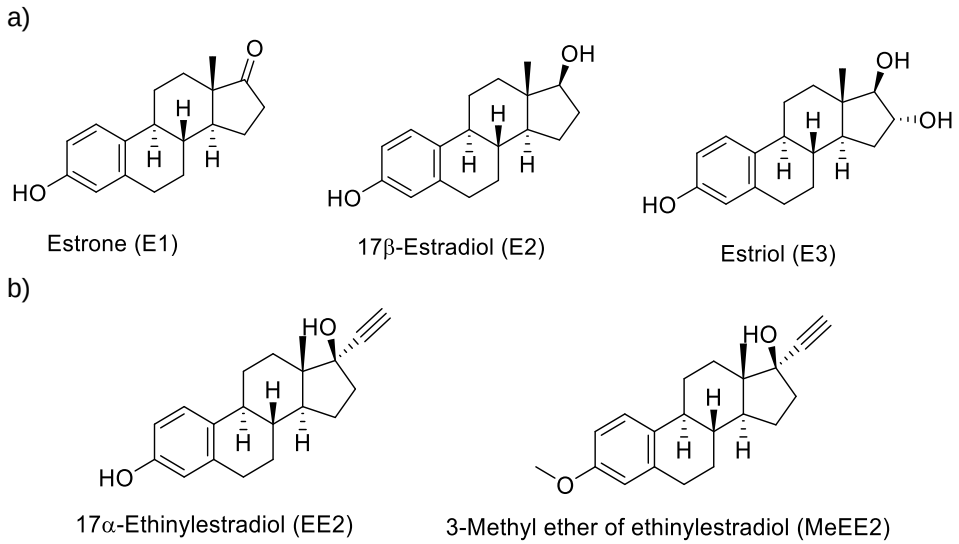

Figure 1.2. Molecular structure of a) natural and b) synthetic estrogens.

Estrogens are the primary female sex hormones and play important roles in both reproductive and non-reproductive systems. In humans and animals, estrogens are produced mainly in the ovary, but can also be synthesized in other organs such as the testis, brain, hypothalamus, adipose tissue, and placenta. In the organism, the catabolism of estrogens occurs in the liver, where they are conjugated to sulfate, glucuronide or sulfoglucuronide forms, made up by the substitution of hydroxyl groups of free estrogens. These substitutions may increase estrogen aqueous solubility and facilitate their elimination *via* urine. However, a fraction of estrogens is eliminated *via* feces in the unconjugated or free forms.[19] Conjugated estrogens display very low estrogenic activity compared to unconjugated forms (Table 1.1).

Table 1.1. Properties and relative estrogenic activity related to 17β-estradiol of free and conjugated estrogens.[18]

Compound		Molecular weight	Water solubility ($mg \cdot L^{-1}$ at 20 °C)	Log K_{OW}	Relative estrogenic activity
Non-conjugated estrogens	E1	270.4	13	3.43	25.4
	E2	272.4	13	3.94	100.0
	E3	288.4	32	2.81	17.6
	EE2	296.4	4.8	4.15	246.0
	MeEE2	310.4	0.3	4.67	11.0
Conjugated estrogens	ß-E2 3-sulfate	352.4	3.6	2.9	2.6×10^{-2}
	ß-E2 3ß-D-glucuronide	448.4	347	1.46	2.4×10^{-2}
	E1-sulfate	350.4	5.9	0.29	5.0×10^{-3}
	E1-ß-D-glucuronide	446.4	303	1.9	$<1 \times 10^{-3}$

Conjugated hormones excreted are broken down by intestinal and faecal flora, producing estrogenically active free forms. It can be anticipated that after excretion, conjugated estrogens in urine will follow deconjugation, becoming more hydrophobic, and will be partially eliminated from the liquid fraction by sorption onto solids. Free estrogens eliminated *via* faeces remain associated to the hydrophobic fraction of this matrix. Estrogen loss by volatilization is insignificant in both cases.[20]

Humans and animals excrete estrogens, which end up in the environment through sewage discharge and animal waste disposal (Table 2.1).[21] Those steroids have been detected in effluents of WWTPs and surface water.

Table 1.2. Daily excretions (μg) of estrogenic steroids in humans.[21]

Category	E2	E1	E3	EE2
Males	1.6	3.9	1.5	-
Menstruating females	3.5	8	4.8	-
Menopausal females	2.3	4	1	-
Pregnant women	259	600	6000	-
Women	-	-	-	35

1.2. Water treatment processes for organic pollutants removal

To assess the relevance of water treatment as a research topic in the context of environmental quality, a literature search was performed (Fig. 1.3) using Scopus as a data base of peer-reviewed literature, with the following variables: document type, all; data range, 1997–2015 (included); subject areas, all; and search for, “Environmental water risk assessment” (1782 items in 2015) and “Wastewater treatment” (7612 items in 2015). It is quite evident that in the last 2 decades, the number of studies dealing with these topics has greatly increased. There are different processes for the elimination of organic pollutants from water, grouped according to their nature. To refine the search, these studies were screened by “Water treatment biodegradation” (1064 items in 2015), “Water treatment physical processes” (588 items in 2015), and “Advanced oxidation processes” (791 items in 2015). The following sections will present and discuss the major findings on these topics.

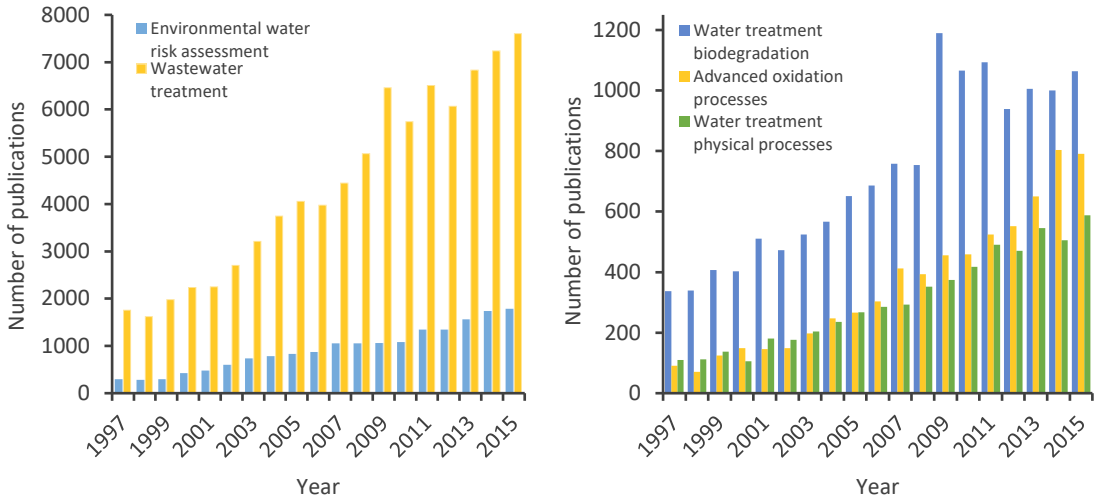

Figure 1.3. Scopus search for relevant publications in the field of water treatment, reported by year.

- Physical processes

The sorption elimination is a physical process based on the uptake of pollutants from the aqueous onto a solid phase. Isotherm equations are usually used to obtain insight description and predict the removal of a target compound by sorption onto different sorbents. The affinity of a target compound for a sorbent can be calculated by the specific sorption coefficient, which relates the ratio between the sorbed and the freely dissolved concentrations of the compound at the equilibrium. The application of activated carbon is a well-known physical process used to remove different organic pollutants. Various studies have indicated the efficiency of activated carbon for the removal of trace levels of EDCs in water.[22] In 2005, Zhang and Zhou studied the removal of E1 and E2 by sorption onto activated carbon under different environmental parameters, such as adsorbent concentration, pH, salinity and the presence of humic acid and surfactants. The results showed that adsorption capacity of activated carbon decreased with increasing adsorbent concentration, due to the presence of colloids, which may bind to the EDCs. The presence of surfactants and humic acids resulted in a reduction of the adsorption constant, which can be explained by the ability of surfactants to enhance the solubility of pollutants in water and the ability of humic acids in complexing with pollutants.[23]

The membrane filtration is another physical approach. It is defined as the separation process based on the difference in physical or chemical properties of two phases separated by a semi-permeable membrane. This membrane operates as a separation barrier, through

which certain substances can pass, while others are retained. Membrane processes are acquiring wide use for estrogens removal in wastewater treatment.[24]

One major drawback of physical process, specifically when dealing with toxic compounds, is that it based on the accumulation and exchange of the pollutants from the aqueous to the adsorbent phase. Therefore, pollutants are not actually destroyed, but just transferred between different phases.

- Biological processes

The biological approach for water treatment is based on the natural role of microorganisms in the elemental cycles, such as the C, N and P cycles, which is related to their biodegradation capacity.[25] Accordingly, biodegradation is the mechanism by which microbial organisms transform, through metabolic routes or enzymatic action, the structure of chemicals present into the medium.[26] Many factors may induce microorganisms to use pollutants as substrates or cometabolize them, such as their genetic potential, temperature, pH, and available nitrogen and phosphorus sources. These conditions determine the rate and the extent of the pollutant degradation.[27]

Some microorganisms have the naturally-occurring metabolic diversity to degrade, transform or accumulate a huge range of compounds including hydrocarbons, polychlorinated biphenyls, polyaromatic hydrocarbons, radionuclides and metals.[28] Several studies have demonstrated that both heterotrophic and autotrophic aquatic microorganisms can degrade estrogens, and that some of them can transform estrogens into non-estrogenic compounds.[4b, 29] The mechanisms of biodegradation of estrogens in WWTPs reported in the literature also include sorption to biosolids[30] and sludge.[26, 31]

- Advanced oxidation processes

Generally, organic pollutants present in water media can be degraded by direct photolysis to variable degrees, depending on their chemical structure. The presence of aromatic rings and conjugated π-systems, as well as certain functional groups and heteroatoms, may increase the direct absorption of sunlight. Such structures produce absorption spectral bands in the UVC wavelength range (280-100 nm), with tailing absorption into the UVB (315-280 nm) and in some cases UVA ranges (400-315 nm). The potential spectral overlap with natural sunlight ($\lambda > 290$ nm) suggests that these organic pollutants may degrade, at least partially, by direct photolysis.[32]

Organic pollutants in water can also be degraded by indirect photolysis. Advanced oxidation processes (AOPs) refer specifically to processes in which the oxidation of

compounds occurs primarily through reactions with reactive oxygen species (ROS), such as radicals and singlet oxygen ($^1O_2$).[33] These processes comprise two phases: the formation of ROS under irradiation, and the reaction of these species with the target pollutants. AOPs are considered as effective water treatment techniques for removing organic pollutants which, due to their high chemical stability and/or low biodegradability, are not treatable by ordinary approaches.[34] In the last decade, the photocatalytic degradation of various toxic organic compounds has been analysed[35]

Semiconductor photocatalysis is one of the most effective AOP technology for the destruction of pollutants in water. In the last two decades, TiO_2 has received considerable interest as a semiconductor photocatalyst due to its photochemical stability, non-toxic nature and low cost.[36] However, the efficiency of the use of TiO_2 is limited by its relatively large band gap energy, which corresponds to the wavelength of 370 nm, where only *ca*. 3-5% of the solar energy is overlapped and therefore effective. The high recombination rate of electron-hole pairs formed during the photocatalytic process is also a disadvantage of this technology.[37] The use of solar energy in photosensitized applications for water treatment emerges as an affordable approach to a difficult environmental problem.

As previously stated, organic pollutants under solar irradiation in environmental waters can be subjected to direct photolysis. Upon a photon absorption by the pollutant, the excited form will undergo a chemical transformation, thus generating one or more different product species. However, depending on different environmental conditions, such as fluence rate (total number of particles crossing over a sphere of unit cross section which surrounds a point source of radiation) of the solar irradiation, water turbidity, pH of the media, presence of natural organic matter, salinity, biological activity or oxygen content, the degradation of the pollutant can be significantly delayed or inhibited.[38] Photodegradation of pollutants in water may also occur by indirect photolysis, by means of other substances present in water able to absorb solar irradiation and subsequently generate ROS, mainly $^1O_2$ and hydroxyl ($HO^{\bullet}$), peroxyl ($ROO^{\bullet}$) and superoxide anion ($O_2^{-\bullet}$) radicals.[39] The photocatalytic treatment for water remediation is especially convenient because it may achieve the mineralization of the organic pollutant (in particular when high doses of light are applied), which minimizes the release of potential hazardous degradation products,[40] in addition to the possibility of using sunlight as energy source.[41] This methodology requires light of an appropriate wavelength, a photocatalyst or photosensitizer (PS) capable of absorbing that light, and molecular oxygen and/or an appropriate substrate (Fig. 1.4). The excitation of the PS is generally achieved *via* one photon absorption (hυ), originating an electron transition between the ground state, S_0, and the singlet excited state, S_1^*.

Vibrational relaxation of S_1^* by a non-radiative process yields the lowest vibrational level of S_1^*. Intersystem crossing (ISC) from S_1^* generates the first excited triplet state of the PS, T_1^*. The lifetime of T_1^* is longer (µs scale) than that of S_1^* (ns scale), which allows the interaction of the PS in the excited state in one of two ways, defined as Types I and II photochemical mechanisms. A Type I mechanism involves reactions of electron-transfer between the excited PS and oxygen or other substrate present in the medium, yielding free radicals; while in type II mechanism $^1O_2$ ($^1\Delta$) is generated *via* an energy transfer process during a collision of the excited PS, T_1^*, with triplet oxygen ($^3\Sigma$).[42]

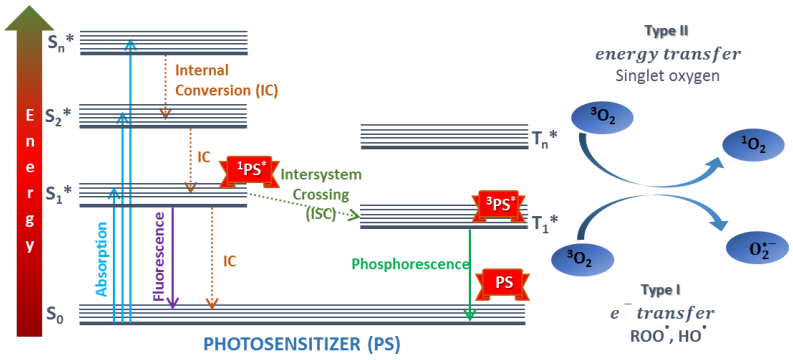

Figure 1.4. Schematic representation of ROS generation by photochemical processes.

Amongst PS, porphyrins (Pors) and phthalocyanines (Pcs) have attracted considerable attention because of their prospective applications in photodynamic therapy,[43] photodynamic inactivation of microorganisms,[44] mimicking enzymes,[45] sensing,[46] catalytic[47] and photocatalytic reactions,[48] molecular electronic devices[49] and conversion of solar energy.[50] Both Pors and Pcs are considered as suitable PS due to their high absorption in the UV-Vis range, which represents an important component of sunlight. Some Pors and Pcs have remarkably high quantum yields for triplet state formation, which determines the ability of a PS to generate $^1O_2$. The yield of the triplet state can be modulated by the incorporation of certain metals into the core and/or by replacing some of the hydrogen atoms with halogens or other heavy atoms, enhancing ISC from the initially formed singlet state to the triplet state.[51] These features of Pors and Pcs may minimize the energetic requirements and maximize the global efficiency of the process.

Being an electrophilic agent, $^1O_2$ is able to oxidize double bonds, sulfide, phenolic, amino groups, and other electron-donor groups in organic compounds.[52] Recent work has focused on immobilized PS for singlet oxygen generation, since this presents several advantages in practical applications. For its use in water treatment, the ability to recover and reuse the PS in successive runs avoiding, to the extent possible, the loss of the original catalytic properties provided by the system, is environmentally and economically sensible.

In general, immobilized PS show reduced quantum yields in comparison with their free form, due in part to the difficulty for oxygen to diffuse into and out of the material matrix, in order to be activated. However, the easy reuse of these systems tends to overcome this drawback.[53]

1.3. Porphyrins and phthalocyanines as photosensitizers in water treatment applications

1.3.1. General considerations of porphyrins and phthalocyanines

Porphyrins, from the Greek word *porphyros*, meaning *purple*, are an important class of naturally occurring macrocyclic compounds found in biological systems that play a very important role in the metabolism of living organisms. Some of the best examples are the iron-containing Pors found as heme (of hemoglobin) and the magnesium-containing reduced Por, or chlorine, found in chlorophyll.[54] Pors are heteroaromatic compounds composed by a tetrapyrrole structure, consisting in four pentagonal pryrroles linked together by four methine bridges. Aromaticity among the macrocycle is constituted by 22 π-electrons (Fig. 1.5a).

On the other hand, phthalocyanines, synthetic analogous of Pors, are intensely blue-green-coloured aromatic macrocyclic compounds which are widely used in dyeing. Their chemical structure present an aromatic macrocycle constituted by four isoindole subunits linked together by their 1,3-positions by *aza* bridges. Their structure consists of 42 π-electrons extended among 32 carbon atoms and 8 nitrogen atoms. However, electron delocalization takes place preferentially over the internal ring system, so that Pcs are considered as aromatic systems formed by 16 atoms and 18 π-electrons, condensed in 4 benzene rings, which preserve their electronic structure (Fig. 1.5b).[55]

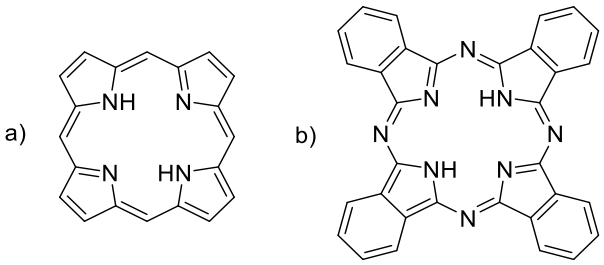

Figure 1.5. Molecular structure of a) porphine, the simplest Por macrocycle; and (b) free-base Pc.

The specific optical properties of Pors and Pcs make them a target of choice as photosensitizing agents. Their excited state properties can be adjusted through conformational design, molecular symmetry, metal complexation, orientation and strength of the molecular dipole moment, size and degree of conjugation of the π-systems, and appropriate donor-acceptor substituents.[56]

Pors and Pcs absorb light in different UV-Vis ranges. UV-Vis absorption spectra of Pcs are characterized by Q-bands and an intense Soret-band clearly differentiated (Fig. 1.6). Metallophthalocyanines (MPcs) present the Q-band maximum in the red region of the visible range, while for free-base Pcs a split Q-band is observed due to a lower structural symmetry. Note that this fact is only valid for symmetrically substituted MPcs. If the periphery of the MPc is unsymmetrically derivatized, the breakage of the symmetry leads to the split of the Q-band.[57] Extended conjugation by the peripheral benzene rings may strengthen the absorption bands at longer wavelengths.[58]

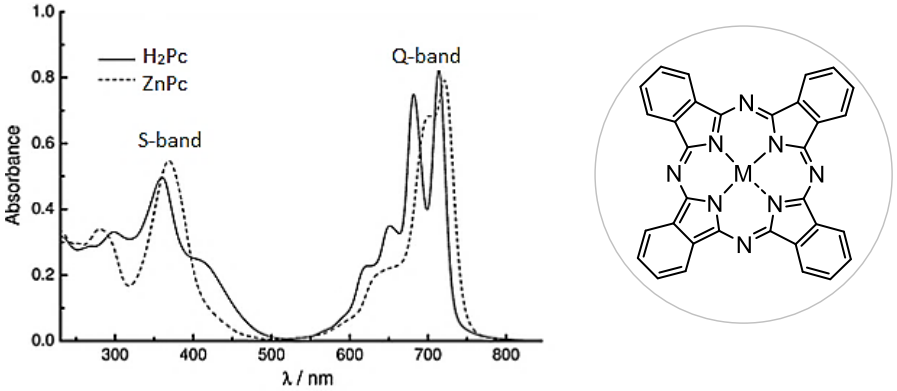

Figure 1.6. Structure and typical absorption spectra of free-base Pc (black line, M = H_2) and metal complex ZnPc (dashed line, M = Zn).[59]

The intense Soret absorption band of Pors in the 420-430 nm spectral region allows a very efficient interaction with blue light wavelengths which, within solar spectrum, are the most penetrating in natural waters.[60] Typically, free-base Pors present four Q bands: IV, III, II and I. Depending on the intensity of these bands, Por spectra may be designated *etio* type (IV>III>II>I), *rhodo* type (III>IV>II>I), *oxo-rhodo* type (III>II>IV>I), *phyllo* type (IV>II>III>I) (Fig. 1.7a).[61]

Similarly to MPcs, absorption spectra of metalloporphyrins (MPors) molecules present higher symmetry than free-base Pors.[62] This feature results in a simplification in the visible spectra with just two Q bands, designated as β and α (Fig. 1.7b).

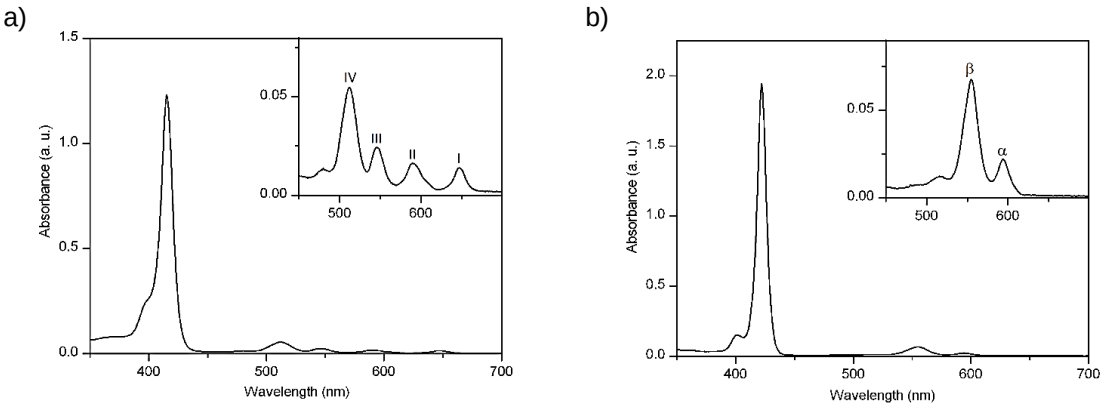

Figure 1.7. Typical UV–vis absorption spectra for (a) a free-base Por and (b) a Por–metal complex.

1.3.2. Synthetic strategies for the preparation of porphyrins

The important biological roles and photophysical properties of Pors captured the attention of investigators during the XX Century since Fischer, considered the *father of porphyrin chemistry*, reported the first total synthesis of the Pors *ethio* porphyrin-III and octamethylporphyrin, in 1926, and protoporphyrin-IX in 1929 (Fig. 1.8).[63]

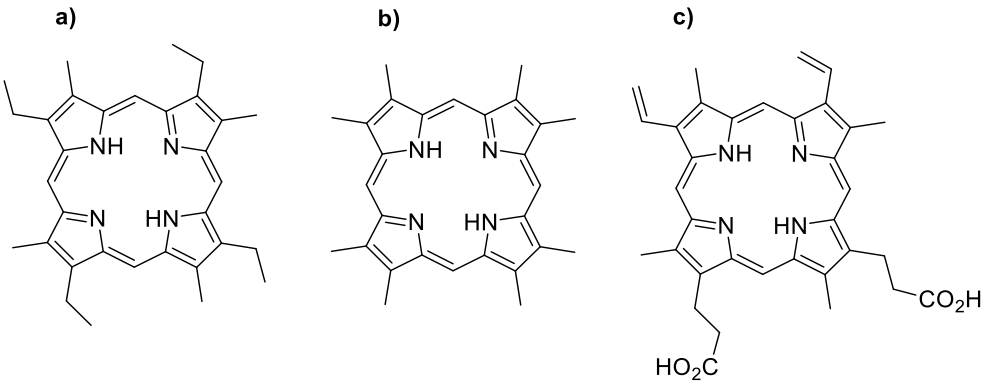

Figure 1.8. Historically important Pors prepared by Fischer: a) ethio porphyrin III, b) octamethytlporphyrin, c) protoporphyrin IX.

Initially, the exploration of Pors was extremely restricted by their synthetic availability. This gave the stimulus for researchers to design efficient synthetic methods for their synthesis. The preparation of Pors can be categorized into three main categories: β- and *meso*-unsubstituted porphine; β-substituted Pors or octalkylporphyrins (OAPs); and *meso*-aryl substituted Pors (Fig. 1.9). This work is focused on *meso*-aryl substituted Pors, for which the most common synthetic routes are presented below.

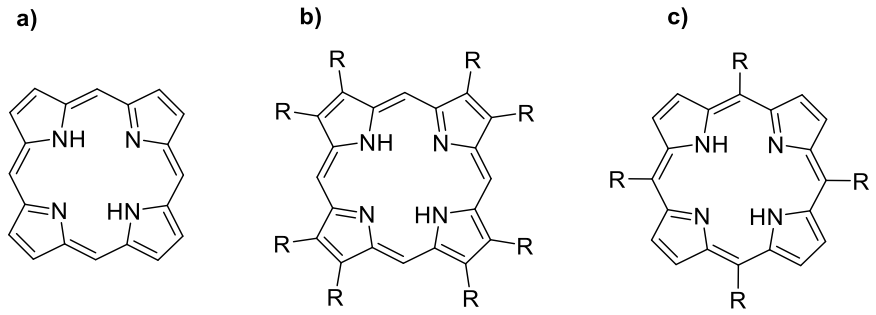

Figure 1.9. Most common substitution patterns found around the Por macrocycle: a) β- and meso-unsubstituted porphine, b) β-substituted OAPs, c) meso-aryl substituted Por.

1.3.3. Synthesis of *meso*-substituted porphyrins

For the synthesis of Pors, one of the most commonly used method is based on the condensation of pyrrole with an aromatic aldehyde. Due to the simplicity of this synthesis, this method has been used extensively to prepare symmetric Pors. *meso*-Tetrasubstituted Pors were first prepared in 1936 by Rothemund by heating pyrrole and an aldehyde in pyridine in a sealed tube at 120 °C for 48 h (Scheme 1.1).[64]

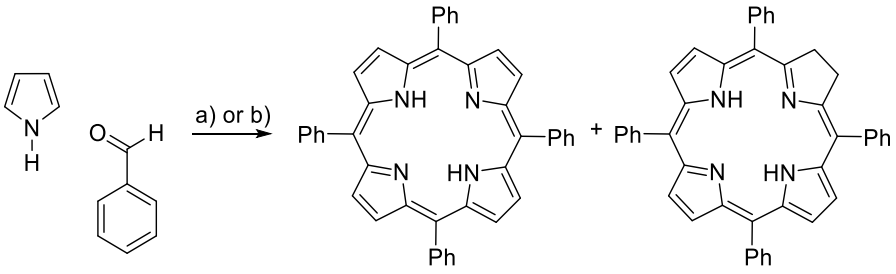

a) Rothmund: Pyridine, 120 ºC, 48 h

b) Adler and Longo: $CH_3CH_2CO_2H$, 140 ºC, 30 min

Scheme 1.1

The yields of Pors from this reaction were in general less than 3% and the product was contaminated with the corresponding chlorin, the 2,3-dihydroporphyrin. Calvin *et al.* discovered that the addition of metal salts to the reaction mixture, such as zinc acetate, increased the yield of Por from 4-5% for the free-base derivative, and decreased the amount of chlorin compound.[65]

An important improvement in the condensation reaction of pyrrole and aldehydes came from the work of Adler and Longo, after demonstrating that the yields of Pors could be largely increased by performing the reaction in acidic media, in open air (Scheme 1.1).[66]

In refluxing propionic acid, this condensation gave yields higher than 20%. Greater yields, *ca.* 30- 40%, were obtained by using acetic acid as solvent. However, in this case the product did not crystallize due to the higher pK_a of acetic acid, resulting in a more difficult isolation and purification of the Por. As previously reported in the Rothemund synthesis, the produced Por was contaminated by the corresponding chlorin, observed in the UV-Vis spectrum by the presence of a strong band centred around 650 nm.

Lindsey *et al*. reported another general synthetic method for *meso*-tetraphenylporphyrins in 1987.[67] This strategy considers that under equilibrium conditions, the acid catalysed condensation proceeds by the formation of a porphyrinogen. The Lindsey method is a two-step and one-pot procedure, in which pyrrole and the aldehyde are condensed in presence of a trace of acid catalysis under anaerobic conditions to produce the porphyrinogen. Then, the porphyrinogen is oxidized to the Por by subsequently adding an oxidant such as 2,3-dichloro-5,6-dicyanobenzoquinone (DDQ) or *p*-chloranil (Scheme 1.2).

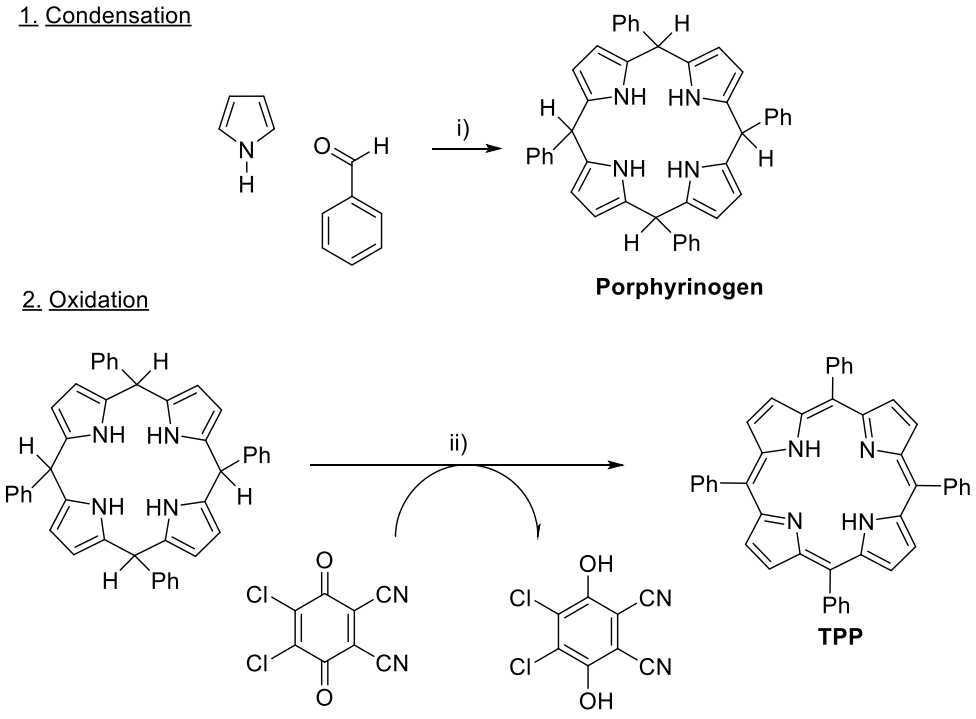

i)TFA or BF_3, CH_2Cl_2, Ar, rt, 30-60 min; ii) DDQ (2 equiv), 45 ºC, 1 h

Scheme 1.2

Maximum yields of the Por (30-40%) are obtained when equimolar concentrations of pyrrole and aldehyde are condensed in the presence of boron trifluoride etherate (BF_3). This reaction is usually performed in dichloromethane at room temperature for 1 h before

the oxidant (*p*-chloranil or DDQ) is added. In most cases, removal of the solvent followed by flash chromatography in a column yields the pure Por.

In 1991, Rocha Gonçalves *et al.* developed a synthetic route to prepare, in one step, *meso*-tetra-aryl substituted Pors in good yields and without chlorin derivatives. Currently, this method is widely used to produce *meso*–substituted Pors, consisting in the condensation of pyrrole with benzaldehyde, in presence of acetic acid with 30% of nitrobenzene at reflux (120 ºC) for 1 hour. The acetic acid acts as solvent and catalyst, and the nitrobenzene as oxidizing agent.[68]

Due to the simplicity of this method, it can be applied to produce a broad variety of tetra-substituted Pors having four identical aryl units. This approach also permits the preparation of asymmetric *meso*-substituted Pors, by condensation of pyrrole with an appropriate mixture of aldehydes. The ratio of the different compounds formed varies depending on the proportion of aldehydes present in the reaction and their reactivity.

1.3.4. Synthetic strategies for the preparation of phthalocyanines

The earliest exhaustive study of the synthesis of Pcs was conducted by Linstead and co-workers in 1930s.[69] At first, almost all Pcs were unsubstituted on their peripheral positions, resulting in poorly soluble compounds in most organic solvents, including with high-boiling points such as 1-chloronaphthalene or 1-bromonaphthalene. The best way to modulate the aggregation nature of Pcs is by replacing the central atom and/or its axial coordination position with one or two ligands, or by modifying its peripheral positions.[70] Structural modifications of Pcs also allow the design of electrophysical characteristics over a wide range. The photophysical properties of MPcs greatly depends on the nature of the central metal ion. MPcs containing transition metals give short triplet lifetimes. A long triplet lifetime and a relatively high triplet quantum yield, which are useful qualities for a PS, characterize MPcs metallated with diamagnetic metal ions such as Zn^{2+}, Al^{3+}, Ga^{3+} and Si^{4+}.[58] Specifically, ZnPcs have been largely explored due to the d^{10} configuration of the central metal ion, Zn^{2+}, which results in optical spectra that are not complicated by additional bands, as in transition-metal Pc complexes.[71]

The preparation of Pcs with identical substituents in the 4 isoindole rings can be performed by cyclotetramerization of the suitably substituted precursors, or by the consecutive derivatization of the already constituted Pc. Different precursors, such as

isoindoline-1,3-diimine, 2-cyanobenzamide, phthalamide, phthalic acid, isobenzofuran-1,3-dione, or isoindoline-1,3-dione, can be used in the preparation of MPcs. However, the synthesis of Pcs usually involves the tetramerization of either phthalonitrile or diiminoisoindoline.[72] Scheme 1.3 summarizes some common synthetic methods to prepare H_2Pcs and MPcs. Most used strategy in the preparation of Pcs involves heating a mixture of a phthalonitrile and a metallic salt in a high boiling point solvent as dimethylethanolamine (DMAE), dimethylformamide (DMF) or *o*-dichlorobenzene (*o*-DCB).[73]

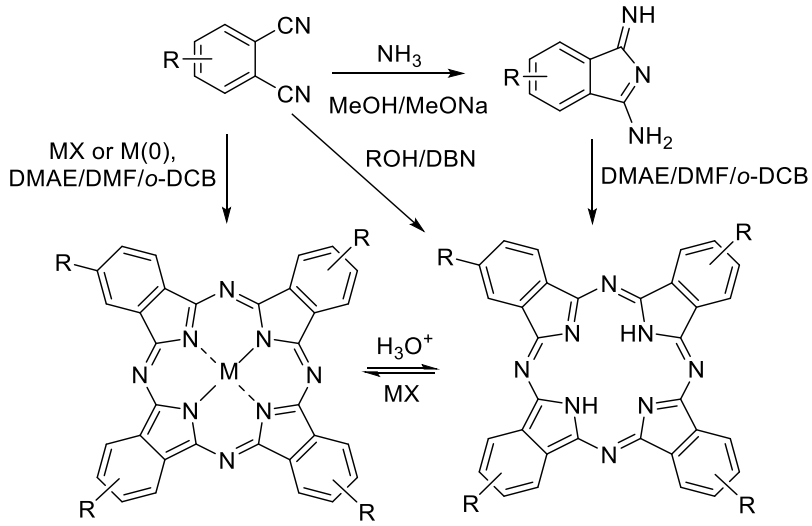

Scheme 1.3

In the preparation of H_2Pcs, most common methodology is the condensation of 1,3-diiminoisoindolines under the same reaction conditions previously described.[74] There are other synthetic routes that can be carried out at lower temperatures with the utilization of alcohols, as 1-butanol, in presence of a non-nucleophilic hindered base, as 1,5-diazabicyclo(4.3.0)non-5-ene (DBN),[75] or even at room temperature by using metallic lithium in DMAE as solvent.[76] Both types of Pcs can be interconverted. The treatment of a MPc with a refluxing non-oxidant mineral acid produces its demetallation, obtaining the corresponding H_2Pc. In contrast, when H_2Pc is refluxed in the presence of a metallic salt in a high boiling point solvent, the MPc will be obtained.

Most recently, some other procedures have been proposed for the preparation of symmetrically substituted Pcs with higher yields and under mild conditions. Shaabani *et al.* developed a fast and effective procedure for the synthesis of MPcs from phthalonitrile, phthalimide and phthalic anhydride, upon treatment with hexamethyldisilazane (HMDS) using microwave irradiation.[77]

Octa-substituted Pcs can be derivatized in the peripheral β-positions (2, 3, 9, 10, 16, 17, 23, 24) or in non-peripheral α-positions (1, 4, 8, 11, 15, 18, 22, 25). Substitution at the more sterically crowded α-position presents reduced aggregation tendencies. They are typically prepared from 4,5- or 3,6-disubstituted phthalonitriles (Scheme 1.4).[78]

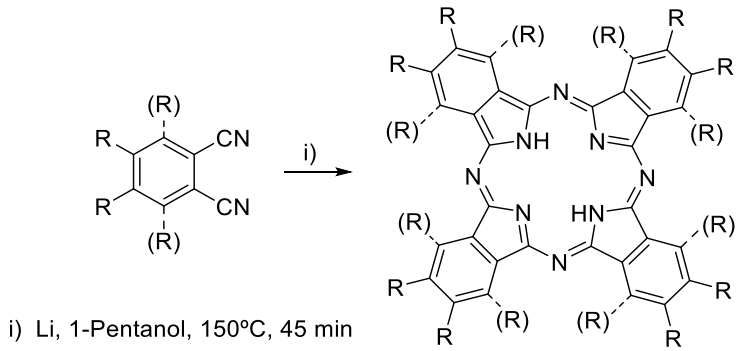

Scheme 1.4

1.3.5. Water-stable porphyrins and phthalocyanines

For water treatment applications, PS are required to be stable in aqueous media. Due to the high hydrophobic nature of Pors and Pcs, hydrophilic substituents can be attached into the structure of the PS to overcome aggregation. During the past few decades, different kinds of water-soluble PS have been synthesized and studied. In this context, most common derivatization of Pors and Pcs are with sulfonic[79] and carboxy acid groups[80] and phosphorus-based functions[81], resulting in anionic PS. On the other hand, introduction of quaternary amino[82] or pyridino[83] groups leads to cationic ones. Water-solubility of anionic and cationic PS is strongly pH-dependent, being not necessary water-soluble in acidic or basic media, depending on their pKa, which determines the extent of ionisation. One of the most important water-soluble PS in current usage, *meso*-substituted tetrakis (4-sulfonatophenyl)porphyrin, presents a high quantum yield of singlet oxygen generation in phosphate buffer (pH 7.4) at concentration ranging from 8×10^{-5} to 20×10^{-5} M, of 0.51.[84]

Several types of neutral substituents are also able to confer water-solubility to Pors and Pcs. A suitable derivatization may be easily afforded with sugar moieties as hydrophilic substituents, which can act as water-solubilizing agents. Perfluorophenyl derivatives of Pors and Pcs are especially suited, since their *para*- and β- fluorine atoms, respectively, allow an easy substitution with a variety of nucleophiles. In 2010, Drain *et al.* described the preparation of glycoconjugated fluorophenyl Pors by nucleophilic substitution if the

pentafluorophenyl groups with β-D-thioglucopyranosyl, affording $Por(SGlcAc)_4$ (Scheme 1.5). In a second reaction step, acetate protecting groups of the glucose moieties were easily removed by basic hydrolysis at room temperature, obtaining the tetra-thioglycosylated porphyrin, $Por(SGlc)_4$.[85]

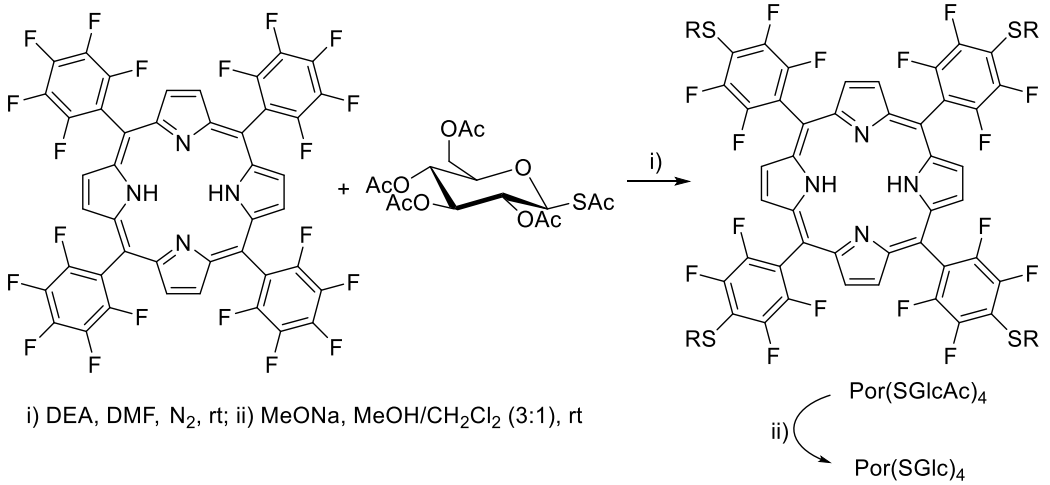

Scheme 1.5

In a similar synthetic approach, the symmetric octathioglycosylated zinc (II) perfluorophthalocyanine was reported in 2011 also by Drain and co-workers.[86]

The preparation of Pcs bearing sugar moieties can be also performed by the tetramerization of glycosylated phthalonitriles. Soares *et al.* reported the synthesis of Pcs bearing eight galactose units separated from the macrocycle by methylenic spacers. The synthesis involved the tetramerization of a previously prepared di-glycosylated phthalonitrile, having two 1,2:3,4-di-*O*-isopropylidene-α-D-galactose units, in the presence of $ZnCl_2$ in DMAE, obtaining $ZnPc(GalPr)_8$. The deprotection of the isopropylidene groups of the sugar moieties was performed under acidic conditions, thus obtaining a highly water soluble octasubstituted galactose zinc(II) phthalocyanine, $ZnPc(Gal)_8$ (Scheme 1.6).[87]

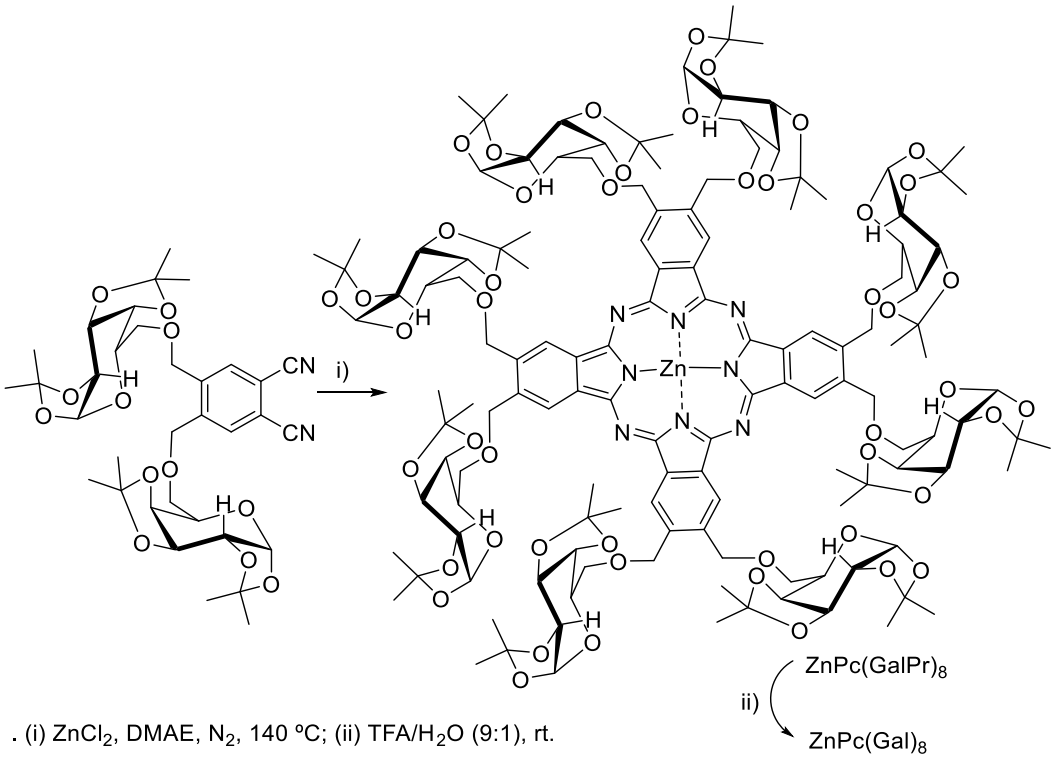

. (i) $ZnCl_2$, DMAE, N_2, 140 ºC; (ii) TFA/H_2O (9:1), rt.

Scheme 1.6

1.3.6. Photocatalytic performance of immobilized porphyrins and phthalocyanines in the degradation of organic pollutants in water

Different types of supports, both organic and inorganic, can be used in the immobilization of PS. However, in case of photo-oxidation processes, more resistant inorganic solids are usually preferred, in order to provide stability of the material under the reaction conditions. The support must also be easily functionalized with the PS, inexpensive and widely available. A fundamental requirement for a PS carrier is that it should not significantly quench $^1O_2$. It is important for the PS to be embedded predominantly in the monomeric form, since aggregation promotes the non-radiative internal conversion, causing a decrease of the triplet lifetime and a drastic reduction in the overall efficiency of $^1O_2$ production.

Physical adsorption of PS onto the support surface, either by van der Waals or by dipole-dipole interactions, is the simplest and most straightforward approach to support catalysts, since no modification of the support and/or the complex is needed. However, in order to avoid PS leaching, the physically adsorbed catalysts cannot be used in solvents in which the PS is soluble. This is particularly relevant for Pcs, which due to the flat aromatic

structure show strong affinity for hydrophobic surfaces. Guo *et al.* reported the preparation of 2,9,16,23-tetra-nitrophthalocyaninato iron (II) ($FePc(NO_2)_4$) nanostructures grown on a substrate constituted by TiO_2 nanofibers, by combining the electrospinning technique and the solvothermal method (Scheme 1.7).[88] These heterostructures exhibited excellent photocatalytic performance for the photodegradation of methyl orange (MO), assisted with H_2O_2 under visible light irradiation, achieving a total degradation of MO after 3 h of irradiation.

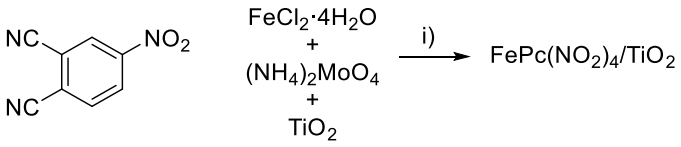

i) Ethylene glycol, 160 ºC, 20 h

Scheme 1.7

Water-soluble charged PS are often immobilized by using ionic interactions on ion-exchanging zeolites and resins. Pcs and Pors substituted with carboxyl or sulfonate groups have been attached to Amberlite.[89] Pcs and Pors bound to exchange resins were reported to behave as homogeneous compounds (Fig. 1.10). PS adsorbed on porous materials (silica, zeolites), are usually encapsulated within the matrix and most of them show reduced $^1O_2$ quantum yield due to the limited diffusion of oxygen into the support and of the reactive oxygen species back to the surrounding medium.

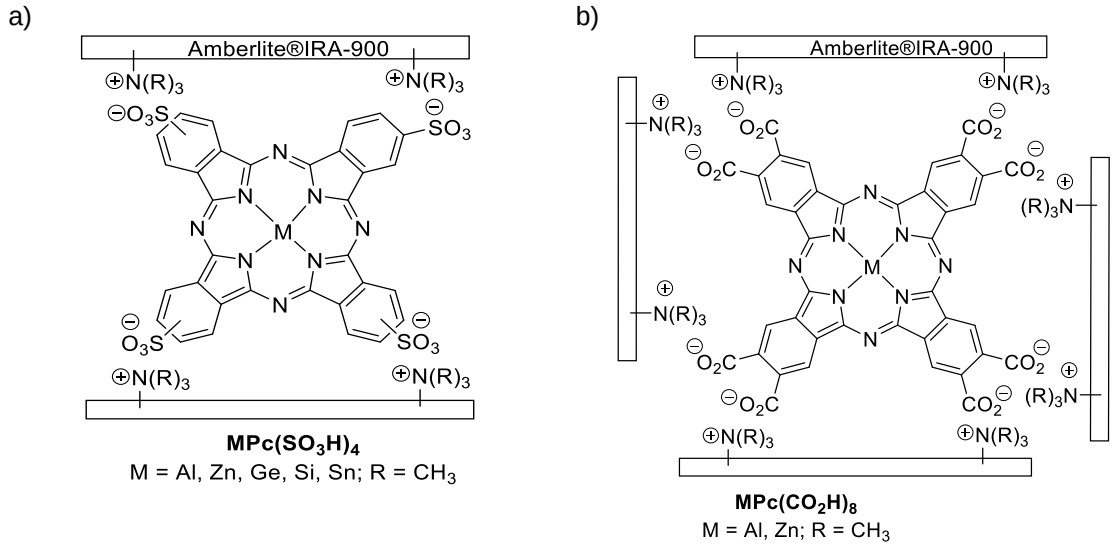

Figure 1.10. Schematic representation of (a) $MPc(SO_3H)_4$ and (b) $MPc(CO_2H)_8$, both immobilized onto Amberlite®IRA-900.[90]

PS can be covalently bound to the surface of the support. This immobilization approach may prevent PS from leaching, providing a strong immobilization. In addition, $^1O_2$ is more available when generated from the surface, since it diffuses into the solution more easily. In recent years, an increasing number of researchers have considered nanomaterials as carriers of PS. The efficiency of PS immobilized on nanomaterials may be comparable with that in homogeneous medium due to the enormous surface of the nanocarriers.

In heterogeneous catalysis, the reaction rate is restricted to the limited surface area of the catalyst, while homogeneous catalysts can react very fast and provide a good conversion rate per molecule. The link between heterogeneous and homogeneous catalysts can be achieved using nanoparticles (NPs), which provide the benefit of increased surface area. The nanostructured catalyst forms stable suspensions in the reaction media that allow increased reaction rates, especially when well dispersed. Furthermore, NPs may allow additional catalytic action due to their unique properties, as in the case of TiO_2 NPs, which exhibit photooxidation on their surfaces.[48] One particularly useful and important group of NPs is magnetic nanoparticles (MNPs), which are typically based on metals such as iron, cobalt and nickel, or metal oxides. In the absence of a magnetic field, and when a suitable surface stabilization is provided, MNPs may be dispersed in the same manner as any NP. However, in the presence of a magnetic field, MNPs can be selectively separated, enabling the easy removal from the reaction media to then be re-dispersed and re-used.[91] The surface of MNPs can be functionalized to allow the attachment of PS. Modisha *et al.* described a conjugate of octacarboxyphthalocyaninato zinc(II) ($ZnPc(CO_2H)_8$) with Fe_3O_4 NPs coated with a silica shell (Fig. 1.11), which was then tested in the photodegradation of 1-phenylazo-2-naphthol-6,8-disulfonic acid disodium salt, commonly known as Orange G (OG), under visible light irradiation.[92] The catalyst could be easily recovered using an external magnet for its reuse.

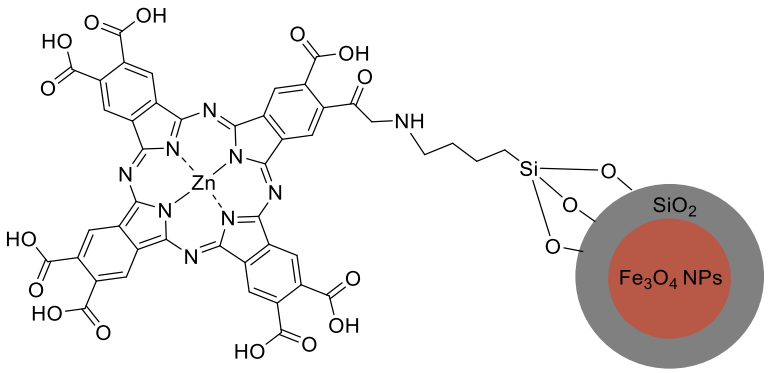

Figure 1.11. Covalent attachment of $ZnPc(CO_2H)_8$ onto MNPs.

In the context of wastewater treatment, and particularly for the photodynamic inactivation of microorganisms, Carvalho *et al.* proposed the development of efficient PS immobilized on MNPs in order to recover these materials after the wastewater treatment just by applying a magnetic field.[93] Then, recycling and reuse abilities of these materials were explored, showing an environmentally-friendly and economically feasible approach to disinfect water.[94]

The use of single walled carbon nanotubes (SWNTs) as support material for Pc complexes was reported for the first time in 2011 by Ogunbayo *et al.* SWNTs were chosen as support because of the easy immobilization of Pcs due to the strong π–π interaction between SWNTs and Pc complexes. In that study, conjugates formed by thioalkyl derivatized PdPcs adsorbed onto SWNTs were used for the photodegradation of 4-nitrophenol.[95]

1.4. Degradation of organic pollutants by bacteria

1.4.1. General considerations about biodegradation of organic pollutants

Bioremediation is based on the metabolic versatility of microorganisms to interact, both physically and chemically, with hazardous substances leading to structural changes (harmless metabolites) or complete degradation into carbon dioxide and water (termed mineralization) of target molecules. Bioremediation requires a redox reaction within the microbial cells to produce energy. These reactions comprise respiration and other biological functions needed for cell survival and reproduction. A delivery system providing one or more of the following elements is usually required: an energy source (electron donor), an electron acceptor and nutrients.[96] Microorganisms must gain energy from the transformation of the pollutants and a source of carbon to build new cell material. Otherwise, biodegradation will not occur.

In the case of biodegradation of organic pollutants, the carbon typically comes from the pollutant being degraded. Although a multitude of reactions are used by microbes to degrade and transform pollutants, all energy-yielding reactions are oxidation-reduction reactions. In oxidative attacks, microbes oxidize a contaminant by transferring electrons from the contaminant (termed the electron donor) to an electron acceptor to gain energy.

Typical electron acceptors are oxygen, nitrate, Fe(III), sulfate, and carbon dioxide (Fig. 1.12a).[97]

On this basis, biodegradation of estrogens must be an oxidation process which involves an electron acceptor. The role of the latter is commonly played by oxygen, thus most rapid and complete degradation of the majority of pollutants is carried out under aerobic conditions.[98] However, in many cases, including the application of anaerobic microorganisms and/or poor aeration of the polluted site, an alternative electron acceptor has to be utilized, which may be both inorganic (nitrate, nitrite, sulphate, multivalent metal ions in a higher oxidation state) and/or organic substrates, such as humic substances, or (poly) phenolics.[99]

In reductive attacks, microbes utilize some easily metabolized organic electron donor, such as sugars or short chain fatty acids, and transfer the electrons to the pollutant to gain energy (Fig. 1.12b). This process is only possible with electrophilic pollutants, such as halogenated aliphatics and explosives which contain nitro groups.[97]

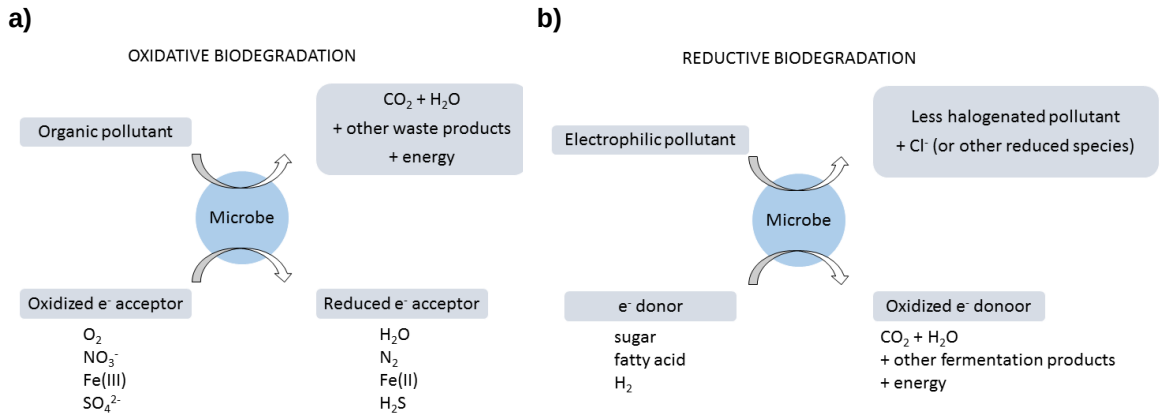

Figure 1.12. General schemes to biodegrade organic pollutants: a) oxidative biodegradation and b) reductive biodegradation.[97]

A number of limiting factors can affect the efficiency of the biodegradation process. The composition and inherent biodegradability of the organic pollutant is the most important consideration when the viability of a remediation approach is evaluated.[100]

Temperature plays an important role in biodegradation of organics, by directly affecting the chemistry of the pollutants as well as affecting the physiology and diversity of the microbial flora. Although biodegradation can occur over a wide range of temperatures, kinetics generally decreases with the decreasing of temperature.[101]

The availability of nutrients, especially nitrogen, phosphorus, and in some cases iron; is also an important factor for the successful bioremediation process. Some of these nutrients can become limiting factors, thus affecting the biodegradation rates. Atlas reported that when a major oil spill occurred in marine and freshwater environments, the supply of carbon was significantly increased and the availability of nitrogen and phosphorus generally became the limiting factor for oil degradation.[102] Excessively high nutrient concentrations can also inhibit the biodegradation activity.[103]

Interest in the biodegradation mechanisms of petroleum hydrocarbons is prompted by their ubiquitous distribution in the environment and their deleterious effects on human health. The essential processes of microbial aerobic degradation of hydrocarbons are shown in Fig. 1.13 and can be described as follows.

- Metabolic processes for optimizing the contact between the microbial cells and the organic pollutants. The chemicals must be accessible to the organisms having biodegrading activities. For example, hydrocarbons are water-insoluble and their degradation often requires the production of biosurfactants.

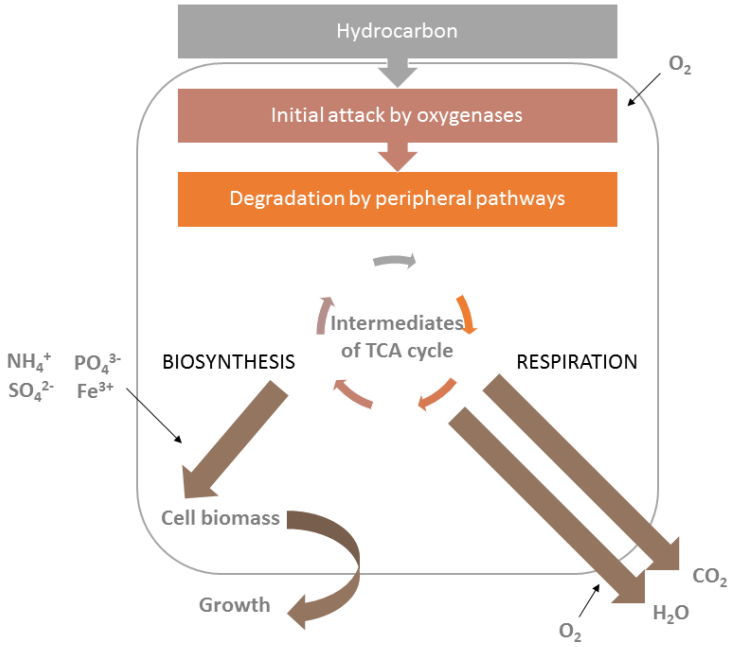

Figure 1.13. Main principle of aerobic degradation of hydrocarbons by microorganisms.

- The initial intracellular attack of hydrocarbons is an oxidative process; therefore, the activation and incorporation of oxygen is an enzymatic key reaction, which is catalysed by oxygenases and peroxidases.

- Peripheral degradation pathways convert these organic pollutants step by step into intermediates of the central intermediary metabolism, such as the tricarboxylic acid cycle.
- Biosynthesis of cell biomass from the central precursor metabolites, such as acetyl-CoA, succinate, pyruvate., and cell respiration.[104]

Microorganisms can degrade organic pollutants using two possible degradation mechanisms: growth-linked (metabolic) and non-growth-linked (cometabolic).[105]

When estrogens are the target molecules for metabolic degradation, microorganisms utilize them as energy and/or carbon source for microbial growth. When a cometabolic transformation reaction is involved, bacteria use their existing enzymes to degrade estrogens. As cometabolic degradation yields no carbon or energy benefits to the degrading microorganisms, a primary growth substrate is needed for sustainable bacterial growth and/or required for inducing the expression of degrading enzymes. A third mechanism for E2 and EE2 transformation, occurring in the presence of selected microorganisms, is abiotic nitration or oxidation.[106]

1.4.2. Estrogen-degrading bacteria

Aerobic estrogen-degrading bacteria have been isolated from various built and natural environments, including activated sludge, compost, soils, sandy aquifers, and the Baltic Sea. These isolates are widespread among different phyla: *Proteobacteria, Actinobacteria, Bacteroidetes*, and *Firmicutes*.[106] Detailed information of some bacteria which can degrade estrogens is listed in Table 1.2.

In 2002, Fujii *et al.* isolated the first 17ß-estradiol-degrading bacterium, a *Novosphingobium* species, from activated sludge.[107] Later in 2004, the biodegradation of natural (E1, E2 and E3) and synthetic (EE2) estrogens using nitrifying activated sludge (NAS) and the ammonia-oxidizing bacteria *Nitrosomonas europaea* was reported. These results indicated that E2 was the most biodegradable estrogen, and was consecutively degraded to other products *via* E1 by using NAS. However, in the presence of an ammonia oxidizing inhibitor, *N. europaea* could only degrade estrogens with no further degradation of their intermediates. This suggested that other microorganisms existed in NAS, which were not ammonia-oxidizing bacteria, and that were responsible for intermediate of estrogens.[26] Another six estrogen-degrading isolates (four *Rhodococcus* strains, an

Achromobacter strain, and a *Ralstonia* strain) from activated sludge were reported by Yoshimoto *et al.*[108] and by Weber *et al*.[109]

Table 1.3. Partial list of estrogen-degrading bacteria.

Bacteria	Classification	Compounds degraded	Origin	Ref.
Novosphingobium ARI-1	α-Proteobacteria Sphingomonadales	E1,E2,EE2	Activated sludge	107
Aminobacter sp. C4	α-Proteobacteria Rhizobiales	E1,E2	Activated sludge	105
Phyllobacterium myrsinacearum	α-Proteobacteria Rhizobiales	E1,E2,E3, EE2	NA	29b
Nitrosomonas europeae NCIMB	β-Proteobacteria	E1,E2,EE2	Activated sludge	26
Ralstonia picketti	β-Proteobacteria Burkholderiales	E1,E2	Activated sludge mixed culture	109
Buttiauxella S19-1	γ-Proteobacteria Enterobacteriales	E2	Sea water	110
Vibrio H5	γ-Proteobacteria Enterobacteriales	E2	Sea water	111
Pseudomonas sp.	γ-Proteobacteria Pseudomonadales	E1,E2,E3, EE2	Activated sludge	29b
Actinetobacter sp.	γ-Proteobacteria Pseudomonadales	E1,E2,E3, EE2	Compost	29b
Steroidobacter denitrificants	γ-Proteobacteria Xanthomonadales	E2	Anoxic digested sludge	112
Rhodococcus rhodochrous DSM	Actinobacteria	E1,E2,E3	NA	113
Nocardia sp. E110	Actinobacteria	E2	NA	114
Sphingobacterium sp. JCR5	Actinobacteria	E1,E2,E3, EE2	Activated sludge	115
Flavobacterium sp.	Bacteroidetes	E2	Activated sludge	105
Bacillus subtilis	Firmicutes	E1,E2	Activated sludge	29a

NA - Data not available

In 2007, Yu *et al.* reported 14 E2-degrading bacteria, which were successfully isolated from a WWTP. Analysis of 16S rRNA gene sequences revealed that they were

phylogenetically affiliated with different genera: *Aminobacter, Brevundimonas, Escherichia, Flavobacterium, Microbacterium, Nocardioides, Rhodococcus*, and *Sphingomonas*. All isolates could convert E2 to E1 within 7 days, but only three strains (*Aminobacter sp.* C4, *Aminobacter aminovorans* and *Sphingomonas sp.* KC8) could degrade also E1. Only *Sphingomonas* strain KC8 could completely degrade E2 and E1 into non-estrogenic compounds.[105] In 2008, Pauwels and co-workers isolated from compost six bacteria which were able to metabolize E1, E2 and E3, and to cometabolize EE2.[29b]

In 2010, Jiang *et al.* isolated five new E2-degrading *Bacillus spp* from activated sludge obtained from a sewage treatment plant located close to a steroid-contraceptives production factory. In this study, all five isolated strains converted E2 to E1 in wastewaters. E1 was degraded by only two strains, whereas it accumulated in cultures of the other three strains.[29a]

1.4.3. Pathways of aerobic biodegradation of estrogens

In recent years, despite the efforts that have been put in understanding the biodegradation pathways of E2, it still remains greatly unclear. The formation of E1 as major metabolite in the biotransformation of E2 in batch tests with activated sludge or pure cultures has been described with different isolated strains. This mechanism is understood as the dehydrogenation of ring D at C-17 (Scheme 1.8).

Initial stages of E1 degradation pathways were first proposed by Coombe *et al*., where incubation of *Nocardia sp*. with E1 resulted in the oxidative fission between C-4 and C-5 in the aromatic ring, leading to the formation of a dicarboxylic acid intermediate. Further degradation pathways were not elucidated, as the organism did not oxidize the proposed intermediates.[114] Later in 2010, Kurisu *et al*. reported that through hydroxylation at the A ring on C-4 position of E1, E1 could be transformed into 4-OH E1, which could be further degraded *via* meta-cleavage (**Scheme 1.8**).[116]

In 2002, Lee and Liu reported another biodegradation pathway of E2 through E1 by sewage bacteria. Here, a previously unreported metabolite, which was identified as a lactone, formed by the further oxidation of E1. However, its role in the biodegradation of E2 remained to be elucidated (Scheme 1.8).[117]

However, E2 is not systematically degraded with E1 as an intermediate metabolite. According to the literature, pathways of initial stages of E2 biodegradation can be classified into the following groups.

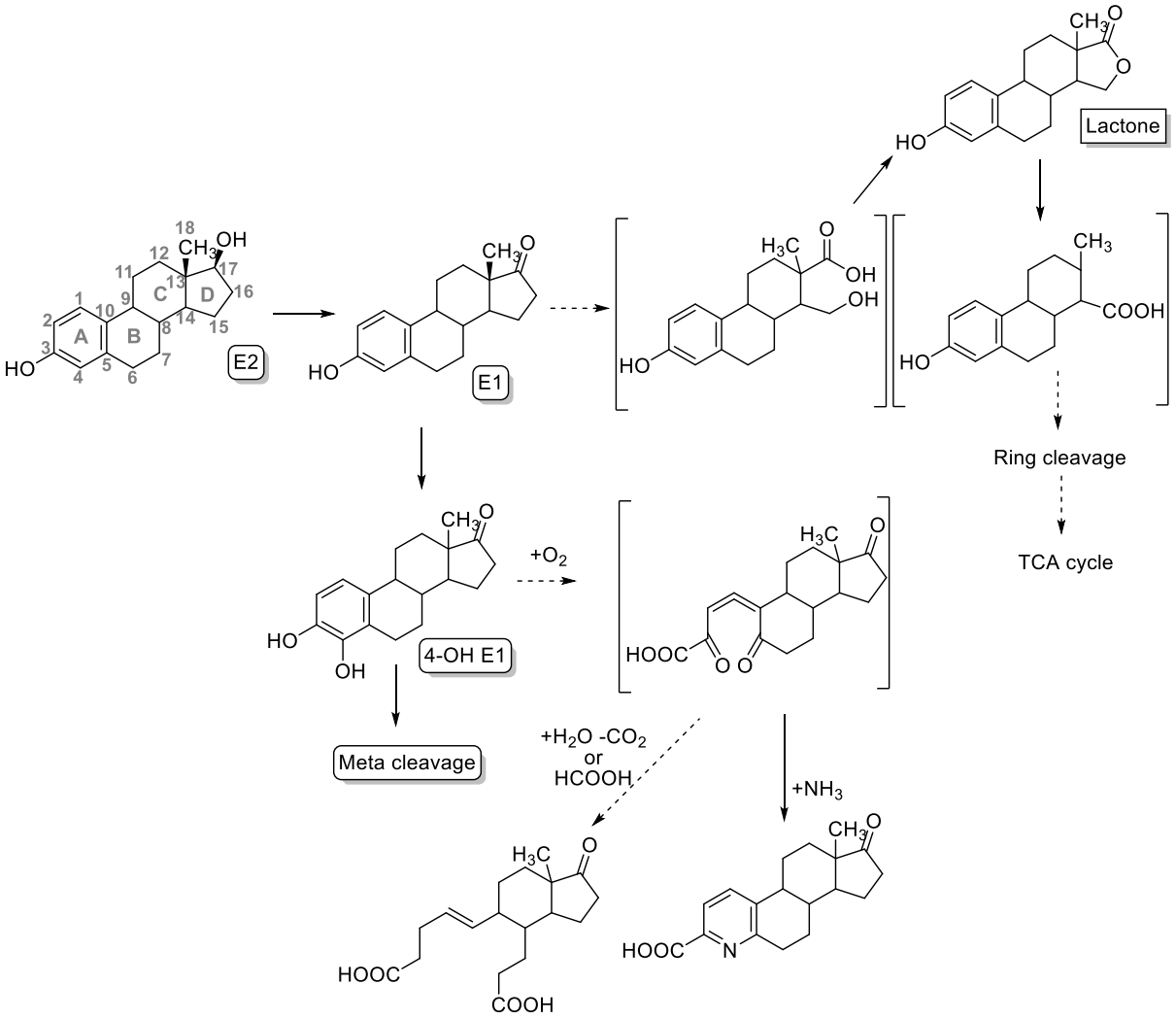

Scheme 1.8

- **Hydroxylation of ring A at C-4** (**Scheme 1.9**). Kurisu *et al.* detected an intermediate metabolite, 4-OH-E2, during E2 degradation by a soil estrogen-utilizing isolate, *Sphingomonas sp.* ED8. In their study, they suggested that 4-OH-E2 was further degraded *via* meta cleavage.[116]

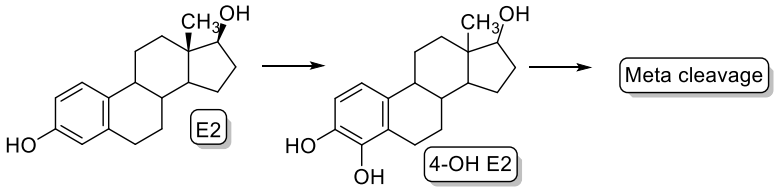

Scheme 1.9

- **Hydroxylation of saturated ring** (**Scheme 1.10**). Kurisu *et al.* also identified a degradation pathway for E2 *via* ring hydroxylation on different positions by the strain *Sphingomonas sp*. ED8, based on the detection of hydroxy-E2, keto-E2, keto-E1, and 3-(4-hydroxyphenyl)-2-hydroxyprop-2-enoic acid.[116]

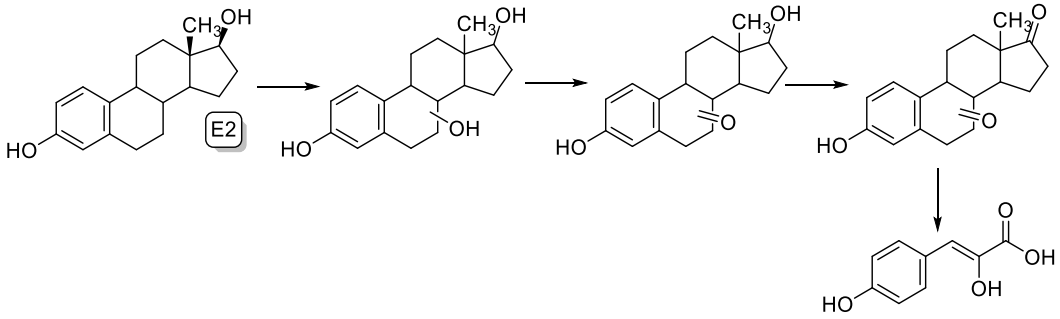

Scheme 1.10

- **Dehydration of ring D at C-17** (**Scheme 1.11**). Nakai *et al.* identified a new intermediate metabolite, estra-1,3 ,5(10),16-tetraen-3-ol (estratetraenol, E0), produced by E0-degrading *Nitrosomonas europaea* .[26]

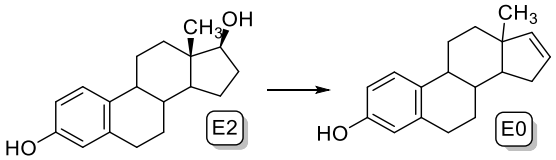

Scheme 1.11

Ternes showed that E1 was quickly degraded in activated sludge from a sewage treatment plant under aerobic conditions, and no other intermediate metabolites were detected.[31] In addition, two other aerobic strains (*Rhodococcus zopfii* and *Novosphingobium spp*.) could use E2 as sole carbon source without E1 accumulation.[113] These evidences suggest the existence of some non-detected metabolic pathways.

1.5. Combined photodegradation and biological processes for water treatment

The main routes for the clearance of toxic compounds from natural waters are biodegradation and photodegradation. Photodegradation is an important mechanism for degrading aromatic hydrocarbons, chlorinated aromatic hydrocarbons, chlorinated phenols, and many pesticides.[118] Biological degradation of a chemical refers to the elimination of the pollutant by the metabolic activity of living organisms, most often bacteria and fungi naturally

occurring in water and soil. In this context, conventional biological processes do not always provide satisfactory results, especially for industrial wastewater treatment, since many of the organic substances produced by the chemical industry are toxic or resistant to biological treatment.[119] Therefore, the only feasible option for such biologically persistent wastewater is the use of AOPs.

AOPs are an efficient approach for the removal of organic pollutants in wastewater effluents. However, operating costs related to energy consumption when applying AOPs is an important drawback. In addition, high photocatalyst concentrations can be required in real water samples which determine significant increases in operating costs. On the other hand, low photocatalyst doses could result in inadequate pre-treatment of wastewaters. Furthermore, chemical oxidation for complete mineralization is generally expensive because the oxidation intermediates formed during treatment tend to be more and more resistant to their complete chemical degradation.[120]

Combination of AOPs with conventional biological systems has been proved not only to be more sustainable, but also to increase biodegradability of pollutants and their complete removal.[121] Zapata *et al.* reported the design of an industrial-scale combined solar photo-Fenton/aerobic biological system for the degradation of pesticides. Results showed an increase in the biodegradability and a reduction of its toxicity.[122]

The assessment of biodegradability variation after the application of AOPs plays a fundamental role, so that specific procedures have been standardized in time. Scientific research should cover the identification of photodegradation intermediates, as well as certain parameters such as five-day biochemical oxygen deman (BOD_5), chemical oxygen demand (COD), BOD_5/COD ratio, or total organic carbon (TOC). In order to assess the technical and economic feasibility of AOPs as treatment of wastewater before its conventional biological processing, removal kinetics of pollutants need to be defined, in order to optimize operating conditions and promote its scale up.[123]

1.6. Layout and objectives of the Ph.D. thesis

Chapter I

The present Chapter I is aimed at presenting a brief overview concerning possible consequences of the presence of organic pollutants in aquatic ecosystems and how to eliminate them *via* biodegradation and photodegradation processes.

Part of this work resulted in the following publication:

Fernández, L., Esteves, V.I., Cunha, Â., Schneider, R.J., Tomé, J.P.C., Photodegradation of organic pollutants in water by immobilized porphyrins and phthalocyanines. *J. Porphyrins Phthalocyanines.* **2016**, *20*, 150-166

Research of this Ph.D. thesis is mainly focused on the removal of E2, as a model of persistent organic pollutant in water, by means of the photodynamic effect or biodegradation routes. The experimental work may be divided into two parts, attending to the nature of the water treatment.

Part I. Porphyrins and phthalocyanines as photosensitizers in water treatment applications (Chapters II and III)

Chapter II

This chapter studies the preparation and evaluation of homogeneous and heterogeneous PS as photocatalysts in E2 degradation. Specific aims include:

- Preparation of photoactive materials based on water-soluble Pors and Pcs covalently anchored onto MNPs, and characterization of their structural and photophysical properties.
- Study of these materials, both non-immobilized and immobilized PS (NP-PS), in the photocatalytic degradation of E2 in water by using batch and flow modes. By using the flow mode system, which usually potentiates the photocatalytic performance, reaction conditions can be optimized by studying different flow rates, load of photocatalyst and pH of the samples. The immobilization of PS allows its recovery after the photo-treatment, so recycling capabilities can be studied.

This work resulted in the following publication:

Fernández, L., Borzecka, W., Lin, Z., Schneider, R.J., Huvaere, K., Esteves, V.I., Cunha, Â, Tomé, J.P.C., Nanomagnet-photosensitizer hybrid materials for the degradation of 17β-estradiol in batch and flow modes. *Dyes Pigm.* **2017**, *142*, 535-543.

Chapter III

This chapter focuses on the disinfection of aqueous samples using photodynamic therapy with hybrid materials composed by Pors and Pc covalently anchored onto MNPs. Specific aims include:

- Cationization of hybrid materials previously prepared in Chapter II (NP-PS) and characterization of the structural and photophysical properties of the new photocatalysts obtained (NP^+-PS). This slight modification of NP-PS allows their use for water disinfection purposes.
- Study of NP^+-PS as photodynamic agents against pathogens in water, using a recombinant bioluminescent *E. coli* strain as a model of Gram-negative bacteria. Study of the recycling of NP^+-PS in further photoinactivation processes.

This work resulted in the following publication:

Fernández, L., Lin, Z., Schneider, R.J., Esteves, V.I., Cunha, Â, Tomé, J.P.C., Antimicrobial photodynamic activity of cationic nanoparticles decorated with glycosylated porphyrins or phthalocyanines for water disinfection. Under preparation

Part II. Degradation of estrogens by bacteria (Chapters IV and V)

Chapter IV

This chapter studies biodegradation processes to eliminate estrogens from aqueous samples, both prepared and collected from a WWTP. Specific aims include:

- Screening of E2-degrading bacterial strains isolated from different sources.
- Optimization of the growth cell and the culture media of those strains with better capabilities to remove E2 from the aqueous samples.
- Biodegradation tests with more realistic conditions found in natural environments or wastewaters by changing the starting concentration of E2 and by preparing samples with different types of estrogens.
- Study of transformation products arising from the biodegradation process using mass spectrometry.

- Biodegradation tests with real water samples collected from a WWTP, after an adequate sample treatment.

This work resulted in the following publications:

Fernández, L., Louvado, A., Esteves, V.I., Gomes, N.C.M., Almeida, A., Cunha, Â, Biodegradation of 17β-estradiol by bacteria isolated from deep sea sediments in aerobic and anaerobic media. *J. Hazard. Mater.*, **2017**, *323*, 359-366.

Fernández, L., Esteves, V.I., Schneider, R.J., Cunha, Â., Aerobic bioremediation of estrogens in wastewaters by the deep-sea isolate *Bacillus licheniformis*. Under preparation

Chapter V

This chapter proposes the combination of photodegradation with a biological process to eliminate E2 from aqueous samples. Specific aims include:

- Evaluation of an efficient photoactive material, previously prepared, towards different organic pollutants in prepared samples and in real water samples collected from a WWTP. Study of its stability under white and UVA light for practical applications.
- Study of transformation products arising from the photodegradation of E2, by mass spectrometry.
- Biodegradation studies of the intermediate products arising from a partial phototreatment process of E2 with the selected photoactive material.

Chapter VI

This chapter is aimed at presenting the conclusions obtained within the frame of this Ph.D. thesis, as well as future perspectives of research work.

CHAPTER 2

NANOMAGNET-PHOTOSENSITIZER HYBRID MATERIALS FOR THE PHOTODEGRADATION OF 17β-ESTRADIOL IN BATCH AND FLOW MODES

Fernández, L., Borzecka, W., Lin, Z., Schneider, R.J., Huvaere, K., Esteves, V.I., Cunha, Â, Tomé, J.P.C., Nanomagnet-photosensitizer hybrid materials for the degradation of 17β-estradiol in batch and flow modes. *Dyes Pigm*. **2017**, 142, 535-543.

Summary

This work carries out the preparation of porphyrins and phthalocyanines, which were then covalently attached onto nanostructured magnetic supports consisting of Fe_3O_4 nanoparticles coated with an amorphous silica shell. To increase the water solubility of the free photosensitizers and, consequently, to improve the stability of the corresponding nanomagnetic hybrids, thio-glucose porphyrin and phthalocyanine derivatives were prepared.

The photocatalytic activity of the non-immobilized photosensitizers and the obtained hybrid materials was evaluated in the photodegradation of 17β-estradiol, as a model of organic pollutant present in waste- and environmental waters, using batch and flow mode treatment systems, assisted by low doses of visible light radiation (4 $mW \cdot cm^{-2}$). The easy recovery of the heterogeneous hybrid materials, just by applying an external magnetic field, allows their reuse in multiple treatment cycles.

Flow mode system potentiates the photocatalytic performance of these novel hybrid materials and is intended to be beneficial for industrial applications.

2.1. Introduction

Assisted-photocatalytic degradation of pollutants in water is a particularly interesting treatment because of its high mineralization efficiency, which minimizes the release of hazardous degradation products,[124] and the possibility of using sunlight as energy source.[36a, 41]

Over the past few years, the scientific community has witnessed a dramatic increase in the number of papers published on applications of magnetite (Fe_3O_4) nanoparticles (MNPs). Magnetite is a common iron oxide that exhibits outstanding physico-chemical properties due to the presence of both Fe(II) and Fe(III) in its structure. It behaves as superparamagnetic as the particle size is reduced to a few nanometres. Nanoscale iron-based catalysts are of considerable current interest because iron is an abundant, eco-friendly, relatively non-toxic, and inexpensive element, and thus, a very welcome alternative to the use of precious metal catalysts. The miniaturization of these catalytic materials to the nanoscale leads to a large surface area to volume ratio and, therefore, to an enhancement in the contact between reactants and catalyst, which may increase the activity dramatically.

The design of efficient processes for photocatalytic degradation of organic pollutants, in terms of photocatalytic materials, energy and time, is needed for a sustainable approach. This can be considered directly related to some of the main advantages of the flow photochemistry, which overcomes certain conventional batch hindrance, such as controlled exposure times, temperature and removal of photodegradation products, while allowing feasible scalability.[125]

This work carries out the preparation of porphyrins and phthalocyanines covalently attached onto a nanostructured magnetic support consisting of MNPs coated with an amorphous silica shell. The easy recovery of these heterogeneous photocatalysts, just by applying an external magnetic field, allows their potential reuse in multiple treatment cycles. The photocatalytic activity of non-immobilized photosensitizer (PS) and the obtained hybrid materials was evaluated in the degradation of 17β-estradiol, as a model of organic pollutant present in water, using both batch and flow mode treatment systems, assisted by visible light radiation (4 $mW \cdot cm^{-2}$). By using the flow mode system, which potentiates the photocatalytic capacity of these novel hybrid materials, further studies based on different photocatalyst concentrations and pH conditions were performed. Reuse capacity of these materials was investigated upon three photocatalytic cycles.

2.2. Results and discussion

Synthesis and characterization of non-immobilized PSs based on fluorophenyl-Pors and perfluoro-Pcs were selected because their peripheral fluorine atoms allow easy substitutions with a large variety of nucleophiles.[49, 126] As a result, PS derivatives with suitable physical, electronic and optical properties can be easily prepared. For water treatment applications, PSs are required to be stable in aqueous media, since it is known that aggregation of the PS decreases the efficiency of $^1O_2$ generation.[127] Due to the high hydrophobic nature of Pors and Pcs, hydrophilic substituents need to be introduced. A suitable derivatization is easily afforded with sugar moieties as hydrophilic substituents.[128] The non-hydrolysable 1-thio-β-D-glucose was selected as water-solubilizing agent of PSs based on **$TPPF_{20}$** and **$ZnPcF_{16}$**.

2.2.1. Synthesis and characterization of non-immobilized porphyrin and phthalocyanine based PSs

Initially, 5,10,15,20-tetrakis(pentafluorophenyl)porphyrin (**$TPPF_{20}$**) was prepared using modified Rothemund conditions,[129] according to Gonçalves *et al.* methodology,[130] by the equimolar condensation of pyrrole with pentafluorobenzaldehyde in a mixture of acetic acid and nitrobenzene, under refluxing conditions (Scheme 2.1). After 2 hours of reaction, **$TPPF_{20}$** was obtained after removal of the solvents and purification of the crude residue by silica gel chromatography.

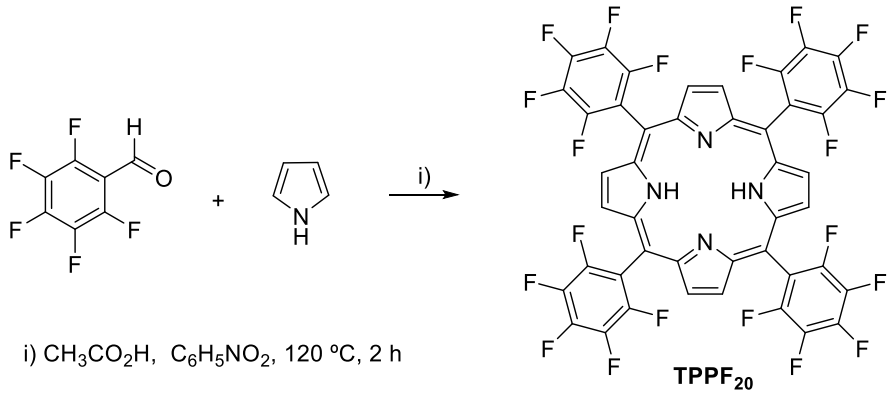

Scheme 2.1

^{1}H and ^{19}F NMR spectra of **TPPF$_{20}$** in $CDCl_3$ agreed with those reported in the literature. The proton resonances of the inner -NH appear at *δ* -2.92 ppm (characteristic of free base porphyrins) and the signal due to the β-protons at *δ* 8.92 ppm (data not shown). The ^{19}F NMR spectrum of **TPPF$_{20}$** shows three signals corresponding to the resonances of *meta*-, *para*-, and *ortho*- fluorine atoms, respectively at *δ* -184.49–-184.41, -174.33, and -159.69–-159.58 ppm, as a triplet of doublets, triplet and doublet of doublets (Fig. 2.1). The mass spectrum presented one pick, m/z 975, corresponding to the molecular ion $(M+H)^+$ of **TPPF$_{20}$** (data not shown).

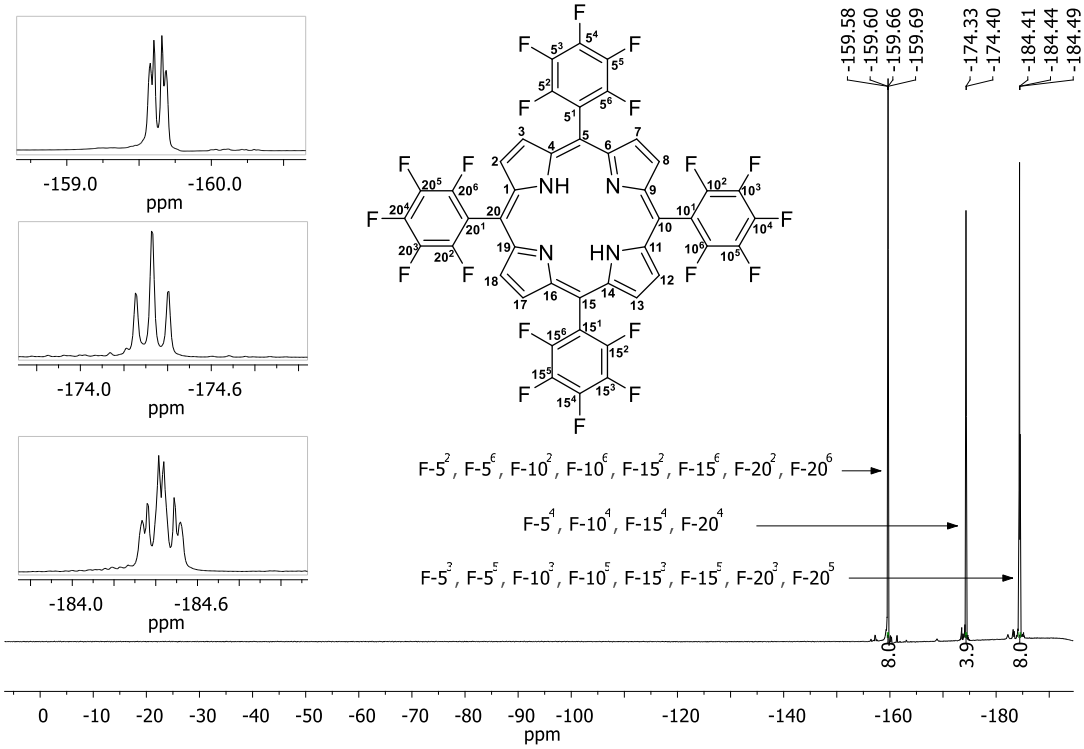

Figure 2.1. ^{19}F NMR spectrum of **TPPF$_{20}$** in $CDCl_3$.

Synthesis of the sugar derivative 2,3,4,6-tetra-*O*-acetyl-glucosylthioacetate (**GlcAcSAc**) was performed by mixing 2,3,4,6-tetra-*O*-acetyl-glucosylbromide with potassium thioacetate in acetone overnight at room temperature (Scheme 2.2).[131]

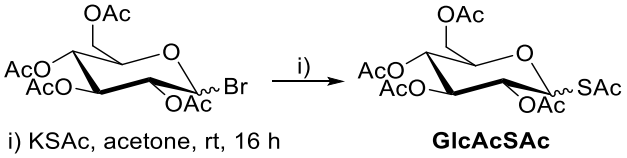

Scheme 2.2

GlcAcSAc was afforded after removal of the solvent and purification over a silica gel chromatography column). ^{1}H NMR spectrum of **GlcAcSAc** is in agreement with

previously reported data in the literature (Fig. 2.2).[132] It shows similar chemical shifts for the protons of the four acetoxy groups, in the range of 2.01 and 2.09 ppm, as singlets. The chemical shift of the protons of the thioacetate group appears farther downfield, at δ 2.39 ppm, due to the deshielding effect of the sulphur atom. Similarly, the proton of the anomeric carbon can be recognized from its chemical shift as a multiplet at δ 5.31-5.26 ppm. Due to the mobility of the two protons of C-6 and the coupling with their only vicinal proton, the resonance signal results in two doublet of doublets at δ 4.27 and 4.16 ppm, and the proton of C-5 appears at δ 3.84 ppm as a doublet of doublet of doublets. The ESI-MS spectrum of **GlcAcSAc** confirmed also the success of the thioacetate insertion by showing the peak corresponding to the molecular ion $(M+Na)^+$ at *m/z* 429.1 (data not shown).

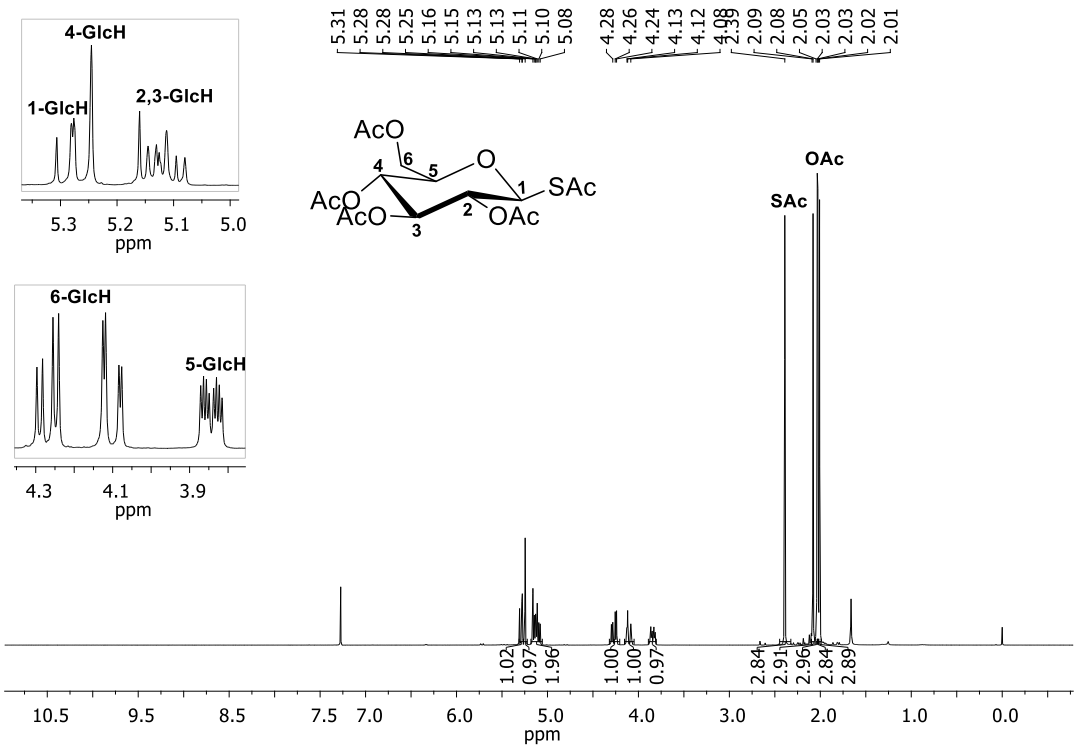

Figure 2.2. ^{1}H NMR spectrum of **GlcAcSAc** in $CDCl_3$.

According to the optimized procedure developed by Drain *et al.* to synthesize thioglycosylated porphyrins from **$TPPF_{20}$**, the non-hydrolysable thioglycosylated porphyrin 5,10,15,20-tetrakis[4-(2,3,4,6-tetra-*O*-acetyl-β-D-glucopyranosylthio)-2,3,5,6-tetrafluorophenyl)]porphyrin (**$TPPF_{16}(SGlcAc)_4$**) was prepared by the nucleophilic substitution of the *para* fluorine atoms of **$TPPF_{20}$** with **GlcAcSAc** in dimethylformamide (DMF) in the presence of diethylamine (DEA), at room temperature.[133] Then, **$TPPF_{16}(SGlcAc)_4$** was precipitated by the addition of water and methanol to the mixture.

After removal of the solvent and purification of the crude by silica chromatography, **$TPPF_{16}(SGlcAc)_4$** was afforded (Scheme 2.3).

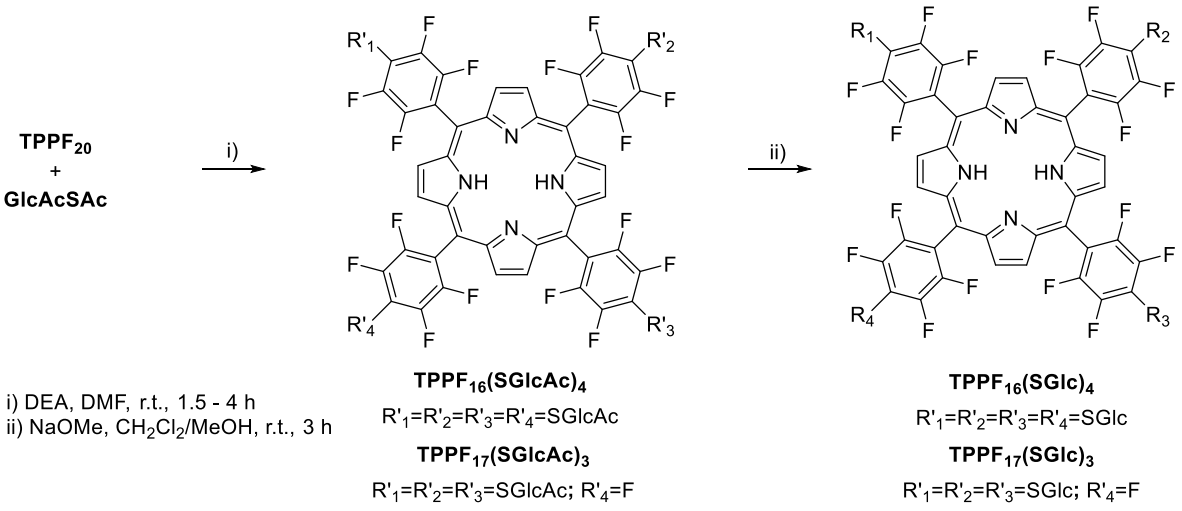

Scheme 2.3

^{1}H spectrum of **$TPPF_{16}(SGlc)_4$** in DMSO-d_6 (deuterated dimethyl sulfoxide) is governed by the symmetry properties of the molecule and by the orientation of *meso* substituents, thus showing only one set of glucopyranosyl peaks owing to the C4 symmetry (Fig. 2.3).

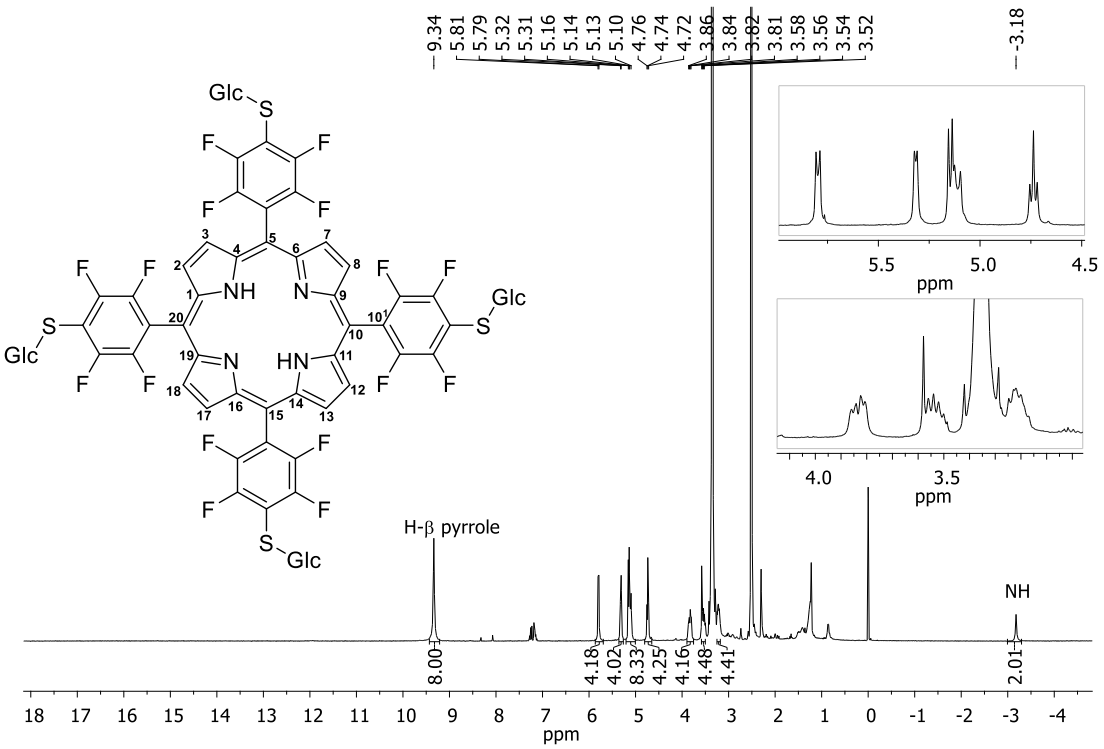

Figure 2.3. ^{1}H NMR spectrum of **$TPPF_{16}(SGlc)_4$** in DMSO-d_6.

The removal of acetyl groups from **TPPF$_{16}$(SGlcAc)$_4$** to **TPPF$_{16}$(SGlc)$_4$** could be confirmed by means of the ^{1}H NMR spectra analysis, since characteristic peaks at δ 2.3–2.0 ppm due to CH_3 disappeared in the spectrum of the final compound. ^{19}F NMR spectra of **TPPF$_{16}$(SGlc)$_4$** showed two peaks with equal intensities and patterns, indicating *para* substitution in the tetrafluorophenyl groups (Fig. 2.4). ESI-Q-TOF-MS spectrum of **TPPF$_{16}$(SGlc)$_4$** showed a peak at *m/z* 1679.6, corresponding to the molecular ion $(M+H)^+$ (data not shown).

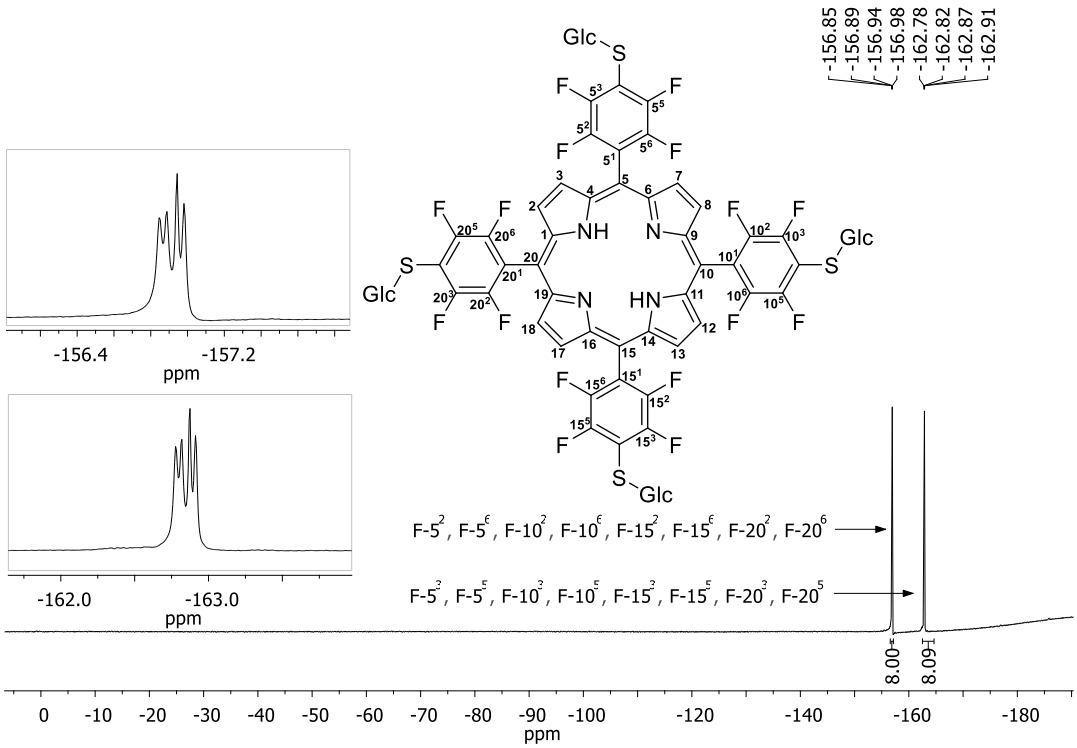

Figure 2.4. ^{19}F NMR spectrum of **TPPF$_{16}$(SGlc)$_4$** in DMSO-*d$_6$*.

The degree of S-glycosylation of **TPPF$_{20}$** could be controlled by the ratio of **GlcAcSAc** to **TPPF$_{20}$** in the feed, thus the novel 5,10,15-tris[4-(2,3,4,6-tetra-*O*-acetyl-β–D-glucopyranosylthio)-2,3,5,6-tetrafluorophenyl)]-20-(2,3,4,5,6-pentafluorophenyl)porphyrin (**TPPF$_{17}$(SGlcAc)$_3$**) was obtained in a similar procedure. To obtain a degree of S-glycosylation of 3, a synthetic procedure with 3.1 equivalents of GlcAcSAc was used, and a distribution of products with varying degrees of substitution was obtained. **TPPF$_{17}$(SGlcAc)$_3$** was purified using flash column chromatography.

The peak area ratios between the two β-pyrrole signals (9.02 and 8.94 ppm) and the sugar moieties in the ^{1}H NMR spectra of **TPPF$_{17}$(SGlcAc)$_3$** coincide well with the expected grade of thioglycosylation in the porphyrin (Fig. 2.5). ^{19}F NMR spectra of **TPPF$_{17}$(SGlcAc)$_3$** (data non-shown) confirmed the asymmetry of the molecule by showing a set of 5 peaks

corresponding to *ortho* and *meta* fluorine atoms of the three *para* glycosylated fluorophenyl groups, with an integration of 6 fluorine atoms each; and *ortho*, *meta* and *para* fluorine atoms of the pentafluorophenyl group, similar to the ^{19}F NMR spectrum of **$TPPF_{20}$**.

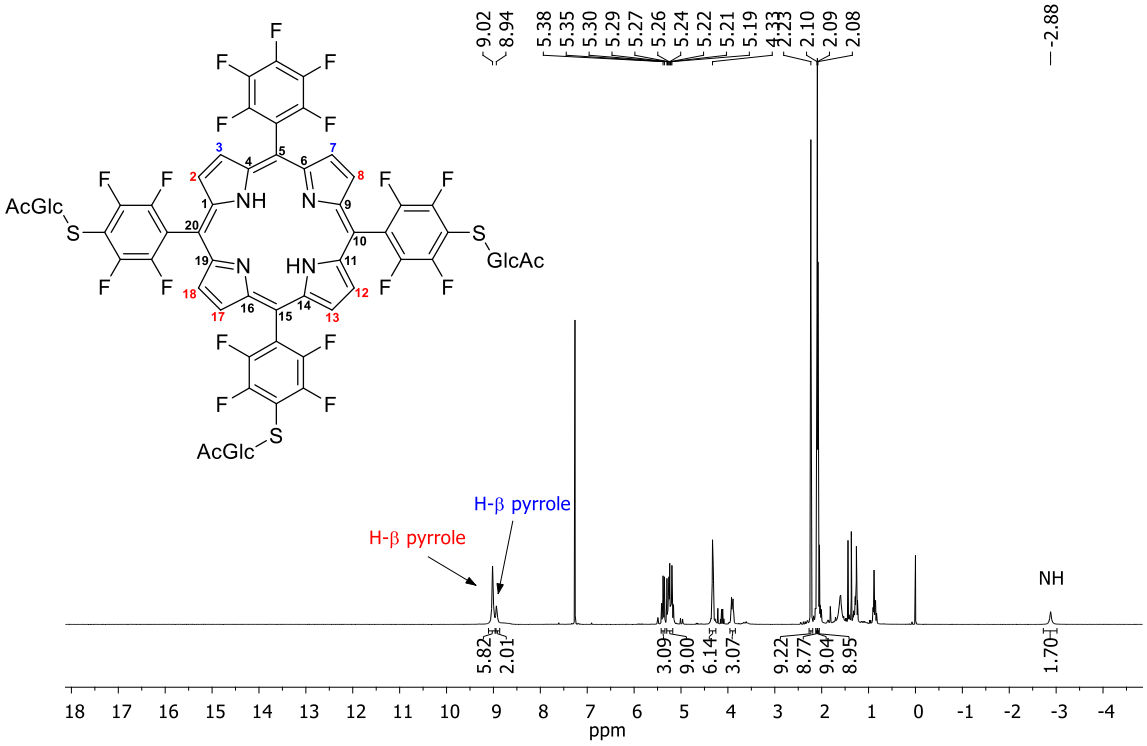

Figure 2.5. ^{1}H NMR spectrum of **$TPPF_{17}(SGlcAc)_3$** in $CDCl_3$.

ESI-Q-TOF-HRMS spectrum of **$TPPF_{17}(SGlcAc)_3$** showed two peaks at *m/z* 2007.2867 and 1004.8048, corresponding to the single and double charged molecular ions $(M+H)^+$ and $(M+2H)^{2+}$(Fig. 2.6).

Figure 2.6. ESI-QTOF-HRMS spectrum of **$TPPF_{17}(SGlcAc)_3$**, with *m/z*: 2007.2867 Da $(M+H)^+$ and 1004.8048 Da $(M+2H)^{2+}$.

ESI-Q-TOF-HRMS spectrum of **TPPF$_{17}$(SGlc)$_3$** confirmed showed one peak corresponding to the molecular ion $(M+H)^+$ at *m/z* 1503.1650 (Fig. 2.7).

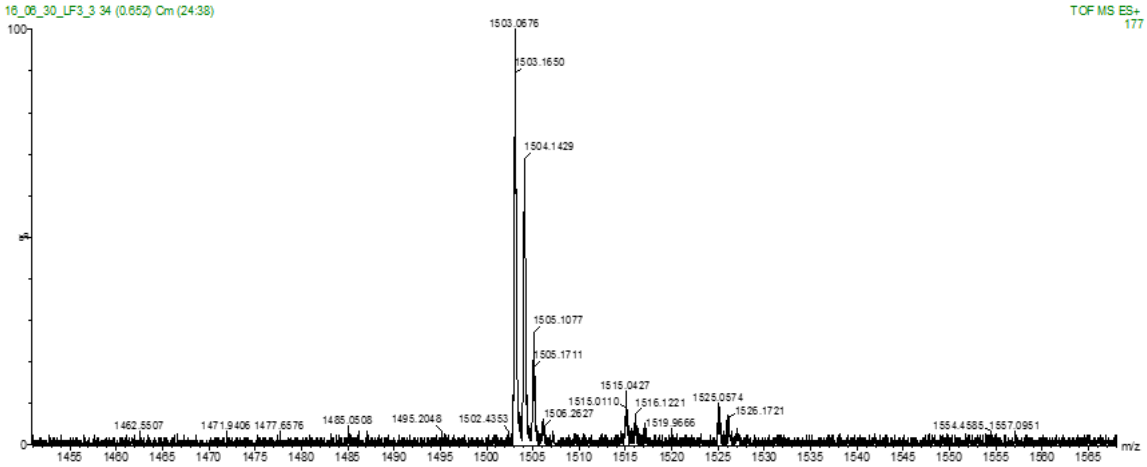

Figure 2.7. ESI-QTOF-HRMS spectrum of **TPPF$_{17}$(SGlc)$_3$**, with *m/z*: 1503.1650 Da $(M+H)^+$.

Deprotection of **TPPF$_{17}$(SGlcAc)$_3$** to obtain **TPPF$_{17}$(SGlc)$_3$** could be confirmed again by ^{1}H NMR (Fig.2.8) spectrum analysis, with the disappearance of the typical proton peaks due to acetyl groups, and ^{19}F NMR spectrum of **TPPF$_{17}$(SGlc)$_3$** (Fig. 2.9) showed again the asymmetry of the molecule.

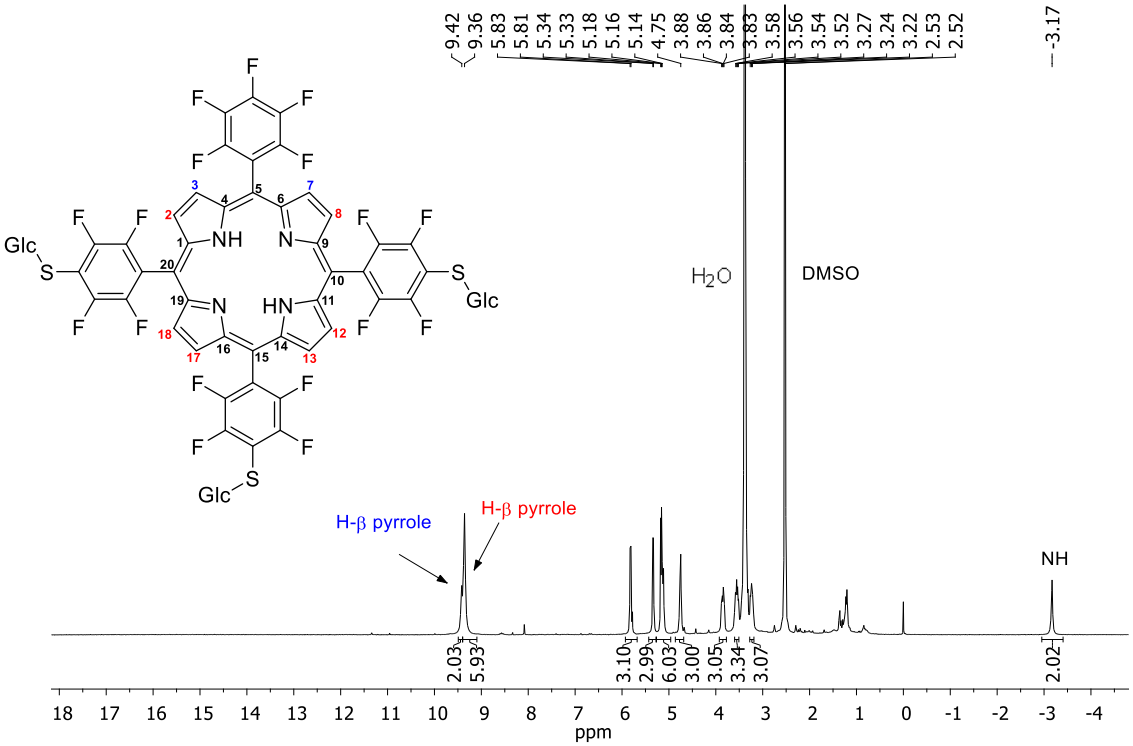

Figure 2.8. ^{1}H NMR spectrum of **TPPF$_{17}$(SGlc)$_3$** in DMSO-d_6.

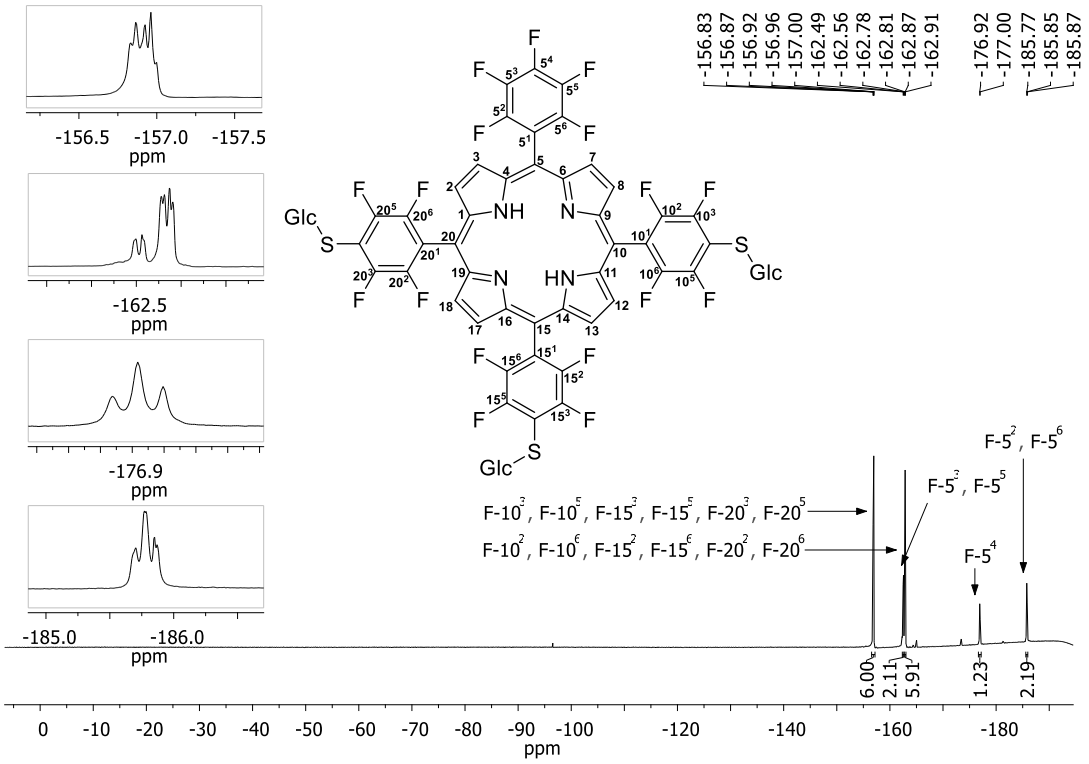

Figure 2.9. ^{19}F NMR spectrum of **$TPPF_{17}(SGlc)_3$** in DMSO-d_6.

Octathioglycosylated zinc(II) phthalocyanine (**$ZnPcF_8(SGlc)_8$**)* was prepared according to the procedure of A. Aggarwal *et al* (Scheme 2.4).[86] This compound was kindly provided by Wioleta Borzęcka.

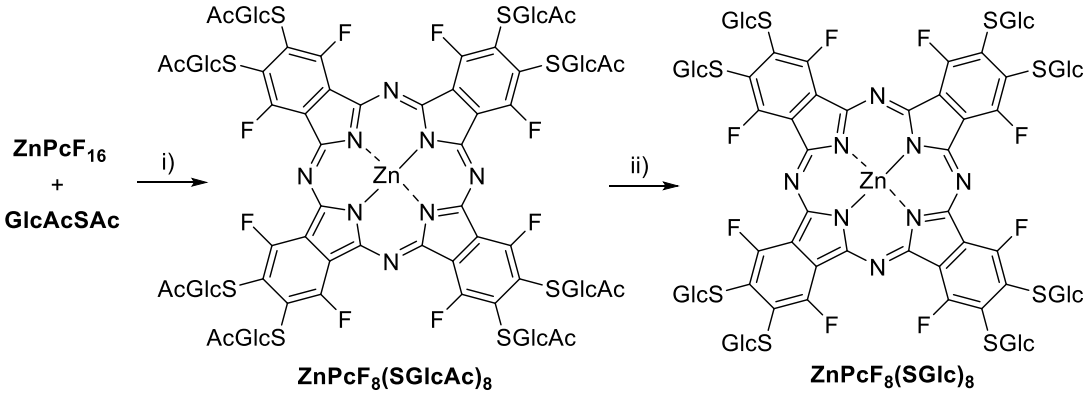

i) DEA, DMF, rt, 24 h; ii) NaOMe, CH_2Cl_2/MeOH, rt, 24 h

Scheme 2.4

Commercially available **$ZnPcF_{16}$** was treated in dry DMF under nitrogen atmosphere with 8.5 equiv. of **GlcAcSAc** in the presence of DEA as a base, at room temperature. After removal of the solvent, the crude was submitted to a silica gel column, thus affording

ZnPc(SGlcAc)$_8$. Deprotection of the sugars was accomplished using sodium methoxide in a slight excess relative to the equivalents of acetate moieties, in a mixture of dichloromethane and methanol as solvent, at room temperature. **ZnPcF$_8$(SGlc)$_8$** was afforded after purification of the crude in reverse phase chromatography.

^{1}H NMR of **ZnPcF$_8$(SGlc)$_8$** in DMSO-d_6 confirmed the deprotection of the carbohydrate units (data non-shown). The ^{19}F NMR of **ZnPcF$_8$(SGlc)$_8$** showed a singlet around -107.7 ppm and the disappearance of the peak at around -85 ppm of **ZnPcF$_{16}$**, indicating that the β-F atoms were substituted by the thioglucose (data non-shown).

2.2.2. Photophysical properties of non-immobilized porphyrin and phthalocyanine based PSs

Pors and Pcs are well-known optical absorbers, with high chemical stability and tailorability, and possess unequivocally strong absorption bands in the UV-Vis region.[134] Non-immobilized Pors **TPPF$_{20}$**, **TPPF$_{16}$(SGlc)$_4$** and **TPPF$_{17}$(SGlc)$_3$**, showed phyllo-type UV–Vis spectra (IV > II > III > I), with absorption maximum at *ca.* 415 nm in the Soret region and four maxima in the Q region (from 506 to 636 nm) in DMSO solutions. Absorption spectra of **ZnPcF$_{16}$** and **ZnPcF$_8$(SGlc)$_8$** showed a clearly differentiated Soret band in the range of *ca.* 320-440 nm, and Q-bands with maxima in the red region of the visible range at 643 and 746 nm respectively. Glycosylated conjugation of **ZnPcF$_{16}$** showed to strengthen its absorption at longer wavelengths and increase its solubility in DMSO (Fig. 2.10).

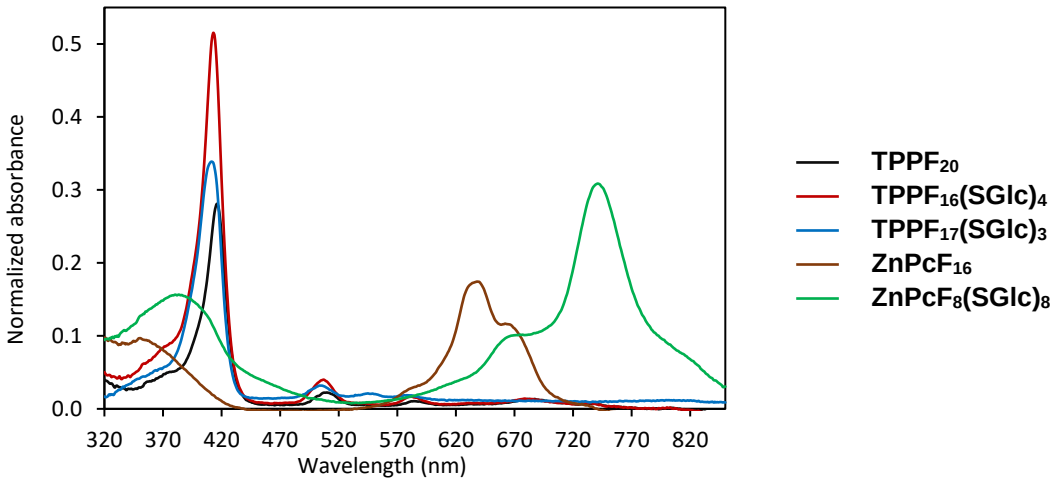

Figure 2.10. UV-Vis absorption spectra of DMSO solutions containing **TPPF$_{20}$**, **TPPF$_{16}$(SGlc)$_4$**, **TPPF$_{17}$(SGlc)$_3$**, **ZnPcF$_{16}$** or **ZnPcF$_8$(SGlc)$_8$** at 2.0 µM.

To evaluate the effect on the glycosylation degree of the unprotected Pors and Pcs in aqueous media, stock solutions of the non-immobilized PSs in H_2O MilliQ containing 1 vol % dimethyl sulfoxide (DMSO) at different concentrations (0.5, 1.0, 2.0, 3.0 and 4.0 μM) were prepared. Since these PSs were initially dissolved in a stock solution in DMSO and then were dispersed in water, herein the term water-stability is preferred to be used instead of water-solubility.

As anticipated, introduction of thioglucose units on the macrocyclic perimeter of **$TPPF_{20}$** increased its stability in water (Fig. 2.11). Maximum intensities of absorption indicate that **$TPPF_{16}(SGlc)_4$** is slightly more water stable than **$TPPF_{17}(SGlc)_3$**. For **$TPPF_{16}(SGlc)_4$** aqueous solutions, the shape of the absorption spectra remained constant upon increasing the concentration, suggesting that any aggregation across this range of concentrations is at most very slight. However, porphyrin **$TPPF_{17}(SGlc)_3$** showed one shoulder in each side next to the Soret maximum when concentration is increased, suggesting the aggregation of the compound is produced under these conditions. UV-Vis spectra of **$TPPF_{20}$**, **$TPPF_{16}(SGlc)_4$** and **$TPPF_{17}(SGlc)_3$** showed slight shifts toward longer wavelengths in comparison with those recorded in DMSO, with Soret band maxima centred at 424, 417 and 416 respectively.

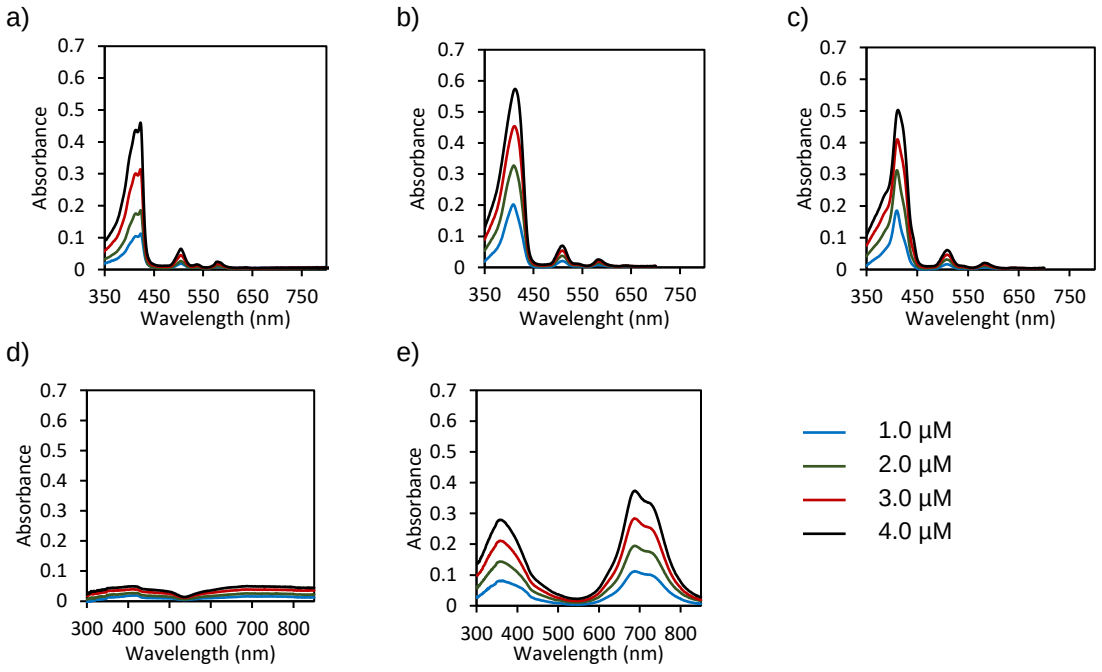

Figure 2.11. UV-Vis absorption spectra of water solutions with 1 vol % DMSO containing different concentrations of (a) **$TPPF_{20}$**; (b) **$TPPF_{16}(SGlc)_4$**; (c) **$TPPF_{17}(SGlc)_3$**; (d) **$ZnPcF_{16}$;** (e) **$ZnPcF_8(SGlc)_8$**.

Stock solutions of **$ZnPcF_{16}$** were not able to be homogeneously dispersed in water, while its glycosylated derivative, **$ZnPcF_8(SGlc)_8$**, presented stability in aqueous solution, with Q and Soret bands shifted to the blue, comparing to those previously reported in DMSO (Fig. 2.11).

Photostability studies were conducted by exposing aqueous solutions of a non-immobilized PS at 2 µM, under white light irradiation (4 $mW \cdot cm^{-2}$), at room temperature, with vigorous magnetic stirring, for 180 min. At fixed intervals of time, visible absorption spectra of the samples were recorded. The intensity of the Soret and Q bands of the non-immobilized PSs showed that all the samples were stable under these irradiation conditions upon 3 h of irradiation.

2.2.3. Synthesis and characterization of immobilized porphyrins and phthalocyanines (NP-PS)

PSs were immobilized onto a magnetic nanostructured support, constituted by Fe_3O_4 NPs coated with an amorphous silica shell (which were gently provided by Dr. Zhi Lin), by nucleophilic substitution of the fluorine atoms with the amine groups of the NPs in DMSO at 160 °C (Scheme 2.5).

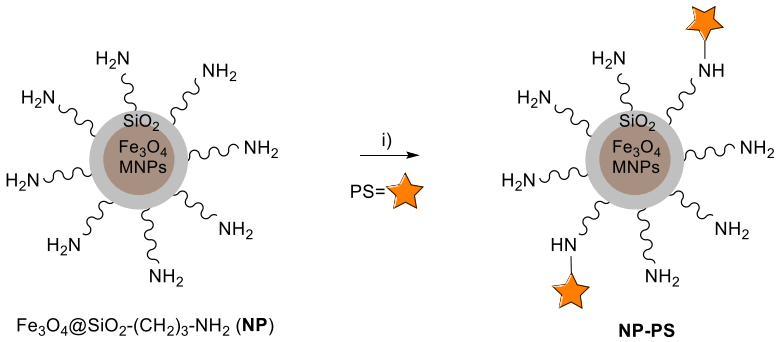

Por-based PS		ZnPc-based PS	
PS	NP-PS	PS	NP-PS
$TPPF_{20}$	NP-$TPPF_{20}$	$ZnPcF_{16}$	NP-$ZnPcF_{16}$
$TPPF_{16}(SGlc)_4$	NP-$TPPF_{16}(SGlc)_4$	$ZnPcF_8(SGlc)_8$	NP-$ZnPcF_8(SGlc)_8$
$TPPF_{17}(SGlc)_3$	NP-$TPPF_{17}(SGlc)_3$		

Scheme 2.5

After 24 – 96 h of reaction, red (**NP-TPPF$_{20}$**, **NP-TPPF$_{16}$(SGlc)$_4$**, **NP-TPPF$_{17}$(SGlc)$_3$**), dark blue (**NP-ZnPcF$_{16}$**) or green (**NP-ZnPcF$_8$(SGlc)$_8$**) insoluble products were obtained. The immobilization of the PSs was monitored by TLC until each reaction mixture showed that all or most of the starting PS had been converted into a new coloured material that remained in the baseline of the TLC. The resulting hybrid materials were washed several times with an appropriate washing solvent (Table 2.1) until no Soret and Q bands belonging to the unreacted PSs were observed by UV-Vis spectroscopy in the rinse solvent. The total amount of reacted PS was calculated by subtracting the unreacted PS, determined by absorption measurements in the rinse solvent. Final materials presented a relative amount of PS between 5 and 14% (w/w). The content of PS in the final hybrid material varied according to each preparation.

Table 2.1. Detailed experimental data of the preparation of NP-PSs, by introduction of Pors or Pcs on **Fe$_3$O$_4$@SiO$_2$-PrNH$_2$** NPs.

Photocatalyst	Reaction time (h)	Rinse solvent	% of reacted PS	% PS in NP-PSs (w/w)	μmol PS/g NPs
NP-TPPF$_{20}$	24	Chloroform	93.4	13.8	164.5
NP-TPPF$_{16}$(SGlc)$_4$	96	Ethanol	78.1	8.8	57.4
NP-TPPF$_{17}$(SGlc)$_3$	24	Ethanol	90.5	9.2	67.5
NP-ZnPcF$_{16}$	24	DMSO	92.3	5.5	66.9
NP-ZnPcF$_8$(SGlc)$_8$	96	Ethanol	71.7	10.7	52.5

As it was expectable, a lower efficiency in the attachment of **TPPF$_{16}$(SGlc)$_4$** and **ZnPcF$_8$(SGlc)$_8$** onto the NPs was obtained, since the *meta* and *ortho* fluorine atoms of **TPPF$_{16}$(SGlc)$_4$** and *alpha* fluorine atoms of **ZnPcF$_8$(SGlc)$_8$**, are not so reactive towards nucleophilic substitution with the amino groups of the NPs compared to the *para* ones in **TPPF$_{17}$(SGlc)$_3$** and **TPPF$_{20}$** or the *beta* in **ZnPcF$_{16}$**, respectively.

Powder XRD pattern of NP-PSs confirmed the preservation of the starting NPs in the photocatalysts, being magnetite (Fe_3O_4) the main crystal phase present. The hump between 2θ 16° and 27° results from the amorphous SiO_2 shell, while peaks centred at 2θ 30.3, 35.5, 43.3 and 57.2° belong to the core of magnetite (Fig. 2.12). The peaks due to the presence of the PSs do not appear in powder XRD pattern of the hybrid materials, maybe because the relative amount of PS is low or because the molecules are well separated on the NP surface. Fe_3O_4 diffraction peaks of NP-PSs present a decrease in the intensity of the hump of SiO_2, maybe due to some loss of the coating during the treatment at high

temperature. The very weak peaks centred at around 2θ 18 and 53.5° in the spectra of NP-PSs also belong to magnetite.

The crystallite size may be estimated *via* the full-width at half-maximum of the strongest XRD reflection, using the well-known Scherrer formula: $\tau = \frac{K\lambda}{\beta\theta}$, where τ is the mean size of the ordered (crystalline) domains, which may be smaller or equal to the grain size; K is a dimensionless shape factor, with a value close to unity; λ is the X-ray wavelength; β is the line broadening at half the maximum intensity, after subtracting the instrumental line broadening, in radians; θ is the Bragg angle (in degrees).[135]

Considering the peak centred at 35.56°, the crystallite size of magnetite is estimated to be *ca.* 18 nm. This result agreed with the diameter of the hybrid materials observed in transmission electron microscopy (TEM) images, which showed average diameters around 15 nm (Fig. 2.13).

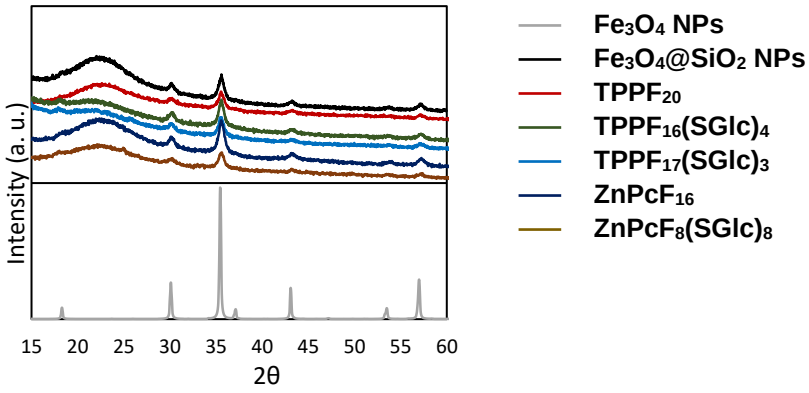

Figure 2.12. XRD powder patterns of Fe_3O_4 NPs, Fe_3O_4@SiO_2 NPs and hybrid materials. The XRD pattern of magnetite is calculated from crystallographic data. Patterns show that magnetite is the main crystal phase.

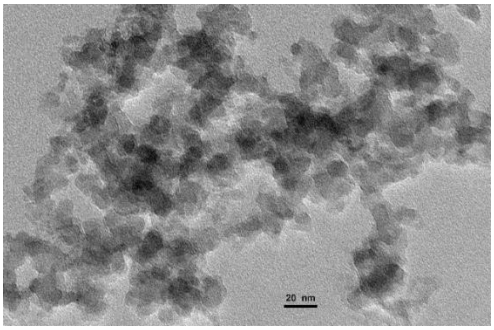

Figure 2.13. Typical TEM image of the prepared hybrid materials showing that the particle size is *ca.* 15 nm.

2.2.4. Photophysical properties of NP-PS

The UV-Vis absorption spectra of the hybrid materials at 2 μM dispersed in H_2O Milli-Q were recorded. Note that concentration of NP-PS always refers to the PS concentration in the hybrid material. **NP-TPPF$_{20}$**, **NP-TPPF$_{16}$(SGlc)$_4$** and **NP-TPPF$_{17}$(SGlc)$_3$** showed the characteristic Soret bands of the porphyrin derivatives, with band maxima centred at *ca.* 415 nm, which indicated the success of the immobilization process and the preservation of the structural features of the PSs. In case of **NP-TPPF$_{20}$** and **NP-TPPF$_{17}$(SGlc)$_3$**, both IV and II Q bands appear clearly differentiated in the spectra, most probably due to a higher relative distribution of the Por in the hybrid material. **NP-ZnPcF$_{16}$** and **NP-ZnPcF$_8$(SGlc)$_8$** showed the typical shape of a Pc absorption spectrum, with Q bands in the range of 550 and 800 nm with higher intensity in case of **NP-ZnPcF$_{16}$**. After drying the samples in the oven, UV-Vis absorption spectra of solids were recorded, which provided again evidence of the successful attachment of the Pors and ZnPcs to the nanostructured support, with maxima in typical regions where the PSs present their typical absorption bands. Solid and liquid UV-Vis absorption spectra of unmodified NPs did not show overlap in the absorption region of Pors and Pcs.

Photostability studies were conducted by exposing aqueous solutions of NP-PS at 2 μM, under white light irradiation (4 mW·cm^{-2}), at room temperature, with vigorous magnetic stirring, for 180 min. At fixed intervals of time, visible absorption spectra of the samples were recorded. NP-PSs showed a decrease in intensity of their absorption bands upon irradiation (Fig. 2.14). However, absorption spectra of control samples kept in dark conditions showed the same behaviour, revealing that this decrease was due to aggregation of the aqueous suspensions. These results showed the need of an appropriate dispersion of the NP-PSs in water in the photocatalytic studies.

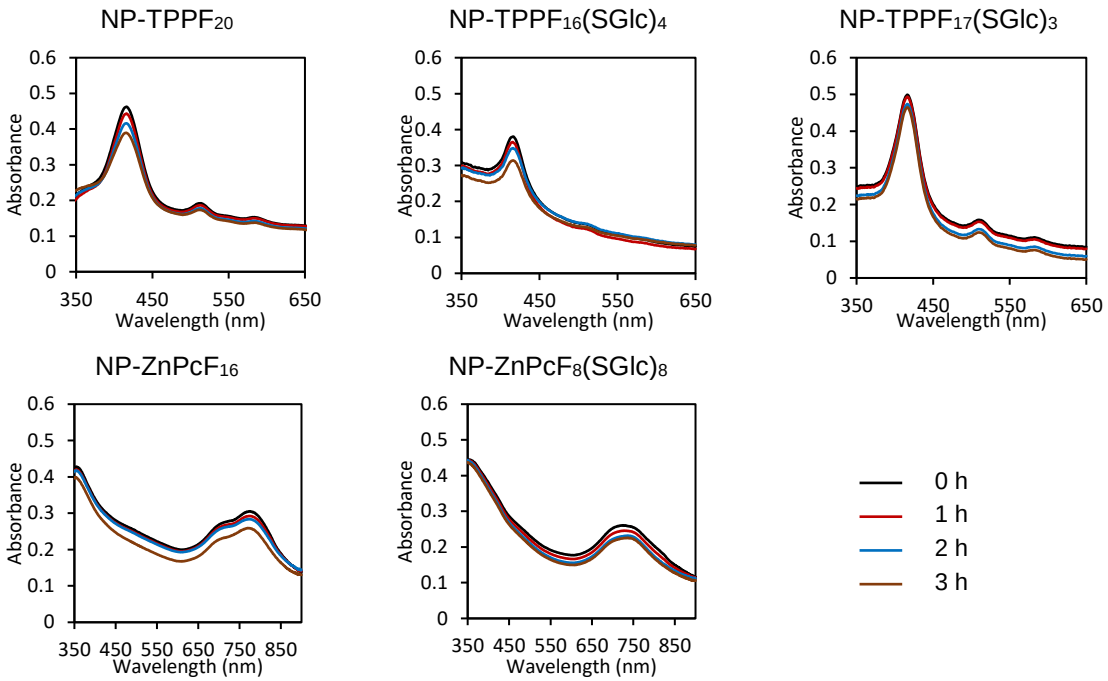

Figure 2.14. UV-Vis absorption spectra of aqueous suspensions containing NP-PS at 2 µM upon different times of artificial white light irradiation.

2.2.5. pH stability studies of PS and NP-PS

The stability of the PSs at different pH conditions was evaluated in aqueous solutions of the non-immobilized PSs at 2 µM, or aqueous suspensions of NP-PSs at 2 µM, by adjusting pH (unmodified samples presented pH 6) with HCl 10% vol. to pH 3, 4 and 5, with saturated $NaHCO_3$ to pH 7 and 8, or with NaOH 10 M to pH 9 and 10. Samples were kept under agitation, at room temperature, for 24 h. UV-vis absorption spectra of samples containing non-immobilized PSs were recorded at time 0 and 24 h. To evaluate a possible cleavage of the Pors and/or Pcs from the NP-PSs after 24 h, samples were filtered with polyvinylidene fluoride (PVDF) syringe filters with a 0.22 µm pore size, and the UV-vis absorption spectra of each filtrate was recorded. In addition, DLS measurements of NP-PSs suspensions in water at different pH were recorded.

Between pH 4 and 10, samples containing a non-immobilized PS at 2 µM showed stability, thus not observing significant changes in the absorption spectra after 24 h compared to those at starting conditions. At pH 3, absorption spectra of the samples containing **$TPPF_{16}(SGlc)_4$**, **$TPPF_{17}(SGlc)_3$** and **$ZnPcF_8(SGlc)_8$** showed changes attending to the shape of the spectra, with broad absorption curves (Fig. 2.15). Additionally, the

sample containing **$TPPF_{20}$** showed a split in the Soret band absorption, which is attributed to the protonation of the inner nitrogen atoms.[79b] The absorption spectrum of the sample of **$ZnPcF_{16}$** showed no water solubility.

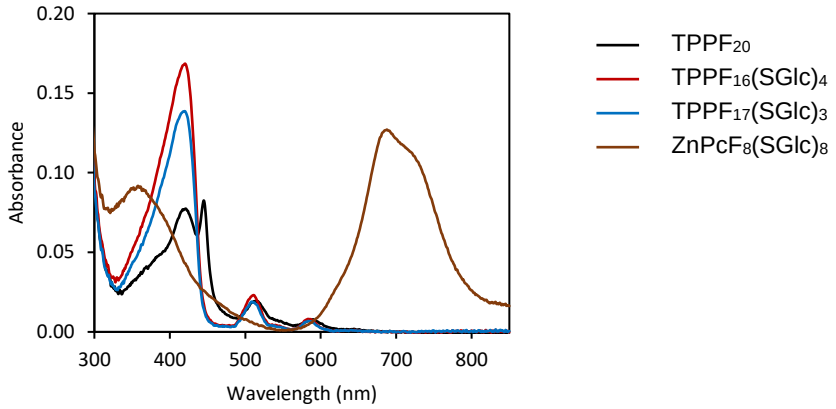

Figure 2.15. UV-Vis absorption spectra of aqueous samples (pH 3) containing a non-immobilized PS at 2 μM after 24 h.

Samples containing NP-PSs at 2 μM at different pH were filtrated after 24 h and the absorption spectra of the liquid fractions were recorded. The UV-Vis spectra of filtrates of samples at pH 4, 5, 6, 7 and 8 did not reveal any release of the PS from the hybrid materials. However, spectra of samples at pH 3 showed low concentrations of PS, which can be attributed to the hydrolytic cleavage of the PS linked to the NPs (Fig. 2.16).

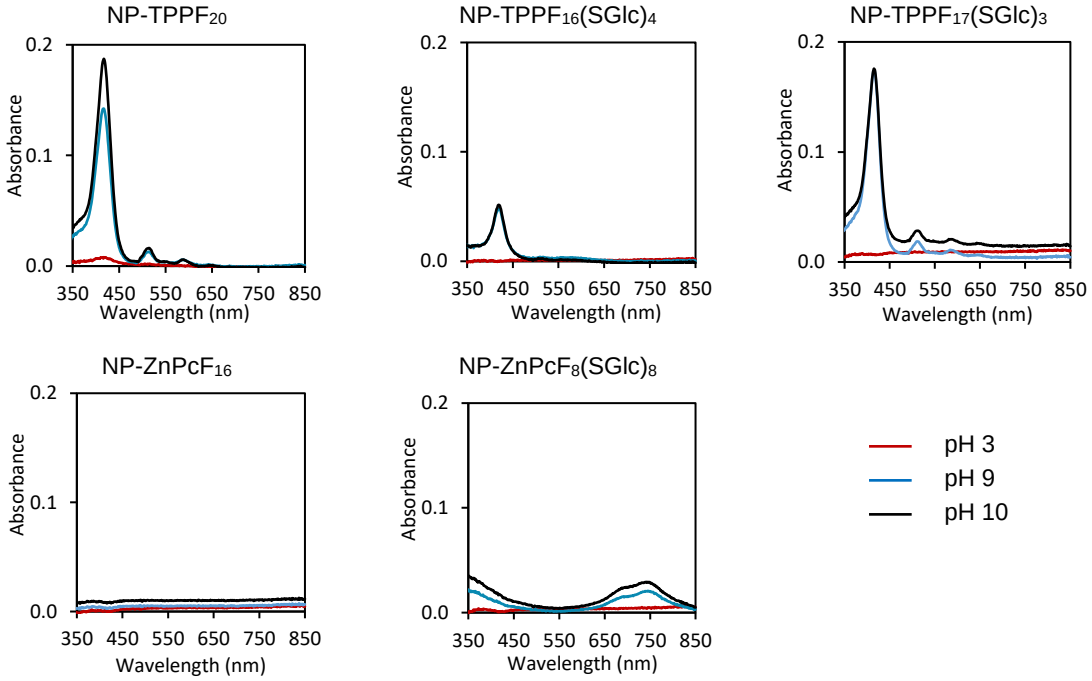

Figure 2.16. UV-Vis absorption spectra of liquid fractions resulting from filtrating aqueous suspensions of NP-PSs subjected to different conditions of pH for 24 h.

By using the absorption molar absorption coefficient of each Por in water (previously calculated at pH 3), the degree of PS cleavage at pH 3 was calculated. **NP-TPPF$_{20}$** presented higher levels of unbound PS (6.23%), than **NP-TPPF$_{16}$(SGlc)$_4$** (0.98%) and **NP-TPPF$_{17}$(SGlc)$_3$** (1.23%). **NP-ZnPcF$_{16}$** and **NP-ZnPcF$_8$(SGlc)$_8$** did not show cleavage at pH 3. However, the lower aqueous stability of Pcs may result in a lack of evidence due to adsorption of the presumed unbound PS into the PVDF filter. Samples showed stability at pH 7 and 8, but all the NP-PSs showed a considerable degree of cleavage at pH 9 and 10, probably due to the dissolution of the silica shell. Therefore, the operative pH range for the hybrid photocatalysts was considered as being between 4 and 8.

Water stability of NP-PSs dispersions was also investigated by dynamic light scattering (DLS). Measurements were taken from dispersed particles in water with pH ranging from 4 to 8, after being stirred for 24 h. Results recorded with **NP-ZnPcF$_8$(SGlc)$_8$** show a representative behaviour for all the nanomaterials (Fig. 2.17). Size distribution becomes wider when increasing pH, as well as the average size of the aggregates, ranging from 78 to 230 nm from pH 4 to pH 8. Acidic pH promotes the protonation of the amino groups in the NP-PSs, thus the electrostatic repulsion between the surfaces stabilizes the suspensions in water.

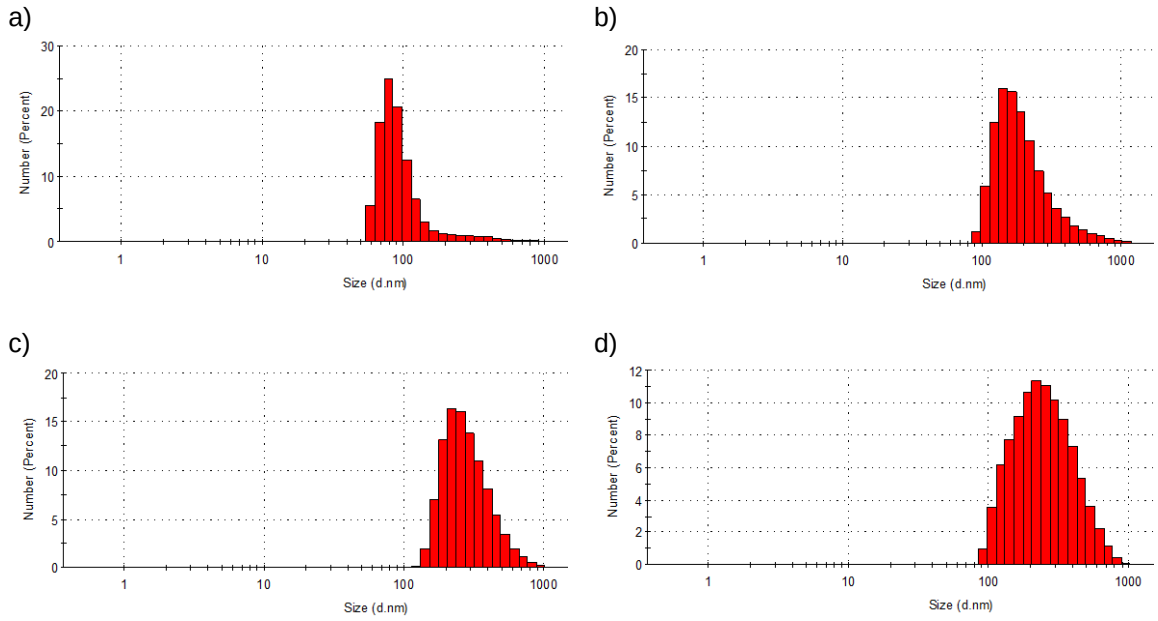

Figure 2.17. DLS size distributions of NP-ZnPcF$_8$(SGlc)$_8$ at 2 µM in water at: a) pH 4; b) pH 5; c) pH 7; d) pH 8.

2.2.6. $^1O_2$ generation by PS and NP-PS

For the qualitatively determination of $^1O_2$ generated by the photocatalysts, samples in DMF/water (9:1) containing a PS (0.5 μM) or a NP-PS (0.5, 2.0 or 5.0 μM) and 50 μM of diphenylisobenzofuran (DPBF) were irradiated with a red LED array, at a fluence rate of 4.0 mW cm^{-2}. Another sample in DMF/water (9:1) containing just DPBF 50 μM was submitted to the same irradiation conditions as control of direct photolysis. The LED array presented an emission peak at 640 nm and a bandwidth at half maximum of ±20 nm. During the irradiation, samples were kept under vigorous stirring at room temperature.

The yellow-coloured DPBF reacts specifically with $^1O_2$ in a [4+2] Diels-Alder cycloaddition reaction, being oxidized to the colorless *o*-dibenzoylbenzene. The generation of $^1O_2$ was followed by its reaction with DPBF. The breakdown of DPBF was monitored by measuring the decreasing of the absorbance at 413 nm.

Light control samples showed low rates of direct photolysis, between 1 and 3%. The decay in the absorption maximum of DPBF (50 μM) in the samples containing PSs is attributed to the ability of $^1O_2$ generation of the PSs. Glycosylated free Pors are more efficient in the $^1O_2$ generation than their related compound **$TPPF_{20}$**, having that **$TPPF_{16}(SGlc)_4$** presents slightly better results in the degradation of DPBF than **$TPPF_{17}(SGlc)_3$** (Fig. 2.18a).

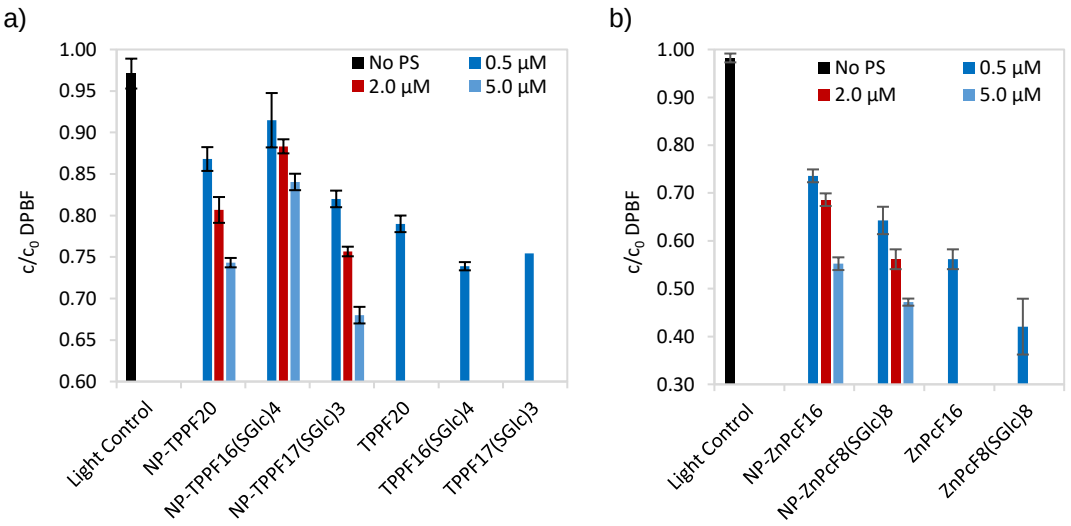

Figure 2.18. Degradation of DPBF (50 μM) in DMF/H_2O (9:1) upon irradiation with a red LED array at a fluence rate of 4.0 mW cm^{-2} and room temperature for: (a) 20 min with or without Por-based PS; (b) for 5 min with or without Pc-based PSs.

As expected, the DPBF assisted decomposition showed that free PSs have higher efficiency to generate $^1O_2$ than their corresponding immobilized derivatives. Due to this, experiments containing higher concentration of NP-PSs were performed. **NP-TPPF$_{20}$** and **NP-TPPF$_{17}$(SGlc)$_3$** showed to be more efficient in the $^1O_2$ generation when compared to **NP-TPPF$_{16}$(SGlc)$_4$**. This could be explained considering that *para* fluorine atoms in **TPPF$_{20}$** and **TPPF$_{17}$(SGlc)$_3$** determine the position for the nucleophilic substitution in the preparation of these materials, which can turn out to be a more ordered material, thus retaining better photophysical properties of the PS.

In this test, samples were irradiated with red light in order to prevent direct photodegradation of DPBF. Since in that region of the spectra is where Pcs present high intense absorption of their Q bands, less irradiation time was required to qualitatively determine the generation of $^1O_2$. Glycosylation of **ZnPcF$_{16}$** improves the dispersion of the PS in aqueous solution, and as it was expectable, **ZnPcF$_8$(SGlc)$_8$** presented better abilities for the generation of $^1O_2$ than its related **ZnPcF$_{16}$** (Fig. 2.18b). ZnPc based hybrid materials showed similar results, being **NP-ZnPcF$_8$(SGlc)$_8$** more efficient.

2.2.7. Radicals generation by PS and NP-PS

The formed radicals during the irradiation of a PS causes chain reactions. For instance, the carbon-centred radicals ($R^{\bullet}$) react with dissolved oxygen leading to peroxyl ($ROO^{\bullet}$) and oxy ($RO^{\bullet}$) radicals. Along with $^1O_2$, these species generated *in situ* have demonstrated strong oxidizing ability in the degradation of organic pollutants like 3,30,5,50-tetrabromobisphenol A,[136] tetrachloromethane[137] and 2,4,6-trichlorophenol in wastewater.[138]

The ability of the PSs to generate radicals was determined by adding NaN_3 (100 mM), a specific quencher of $^1O_2$, to the samples containing a PS (5 µM) and E2 (5 mg·L^{-1}). E2 in all the tests described in Chapter II was quantified using high-performance liquid chromatography with UV-vis absorbance detection, HPLC-UV (see experimental section). As it was expectable, light control samples containing just 5 mg·L^{-1} of E2 showed high photostability of E2 after 90 min of irradiation (Fig. 2.19c).

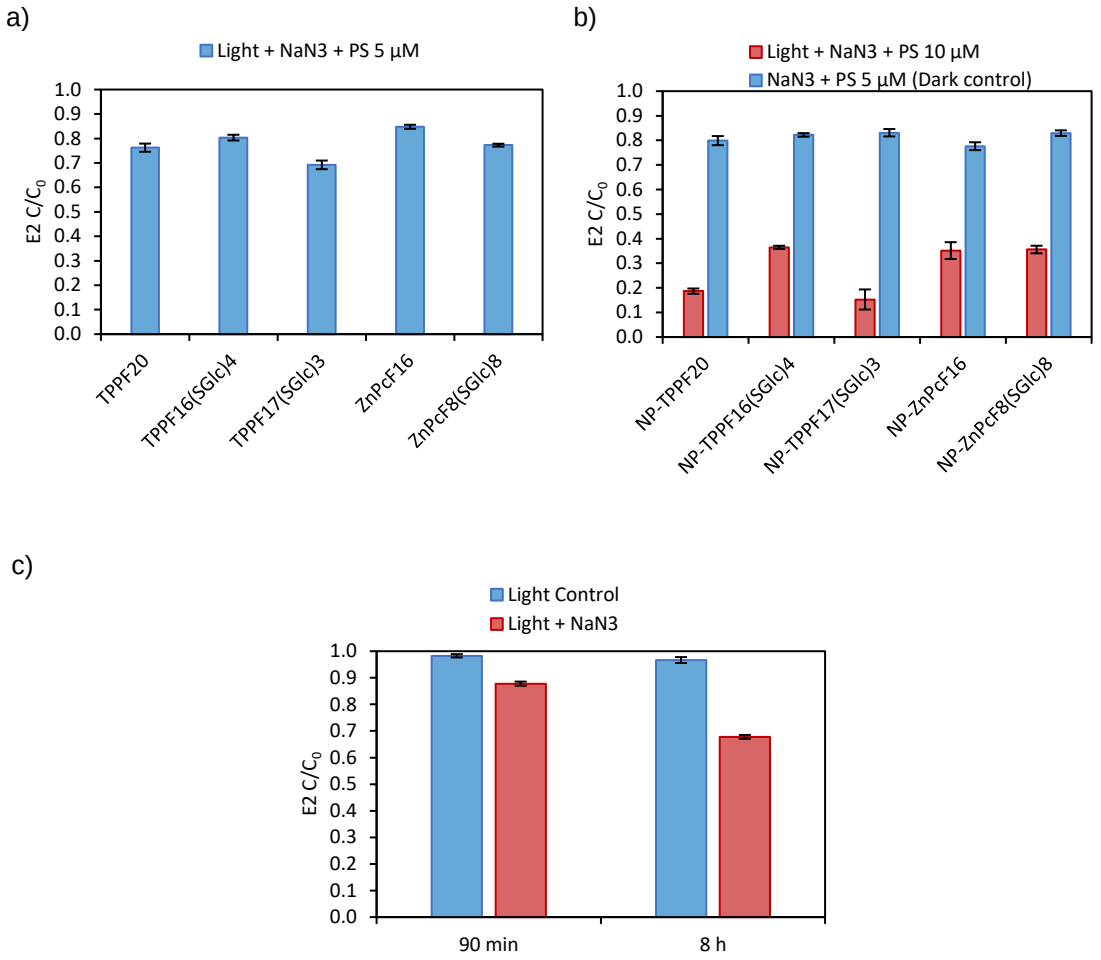

Figure 2.19. Profile of E2 (5 mg·L^{-1}) in presence of NaN_3 (100 mM) as quencher of $^1O_2$ upon: (a) 90 min of artificial white light irradiation with non-immobilized PS (5 µM); and (b) 8 h with NP-PSs (10 µM) with artificial white light irradiation or dark conditions. c) Light control sample of E2, and light control of E2 in presence of NaN_3 (100 mM).

On the other hand, control samples containing E2 (5 mg·L^{-1}) and NaN_3 (100 mM) revealed that after 90 min of irradiation, 12.9% of the starting E2 was degraded due to the presence of NaN_3. Among test samples containing a PS (5 µM), E2 (5 mg·L^{-1}) and NaN_3 (100 mM), **$TPPF_{17}(SGlc)_3$** was the PS with better ability to generate radicals, having that after 90 min of irradiation, only 69.2% of the starting E2 remained in the sample (Fig. 2.19a). Among the 30.8% of removed E2 after the treatment, 1.7% is due to the direct photolysis and 12.9% is due to the presence of NaN_3, which means that 16.2% of the starting E2 was degraded by the radicals *in situ* generated (Table 2.2).

Tests with NP-PSs (10 µM) were performed for 8 h of irradiation. Light control samples showed a E2 direct photolysis of 3.3%. Control samples containing E2 (5 mg·L^{-1}) and NaN_3 (100 mM), submitted to irradiation, showed that 32.2% of the initial E2 was degraded by NaN_3 (Fig. 2.19c). Due to the adsorption capacity of the silica shell of the NPs,

dark control samples containing E2 (5 mg·L^{-1}), NaN_3 (100 mM) and a NP-PS (10 μM), kept in dark conditions, were also included (Fig. 2.19b). Adsorption of E2 was between 16.9 and 22.4%, depending on each NP-PS. The sum of E2 direct photolysis, NaN_3 contribution for E2 degradation and the adsorption ranged between 52.4 and 57.9% of the starting E2 (depending on the NP-PS). The difference of this value respect to the concentration of E2 in the test samples after the treatment is related to the ability of the NP-PS to generate radicals, assuming that $^1O_2$ generated is quenched by NaN_3 (Table 2.2). **NP-TPPF$_{17}$(SGlc)$_3$** displayed the best efficiency in radical generation. After 8 h of irradiation, the sample containing **NP-TPPF$_{17}$(SGlc)$_3$** (10 μM), E2 (5 mg·L^{-1}) and NaN_3 (100 mM), showed a removal of 84.7% of the starting E2: 3.3% of E2 direct photolysis, 32.2% of NaN_3 contribution, 16.9% of adsorption and 32.3% due to the action of radicals generated *in situ* by the PS.

Table 2.2. Ability of PS (5 μM) and NP-PS (10 μM) to generate radicals *in situ* under irradiation (90 min or 8 h), in presence of NaN_3 (100 mM) as $^1O_2$ quencher, using E2 (5 mg·L^{-1}) as a model of organic pollutant. Values correspond to the average of three independent experiments.

Photocatalyst	Irradiation time	% of E2 degraded by direct photolysis	% of E2 degraded in presence of NaN_3	% of E2 adsorbed onto NP-PS	% of E2 in solution after treatment	% of E2 degraded by radicals
$TPPF_{20}$	90 min	1.7	12.9	n/a	76.2	9.2
$TPPF_{16}(SGlc)_4$	90 min	1.7	12.9	n/a	80.4	5.0
$TPPF_{17}(SGlc)_3$	90 min	1.7	12.9	n/a	69.2	16.2
$ZnPcF_{16}$	90 min	1.7	12.9	n/a	84.8	0.6
$ZnPcF_8(SGlc)_8$	90 min	1.7	12.9	n/a	77.3	8.1
NP-$TPPF_{20}$	8 h	3.3	32.2	20.1	18.7	25.7
NP-$TPPF_{16}(SGlc)_4$	8 h	3.3	32.2	17.8	36.5	10.2
NP-$TPPF_{17}(SGlc)_3$	8 h	3.3	32.2	16.9	15.3	32.3
NP-$ZnPcF_{16}$	8 h	3.3	32.2	22.4	35.2	6.9
NP-$ZnPcF_8(SGlc)_8$	8 h	3.3	32.2	17.1	35.6	11.8

n/a: not applicable

2.2.8. Batch mode photodegradation studies of E2 in presence of PS and NP-PS

Visible-light assisted photodegradation of E2 studies with free Pors and ZnPcs photocatalysts were conducted in batch mode to examine the photocatalytic performance of the PSs at different concentrations in water. Photodegradation studies in batch were performed using 100 mL cylindrical glasses. The photocatalytic activity of the PSs was evaluated in the degradation of 50 mL of aqueous samples containing 5 $mg \cdot L^{-1}$ of E2 (18.4 µM) under visible light irradiation (4 $mW \cdot cm^{-2}$) with different concentrations of a non-immobilized PS (2.5, 5.0 and 10.0 µM) or a NP-PS at 10 µM. Two control samples were included in each irradiation experiment: a light control containing 5 $mg \cdot L^{-1}$ of E2, without PS, and submitted to the same irradiation conditions as the samples, and a dark control containing 5 $mg \cdot L^{-1}$ of E2 and the PS at the highest concentration (10.0 µM), but kept in dark conditions. In order to estimate the reproducibility of the experimental results, photodegradation experiments were carried out in triplicate, showing in the graphs the average value corresponding for each experimental condition.

Light control samples showed that around 8% of E2 was degraded by direct photolysis after 8 h of irradiation (Fig. 2.20). No significant alterations in E2 concentration were detected in dark controls, which contained a PS (10 µM) and E2 (5 $mg \cdot L^{-1}$), but were kept in dark conditions.

As general conclusion, E2 degradation was faster with Pors than with Pcs herein tested. Both non-immobilized thioglycosylated Pors, **$TPPF_{17}(SGlc)_3$** and **$TPPF_{16}(SGlc)_4$**, showed better performance for E2 photodegradation in water comparing to **$TPPF_{20}$**, obtaining a full degradation of E2 after 2 h of irradiation in presence of 10 µM **$TPPF_{17}(SGlc)_3$**, and after 3 h with 10 µM **$TPPF_{16}(SGlc)_4$**. Despite the efficiency of **$ZnPcF_{16}$** and **$ZnPcF_8(SGlc)_8$** in singlet oxygen generation, the marked trend of Pcs to aggregate in water may be a possible explanation for the results obtained. In case of 10.0 µM **$ZnPcF_8(SGlc)_8$**, 7 h of irradiation were needed to degrade 5 $mg \cdot L^{-1}$ of E2, while after 8 h of irradiation, 10.0 µM **$ZnPcF_{16}$** caused only a small degradation (< 60% of the starting concentration of E2).

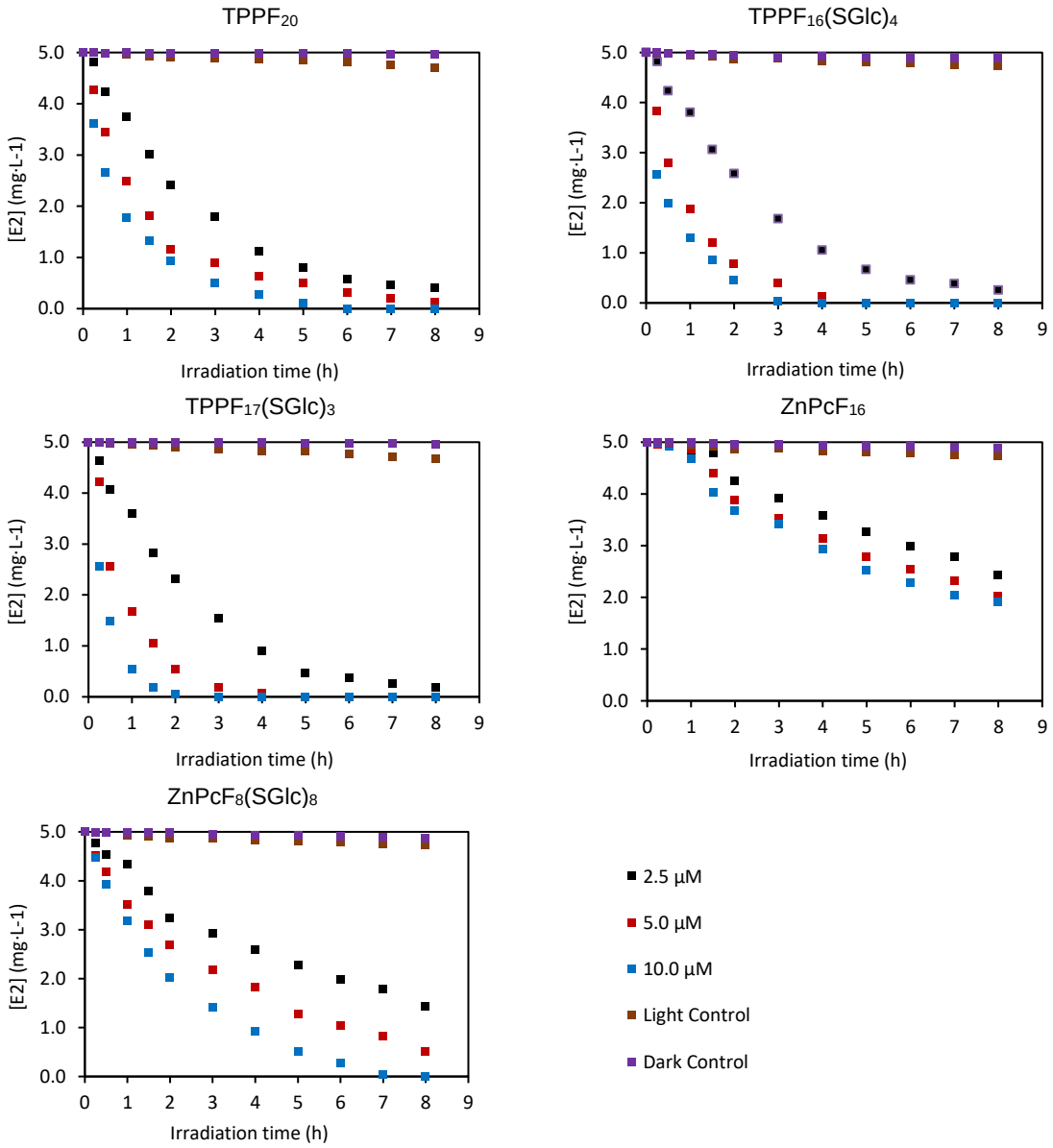

Figure 2.20. Visible-light assisted photodegradation of E2 in batch mode in presence of different concentrations of non-immobilized PSs. Values correspond to the average of three independent experiments.

The determination of kinetic parameters was performed by fitting a pseudo-first order kinetic model to each set of PS concentration used in the studies (Fig. 2.21). Accordingly, the natural logarithm of the ratio between E2 concentration, at a given irradiation time, and its initial concentration, was plotted as a function of the irradiation time and a linear regression was obtained. Correlation coefficients (*r*), number of data (*n*), apparent pseudo-first order rate constants (*k*) and half-lives ($t_{1/2}$) are presented in **Table 2.3**. *r* ranges from 0.964 to 0.999, confirming the adequacy of the pseudo-first order model to describe the E2 indirect photodegradation kinetics.

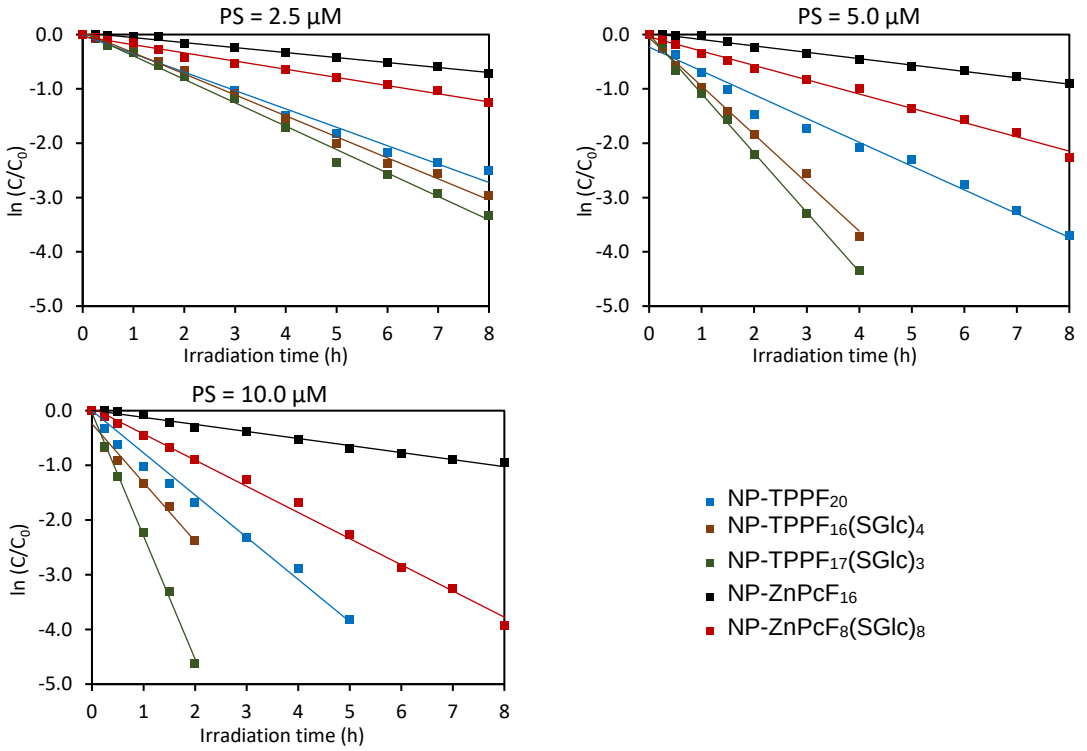

Figure 2.21. Pseudo-first order photodegradation kinetics of E2 in presence of different concentrations of non-immobilized PSs. Values correspond to the average of three independent experiments.

Table 2.3. Kinetic parameters for the photodegradation of E2 in batch mode in presence of different concentrations of non-immobilized PSs. Values correspond to the average of three independent experiments.

PS	Conc. (µM)	r	n	k (h^{-1})	$t_{1/2}$ (h)
$TPPF_{20}$	2.5	0.995	36	0.3414	121.8
	5.0	0.982	36	0.4809	86.5
	10.0	0.991	27	0.7714	53.9
$TPPF_{16}(SGlc)_4$	2.5	0.997	36	0.3775	110.2
	5.0	0.997	24	0.9122	45.6
	10.0	0.964	18	1.2404	33.5
$TPPF_{17}(SGlc)_3$	2.5	0.997	36	0.4243	98.0
	5.0	0.999	24	1.091	38.1
	10.0	0.999	18	2.2782	18.3
$ZnPcF_{16}$	2.5	0.991	36	0.0852	488.1
	5.0	0.994	36	0.1127	369.0
	10.0	0.994	36	0.1276	325.9
$ZnPcF_8(SGlc)_8$	2.5	0.993	36	0.1573	264.4
	5.0	0.996	36	0.2709	153.5
	10.0	0.997	36	0.4688	88.7

Batch mode photocatalysis studies with NP-PSs started with the adsorption/desorption equilibrium attributed to the adsorption capacity of E2 onto the silica shell of the NPs. Dark controls containing 10 µM NP-PSs and 5 mg·L^{-1} E2 were magnetically stirred for 120 min in dark conditions. Equilibrium was achieved after 60 minutes for all the NP-PSs (Fig. 2.22a). In photocatalytic tests with NP-PSs, samples were stirred for 60 minutes in dark conditions before starting the irradiation.

After 8 h of phototreatment, light controls showed low rates of direct photolysis of E2. **NP-TPPF$_{17}$(SGlc)$_3$** and **NP-ZnPcF$_8$(SGlc)$_8$** showed a similar performance, with a removal activity of *ca.* 82% of the initial E2, while in presence of **NP-TPPF$_{20}$**, 44% of E2 remained in solution and in presence of **NP-TPPF$_{16}$(SGlc)$_4$** and **NP-ZnPcF$_{16}$** only 40% was degraded (Fig. 2.22b). These results can be understood attending to changes in the aqueous stability of the suspensions, compared to related non-immobilized PSs, which can alter their photophysical properties.

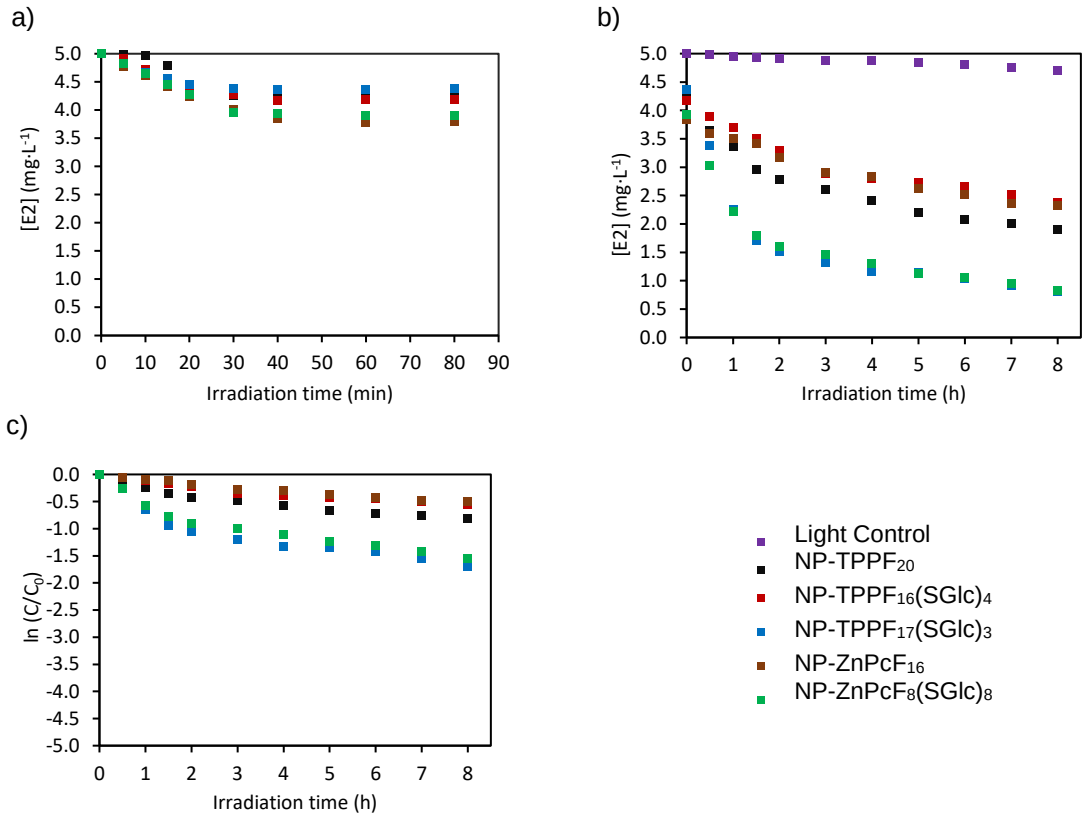

Figure 2.22. a) Kinetic adsorption curves of E2 onto NP-PSs; b) and c) photodegradation of E2 in batch mode in presence of NP-PSs at 10 µM of PS. Values correspond to the average of two independent experiments.

By plotting the natural logarithm of the ratio between E2 concentration, at a given irradiation time, and its initial concentration, results of E2 photodegradation with NP-PS in

batch mode do not fit pseudo first order trend (Fig. 2.22c). Second order trend adjustment of results obtained *r* below 0.873.

Catalyst recovery and reuse are important features for many catalytic processes. The homogeneous Por and Pc based PSs could not be recovered, but the heterogeneous catalysts could be separated and reused without significant loss of catalytic activity. For subsequent uses in E2 photodegradation, NP-PSs were recovered by applying a magnetic field and removing the supernatant. The catalysts were cleaned by rinsing in ethanol and water and reused in further experiments. After three runs, efficiency of photocatalytic activity decreased less than 2% in case of **NP-TPPF$_{17}$(SGlc)$_3$**, *ca.* 4% in case of **NP-TPPF$_{20}$**, **TPPF$_{16}$(SGlc)$_4$** and **NP-ZnPcF$_8$(SGlc)$_8$**; and around 9% in case of **NP-ZnPcF$_{16}$** (Fig. 2.23). Analysis of HPLC chromatograms of the rinse solvent from the NP-PSs washing processes did not show presence of E2, revealing that the E2 fraction adsorbed onto the NP-PSs is also degraded during the process. This could be expected since ROS generated during the phototreatment can more easily reach E2 in the shell of the NP-PSs.

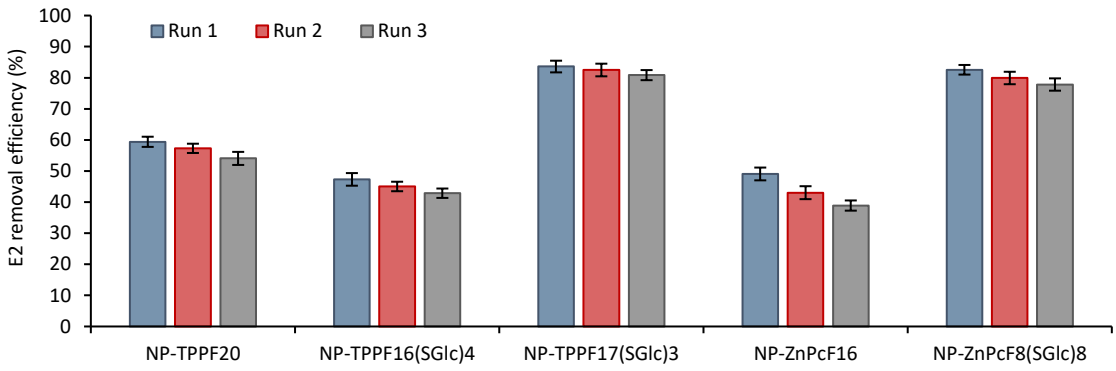

Figure 2.23. Reuse of NP-PSs after recovering and washing processes.

2.2.9. Flow mode photodegradation studies of E2 in presence of PS and NP-PS

Flow mode studies here presented were performed in EcoSynth, Belgium. In order to improve assisted photodegradation of E2, both in homogeneous and heterogeneous photocatalysis, a flow setup using reactor channels was substituted for the batch vessel (Fig. 2.24). As such, samples from the reservoir were pumped with a piston pump through a narrow-bore ($ø_{inner}$: 0.8 mm, $ø_{outer}$: 1.6 mm), transparent tube of fluorinated ethylene propylene while being irradiated, with final material collected at the reactor outlet.

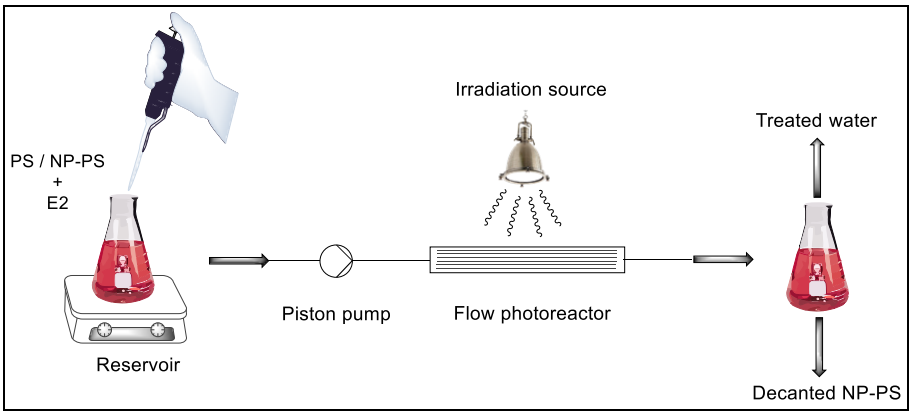

Figure 2.24. Design of the flow photoreactor setup used for photodegradation assays.

Residence time plays an important role in the complete decomposition of the target compound when using a flow photodegradation reactor. The photocatalytic degradation of 5 mg·L^{-1} of E2 was performed using different flow rates, ranging from 0.1 to 0.4 mL·min^{-1}. To build the kinetic profile of E2 degradation, samples with 10 µM of non-immobilized PS were tested with different residence times (Fig. 2.25a and c). Compared to results obtained in batch mode using a non-immobilized PS at 10 µM, photocatalytic rates were greatly enhanced, and the Por-based PSs showed E2 $t_{1/2}$ ranging 3.6 - 9.7 min (Table 2.4). Especially remarkable were the results obtained with Pc-based PSs, that show a decrease of E2 $t_{1/2}$ from 325.9 to 59.2 min in presence of **$ZnPcF_{16}$**, and from 88.7 to 18.4 min in presence of **$ZnPcF_8(SGlc)_8$**.

As previously described, samples containing NP-PS were stirred for 60 min and kept in the dark before being pumped into the system, in order to achieve the adsorption/desorption equilibrium. Compared to batch mode, results obtained in flow mode (Fig. 2.25b and d) show a marked increase in degradation efficiency. After 60 min of irradiation, all the starting E2 was degraded in presence of **$NP\text{-}TPPF_{17}(SGlc)_3$**, and in presence of **$NP\text{-}TPPF_{16}(SGlc)_4$**, **$NP\text{-}ZnPcF_8(SGlc)_8$** or **$NP\text{-}ZnPcF_{16}$**, only 0.32, 0.50 or 0.98 mg L^{-1} of E2 remained in solution, respectively.

Flow mode photocatalysis produced remarkable high degradation rates in comparison with the experiments in batch, resulting in E2 half-lives between 12.1 and 33.5 min in case of NPs-Pors, while in previous results obtained in batch mode under the same conditions of irradiation and sample preparation, $t_{1/2}$ of E2 ranged from 48 min (**$NP\text{-}TPPF_{17}(SGlc)_3$**), to 210 min (**$NP\text{-}TPPF_{20}$**) and 420 min (**$NP\text{-}TPPF_{16}(SGlc)_4$**). Results in flow mode were also improved in the case of ZnPc based PSs, obtaining E2 $t_{1/2}$ of 18.4 min in case of **$NP\text{-}ZnPcF_8(SGlc)_8$** (45 min in batch mode). Especially remarkable were results of degradation of E2 with **$NP\text{-}ZnPcF_{16}$**, showing that half of the starting E2 was degraded after

24.9 min of irradiation, while 360 min were needed in batch mode to achieve the same percentage of degradation.

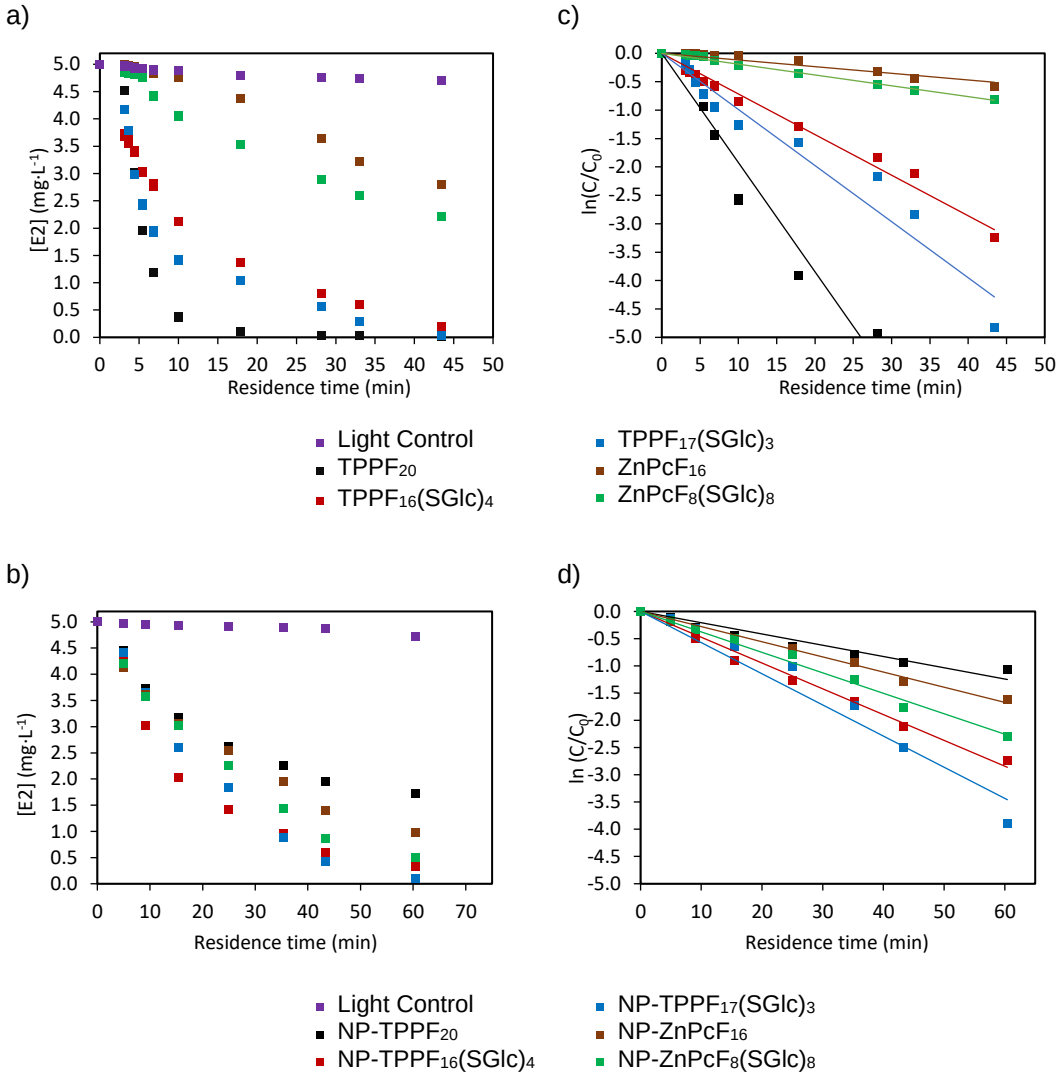

Figure 2.25. Photodegradation of E2 in flow mode in presence of: a) non-immobilized PSs at 10 μM, b) NP-PS at 10 μM of PS. Values correspond to the average of two independent experiments. Pseudo-first order photodegradation kinetics of E2 in flow mode in presence of: c) non-immobilized PSs at 10 μM, d) NP-PS at 10 μM. Values correspond to the average of three independent experiments.

Table 2.4. Kinetic parameters for the photodegradation of E2 in flow mode in presence of a non-immobilized PS (10 μM) or a NP-PS (10 μM). Values correspond to the average of three independent experiments.

PS or NP-PS (10 μM)	r	n	k (min^{-1})	$t_{1/2}$ (min)

$TPPF_{20}$	0.961	24	0.1922	3.6
$TPPF_{16}(SGlc)_4$	0.990	27	0.0715	9.7
$TPPF_{17}(SGlc)_3$	0.971	27	0.0988	7.0
$ZnPcF_{16}$	0.958	27	0.0117	59.2
$ZnPcF_8(SGlc)_8$	0.992	27	0.0190	36.5
NP-$TPPF_{20}$	0.959	24	0.0207	33.5
NP-$TPPF_{16}(SGlc)_4$	0.995	24	0.0474	14.6
NP-$TPPF_{17}(SGlc)_3$	0.977	24	0.0572	12.1
NP-$ZnPcF_{16}$	0.995	24	0.0278	24.9
NP-$ZnPcF_8(SGlc)_8$	0.994	24	0.0376	18.4

The higher efficiency in flow mode is largely due to the better penetration of light into the suspension. Unlike in a batch procedure, the narrow reactor channels guarantee homogeneous irradiation conditions for the small reaction volume inside the reactor (~ 2 mL). With accurate control over residence time, this continuous processing eventually allows for photochemical treatment of large sample volumes under identical irradiation conditions. Furthermore, absorption spectra of samples recorded before and after the irradiation tests showed a better stabilization of the suspensions in the system output, thus demonstrating that flow mode maximizes the performance of NP-PSs.

In addition to different exposure times of irradiation, photodegradation studies with NP-PSs in flow mode were performed under different operational parameters, such as pH of the samples and concentration of NP-PSs. The effect of the load of NP-PSs on the efficiency of E2 photodegradation was investigated in the range of 10-20 μM, with a residence time in the flow system of 35 min (Fig. 2.26). The results show that, in the presence of all the NP-PSs, degradation rate and E2 adsorption were, respectively, directly and indirectly proportional to catalyst concentration. At higher concentrations, aggregation of the suspensions in the output of the system was not observed.

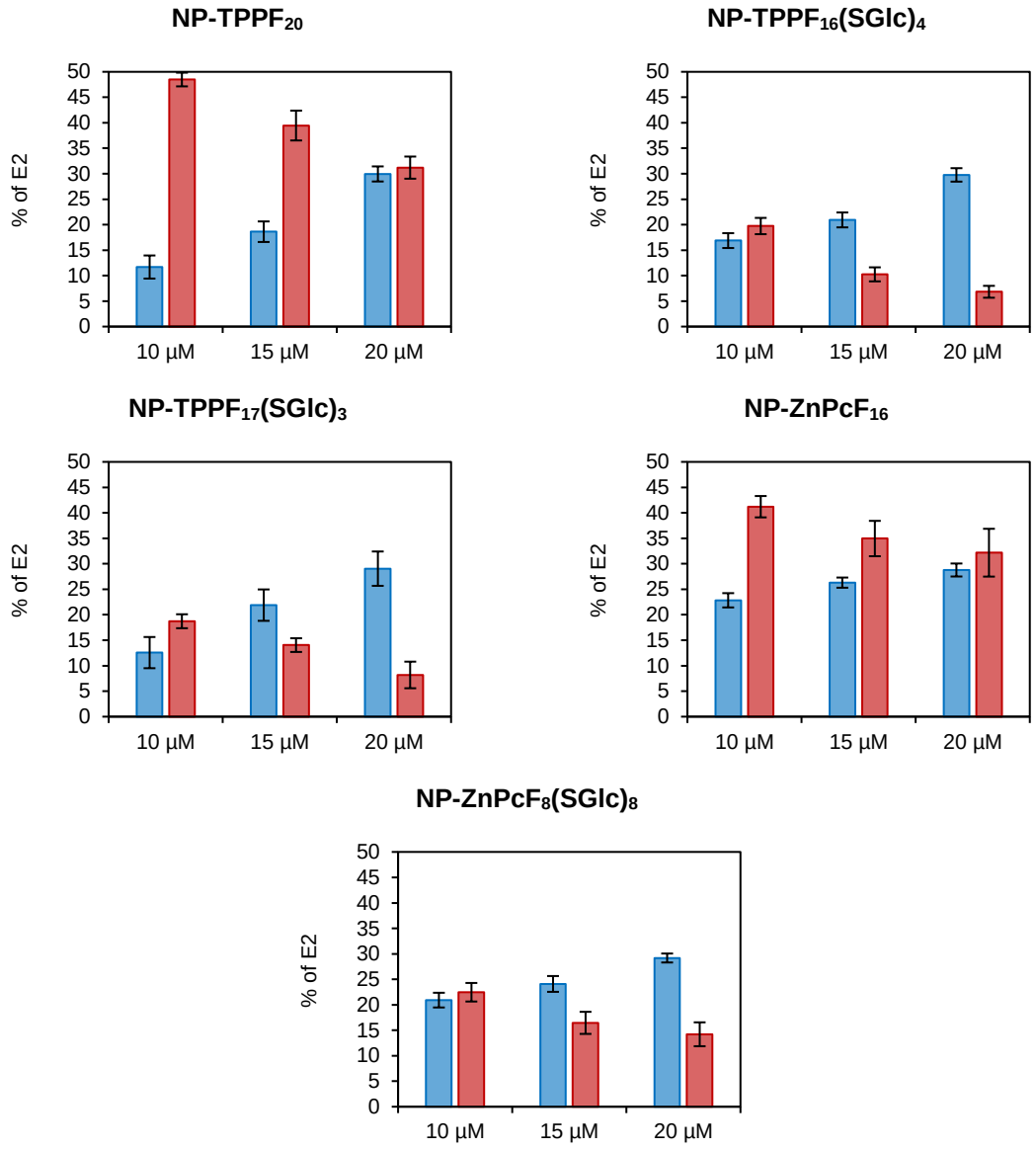

Figure 2.26. Effect of NP-PSs' concentration in flow mode tests of E2 photodegradation. Blue bars represent E2 adsorbed into the hybrid material; red bars represent E2 in solution, after 35 min of residence time.

Following the results of preliminary tests of the effect of pH on NP-PSs stability, assisted flow photodegradation of E2 was investigated at pH 8, 6 and 4. Concentration of NP-PSs was kept at 10 µM and initial concentration of E2 was 5 $mg \cdot L^{-1}$. Samples were stirred in dark conditions for 40 min and then pumped into the system adjusting the flow for a residence time of 35 min. The pH is an important parameter in photocatalytic degradation processes, since it influences the rate of formation of hydroxyl radicals. While in acidic solutions the formation of hydroxyl radicals is thermodynamically unfavourable, in basic conditions the formation of hydroxyl radicals increases.[139]

In this study, degradation of E2 was faster at pH 8 than in unmodified samples at pH 6 (Fig. 2.27). However, NP-PSs showed an improved photocatalytic performance at pH 4. DLS results showed a smaller average size of the aggregates and more monodisperse solutions at pH 4. Acidic pH promotes the protonation of the amino groups in the NP-PSs, thus the electrostatic repulsion between the surfaces stabilizes the suspensions in water. As expectable, more homogeneous dispersions of NP-PSs benefit the diffusion of O_2 into the photocatalyst, which improves the photocatalytic performance.

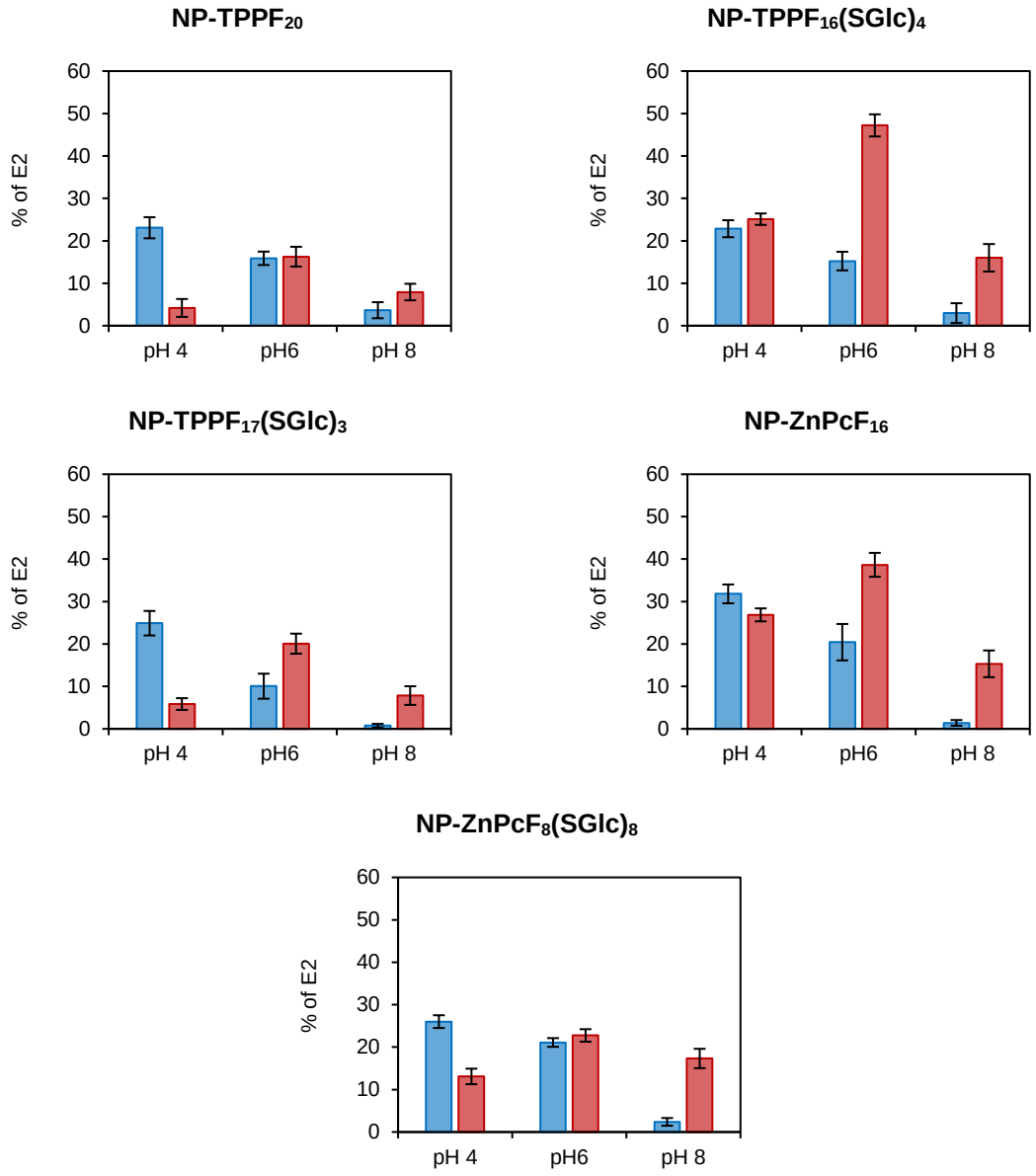

Figure 2.27. Effect of the pH on visible-light photodegradation of E2 in flow mode assays with NP-PSs. Blue bars represent E2 adsorbed onto the hybrid material; red bars represent E2 in solution after 35 min of residence time.

Adsorption studies with dark control samples showed that, in comparison to samples at pH 6, the amount of E2 adsorbed was lower at pH 8 and higher at pH 4. In alkaline conditions, E2 becomes from partially to significantly negatively charged (pKa of E2 = 10.46 ± 0.03 [140]). The low aqueous solubility of E2, which has been reported over the range of 3.1 to 12.96 $mg \cdot L^{-1}$ [141], can influence its distribution and availability in the medium. It is expectable that an increase in pH will involve an increase in E2 solubility, and therefore a lower adsorption and a positive effect on the degradation rate due to a higher availability of E2 in the samples. Under this assumption, a higher amount of E2 is expected to get adsorbed onto the SiO_2 coating of the NPs at lower pH ranges. Variations in E2 adsorption levels at different pH values can be also explained attending to the morphological changes in the dispersions of NP-PSs observed in the DLS measurements. The reduction of the average aggregate size at acidic pH increases the ratio between area and volume, thus benefiting the adsorption of E2 onto the surface of the NPs.

To demonstrate that these NP-PSs can be used as photocatalysts in practical applications of water treatment, the reusability of the photocatalysts at 10 µM was investigated by successive runs for the degradation of E2 (5 $mg \cdot L^{-1}$) with a residence time in the flow system of 35 min. The catalysts were separated from their corresponding reaction mixture after each run, washed with ethanol and water, and re-suspended in water before reuse. After three cycles of assisted photodegradation of E2, none of the catalysts exhibited any significant loss of activity (Fig. 2.28). Again, analysis of the rinse solvent from the washing processes showed that the E2 adsorbed is also degraded during the photocatalytic test.

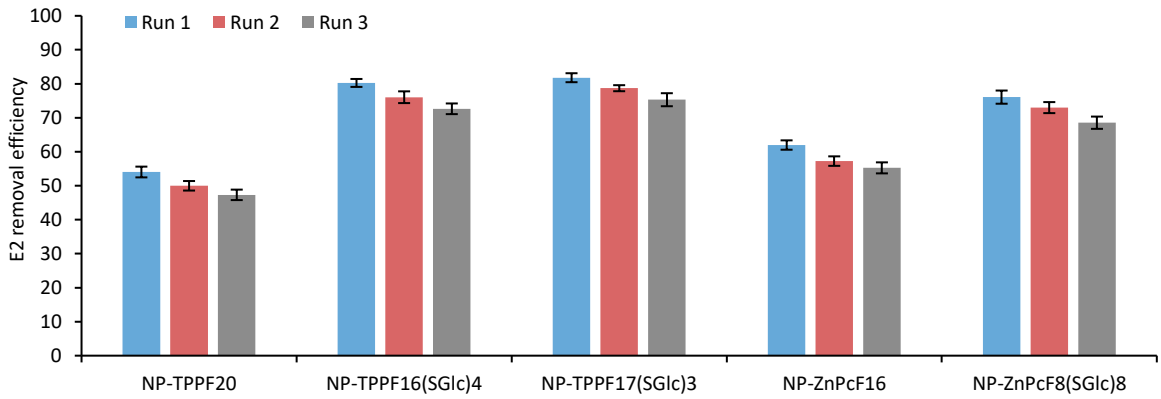

Figure 2.28. Recycling tests of visible-light assisted photodegradation of E2 in flow mode.

2.3. Conclusions

Five novel hybrid materials based on Pors and Pcs anchored onto MNPs were prepared and tested as photocatalysts. Studies of degradation of E2 in batch mode showed efficient E2 removal in presence of the free PSs **$TPPF_{20}$**, **$TPPF_{16}(SGlc)_4$**, **$TPPF_{17}(SGlc)_3$** and **$ZnPcF_8(SGlc)_8$**, even at just 4 mW cm^{-2}. However, the lower aqueous stability of the NP-PSs, due to the tendency of these materials to aggregate in water and therefore form non-homogeneous dispersions, caused reduction of E2 photodegradation rates. By substituting batch for flow mode, the E2 photodegradation efficiency was increased in presence of all the free and immobilized PSs. Optimization of reaction conditions in flow mode suggested that lower flow rates (*ca.* 0.1 $mL \cdot min^{-1}$) and higher load of the photocatalysts (20 μM) enhanced the degradation of E2.

Upon testing different pH conditions, pH 4 showed a more efficient removal of E2. Also, a higher adsorption of the pollutant onto the NPs was observed, which is related to a better stability of the hybrids in acidic aqueous solutions. In addition, recycling tests of NP-PSs used in the flow system indicated the viability of these photocatalysts, as photocatalytic activity remained practically constant during three cycles.

2.4. Experimental section

2.4.1. Apparatus and characterization

Absorption spectra of liquid samples were recorded using a Shimadzu UV-2501-PC photometer. Absorption spectra of solid samples were recorded using a Jasco V-560 with an integrating sphere ISV-469.

^{1}H, ^{19}F NMR and ^{13}C NMR spectra were recorded on a Bruker Avance-300 spectrometer at 300, 282.38 and 75.47 MHz, respectively, or on a Bruker Avance-500 at 125.77 MHz for ^{13}C. Tetramethylsilane (TMS) was used as internal reference. The chemical shifts are expressed in δ (ppm) and the coupling constants (*J*) in Hz. The multiplicity is presented as follows: s = singlet, br = broad singlet, d = doublet, t = triplet, dd = double doublet, dt = doublet of triplet, m = multiplet.

Electrospray ionization mass spectrometric analyses were performed at the Division 1.8 of Bundesanstalt für Materialforschung und -prüfung (Berlin, Germany), using a Waters/Micromass Q-Tof Ultima Mass Spectrometer instrument. The electrospray ionization was run in $CHCl_3$/EtOH (80/20), with 0.1% formic acid.

Analytical TLC was carried out on pre-coated silica gel sheets (Merck, 60, 0.2 mm).

Powder XRD was performed in the range 10-90° 2θ on a Philips X'pert MPD diffractometer using Cu Kα radiation.

TEM images were recorded on a Hitachi H9000 NA microscope operated at 200 kV.

The irradiation system used to determine the production of $^{1}O_2$ was a Lumacare source, model LC-122, consisting of a 250 W halogen lamp coupled to an optic fibre beam of red light (620-750 nm).

The irradiation system used in the photocatalytic tests was a PAR irradiation system consisted of 13 fluorescent lamps of type OSRAM 21 of 18 W each with a broad emission spectrum of 380 – 700 nm. The radiation power was measured with a potentiometer bright Spectra Physics, model 407A and the sensor of the same brand, model 407A-2.

Chromatographic separation of E2 was performed using a Waters Alliance 2695 HPLC System, coupled to a 2487 UV Detector.

2.4.2. Materials and reagents

All reagents were obtained from commercial sources and were used without further purification steps. Reversed-phase column chromatography was carried out on Waters Sep-Pak C18 35 cm^3 cartridges. Analytical thin-layer chromatography (TLC) was carried out on pre-coated silica gel sheets (Merck, 60, 0.2 mm).

2.4.3. Synthesis of 5,10,15,20-tetrakis(2,3,4,5,6-pentafluorophenyl)porphyrin ($TPPF_{20}$)

Pentafluorobenzaldehyde (8 mL, 65.0 mmol) was added to a refluxing mixture of glacial acetic acid (400 mL) and nitrobenzene (300 mL). Pyrrole (5 mL, 72.0 mmol) was then added dropwise over 15 min and the mixture was refluxed for 1 h. After cooling to room temperature, the acetic acid and nitrobenzene were distilled under reduced pressure to dryness. The crude material was then taken up in chloroform and submitted to column chromatography (silica gel) using a mixture of chloroform–petroleum ether (1:1) as eluent. After evaporation of the solvent, **$TPPF_{20}$** was crystallized in dichloromethane/petroleum ether as a purple solid (1.9 g, 12%).**^{1}H NMR** (300 MHz, $CDCl_3$): δ 8.92 (s, 8H, β-H), -2.92 (s, 2H, NH). **^{19}F NMR** (282.37 MHz, $CDCl_3$): δ -159.69–-159.58 (8F, dd, *J* = 23.2, 7.6 Hz, 3,5-PhF), -174.33 (4F, t, *J* = 20.9 Hz, 4-PhF), -184.43 (8F, td, *J* = 22.5, 7.7 Hz, 8F, 2,6-PhF). **UV-vis** (c = 2.30 μM, DMSO, path length = 1 cm, 25 °C): λ/nm (ε × 10^{-4} /M^{-1} cm^{-1}) = 417 (10.4), 507 (1.59), 553 (0.02), 588 (0.51), 696 (0.03). **ESI-MS** *m/z*: 974 $(M+H)^+$.

2.4.4. Synthesis of 2,3,4,6-tetra-*O*-acetyl-glucosyl thioacetate (GlcAcSAc)

Synthesis of the sugar derivative was performed according to a previously reported method,[131] by mixing 2,3,4,6-tetra-*O*-acetyl-glucosyl bromide (1 g, 2.43 mmol) with potassium thioacetate (555 mg, 4.86 mmol, 2.0 equiv.) in acetone, overnight, at room temperature. This yielded 2,3,4,6-tetra-*O*-acetyl-glucosyl thioacetate (**GlcAcSAc**) (775 mg, 78.5%) after removal of the solvent and purification over a silica column using hexane/ethyl acetate (3:2) as eluent. **^{1}H NMR** (300 MHz, $CDCl_3$): δ 5.31-5.26 (1H, m, 1-GlcH), 5.25 (1H, s, 4-GlcH), 5.18 – 5.16 (2H, m, 2,3-GlcH), 4.27 (1H, dd, *J* = 12.5, 4.4 Hz, 6-GlcH), 4.10 (1H,

dd, *J* = 12.5, 2.1 Hz, 6-GlcH), 3.84 (1H, ddd, *J* = 10.1, 4.4, 2.2 Hz, 5-GlcH), 2.39 (3H, s, $SCOCH_3$), 2.09 (3H, s, CH_3), 2.04 (3H, s, CH_3), 2.03 (3H, s, CH_3), 2.02 (3H, s, CH_3). **^{13}C NMR** (75.47 MHz, $CDCl_3$): δ 170.67 (C=O), 170.07 (C=O), 169.41 (C=O), 169.36 (C=O), 80.18 (1- GlcC), 76.34 (5-GlcC), 73.94 (3-GlcC), 68.94 (2-GlcC), 67.83 (4-GlcC), 61.65 (6-GlcC), 30.86 (CH_3), 20.73 (CH_3). **ESI-MS** *m/z*: 429.1 $(M+Na)^+$.

2.4.5. Synthesis of 5,10,15,20-tetrakis[4-(2,3,4,6-tetra-*O*-acetyl-β-D-glucopyranosylthio)-2,3,5,6-tetrafluorophenyl)]porphyrin ($TPPF_{16}(SGlcAc)_4$)

To a solution of **$TPPF_{20}$** (200 mg, 204 µmol), and 2,3,4,6-tetra-*O*-acetylglucosylthioacetate (360 mg, 932 µmol, 4.6 equiv.) in DMF (10 mL), diethyl amine (4 mL) was added. The reaction mixture was stirred overnight at room temperature. Then, the product was precipitated with methanol/water. The crude mixture was recovered in dichloromethane and purified by flash chromatography (silica gel) using a mixture of ethyl acetate/hexane (2:1) as eluent. **$TPPF_{16}(SGlcAc)_4$** (349 mg, 73%) was obtained after crystallization in dichloromethane/hexane, as a red powder. **^{1}H NMR** (300 MHz, $CDCl_3$): δ 9.02 (8H, s, β-pyrroleH), 5.44 - 5.33 (4H, m, 1-GlcH), 5.31 – 5.21 (8H, m, 2,3-GlcH), 5.18 (4H, d, *J* = 9.9 Hz, 4-GlcH), 4.39 – 4.24 (8H, m, 6-GlcH), 3.91 (4H, dt, *J* = 9.9, 3.6 Hz, 5-GlcH), 2.23 (12H, s, CH_3), 2.10 (12H, s, CH_3), 2.09 (3H, s, CH_3), 2.08 (3H, s, CH_3), -2.87 (2H, br, NH). **^{13}C NMR** (125.77 MHz, $CDCl_3$): δ 170.50 (C=O), 170.24 (C=O), 170.06 (C=O), 169.73 (C=O), 149.64 (2,6- PhC), 145.14 (3,5-PhC, α-pyrroleC), 127.63 (β -pyrroleC), 121.78 (4-PhC), 112.81 (1-PhC), 104.33 (*meso*C), 85.63 (1- GlcC), 75.06 (5-GlcC), 71.93 (3-GlcC), 67.89 (2-GlcC), 67.17 (4-GlcC), 61.43 (6-GlcC), 22.66 (CH_3), 20.79 (CH_3), 20.71 (CH_3), 20.64 (CH_3). **^{19}F NMR** (282.37 MHz, $CDCl_3$): δ -131.72 (8F, dd, *J* = 25.3, 12.1 Hz, 3,5-PhF), -136.00 (8F, dd, *J* = 24.9, 12.2 Hz, 2,6-PhF). **UV-vis** (c = 2.30 µM, DMSO, path length = 1 cm, 25 °C): λ/nm (ε × 10^{-4} /M^{-1} cm^{-1}) = 416 (33.4), 507 (2.36), 539 (0.32), 580 (0.77), 634 (0.08). **ESI-MS** *m/z*: 1177.33 $(M+2H)^{2+}$.

2.4.6. Synthesis of 5,10,15,20-tetrakis[4-(β-D-glucopyranosylthio)-2,3,5,6-tetrafluorophenyl)]porphyrin ($TPPF_{16}(SGlc)_4$)

Porphyrin **$TPPF_{16}(SGlcAc)_4$** (200 mg, 84 μmol) was dissolved in methanol/dichloromethane (3:1, 10 mL) and treated with sodium methoxide (0.5 M solution in methanol, 4 mL). The reaction mixture was stirred at room temperature for 1.5 h and then neutralized by an aqueous citric acid solution. The mixture was filtered through a Waters Sep-Pak C18 35 cm^3 reversed-phase prep column and washed with water. The deprotected glucoporphyrin **$TPPF_{16}(SGlc)_4$** was then purified on flash chromatography (silica gel) eluted using a mixture of ethyl acetate/ methanol (3:1) and crystallized in methanol/CH_2Cl_2 (134 mg, 96%). **^{1}H NMR** (300 MHz, CD_3OD): *δ* 9.64 – 8.67 (8H, br s, β- pyrroleH), 5.29 – 5.10 (4H, m, GlcH), 4.64 (4H, s, GlcH), 4.06 (4H, dd, *J* = 20.7, 9.1 Hz, GlcH), 3.79 (4H, dd, *J* = 11.9, 5.8 Hz, GlcH), 3.60 – 3.44 (16H, m, GlcOH), 3.44 – 3.26 (12H, m, 12H, GlcH), -3.00 (2H, s, NH). **^{13}C NMR** (125.77 MHz, DMSO-d_6): *δ* 148.14 (2,6- PhC), 147.15 (3,5-PhC, α-pyrroleC), 146.28 (β -pyrroleC), 145.20 (4-PhC), 119.54 (1-PhC), 114.27 (*meso*C), 85.13 (1- GlcC), 82.31 (5-GlcC), 79.61 (3-GlcC), 78.58 (2-GlcC), 72.23 (4-GlcC), 70.82 (6-GlcC). **^{19}F NMR** (282.37 MHz, CD_3OD): *δ* -158.22 (8F, dd, *J* = 24.6, 11.9 Hz, 3,5-PhF), -163.63 (8F, dd, *J* = 24.6, 11.9 Hz, 2,6-PhF). **UV-vis** (*c* = 4.00 *μ*M, DMSO, path length = 1 cm, 25 °C): *λ*/nm ($\varepsilon \times 10^{-4}/M^{-1}\ cm^{-1}$) = 414 (35,96), 507 (2.36), 536 (0.31), 580 (0.75), 636 (0.05). **ESI-MS** *m/z*: 1679.60 $(M+H)^+$.

2.4.7. Synthesis of 5,10,15-tris[4-(2,3,4,6-tetra-*O*-acetyl-β–D-glucopyranosylthio)-2,3,5,6-tetrafluorophenyl)]-20-(2,3,4,5,6-pentafluorophenyl)porphyrin ($TPPF_{17}(SGlcAc)_3$)

To a solution of **$TPPF_{20}$** (200 mg, 204 μmol), and 2,3,4,6-tetra-*O*-acetylglucosylthioacetate (250 mg, 648 μmol, 3.2 equiv) in DMF (10 mL), diethyl amine (3 mL) was added. The reaction mixture was stirred at room temperature for 90 min. Then, the product was precipitated with methanol/water and the solid filtered and washed with water. The crude mixture was recovered in dichloromethane and purified by flash chromatography (silica gel) using a mixture of ethyl acetate/hexane (2:1) as eluent. The glucoporphyrin **$TPPF_{17}(SGlcAc)_3$** (233 mg, 57%) was obtained after recrystallization in dichloromethane/hexane, as a red powder. **^{1}H NMR** (300 MHz, $CDCl_3$): δ 9.02 (6H, s,

3,7,8,12,13,17-β-pyrroleH), 8.94 (2H, s, 2,18-β-pyrroleH), 5.39 (3H, dd, *J* = 9.2 and 9.2 Hz, 1-GlcH), 5.25 (9H, ddd, *J* = 14.0, 8.7, 4.5 Hz, 2,3,4-GlcH), 4.33 (6H, m, 6-GlcH), 3.91 (3H, dt, *J* = 9.9, 3.5 Hz, 5-GlcH), 2.23 (9H, s, CH_3), 2.10 (9H, s, CH_3), 2.09 (9H, s, CH_3), 2.08 (9H, s, CH_3), -2.87 (2H, br s, NH). **^{13}C NMR** (125.77 MHz, $CDCl_3$): δ 170.72 (C=O), 170.24 (C=O), 169.53 (C=O), 169.46 (C=O), 148.13–145.25 (2,6-PhC, 3,5-PhC, α-pyrroleC), 131.56 (β-pyrroleC), 122.07 (4-PhC), 111.96 (1-PhC), 104.30 and 103.63 (*meso*C), 84.48 (1-GlcC), 79.94 (5-GlcC), 70.60 (3-GlcC), 68.06 (2-GlcC), 61.82 (4-GlcC), 60.43 (6-GlcC), 24.49 (CH_3), 23.91 (CH_3). **^{19}F NMR** (282.37 MHz, $CDCl_3$): δ -154.79 (6F, dd, *J* = 23.0, 11.0 Hz, 3,5-PhFGlc), -158.97 - -159.28 (6F, m, 2,6-PhFGlc), -159.59 (2F, d, *J* = 16.3 Hz, 3,5-PhF), -174.39 (1F, t, *J* = 20.9 Hz, 4-PhF), -183.91 - -185.12 (2F, m, 2,6-PhF). **UV–vis** (c = 2.30 μM, DMSO, path length = 1 cm, 25 ºC): λ/ nm (ε *x* 10^{-4}/M^{-1} cm^{-1}) = 414 (31.1), 507 (2.27), 534 (0.31), 581 (0.75), 633 (0.07). **HRMS** (ESI) (*m/z*). Found: $[M+H]^+$ 2007.2867; molecular formula $C_{86}H_{67}F_{17}N_4O_{27}S_3$ requires $[M+H]^+$ 2007.2962.

2.4.8. Synthesis of 5,10,15-tris[4-(β-D-glucopyranosylthio)-2,3,5,6-tetrafluorophenyl)]-20-bis(2,3,4,5,6-pentafluorophenyl)porphyrin ($TPPF_{17}(SGlc)_3$)

Porphyrin **$TPPF_{17}(SGlcAc)_3$** (200 mg, 99.6 μmol) was dissolved in methanol/dichloromethane (3:1, 10 mL) and treated with sodium methoxide (0.5 M solution in methanol, 3 mL). The reaction mixture was stirred at room temperature for 1.5 h and then neutralized by an aqueous citric acid solution. The mixture was filtered through a Waters Sep-Pak C18 35 cm^3 reverse-phase prep column and washed with water. The deprotected glucoporphyrin **$TPPF_{17}(SGlc)_3$** was then purified on flash chromatography (silica gel) eluted using a mixture of ethyl acetate/ methanol (3:1) and crystallized in methanol/CH_2Cl_2 (142 mg, 95%). **^{1}H NMR** (300 MHz, DMSO-d_6): δ 9.42 (2H, s, 2,18-β-pyrroleH), 9.36 (6H, s, 3,7,8,12,13,17-β-pyrroleH), 5.82 (3H, t, *J* = 5.5 Hz, GlcH), 5.34 (3H, d, *J* = 3.9 Hz, GlcH), 5.26 – 4.96 (6H, m, GlcH), 4.75 (3H, s, GlcH), 3.85 (3H, dd, *J* = 10.5, 4.7 Hz, GlcH), 3.55 (3H, dd, *J* = 11.6, 5.6 Hz, GlcH), -3.17 (s, 2H, NH). **^{13}C NMR** (125.77 MHz, DMSO-d_6): δ 147.80 – 144.67 (α,β-pyrroleC, 2,6-PhC and 3,5-PhC), 133.01 (β-pyrroleC), 129.63 (4-PhC), 119.26 (1-PhC), 104.83, 103.13 (*meso*C), 84.63 (1-GlcC), 81.89 (5-GlcC), 78.18 (3-GlcC), 74.82 (2-GlcC), 70.44 (4-GlcC), 61.48 (6-GlcC). **^{19}F NMR** (282.37 MHz, DMSO-d_6): δ -156.56 - -157.20 (6F, m, 3,5-PhFGlc), -162.53 (2F, d, *J* = 19.6 Hz, 3,5-PhF), -162.84 (6F, dd, *J* = 26.2, 9.9 Hz, 2,6-PhFGlc), -176.92 (1F, t, *J* = 22.4 Hz, 4-PhF), -158.80 (2F, dd, *J* =

34.5, 12.8 Hz, 2,6-PhF). **UV–vis** (c = 4.00 μM, DMSO, path length = 1 cm, 25 ºC): λ /nm (ε *x* 10^{-4}/M^{-1} cm^{-1}) = 413 (34.49), 506 (2.31), 536 (0.25), 580 (0.71), 632 (0.02). **HRMS** (ESI) (*m/z*). Found: $[M+H]^+$ 1503.1650; molecular formula $C_{62}H_{43}F_{17}N_4O_{15}S_3$ requires $[M+H]^+$ 1503.1694.

2.4.9. Synthesis of 1,4,8,11,15,18,22,25-octafluoro-2,3,9,10,16,17,23,24-octakis(2,3,4,6-tetra-*O*-acetyl-β–D-glucopyranosylthio)phthalocyaninato zinc (II) (ZnPc(SGlcAc)$_8$)

$ZnPcF_{16}$ (200 mg, 0.231 mmol) was treated under nitrogen with 9 equiv. of 2,3,4,6-tetra-*O*-acetylglucosylthioacetate (845 mg, 2.079 mmol) in the presence of diethyl amine (8 mL, 77.37 mmol) in dry DMF (20 mL). The reaction mixture was stirred at room temperature for 24 h. Then, the crude was evaporated to dryness and purified by flash chromatography (silica gel) using a mixture of hexane/ethyl acetate/acetone as eluent. The glucophthalocyanine **ZnPc(SGlcAc)$_8$** (540.9 mg, 65.7 %) was obtained after precipitation in CH_2Cl_2/hexane, as a green product.

2.4.10. Synthesis of 1,4,8,11,15,18,22,25-octafluoro-2,3,9,10,16,17,23,24-octakis(β-D-glucopyranosylthio)phthalocyaninato zinc (II) (ZnPc(SGlc)$_8$)

Phthalocyanine **ZnPc(SGlcAc)$_8$** (200 mg, 55.2 μmol) was dissolved in methanol/dichloromethane (3:1, 30 mL) and treated with sodium methoxide (0.5 M solution in methanol, 4 mL). The reaction mixture was stirred at room temperature for 24 h and then neutralized by an aqueous citric acid solution. The mixture was filtered through a Waters Sep-Pak C18 35 cm^3 reversed-phase prep column and washed with water, thus affording the deprotected glucophthalocyanine **ZnPc(SGlc)$_8$** (83.7 mg, 67%).

2.4.11. Synthesis of magnetic nanoparticles coated with silica (Fe_3O_4@SiO_2-$PrNH_2$)

$FeNH_4(SO_4)_2$ (2.95 g) and $(NH_4)_2Fe(SO_4)_2$ (1.20 g) were dissolved in deionized water (100 mL) with vigorous stirring at 80 °C. $NH_3 \cdot H_2O$ 25% (3.5 mL) was then added

dropwise to the solution. The color of the bulk solution immediately changed from orange to black. The magnetite precipitate was washed twice with deionized water. Sodium metasilicate (23.75 g) was dissolved in deionized water, and the pH value of the solution was adjusted to *ca.* 12 by the addition of a required amount of concentrated hydrochloric acid (37%). The sodium metasilicate solution and the prepared Fe_3O_4 nanocores were poured into a beaker equipped with a mechanical stirrer. The mixture was ultrasonicated for 30 min. Then, the temperature of the mixture was increased to 80 °C. HCl was added dropwise to adjust the pH value to 6-7. The precipitate was washed several times with deionized water and then dispersed in ethanol (800 mL). (3-Aminopropyl)triethoxysilane (APTES) was added to the suspension and the resulting mixture was magnetically stirred at room temperature for 24 h. The precipitate was washed several times with ethanol, and the magnetic nanoparticles were purified by magnetic decantation and then dispersed in the same solvent (600 mL).

2.4.12. Synthesis of the Nanomagnet-Photosensitizer hybrids

Magnetic silica nanoparticles were filtered through a polyamide membrane; then 250 mg of MNPs (371.5 µmol of aminopropyl groups, 20 equiv.) were resuspended in DMSO (1 mL). A solution of each porphyrin and phthalocyanine (18.65 µmol) in DMSO (5 mL) was added to that suspension and the resulting mixture was magnetically stirred at 160 °C during 24 h in case of **$TPPF_{20}$**, **$TPPF_{17}(SGlc)_3$** and **$ZnPcF_{16}$**, and 96 h in case of **$TPPF_{16}(SGlc)_4$** and **$ZnPcF_8(SGlc)_8$**. A red (**NP-$TPPF_{20}$**, **NP-$TPPF_{16}(SGlc)_4$**, **NP-$TPPF_{17}(SGlc)_3$**), dark blue (**NP-$ZnPcF_{16}$**) or green (**NP-$ZnPcF_8(SGlc)_8$**) insoluble product was obtained. The immobilization of the PSs was monitored by TLC. The resulting hybrid materials were washed with the appropriate solvent (*ca*. 1500 mL) (Table 1) until the typical Soret and Q bands were no longer observed in the rinse solvent. The amount of unreacted PS was calculated by UV-vis spectrophotometry.

2.4.13. Photostability tests

The photostability of the PSs was evaluated by exposing aqueous solutions of a non-immobilized PS at 2 µM or an aqueous suspension of NP-PS at 2 µM, under white light irradiation (4 $mW \cdot cm^{-2}$), at room temperature, with vigorous magnetic stirring, for 180 min.

At fixed intervals of time, visible absorption spectra of the samples were recorded. To evaluate the stability of the PSs in water, a procedure similar to that described above but in dark conditions was performed.

2.4.14. pH stability test

The stability of the PSs at different pH conditions was evaluated in aqueous solutions of the non-immobilized PSs at 2 µM, or aqueous suspensions of NP-PSs at 2 µM, by adjusting pH (unmodified samples presented pH 6) with HCl 10% vol. to pH 3, 4 and 5, with saturated $NaHCO_3$ to pH 7 and 8, or with NaOH 10 M to pH 9 and 10. Samples were kept under agitation and at room temperature for 24 h. UV-vis absorption spectra of samples containing non-immobilized PSs were recorded at time 0 and 24 h. To evaluate a possible cleavage of the Pors and/or Pcs from the NP-PSs after 24 h, samples were filtered with polyvinylidene fluoride (PVDF) syringe filters with a 0.22 µm pore size, and the UV-vis absorption spectra of each filtrate was recorded. In addition, DLS measurements of NP-PSs suspensions in water at different pH were recorded.

2.4.15. Determination of sensitized $^1O_2$ generation

$^1O_2$ was qualitatively determined by a chemical method using 1,3-diphenylisobenzofuran (DPBF) as $^1O_2$ scavenger. Samples in DMF/water (9:1) containing 0.5, 2.0 or 5.0 µM of a PS and 50 µM of DPBF were irradiated with a red LED array, at a fluence rate of 4.0 mW cm^{-2}. Another sample in DMF/water (9:1) containing just DPBF 50 µM was submitted to the same irradiation conditions as control of direct photolysis. The LED array was composed of a matrix of 6 × 8 LEDs, thus making a total of 48 light sources, with an emission peak at 640 nm and a bandwidth at half maximum of ± 20 nm. During the irradiation, the solutions of non-immobilized PSs or suspensions of NPs-NPs, as well as the control sample were kept under vigorous stirring at room temperature. The generation of $^1O_2$ was followed by its reaction with DPBF. The breakdown of DPBF was monitored by measuring the decrease of the absorbance at 413 nm.

2.4.16. Determination of sensitized generation of radicals

Indirect determination of radicals generated by the PSs was performed by using sodium azide (NaN_3) as $^1O_2$ quencher.[142] To that end, 50 mL of aqueous samples containing E2 (5 $mg \cdot L^{-1}$) and NaN_3 (100 mM) were kept under artificial white light irradiation of 4 $mW \cdot cm^{-2}$,[143] in the presence of each free PS at 5 µM for 90 min, or in the presence of each NP-PS for 8 h. A light control sample containing 5 $mg \cdot L^{-1}$ of E2, without PS nor NaN_3, and submitted to the same irradiation conditions, was included. An additional control sample containing just E2 (5 $mg \cdot L^{-1}$) and NaN_3 (100 mM) was also included. The final concentration of E2 in the samples was determined by HPLC coupled to an UV detector. See details in Section 2.4.19 (quantification of E2).

2.4.17. Photodegradation of E2 in batch mode

Photodegradation studies in batch were performed using 100 mL cylindrical glasses. The photocatalytic activity of the PSs was evaluated in the degradation of 50 mL of aqueous samples containing 5 $mg \cdot L^{-1}$ of E2 under visible light irradiation (4 $mW \cdot cm^{-2}$) with different concentrations of a non-immobilized PS (2.5, 5.0 and 10.0 µM) or a NP-PS at 10 µM. The stock solution of E2 was prepared at 1.84 mM (500 $mg \cdot L^{-1}$) in DMSO. Preparation of samples consisted in dispersing appropriate volumes of stock solutions of PSs and E2 in water until the desired concentration. Two control samples were included in each irradiation experiment: a light control containing 5 $mg \cdot L^{-1}$ of E2, without PS, and submitted to the same irradiation conditions as the samples, and a dark control containing 5 $mg \cdot L^{-1}$ of E2 and the PS at the highest concentration (10.0 µM), but kept in dark conditions.

In order to estimate the reproducibility of the experimental results, photodegradation experiments were carried out in triplicate, showing in the graphs the average value corresponding for each experimental condition.

2.4.18. Photodegradation of E2 in flow mode

The flow visible-light phototreatment of E2 was carried out in a set up consisting in a light-transparent tubing of fluorinated ethylene propylene (FEP), with an inner diameter of

0.8 mm and outer diameter of 1.6 mm. The tube was mounted on a flatbed to obtain parallel reactor channels with a total reactor volume of 2 mL. After appropriate homogenization, samples in the reservoir (50 mL of aqueous solutions containing 5 $mg \cdot L^{-1}$ of E2 and a PS or NP-PS at 10 µM) were pumped by a rotary piston pump (REGLO-CPF Digital, Ismatec, Wertheim, Germany) through the photo-reactor with flow rates ranging from 0.1 to 0.4 $mL \cdot min^{-1}$ while exposed to white light irradiation (4 $mW \cdot cm^{-2}$). Light and dark control samples were included in each irradiation experiment.

Photodegradation studies with NP-PSs were done with different residence times (0-60 min), loads of photocatalyst (NP-PS at 10, 15 and 20 µM) and pH (4, 6 and 8). pH values were adjusted using NaOH 10 M and HCl 1M.

2.4.19. Quantification of E2

Quantification of E2 was calculated by using HPLC-UV. Aliquots (20 µL) of the samples collected at different times during the phototreatment process were injected without any further sample preparation in case of non-immobilized PSs, or after filtration with a PVDF syringe filter with a 0.22 µm pore size in case of NP-PS, into an HPLC column with UV detection at 200 nm. Separation was achieved on a VDSPher 100 C18-E column (5 µm, 250 *x* 4.6 mm). The mobile phase was a mixture of acetonitrile and Millipore water 3:1 (v/v) with a flow rate of 1.0 $mL \cdot min^{-1}$ in isocratic mode.

CHAPTER 3

ANTIMICROBIAL PHOTODYNAMIC ACTIVITY OF CATIONIC NANOPARTICLES DECORATED WITH GLYCOSYLATED PORPHYRINS OR PHTHALOCYANINES FOR WATER DISINFECTION

Fernández, L., Lin, Z., Schneider, R.J., Esteves, V.I., Cunha, Â, Tomé, J.P.C., Antimicrobial photodynamic activity of cationic nanoparticles decorated with glycosylated porphyrins or phthalocyanines for water disinfection. Under preparation

Summary

The antimicrobial photodynamic approach has been demonstrated as efficient and sustainable for the eradication of microbial pathogens.

The use of silica-coated magnetite nanoparticles as carrier of porphyrins and phthalocyanines, and its subsequent cationization, has resulted in the production of stable and efficient antimicrobial photosensitizing materials against Escherichia Coli. The effect of the photosensitizer glycosylation and size distribution of the nanomaterials in water are discussed. These biocide agents showed to be photostable and maintained their photoactivity performance upon 5 PDI cycles, which makes them promising materials for water disinfection purposes.

3.1 Introduction

Along with the presence of pollutants, the emergence of waterborne pathogens represents a global challenge in ensuring affordable access to clean water. In developing countries, access to both safe and readily drinking water and adequate sanitation are not the rule, and waterborne diseases are common.[144] The term waterborne disease refers to infections caused by the ingestion of water contaminated by human or animal faeces or urine containing pathogenic microorganisms, such as bacteria and viruses.[145] Water related diseases cause between 2 and 5 million deaths each year.[146] Some of most common diseases caused by contaminated water include cholera, dysentery, gastroenteritis, typhoid fever and acute diarrhea.[147]

Among methods for water disinfection, the use of chlorine is considered as one of the most efficient. It is effective against a broad range of microbes and it is inexpensive and easy to use. However, the use of chlorine does not assure the inactivation of parasites, it affects odour and taste, and can lead to harmful disinfection by-products (DBPs).[148] The safety issues related to large storage quantities of chlorine represents also a significant concern in terms of industrial accidents and the possibility of being used as a chemical weapon.[149] Alternative methods, such as the use of ozone, UV light or antibiotics, also have drawbacks namely related with costs, efficiency, mutagenic effects and development of microbial resistance,[150] and the nature of the formed disinfection by-products (DPBs).[151] In this context, new technologies for water treatment have emerged in recent years.

Photodynamic inactivation of microorganisms (PDI) may offer advantages over conventional processes of water remediation, circumventing microbial resistance against antibiotics.[152] In addition, it represents a broad-range approach since it reduces the survival of bacteria (Gram-positive and Gram-negative), fungi, viruses and parasites.[153] PDI involves the simultaneous presence of a photosensitizer (PS), visible light and oxygen, to produce reactive oxygen species (ROS), mainly singlet oxygen ($^1O_2$). ROS cause oxidative damage and eventually lethal effects on cells.[154] Gram-negative bacteria are typically characterized by an impermeable outer cell membrane, which protects the cell from exogenous agents. However, positive charges in the PS improve PS binding to the negatively charged cell wall of Gram-negative bacteria, which increases membrane permeability and improves the PDI efficiency.[155]

Two common problems of PDI agents are their susceptibility to form non-photoactive aggregates and their tendency to undergo photobleaching. Water solubility[155] and

photostability[156] determine the efficiency of PSs in most applications. Addressing the molecular basis of PS performance may help to overcome these limitations. PSs selected in this work are the ones described in Chapter 2: **$TPPF_{20}$**, **$TPPF_{16}(SGlc)_4$**, **$TPPF_{17}(SGlc)_3$**, **$ZnPcF_{16}$** and **$ZnPcF_8(SGlc)_8$**. Polyfluorinated PSs decorated with thioglucose units as hydrophilic agents present improved resistance to both photobleaching[157] and aggregation.[158] In Por and Pc macrocyclic aromatic systems, fluorine substituents bear substantial negative charges, removing electron density from the aromatic system, and therefore providing an increased photostability. Both Pors and Pcs present high absorption coefficients in the spectral region of blue light, which penetrates more efficiently in aqueous media. In addition, the high absorption coefficient of Pcs in the red region of the spectrum makes them also potential candidates for other applications.

The attachment of the PS to a magnetic nanostructured support may be a useful strategy,[159] thus obtaining a more sable PS which can be recovered in a fast, easy and inexpensive way.[160] Previous results of our group have demonstrated the efficient PDI of a Gram-negative bacterium (*Allivibrio fischeri*) using cationic nanomagnet-porphyrin hybrids with a Fe_3O_4 or a $CoFe_2O_4$ core.[94] The recycling and reuse capabilities of these hybrid materials were also proven.

This work describes the cationization of nanomagnet-PS hybrids described in Chapter 2: **NP-$TPPF_{20}$**, **NP-$TPPF_{16}(SGlc)_4$**, **NP-$TPPF_{17}(SGlc)_3$**, **NP-$ZnPcF_{16}$** and **NP-$ZnPcF_8(SGlc)_8$**; and their evaluation as PDI agents. With the introduction of positive charges in the outer shell of the NPs, an improvement on both water stability and PDI efficacy is expected.

3.2 Results and discussion

3.2.1 Preparation of NP^+-PS

Pors and Pcs immobilized onto NPs constituted by a nucleus of Fe_3O_4 and coated with silica described in Chapter 2, **NP-$TPPF_{20}$**, **NP-$TPPF_{16}(SGlc)_4$**, **NP-$TPPF_{17}(SGlc)_3$**, **NP-$ZnPcF_{16}$** and **NP-$ZnPcF_8(SGlc)_8$**, were cationized using a large excess of methyl iodide in DMF at 40 ºC for 16 h. NP^+-PS (**NP^+-$TPPF_{20}$**, **NP^+-$TPPF_{16}(SGlc)_4$**, **NP^+-$TPPF_{17}(SGlc)_3$**, **NP^+-$ZnPcF_{16}$** and **NP^+-$ZnPcF_8(SGlc)_8$**) were obtained after filtration, and then were washed

and resuspended in water (Scheme 3.1). In this chapter, concentration of hybrid materials (in µM), NP-PS or NP$^+$-PS, always refers to the amount of PS in the material.

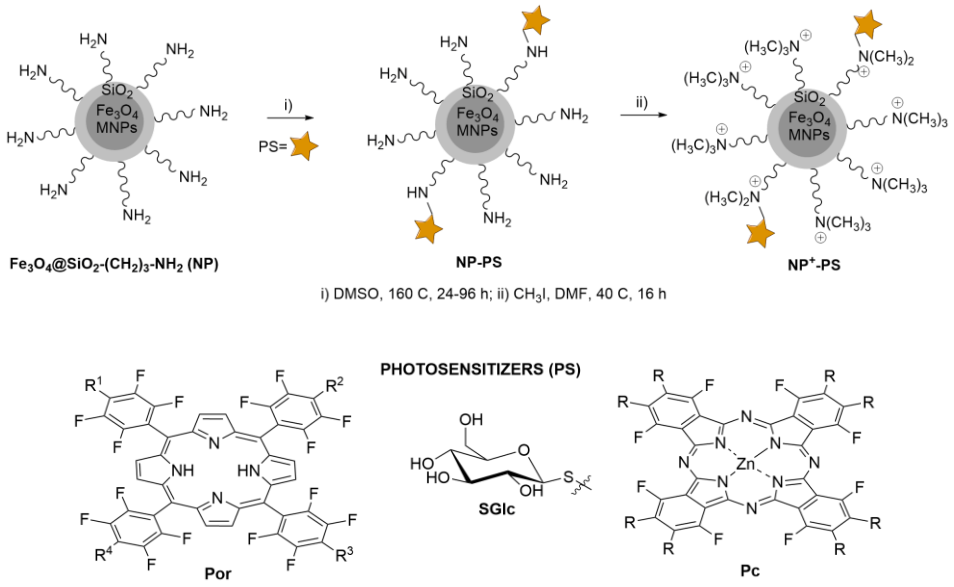

Por based PSs			ZnPc based PSs		
R	PS	NP$^+$-PS	R	PS	NP$^+$-PS
R^1=R^2=R^3=R^4= F	$TPPF_{20}$	NP$^+$-$TPPF_{20}$	F	$ZnPcF_{16}$	NP$^+$-$ZnPcF_{16}$
R^1=R^2=R^3=R^4= SGlc	$TPPF_{16}(SGlc)_4$	NP$^+$-$TPPF_{16}(SGlc)_4$	SGlc	$ZnPcF_8(SGlc)_8$	NP$^+$-$ZnPcF_8(SGlc)_8$
R^1=R^2=R^3= SGlc; R^4= F	$TPPF_{17}(SGlc)_3$	NP$^+$-$TPPF_{17}(SGlc)_3$			

Scheme 3.1

3.2.2 Characterization of NP$^+$-PS

XRD spectra of NP$^+$-PS powders confirmed that magnetite is the main crystal phase in the hybrid materials, presenting peaks centred at 2Θ 18.4º, 29.7º, 35.4º, 37.1º, 43.1º, 53.5º and 57.1º (Fig. 3.1). The hump between 2Θ 17º and 27º belongs to the amorphous silica shell. Peaks belonging to PS are not visible, maybe due to a minor containing in the final material.

Due to their magnetic properties, Fe_3O_4 based NPs can be easily recovered from the aqueous medium after 2 minutes of applying an external magnetic field (Fig. 3.2a). This valuable feature is useful to recycle and reuse NP$^+$-PS. However, these materials are also prone to form aggregates in solution, as typical TEM images show (Fig. 3.2b). Average particle size is below 10 nm, but aggregates of variable number of NPs are prevalent, which suggests that a good homogenization of NP$^+$-PS before employing them will be relevant.

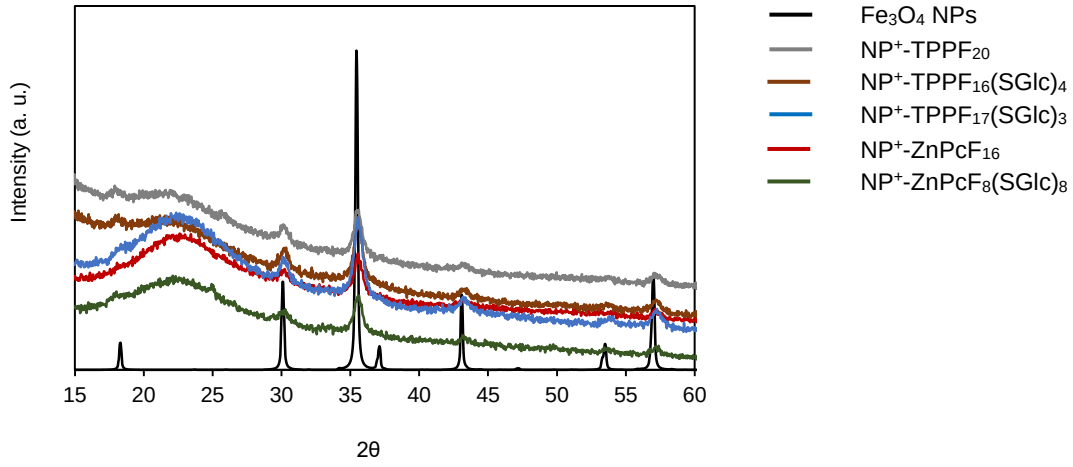

Figure 3.1. XRD powder spectra of the cationic hybrid materials. Patterns show that magnetite is the main crystal phase.

a)

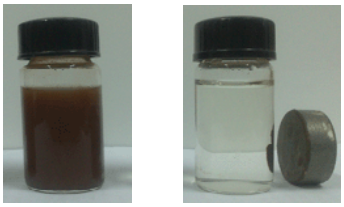

b)

NP⁺-TPPF$_{17}$(SGlc)$_3$ **NP⁺-ZnPcF$_8$(SGlc)$_8$**

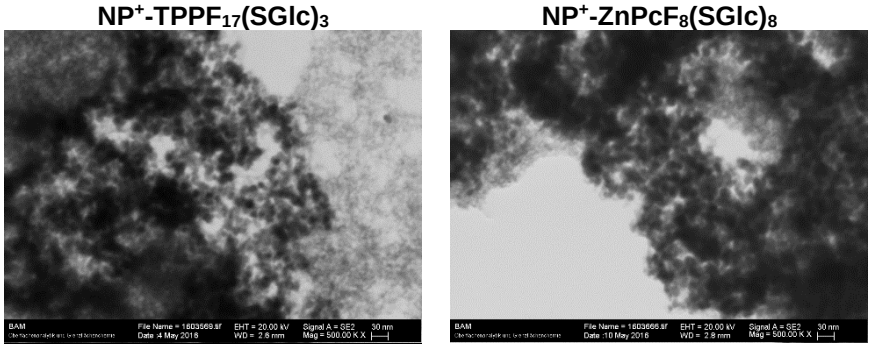

Figure 3.2. a) Photographs of aqueous dispersions of **NP⁺-TPPF$_{17}$(SGlc)$_3$** in vials without and in presence of a magnetic field for 2 minutes; b) TEM images of **NP⁺-TPPF$_{17}$(SGlc)$_3$** and **NP⁺-ZnPcF$_8$(SGlc)$_8$**, which show average particle sizes less than 10 nm.

The successful immobilization of the PS onto the NPs was confirmed by UV-Vis spectroscopy of the suspensions in water (Fig. 3.3), by the presence of the characteristic Soret band at ca. 420 nm and weak Q bands ranging between 506-636 nm in case of Por based NPs, and typical intense Q bands between 600 and 850 nm in case of Pc based PS. Absorption spectrum of **ZnPcF$_{16}$** show the poor water solubility of this PS. Absorption curves of NP-PS and their corresponding NP⁺-PS did not show significant differences.

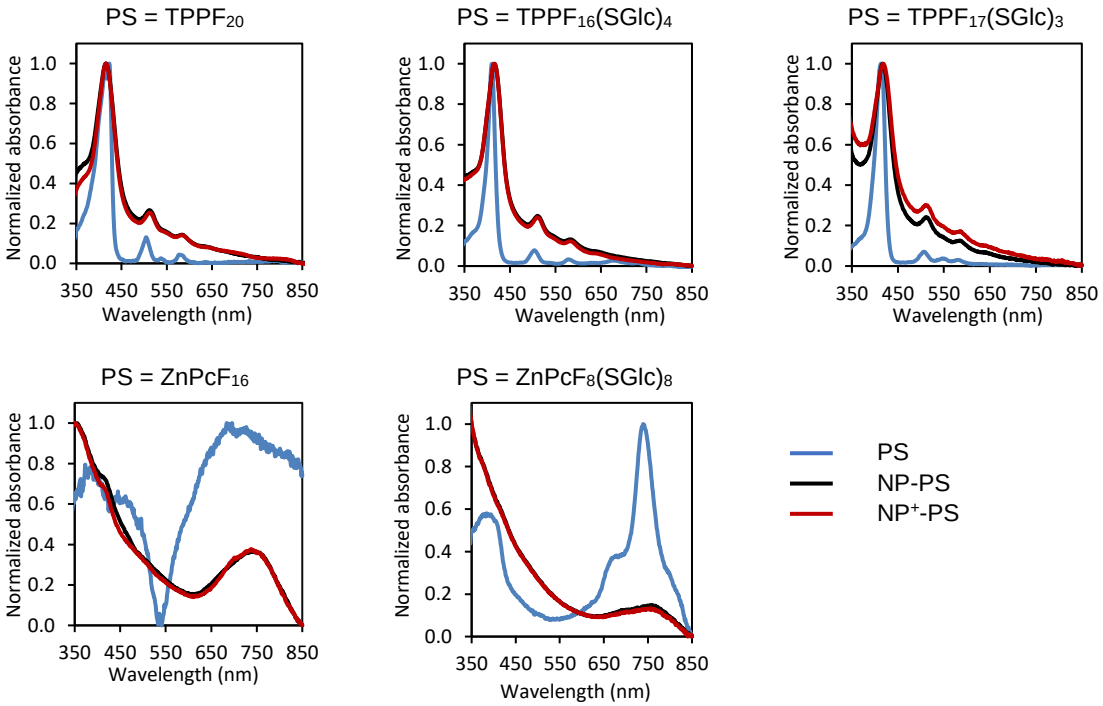

Figure 3.3. Normalized UV-Vis spectra of non-immobilized PS, NP-PS and NP^{+}-PS in water.

Water stability of NP-PS and NP^{+}-PS dispersions was investigated by size distribution analysis obtained by dynamic light scattering (DLS). Size distribution curves of NP-PS aggregates are polydisperse and show high average hydrodynamic radius, ranging from 1115.8 nm (**NP-$TPPF_{20}$**) to 295.1 nm (**NP-$TPPF_{17}(SGlc)_3$**) (Fig. 3.4).

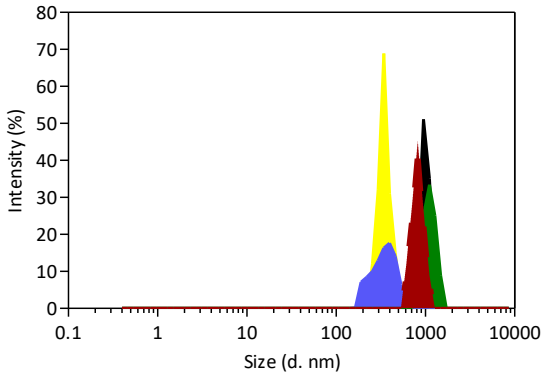

NP-PS	Average hydrodynamic radius (nm)
NP-$TPPF_{20}$	1115.8 ± 119.3
NP-$TPPF_{16}(SGlc)_4$	342.1 ± 52.6
NP-$TPPF_{17}(SGlc)_3$	295.1 ± 158.6
NP-$ZnPcF_{16}$	1100.3 ± 208.6
NP-$ZnPcF_8(SGlc)_8$	825.2 ± 381.3

Figure 3.4. Size distribution analysis of NP-PS using DLS experiments in water. Curves represent the relative population of the corresponding aggregate size given in a logarithmic scale in the x-axis.

Cationization of the amino groups in NP⁺-PSs promotes electrostatic repulsion between the surfaces of the NPs, which improves stabilization of the suspensions in water. However, **NP⁺-TPPF$_{20}$** and **NP⁺-ZnPcF$_{16}$** present broad size distributions with average hydrodynamic diameters of 1108.6 and 855.1 nm, respectively, due to aggregation of nanoparticles (Fig. 3.5).

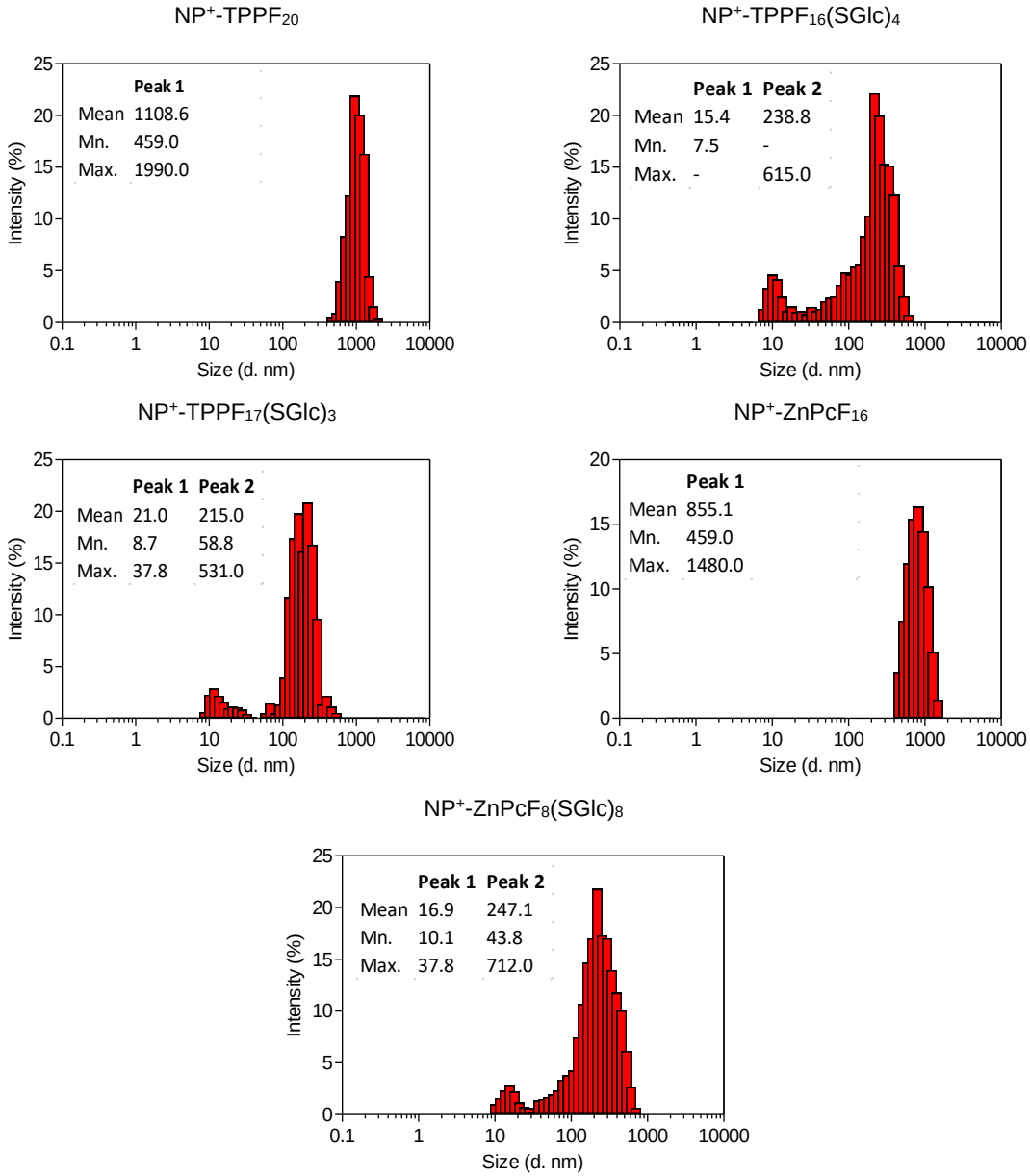

Figure 3.5. Size distribution analysis of NP⁺-PS using DLS experiments in water. Bars represent the relative population of the corresponding aggregate size given in a logarithmic scale.

NP⁺-TPPF$_{16}$(SGlc)$_4$, **NP⁺-TPPF$_{17}$(SGlc)$_3$** and **NP⁺-ZnPcF$_8$(SGlc)$_8$** present broad bimodal size distributions, with intense peaks centred at 215.0 nm (**NP⁺-TPPF$_{17}$(SGlc)$_3$**),

238.8 nm (**NP⁺-TPPF$_{16}$(SGlc)$_4$**) and 247.1 nm (**NP⁺-ZnPcF$_8$(SGlc)$_8$**). These values are in good agreement with other data obtained on magnetite NPs.[161] A second peak, centred at 21.0 nm (**NP⁺-TPPF$_{17}$(SGlc)$_3$**), 15.4 nm (**NP⁺-TPPF$_{16}$(SGlc)$_4$**) and 16.9 nm (**NP⁺-ZnPcF$_8$(SGlc)$_8$**) can be attributed to single NPs, which did not suffer from aggregation (Fig. 3.5).

The different hydrodynamic diameter of aggregates in water can be explained attending to the multiple reactive positions for the nucleophilic attack in **TPPF$_{20}$** and **ZnPcF$_{16}$**, which could have promoted the formation of polymeric materials based on several NPs linked by units of **TPPF$_{20}$** or **ZnPcF$_{16}$** (Fig. 3.6). Attachment of **TPPF$_{17}$(SGlc)$_3$** onto NPs is certain to occur by substitution of its *para* fluorine atom, while available fluorine atoms of **TPPF$_{16}$(SGlc)$_4$** and **NP⁺-ZnPcF$_8$(SGlc)$_8$**) are not so good leaving groups and nucleophilic attack is promoted in less extent.

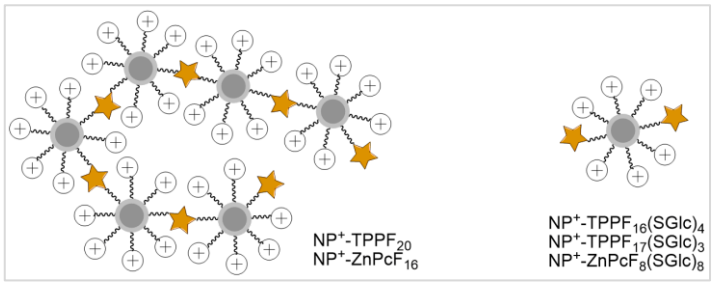

Figure 3.6. Schematic representation of NP⁺-PS according to the reactivity of the starting PS (represented by yellow stars) for covalent attachment onto NP by nucleophilic attack.

3.2.3 Evaluation of photophysical properties of NP⁺-PS

One of the characteristics that are expected from an efficient PS is the ability of generating high amounts of $^1O_2$. $^1O_2$ production for non-immobilized PS, NP-PS and NP⁺-PS, was estimated by measuring the breakdown of diphenylisobenzofuran (DPBF), in absence or in presence of a PS, under artificial white light irradiation (4 mW·cm^{-2}). Light control samples, containing just DPBF, were submitted to the same irradiation conditions for 20 minutes and showed low rates of direct photolysis (*ca.* 3.5%), consequently, a more relevant decay in the DPBF maximum of absorption in the samples containing a PS is attributed to the presence of $^1O_2$ (Fig. 3.7).

As described in Chapter 2, non-immobilized PS were the best $^1O_2$ producers. Free glycosylated Pors are more efficient in the $^1O_2$ generation than their related compound

$TPPF_{20}$, having that **$TPPF_{16}(SGlc)_4$** presents slightly better results in the degradation of DPBF than **$TPPF_{17}(SGlc)_3$**. NP-PS showed lower kinetics in $^1O_2$ generation, which can be understood due to the difficulty of oxygen to diffuse into the aggregates. Charges in NP^+-PS improved their water stability, which improved their ability to generate $^1O_2$. **NP^+-$TPPF_{17}(SGlc)_3$** presents slightly better results in the degradation of DPBF than **NP^+-$TPPF_{20}$** and **NP^+-$TPPF_{16}(SGlc)_4$**. Besides the potential as $^1O_2$ generator of the non-immobilized **$TPPF_{17}(SGlc)_3$**, **NP^+-$TPPF_{17}(SGlc)_3$** could turn out to be the most ordered material, since *para* fluorine atoms in **$TPPF_{17}(SGlc)_3$** determine the position for the nucleophilic substitution in the attachment to the NPs, which could retain better the photophysical properties of the PS.

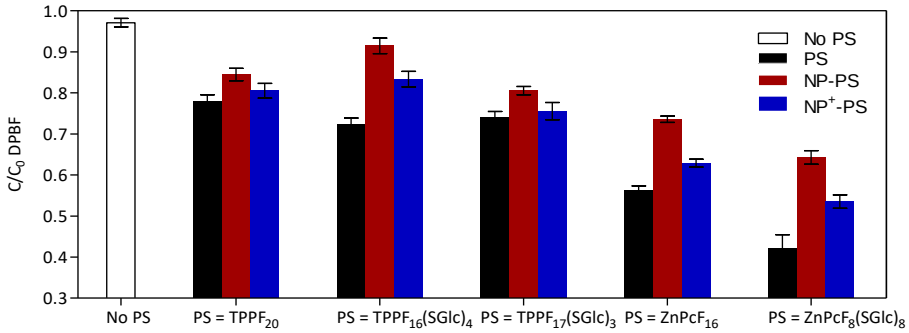

Figure 3.7. Degradation of DPBF (50 µM) in DMF/H_2O (9:1) upon irradiation with a red LED array at a fluence rate of 4.0 mW cm^{-2} and room temperature for 20 min of irradiation in absence of PS, or in presence of a Por-based PS (0.5 µM) for 20 min, or in presence of a Pc-based PS (0.5 µM) for 5 min.

In this test, samples were irradiated with red light in order to prevent direct photodegradation of DPBF, which present its maximum of absorption in the blue region of the electromagnetic spectrum. Since in the red region of the spectrum is where Pc present higher intense absorption of their Q bands, only 5 min of irradiation was required to qualitatively determine the ability to generate $^1O_2$ of Pc-based PS. Results showed a higher $^1O_2$ yield of the glycosylated derivative **NP^+-$ZnPcF_8(SGlc)_8$** when compared to its related **NP^+-$ZnPcF_{16}$**.

Photostability studies were conducted in the same conditions of irradiation of the PDI studies. The intensity of the Soret and Q bands of NP^+-PS showed that all the samples were stable upon 270 min of irradiation (Fig. 3.8). Previous studies (see Chapter 2) showed a slight decrease in intensity of the absorption bands of neutral NP-PS due to an uncertain stability of the aqueous suspensions. In view of the results, cationization improved the

stability of water suspensions of hybrid materials, which would also explain the better photophysical features in $^1O_2$ generation.

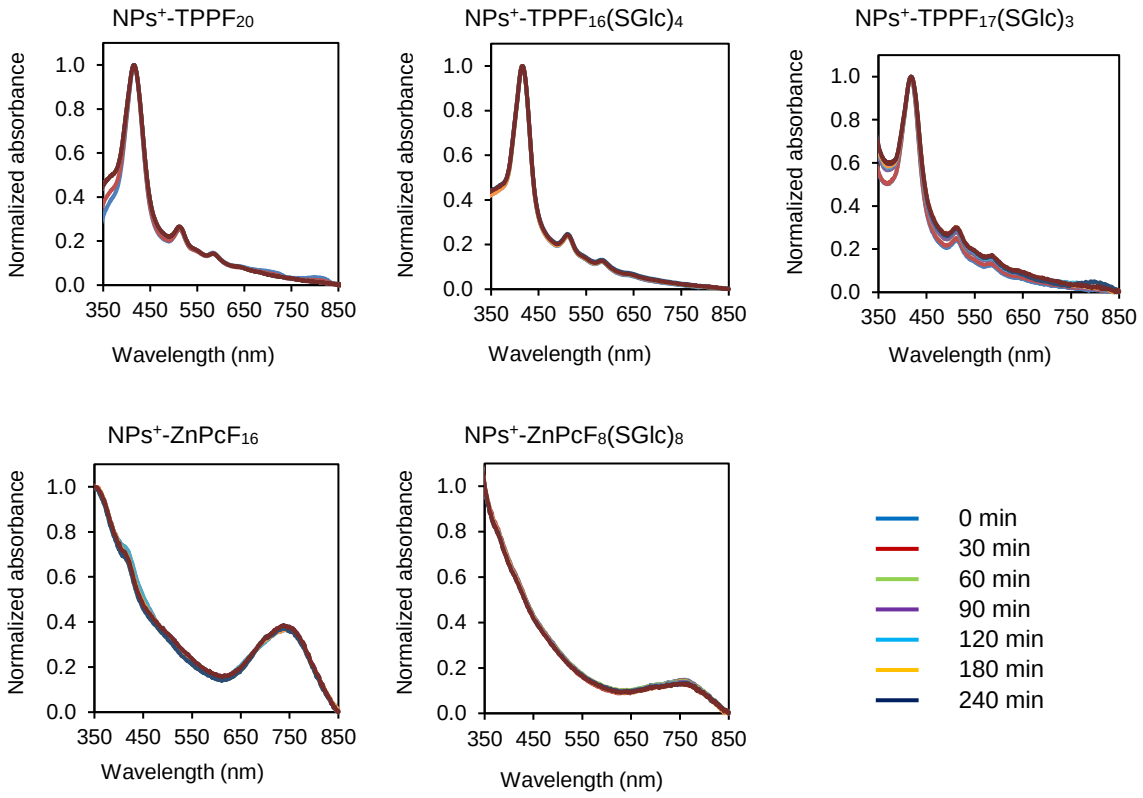

Figure 3.8. UV-Vis absorption spectra of aqueous suspensions of hybrid materials at 2 µM upon different times of artificial white light irradiation at 4 mW·cm^{-2}.

3.2.4 Bioluminescence versus viable counts of an overnight culture of *E. coli*

To assess the correlation between colony counts and the bioluminescent signal of the indicator *E. coli* strain, an overnight culture of bioluminescent *E. coli* was serially diluted in phosphate buffer saline solution (PBS). Light emission of the non-diluted and diluted aliquots was read in a luminometer and simultaneously, and 1 mL of each dilution was pour plated in TSA medium for colony counting. Three independent experiments were conducted and the results were averaged and represented as displays Fig. 3.9, showing that, bioluminescence and viable counts of a growing culture of recombinant *E. coli* presented a linear relationship.

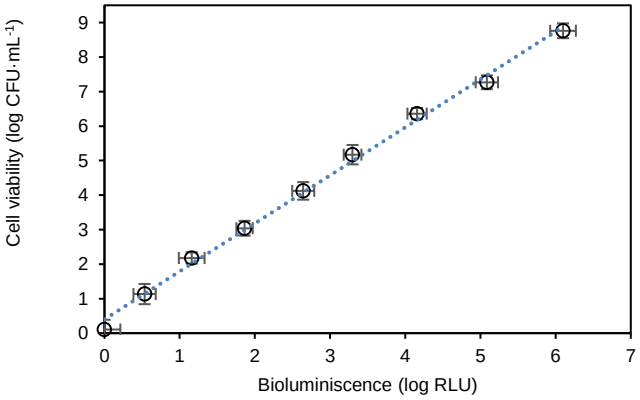

Figure 3.9. Relation between bioluminescence and viable counts in overnight cultures of recombinant *E. coli* (≈ 10^8 CFU·mL^{-1}); R^2 = 0.9964. Values represent the mean of three independent experiments; error bars indicate the standard deviation.

3.2.5 Photosensitization of *E. coli*

Waterborne Gram-negative bacteria, such as *Vibrio cholera*, *Vibrio parahaemolyticus*, *Salmonella enterica*, *Shigella dysenteriae* and *Escherichia coli*, are responsible for many life-threating infections in humans.[145] While Gram-positive bacteria have a thick and porous cell wall of interconnected peptidoglycan layers that surround a cytoplasmic membrane, Gram-negative bacteria present an outer membrane, a thinner peptidoglycan layer and a cytoplasmic membrane.[162] To perform antimicrobial photodynamic therapy, the accumulation of the PS in the bacteria is a prerequisite for cell death.[163] A positively charged PS can achieve an efficient interaction with the Gram-negative bacterial cell wall, which is negatively charged due to, for instance, teichoic acid residues, thus circumventing the difficulty to interact with the complex cell wall. Positive charges bind to the surface and displace cations, thereby changing the arrangement of the lipopolysaccharide external coat, which results in an alteration of the barrier properties of cell wall. This allows the penetration of the PS and enables the further photosensitization process of Gram-negative bacteria (Fig. 3.10).[164] Herein, we tested hybrid materials consisting in an effective PS (as $^1O_2$ generator), which does not possess any intrinsic cationic charges, attached to polycationic NPs, favouring the synergistic combination of the final photoactive materials.

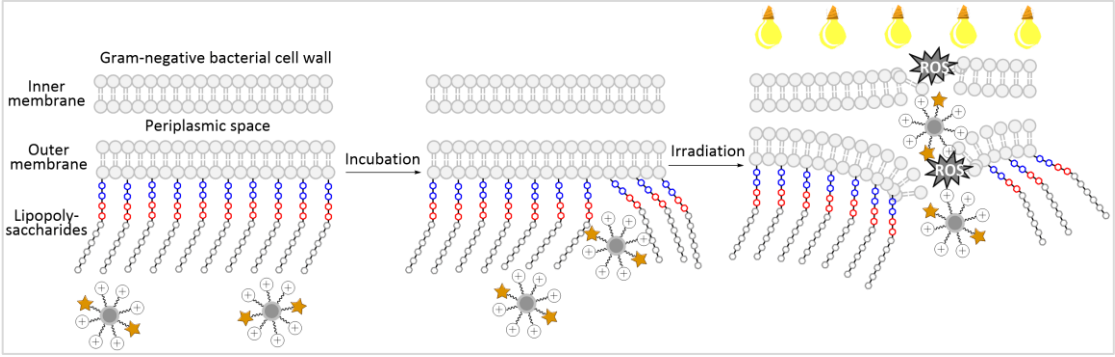

Figure 3.10. Schematic illustration of PDI mechanism of NP^{+}-PS on *E. Coli* as a model Gram-negative bacteria.

The photocytotoxicity action of PS, NP-PS or NP^{+}-PS against a recombinant bioluminescent *E. coli* was assessed by exposing the cells with the photosensitizers at 10 or 20 μM to artificial white light (4 $mW \cdot cm^{-2}$) during different irradiation periods (15, 30, 60, 90, 120, 150, 180, 240 and 270 min). Results of control experiments (data not shown) showed that viability of *E. coli* was affected neither by irradiation itself (light control) nor by any of the photosensitizer tested (dark control). This fact indicates that cell viability reduction observed after irradiation of the treated samples is due to the photosensitization effect of PS, NP-PS or NP^{+}-PS. Among non-immobilized PS (20 μM), no considerable decrease in cell survival was observed in the presence of **$TPPF_{20}$** and **$ZnPcF_{16}$** (Fig. 3.11a). The corresponding glycosylated derivatives showed evidence of a photosensitizing effect with a decrease of 2.3 log (**$TPPF_{16}(SGlc)_4$**), 2.8 log (**$TPPF_{17}(SGlc)_3$**) and 2.6 log (**$ZnPcF_8(SGlc)_8$**) on bioluminescence signal after 270 min of irradiation. Results suggest a positive effect of the PS glycosylation over the PDI efficiency, which could be explained due to a higher efficiency as $^1O_2$ generators, a better solubilisation in water, and/or certain interactions between glucose units and the outer cell membrane. However, several non-immobilized cationic PS have been already documented as more promising PDI agents against *E. coli* at lower concentrations and irradiation times of exposure.[44, 155, 165] The five neutral hybrid materials were tested under the same conditions in PDI experiments and all showed to be even less efficient against *E. coli* (Fig. 3.11b).

In previous studies, Carvalho *et. al* showed that positive charges in the PS of a NP^{+}-PS were essential to achieve a significant photoinactivation of *E. coli,* concluding that positive charges in the nanomaterial play other important roles, such as the stabilization in water suspensions.[93] However, the neutral **$TPPF_{16}(SGlc)_4$**, **$TPPF_{17}(SGlc)_3$** and **$ZnPcF_8(SGlc)_8$**, which were not particularly efficient *per se* as PDI agents, could efficiently inactivate *E. coli* after conjugation to NPs which were further cationized. Their

corresponding **NP⁺-PS** at 10 µM showed already better biocide activity against *E. coli* during 270 min of irradiation than their related precursors at 20 µM, being able to induce a decrease of 2.6 log (**NP⁺-TPPF$_{16}$SGlc)$_4$**), 3.8 log (**NP⁺-TPPF$_{17}$(SGlc)$_3$**) and 3.3 log (**NP⁺-ZnPcF$_8$(SGlc)$_8$**) on the bioluminescence signal (Fig. 3.12a). On the other hand, the slight decrease of the bioluminescence signal in tests with **NP⁺-TPPF$_{20}$** and **NP⁺-ZnPcF$_{16}$** was only due to the adsorption capacity of the silica shell of the materials to host bacterial cells, since these values coincided well with the ones obtained in dark control tests. These results indicate that not only a positively charged support carrying a PS is needed for the PDI effect.

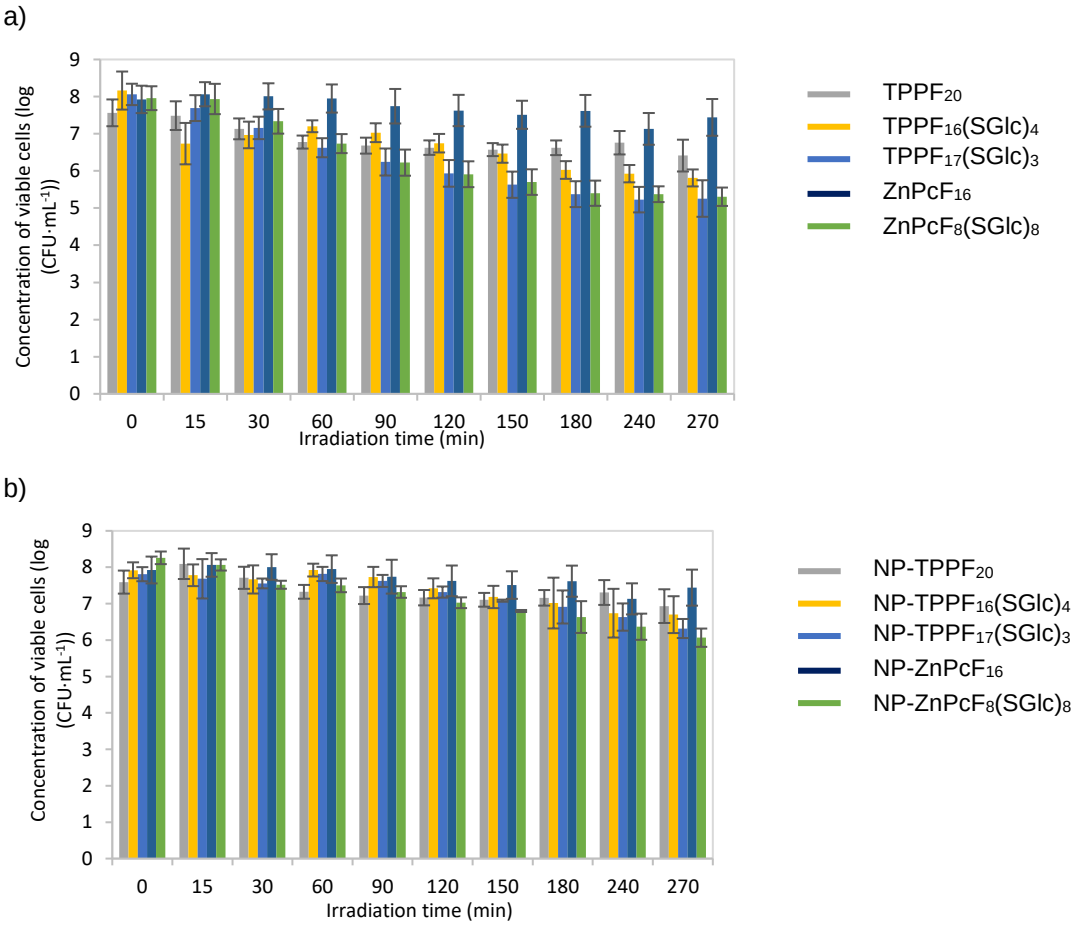

Figure 3.11. Photodynamic inactivation of *E. coli* with a) 20 µM of non-immobilized PS or b) neutral nanomagnet-photosensitizer hybrid (NP-PS). Tests were performed under permanent magnetic stirring (mean ± standard deviation of three PDI experiments of 270 min with a fluence rate of 4 mW·m^{-2}).

Previous studies have demonstrated the efficiency as PDI agents of neutral porphyrins conjugated to cationic moieties. Reddi *et. al* described the preparation of 5-(4-carboxyphenyl)-10,15,20-triphenylporphyrin anchored to cationic peptides, which exhibited

strong interaction capability as well as photoactivity towards *E. coli* and eukaryotic cells, namely, human fibroblasts.[166] The glycosylation derivatization of a PS could have beneficial effects on the photodynamic performance. Sugars in culture media are easily used for cell growth. Because of the ubiquitous metabolic requirements for sugar, microorganisms frequently possess a variety of transport pathways (sometimes called carriers, porters or permeases) to cope with sugar availability under different environmental conditions.[167] Group translocation systems, more commonly known as the phosphotransferase system in *E. coli*, are used primarily for the transport of sugars. An interaction between PS-thioglucose and these carriers could promote the accumulation in the membrane, essential for PDI efficient processes. This assumption can also explain the data obtained in PDI tests with non-immobilized PS.

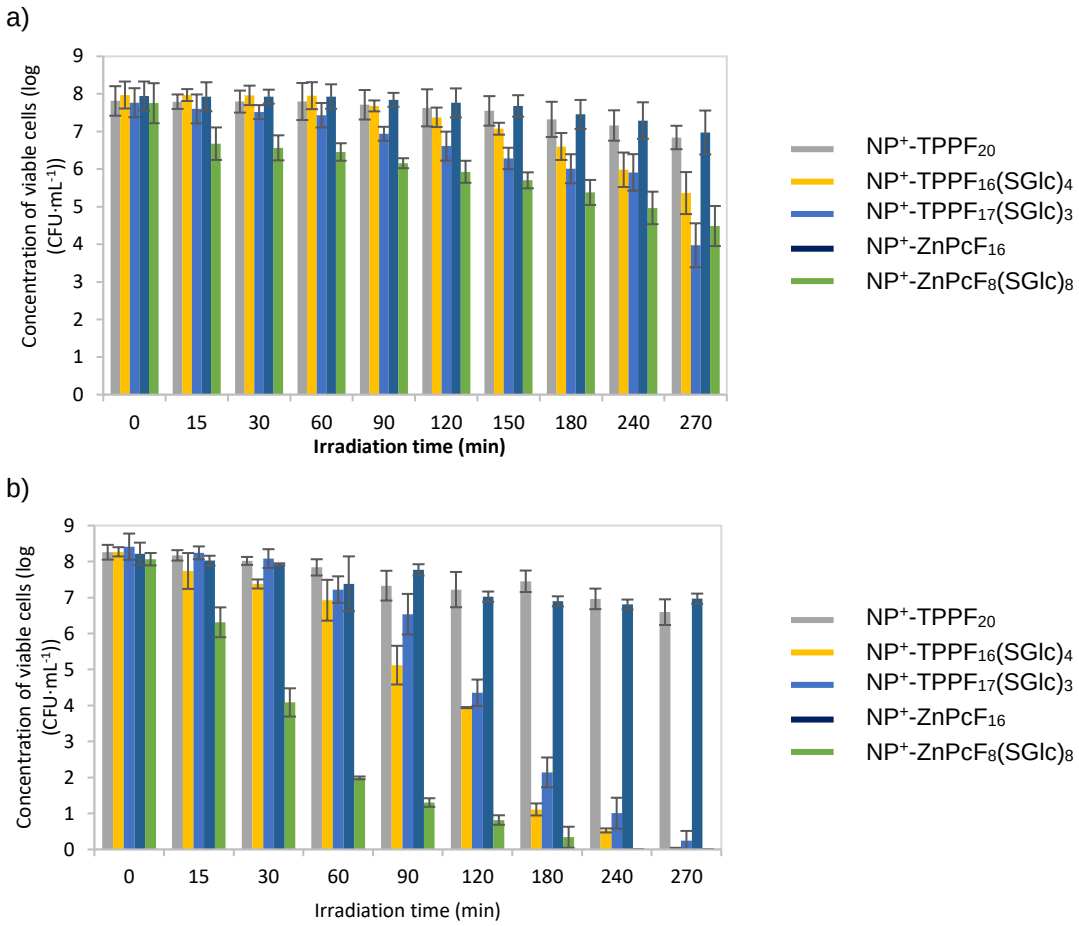

Figure 3.12. Photodynamic inactivation of *E. coli* with a) 10 or b) 20 µM of cationic nanomagnet photosensitizer hybrid (NP^+-PS). Tests were performed under a permanent magnetic stirring (mean ± standard deviation of three PDI experiments of 270 min with a fluence rate of 4 $mW \cdot m^{-2}$).

Additionally, **NP$^+$-TPPF$_{16}$(SGlc)$_4$**, **NP$^+$-TPPF$_{17}$(SGlc)$_3$** and **NP$^+$-ZnPcF$_8$(SGlc)$_8$** present a bimodal size distribution of the aggregates in water, with small NPs of hydrodynamic diameters between 7.5 and 38 nm, which could better diffuse among the cell membrane. Evidences of the influence of scaffold size of NPs on bactericidal activity have been reported.[168]

Biological results using NP$^+$-PS at 20 μM (Fig. 3.12b) confirmed that **NP$^+$-ZnPcF$_8$(SGlc)$_8$** was the most effective material against *E. coli*, where only 240 min were necessary to achieve the complete photoinactivation. **NP$^+$-TPPF$_{16}$(SGlc)$_4$** was the second material more effective, causing total cell death after 270 min of irradiation. **NP$^+$-TPPF$_{17}$(SGlc)$_3$** induced a decrease of ≈8 log on the bioluminescence signal, which was almost a total inactivation of cells.

3.2.6 Recycling of NP$^+$-PS in successive PDI cycles

Previous studies of PDI recycling tests with NP$^+$-PS showed that PDI efficiency suffered a decrease of ≈1.5 log units on the bioluminescence signal in the second cycle, and that this loss of photosensitizention capacity was even more pronounced in the third cycle. This effect was thought to be related with the loss of small active particles disaggregated from the large hybrid clusters, caused by the sonication of the recycled NP$^+$-PS stock suspensions before each PDI cycle.[94] To overcome this, NP$^+$-PS were magnetically recovered and washed with ethanol and water by manually shaking after each run, and then were tested under the same PDI test conditions, avoiding always the use of sonication treatment. Starting bacterial suspension contained log (RLU)= 7.9 ± 0.3. The three materials presented a similar behaviour among 5 recycling runs, in which photosensitization activity was retained and the loss of PDI efficiency was not so pronounced as previous studies (Fig. 3.13). After 5 runs, efficiency suffered a decrease of 1.9 log (**TPPF$_{16}$(SGlc)$_4$**), 1.8 log (**TPPF$_{17}$(SGlc)$_3$**) and 2.2 log (**ZnPcF$_8$(SGlc)$_8$**) on the bioluminescence signal. This drop in photosensitization efficiency can be attributed to the loss of NP$^+$-PS during recycling treatments.

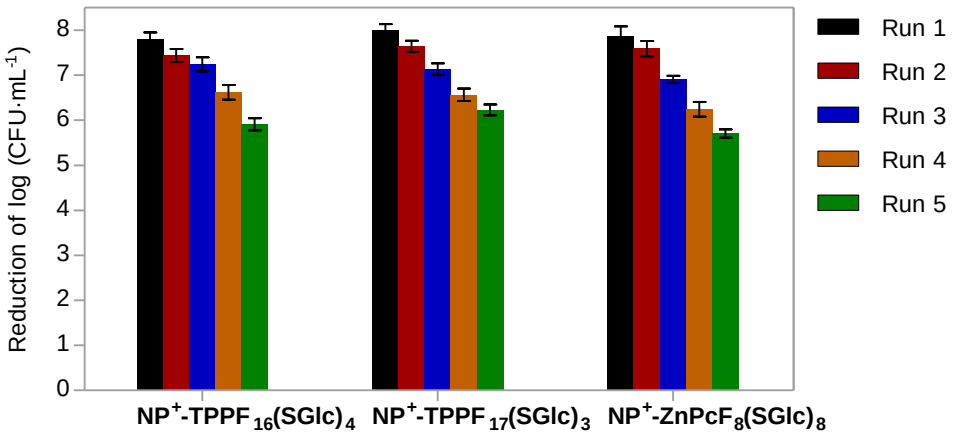

Figure 3.13. Photodynamic inactivation of *E. coli* (starting bacterial suspension contained log (RLU)= 7.9 ± 0.3) with recycling of materials, conducted at a concentration of 20 μM of **NP^+-$TPPF_{16}(SGlc)_4$**, **NP^+-$TPPF_{17}(SGlc)_3$**, or **NP^+-$ZnPcF_8(SGlc)_8$**, under a permanent magnetic field (mean ± standard deviation of three PDI cycles of 270 min with a fluence rate of 4 $mW \cdot m^{-2}$).

Conclusions

The novel cationic nanomagnet-photosensitizer hybrids based on glycosylated porphyrins or phthalocyanines, **NP^+-$TPPF_{16}(SGlc)_4$**, **NP^+-$TPPF_{17}(SGlc)_3$** and **NP^+-$ZnPcF_8(SGlc)_8$**, can be considered as high efficient materials for the photodynamic inactivation of *E. coli*. Aggregates of the three materials in water presented a bimodal size distribution, formed by large clusters of agglomerated NPs and small NPs with hydrodynamic diameters between 7.5 and 38 nm, which could better diffuse among the cell membrane. Glycosylation of the PS showed a beneficial effect on the photosensitizing performance, which can be understood as a result of the interaction between thioglucose units and the outer cell membrane of *E. coli*, which would induce a better accumulation of NP^+-PS. **NP^+-$ZnPcF_8(SGlc)_8$** was the most effective material, causing complete inactivation (to the limit of detection) at 20 μM upon 240 min of white light irradiation at 4mW·cm^{-2}. In addition, the recovery and recycling of NP^+-PS indicated the viability of these materials, as the drop of PDI efficiency was not very pronounced after 5 cycles.

3.3 Experimental section

3.3.1 Apparatus and characterization

Absorption spectra of liquid samples were recorded using a Shimadzu UV-2501-PC. Absorption spectra of solid samples were recorded using a Jasco V-560 with an integrating sphere ISV-469. Powder XRD spectra were performed in the range 10-90° 2θ on a Philips X'pert MPD diffractometer using Cu Kα radiation. Transmission electron microscopy (TEM) images were obtained on a Zeiss Libra 200 MC TEM/STEM electron microscope operating at 200 kV from Bruker (Berlin, Germany). DLS measurements were done in a Marvel ZetaSizer Nano equipment. The irradiation system used to determine the production of $^1O_2$ was a LED array composed of a matrix of 6 × 8 LEDs, thus making a total of 48 light sources, with an emission peak at 640 nm and a bandwidth at half maximum of ±20 nm. The irradiation system used in the PDI tests was a PAR radiation, 13 fluorescent lamps OSRAM 21 of 18 W each, 380-700 nm. The radiation power was measured with a potentiometer bright Spectra Physics, model 407A and the sensor of the same brand, model 407A-2.

3.3.2 Materials and reagents

All reagents were obtained from commercial sources and were used without further purification steps. Reverse phase column chromatography was carried out over Waters Sep-Pak C18 35 cm^3 cartridges. Analytical TLC was carried out on pre-coated silica gel sheets (Merck, 60, 0.2 mm).

3.3.3 Synthesis of the cationic nanomagnet-PS hybrids (NP^+-PS)

NP-PS (**NP-TPPF$_{20}$**, **NP-TPPF$_{16}$(SGlc)$_4$**, **NP-TPPF$_{17}$(SGlc)$_3$**, **NP-ZnPcF$_{16}$** **NP-ZnPc(SGlc)$_8$**) suspended in ethanol (11.5 mL, corresponding to 190 mg) were filtered through a polyamide membrane, washed and resuspended in DMF (6 mL), and subsequently treated with a large excess of methyl iodide (2 mL). The reaction mixture was kept under stirring at 40 ºC for 16 h. Then, suspensions were cooled down in an ice bath and the corresponding cationic nanomagnet materials (NP^+-PS) were filtered, washed with

methanol and water, and resuspended in water (50 mL), obtaining **NP^+-$TPPF_{20}$**, **NP^+-$TPPF_{17}(SGlc)_3$**, **NP^+-$ZnPcF_{16}$**, **NP^+-$TPPF_{16}(SGlc)_4$** and **NP^+-$ZnPcF_8(SGlc)_8$**. These stock suspensions correspond to approximately 18 $mg \cdot mL^{-1}$.

3.3.4 Photostability and aqueous stability tests

Photostability of the cationic hybrid materials was evaluated by exposing aqueous suspensions of NP^+-PSs at 2 μM, under white light irradiation (4 $mW \cdot cm^{-2}$), at room temperature, with vigorous magnetic stirring, for 270 min. At fixed intervals of time, visible absorption spectra of the samples were recorded. To evaluate the stability of the suspensions of the hybrid compounds in water, a procedure similar to that described above was followed but in dark conditions (samples contained in glass cells were covered with aluminium foil).

3.3.5 Determination of sensitized $^1O_2$ generation

Ability of PS, NP-PS and NP^+-PS to generate $^1O_2$ was qualitatively determined by a chemical method using 1,3-diphenylisobenzofuran (DPBF) as $^1O_2$ trapping agent. The yellow-coloured DPBF reacts specifically with $^1O_2$ in a [4+2] cycloaddition Diels-Alder reaction, being oxidized to the colorless *o*-dibenzoylbenzene. For the determination of the $^1O_2$ generation, samples in DMF/water (9:1) containing 0.5 μM of PS, NP-PS or NP^+-PS, and 50 μM of DPBF were irradiated with a red LED array, at a fluence rate of 4.0 $mW \cdot cm^{-2}$. Another sample in DMF/water (9:1) containing just DPBF 50 μM was submitted to the same irradiation conditions as light control of direct photolysis. The LED array used as irradiation system was composed of 6 × 8 LEDs, with an emission peak at 640 nm and a bandwidth at half maximum of ±20 nm. During the irradiation, samples were kept under vigorous stirring at room temperature. The generation of singlet oxygen was followed by its reaction with DPBF. The breakdown of DPBF was monitored by measuring the decreasing of the absorbance at 413 nm at irradiation intervals of 2 min for 20 min for Por-based PS, and at intervals of 0.5 min for 5 min for Pc-based PS.

3.3.6 Bacteria growth conditions

A recombinant bioluminescent *Escherichia coli* strain was selected as model of Gram-negative bacteria for PDI studies due to the possibility of real-time monitoring of the photosensitization process.[169] Cells were grown on tryptic soy agar (TSA), supplemented with 50 $mg \cdot mL^{-1}$ of ampicillin (Amp) and 34 $mg \cdot mL^{-1}$ of chloramphenicol (Cm). One isolated colony was aseptically inoculated in 30 mL of tryptic soy broth (TSB), supplemented with both antibiotics (150 µL Amp/100 mL TSB, 60 µL Cm/100 mL TSB) and grown for one day, at room temperature, at 100 rpm stirring. Before each experiment, an aliquot (140 µL) of this culture was sub-cultured in 30 mL of fresh TSB containing Amp and Cm (same concentrations as before in TSB), and was grown for 16 h, at 26 ºC, at 130 rpm stirring, until reaching stationary phase.

3.3.7 Screening assays with a bioluminescent *E. coli* strain

To assess the correlation between colony counts and the bioluminescent signal of the indicator *E. coli* strain, an overnight culture of bioluminescent *E. coli* (≈10^8 $CFU \cdot mL^{-1}$) was serially diluted in phosphate buffer saline solution (PBS; 1.80 $g \cdot L^{-1}$ of Na_2HPO_4, 0.30 $g \cdot L^{-1}$ of KH_2PO_4, 0.25 $g \cdot L^{-1}$ of KCl, 10.00 $g \cdot L^{-1}$ of NaCl; prepared in MilliQ water; pH 7.4). Light emission of the non-diluted and diluted aliquots was read in a luminometer and simultaneously, 1 mL of each dilution was pour plated in TSA medium for colony counting. Three independent experiments were conducted and the results were averaged.

3.3.8 Assays of photodynamic inactivation with a bioluminescent strain

An aliquot of a fresh culture of the bioluminescent *E. coli* strain (≈10^8 $CFU \cdot mL^{-1}$) centrifuged for 5 min at 13000*g*. The bacterial pellet was washed twice and resuspended in PBS. Cell suspensions were transferred to polystyrene Petri dishes and PS, NP-PS or NP^+-PS were added at the selected concentration (10 or 20 µM). To each Petri dish, a sterile magnetic bar was added. Samples were incubated for 30 min in dark conditions at 26 ºC. Then, the bottom of Petri dishes was immersed in a water bath at 26 ºC and this was placed on a magnetic plate, under the light irradiation system. Aliquots of treated samples were

collected at time 0 and after 15, 30, 60, 90, 120, 180, 240 and 270 min of irradiation for bioluminescence measurement in a luminometer (Turner Designs – 20 ⁄ 20). Three independent experiments were conducted and the results were averaged. A light control (bacteria exposed to irradiation without PS, NP-PS or NP^+-PS) and a dark control (bacteria exposed to PS, NP-PS or NP^+-PS, in dark conditions) were included in each experiment to check potential hybrid toxicity to the bacterial model or direct effects of light on cell viability.

3.3.9 Recycling studies of NP^+-PS

Herein, the term recycling involves processing an already used material after its recovery by removal of the treated liquid and an aqueous rinsing, for its reuse by adding a new volume of bacterial suspension.

After one PDI experiment (1 cycle), samples containing NP^+-PS were transferred into polystyrene tubes and the materials were collected at the bottom with a strong permanent magnetic field, using a neodymium magnet. Supernatant in each tube was removed and NP^+-PS systems were washed with ethanol and water. Then, a new bacterial suspension was added to each tube and these suspensions were transferred again to Petri dishes. After the incubation period in dark conditions, irradiation of the samples was restarted. For each NP^+-PS, five PDI cycles were performed. Three independent experiments, of five cycles each, were done and the results were averaged. Light control (bacteria exposed to irradiation without hybrid) and dark control (bacteria exposed to NP^+-PS without irradiation) samples were included in each of the experiments.

CHAPTER 4

BIODEGRADATION OF ESTROGENS BY BACTERIA ISOLATED FROM NATURAL ENVIRONMENTS

Fernández, L., Louvado, A., Esteves, V.I., Gomes, N.C.M., Almeida, A., Cunha, Â, Biodegradation of 17β-estradiol by bacteria isolated from deep sea sediments in aerobic and anaerobic media. *J. Hazard. Mater.*, **2017**, 323, 359-366.

Fernández, L., Esteves, V.I., Schneider, R.J., Cunha, Â., Aerobic bioremediation of estrogens in wastewaters by the deep-sea isolate *Bacillus licheniformis*. Under preparation

Summary

Eleven bacteria isolated from different natural environments, such as compost, Ria de Aveiro (Portugal) and enrichment cultures of sediments of mud volcanoes of the Gulf of Cadiz (Moroccan-Iberian margin), were identified as aerobic E2 biodegraders, producing estrone (E1) as main metabolite, which could be also degraded by the tested strains. Bacterial strains presenting higher efficiency in E2 removal were investigated under different conditions, including the ability of the strains to clear E2 in presence of other available carbon sources in the medium, the behaviour of isolated strains in presence of different concentrations of E2, the ability of the strains to simultaneously degrade different estrogens, the evaluation of the rate of E2 clearance in real wastewaters, the determination of the E2 transformation products, and the anaerobic biodegradation of E2.

4.1. Introduction

In the last years, despite the observed reduction in the estrogenicity of wastewater effluents, some estrogenic effects still persist in streams discharged to surface waters.[170] The impact of preliminary treatments in a classic urban WWTP, consisting on the elimination of large solids, seems to be insignificant in the removal of estrogens. During primary treatments, sorption techniques are used for the removal of pollutants, through that it is expected that free estrogens, which present relatively high logarithmic values of octanol-water partition coefficient (K_{ow}), can be removed (see section 1.1). However, only negligible amounts of estrogens are eliminated during this stage,[171] and conjugated estrogens, such as sulfate, glucuronide or sulfoglucuronide forms, which present lower levels of estrogenic activity, may undergo deconjugation to be transformed into more active free hormones.[171b, 171c, 172] After this stage, the liquid phase is subjected to a secondary treatment under aerobic, anoxic, and/or anaerobic conditions, allowing the removal of carbon, nitrogen, and phosphorous, among other elements, by microbial activity. Then, treated sewage is directed to a secondary clarifier where water is separated from biomass and residual organic matter or sludge. Here, in addition, free estrogens can be removed by sorption to organic material or be biologically transformed.[18]

According to Wu *et al.*, removal of estrogens in a WWTP has shown to be mainly *via* biodegradation, observing different elimination degrees ranging from 19 to 94% for E1, 76- 92% for E2, and 83-87% for EE2.[105] Consequently, natural and synthetic estrogens reach the aquatic environment through discharges of urban and industrial wastewaters. Due to their high estrogenic potency, the natural hormone E2 and the synthetic estrogen EE2 are the most closely monitored.[173]

Estrogens E1, E2, E3 and EE2, the target organic pollutants to be removed in the present research work, have been previously reported in WWTPs effluents (Table 4.1) and in river waters (Table 4.2), at concentrations which are already considered (or close to be considered) as sufficient to induce estrogenic effects in aquatic organisms (1-10 $ng \cdot L^{-1}$).

Table 4.1. Concentration of estrogens in treated effluents.

Sample site by country	Concentration ($ng \cdot L^{-1}$)				Ref.
	E1	E2	E3	EE2	
France	4.3-7.2	1	5.0-7.3	2.7-4.5	[174]
Canada	3	6	n.a.*	9	[175]
Germany	9	n.d. (1.0)*	n.a.	1	[175]
Netherlands	n.d. (0.4)-47	n.d. (0.6)-12	n.a.	n.d. (0.2)-7.5	[176]
England	6.4-29	1.6-7.4	2.0-4.0	n.d. (0.3)	[177]
Italy	2.5-82.1	0.35-3.5	0.43-18.0	n.d. (0.3)-1.7	[178]
Spain	n.d. (2.5)-8.1	n.d. (5.0)-14.5	0.25-21.5	n.d. (5.0)	[179]
Portugal	n.d. (0.2)-85.3	n.d. (0.2)-9.2	n.a.	n.d.(0.2)	[180]

*n.d. (LOD): not detected (limit of detection)

*n.a.: not analysed

Table 4.2. Concentration of estrogens in river waters.

Sample site by country	Concentration ($ng \cdot L^{-1}$)				Ref.
	E1	E2	E3	EE2	
France	1.1-3.0	1.4-3.2	1.0-2.5	1.1-2.9	[174]
Netherlands	n.d. (0.1)*-3.4	n.d. (0.3)-5.5	n.a.*	n.d. (0.1)-4.3	[176]
England	0.2-17.0	n.d. (0.5)-7.1	n.d. (0.5)-3.1	n.d. (0.5)*	[177]
Italy	1.5	0.11	0.33	0.04	[178]
Spain	4.3	6.3	8.0	n.d. (5.0)	[179]
Portugal	n.d. (0.2)-0.5	n.d. (0.2)-0.8	n.a.	n.d.(0.2)	[180]

*n.d. (LOD): not detected (limit of detection)

*n.a.: not analysed

The use of microorganisms capable of degrading organic pollutants is considered an interesting strategy for water treatment applications because of its reduced environmental impact and its efficiency in the removal of dispersed organics, even at low concentrations,[181] which benefits the efficient removal of pollutants in the nanoscale range. It has the disadvantage of being a slow process when compared to physical methods and advanced oxidation processes (AOPs).[182] In spite of the fact that by using AOPs some

persistent photodegradation products may retain estrogenic activity in water,[183] in general physicochemical techniques are considered as efficient. On the other hand, bioremediation is an advantageous technology for pollutant removal due to low costs and modest energetic requirements, qualities which are not always fulfilled by AOPs.

Different types of estrogen-degrading bacteria have been isolated and characterized, such as *Novosphingobium*,[184] *Sphingomonas*,[185] *Ralstonia*,[109] *Rhodococcus*[108] and *Nitrosomonas*[26] species (see section 1.4.2). Previous studies have reported the formation of E1 as the major metabolite in the biotransformation of E2 in batch tests with either activated sludge or pure cultures.[26, 31, 109, 114, 117] This fact suggests that the biotransformation of E2 by bacteria may start through the most accessible functional group, the 17-hydroxyl group (Scheme 4.1). As a result, E1 is produced, but detailed transformation pathways of E2 by biodegradation are still unclear in most cases. E1 displays approximately one quarter of the estrogenic activity of E2, therefore, E1 is considered an undesired degradation product.

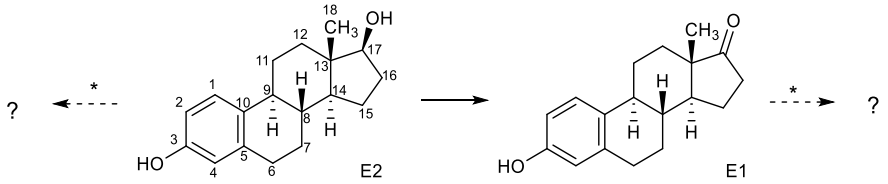

Scheme 4.1

In this work, eleven bacterial strains isolated from compost, estuarine water (Ria de Aveiro, Portugal) and deep sea sediments (mud volcanoes of the Gulf of Cadiz, Moroccan-Iberian margin), were tested in the aerobic and anaerobic biodegradation of estrogens. The motivation of this study lies within the frame of alternative E2 biodegradation routes in which the formation of E1 is reduced or this can be also degraded during the treatment by selected bacterial strains. The versatility of the more efficient bacterial strains to metabolize estrogens was evaluated under different conditions, such as the influence of the presence of other carbon sources, or the ability to degrade other estrogens. Finally, transformation products arising from the biodegradation of E2 were studied using mass spectrometry methods.

4.2. Bacterial strain selected for estrogen removal

Eleven bacterial strains isolated from different environmental matrices were tested in biodegradation studies of estrogens. Codes given for the isolates are displayed in parentheses next to the bacterial strain name.

- Five unidentified bacteria, previously isolated from sediments of mud volcanoes of the Gulf of Cadiz (Moroccan-Iberian margin, Fig 4.1), located at ~4500 m water depth;[186] were kindly provided by The Laboratory of Molecular Ecology of Marine Environments, of University of Aveiro (**LF1**-**LF5**). These isolates were selected since biodegradation of a wide range of hydrocarbons, including aliphatic, aromatic, halogenated and nitrated compounds, has been shown to occur in different extreme habitats. In particular, cold-adapted hydrocarbon degraders have been described as suitable for wastewater treatment applications.[187]

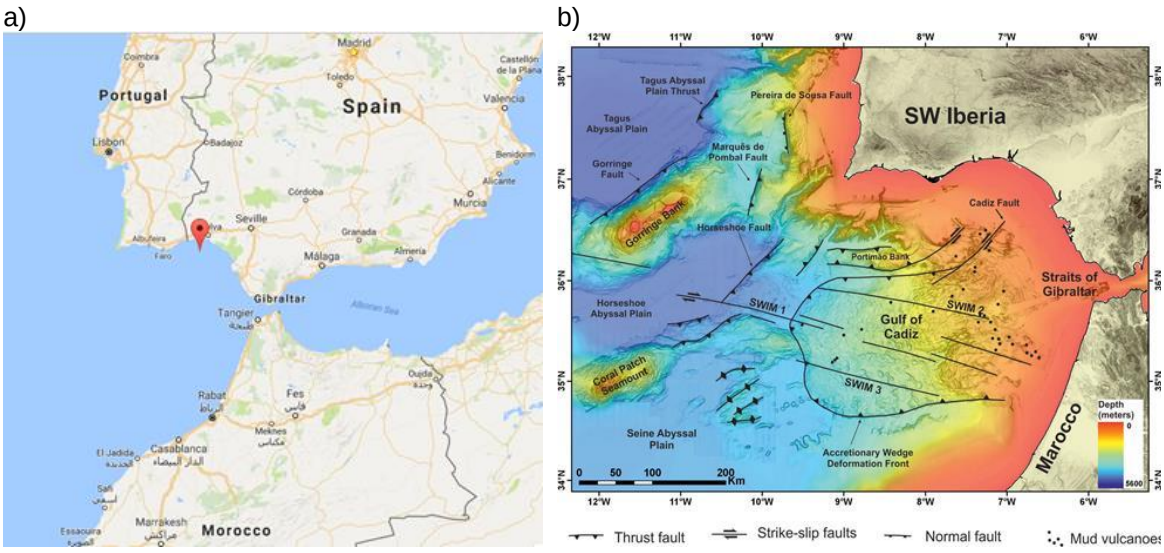

Figure 4.1. a) Map of the SW Iberia-Gulf of Cadiz and b) enlargement of tectonic map of mud volcanoes of this region were LF1-LF5 were isolated.[188]

The deep sea environment is influenced by extreme conditions, broadly characterized by high hydrostatic pressures up to 1100 atm (110 MPa), low temperatures of approximately 2-3 °C, salinity levels of 3.4-3.5%, a pH between 7.5 and 8.0, absence of light and generally oligotrophy.[189] Bacteria isolated from extreme environments able to degrade organic pollutants can be ideal candidates for the biological treatment of wastewaters under certain extreme conditions of pressure, temperature, pH, salinity, etc.

- *Pseudomonas aeruginosa* strain JB2 (**LF6**) and *Acinetobacter* sp. ADP1 (**LF7**), both isolated from compost, were kindly provided by Prof. Dr. Nico Boon, from Laboratory of Microbial Ecology and Technology, of Ghent University. These isolates were selected as positive controls in the biodegradation tests, since they were already reported as estrogen degraders in 2008 by Pauwels *et al.*[29b]

- *Pseudomonas aeruginosa* GIM 32 (**LF8**), *Pseudomonas* sp. JPPB B25 (**LF9**), *Pseudomonas* sp. ANT-2400 S10 (**LF10**) and *Pseudomonas segetis* FR1439 (**LF11**), all of them isolated from Ria de Aveiro (North-West of Portugal), were kindly provided by Antonio Louvado, from the Laboratory of Applied and Environmental Microbiology, Department of Biology, University of Aveiro.[190] These isolates were selected because they were already described as polycyclic aromatic hydrocarbons (PAHs) degraders,[191] and it was though that they could present potential for the removal of other organic pollutants.

4.3. Results and discussion

4.3.1. Identification of isolates from deep sea sediments (LF1-LF5)

For the molecular identification of isolates **LF1**-**LF5**, extraction of total deoxyribonucleic acid (DNA) of bacterial isolates was carried out following the phenol/chloroform extraction procedure,[192] using fresh bacterial cultures grown in Luria-Bertani broth (LB) for 5 days at 26 °C on a rotary shaker. DNA was suspended 50 µL of TE buffer and stored at -20 °C. To evaluate the extraction procedure, 5 µL-aliquots of each sample were subjected to electrophoresis on agarose gel 1.5% with GelRed at 80 V for 30 min in TAE buffer. The gel was then visualized on an imaging system.

The 16S ribosomal DNA (rDNA) gene was amplified by polymerase chain reaction (PCR) using universal bacterial primers U27 and 1492R.[193] A negative control containing all reagents but the biological sample was included for detecting possible contaminations. The DNA amplification product was externally sequenced (Stabvida) using the Sanger method.[194] The sequences obtained were classified and compared to existing sequences in GenBank using the software BLAST (Basic Local Alignment Search Tool) (http://www.ncbi.nlm.nih.gov/).

Positive amplification of PCR reactions with selected primers was only obtained for isolates **LF1**, **LF3** and **LF5**. Consequently, **LF2** and **LF4** remained unidentified. The sequences were identified as closely related (more than 99% sequence similarity) to sequences designed as *Virgibacillus halotolerans* (**LF1**), *Bacillus flexus* (**LF3**) and *Bacillus licheniformis* (**LF5**) (Table 4.3).

Table 4.3. BLAST results obtained for the 16S rDNA gene sequence alignments.

Isolate	Similarity	BLAST	Accession number	Query	Ref.
LF1	99%	*Virgibacillus halotolerans* strain WS 4627	NR108860.1	99%	[195]
LF3	99%	*Bacillus flexus* strain MSBC2	KJ452460.1	99%	[196]
LF5	99%	*Bacillus licheniformis* strain 3	KP119810.1	99%	[197]

The five isolates were positive to the Gram staining method.[198] In general, Gram-positive bacteria are more resistant to extreme conditions of pressure than Gram-negative, due to the rigidity of teichoic acids in their peptidoglycan layer cell wall.[199] Attending to the high hydrostatic pressure levels of deep sea environment, results of staining method can be considered as expectable. The two *Bacillus* isolates identified in this study are commonly occurring in various aquatic habitats. *Bacillus flexus* has been isolated from a Saudi lake (in this study, *Bacillus flexus* was used to degrade microcystin-RR, a potent toxin for humans and animals produced by some cyanobacteria)[200] and from green seaweed *Ulva lactuca* of Indian Ocean.[201] *Bacillus licheniformis* has been isolated from coastal environment in Cochin, in India.[202] In the literature, the presence of *Virgibacillus halotolerans* has only been reported from a dairy product.[195] However, a number of *Virgibacillus* species have been isolated from different marine environments.[203]

- Description of *Virgibacillus halotolerans* WS 4627 (**LF1**)[195]

  Current classification. Domain: *Bacteria*. Phylum: *Firmicutes*. Class: *Bacilli*. Order: *Bacillales*. Family: *Bacillaceae*. Genus: *Virgibacillus*. Species: *Virgibacillus halotolerans.* Type strain: WS 4627.[202]

  Cells are Gram-stain-positive, slightly motile and strictly aerobic rods (0.7–0.8 *x* 3.0–5.0 mm) that produce ellipsoidal endospores that lie centrally or subterminally in sometimes slightly swollen sporangia. Colonies are cream, flat to low-convex and translucent with regular margins. Growth at pH 6.5-8.5 and in 0.5-16.5% NaCl. Growth temperature 8 to 35 ºC (optimum 30 ºC).

- Description of *Bacillus flexus* strain MSBC2 (**LF3**)[196]
  Current classification. Domain: *Bacteria*. Phylum: *Firmicutes*. Class: *Bacilli*. Order: *Bacillales*. Family: *Bacillaceae*. Genus: *Bacillus*. Species: *Bacillus flexus.* Type strain: MSBC2.

  Cells are Gram-stain-positive, motile, aerobic cocci (0.9 µm mean cell width), that produce centrally/paracentrally ellipsoidal endospore in unswollen sporangia. Colonies are cream-colored, opaque and smooth. Growth at pH 4.5-9.5 and in 2-10% NaCl. Growth temperature 17 to 37 ºC (optimum 30 ºC).

- Description of *Bacillus licheniformis* strain 3 (**LF5**)[197]
  Current classification. Domain: *Bacteria*. Phylum: *Firmicutes*. Class: *Bacilli*. Order: *Bacillales*. Family: *Bacillaceae*. Genus: *Bacillus*. Species: *Bacillus licheniformis.* Type strain: 3.

  Cells are Gram-stain-positive, motile, rod-shaped (1.5-3.0 *x* 0.6-0.8 µm), facultative anaerobes (unlike other bacilli that are typically aerobic), that produce ellipsoidal or cylindrical, central, paracentral or subterminal spore, not deforming the vegetative cell. Colonies are whitish or brownish, round to irregular in shape (2-4 mm diameter), with margins varying from undulate to fimbriate. Growth at pH 5.7-6.8 and in NaCl 2-7%. Growth temperature 30 to 68 ºC.

4.3.2. E2 degradation under aerobic conditions

Initial experiments were conducted to identify those bacterial strains capable of degrading E2 as selected estrogen. Among the initially tested isolates, only those bacteria which showed positive results in E2 removal are further described in this chapter, since other isolates from deep sea sediments which did not show capability to degrade or transform E2 were not identified by 16S rDNA. All the four strains isolated from Ria de Aveiro showed ability to degrade E2.

The first degradation experiment, described as abiotic control, was conducted to assess the stability of the estrogens E2 and E1 in the test medium under aerobic conditions. Although starting tests included only biodegradation of E2, in abiotic control samples E1 was included due to expectations of obtaining it during E2 transformation, per the literature.

Samples were prepared in a minimal medium based on a modified phosphate buffer saline, obtained by adding to PBS a nitrogen source arising from NH_4Cl, ammonium ferric citrate and 5 $mL \cdot L^{-1}$ of a micronutrient solution (see section 4.4.3). In addition, a higher content of NaCl (35.00 $g \cdot L^{-1}$) was added in biodegradation tests with strains **LF1**-**LF5**, to simulate salinity levels of deep sea areas. This modified PBS (PBS_{mod}) was designed to provide nutritional requirements for bacterial growth.

Experiments with abiotic control samples were carried out in triplicate, in 30 mL of PBS_{mod} medium containing E2 and E1 at 5 $mg \cdot L^{-1}$. Samples were kept in dark conditions (to avoid direct photolysis of E1 and E2), under permanent orbital stirring, for 5 days, at 26 ºC. Aliquots (500 µL) of the aqueous samples, which were collected each 12 h during the tests, were taken and estrogens in the supernatant were extracted with ethyl acetate and then quantified by high performance liquid chromatography with UV detector (HPLC-UV). Abiotic samples containing E2 and E1 did not show significant differences in the starting concentrations during 5 days of incubation (ANOVA, $p > 0.05$), thus indicating that any variation in the concentration of E2 and the hypothetically E1 bioproduced in further biotic samples would be related with bacterial activity (Fig. 4.2).

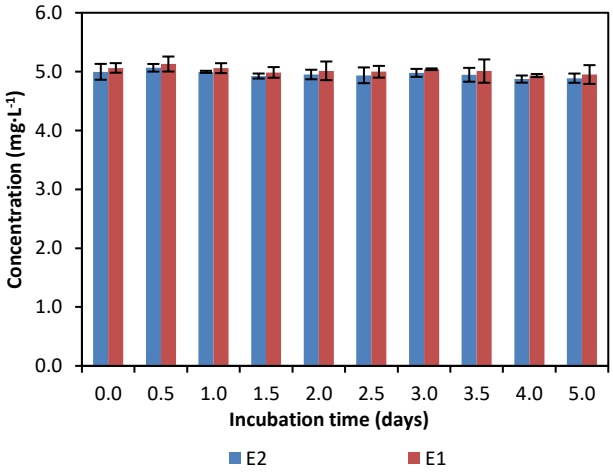

Figure 4.2. Abiotic control samples in absence of bacteria, under dark conditions. Data shown represent the average values of E2 (blue bars) and E1 (red bars), and errors of three independent experiments.

Initial biodegradation experiments were conducted to examine if isolates were capable of degrading E2 in aerobic conditions. Biodegradation tests were carried out in triplicate using each of the eleven bacteria individually. For this purpose, each isolate was grown in its corresponding solid medium (see section 4.4.4) containing 5 $mg \cdot L^{-1}$ of E2 by adding the appropriate volume of a stock solution of E2 in dimethyl sulfoxide (DMSO) at 1 $g \cdot L^{-1}$. Then, one isolated colony was inoculated in liquid medium (see section 4.4.4) and

grown at 26 ºC. Cells were harvested during the exponential phase of growth (OD_{600} = 0.7) from aliquots (2 mL) by centrifugation at 6000 *g* for 7 min. Each cell pellet was washed with PBS_{mod} and then transferred into in 30 mL of PBS_{mod} with 5 $mg \cdot L^{-1}$ of E2, contained in a 100 mL glass Erlenmeyer flask. Samples were kept in a dark incubator shaker (5 days, at 26 ºC, 150 rpm).

During these biodegradation studies, aliquots (500 µL) of the aqueous samples were collected each 12 h, and bacterial cells were separated from the culture medium by centrifugation at 6000 *g*. Estrogens in the supernatant were extracted with ethyl acetate, and attenuation of E2 and formation and attenuation of E1 were monitored using HPLC-UV, using the same chromatographic conditions as previously with abiotic samples. In addition, measurements of optical density at 600 nm (OD_{600}) were done for monitoring of cell culture growth, by collecting aliquots (100 µL) of the aqueous samples each 12 h. OD_{600} measurements were done without any sample treatment.

First tests to be analysed were those with strains **LF6** and **LF7**, which were already described as estrogen-degraders in the literature and therefore were considered as positive biotic controls.[29b] Both strains presented ability to remove 5 $mg \cdot L^{-1}$ of E2 from the samples within the incubation period, and to form and remove E1 to some extent. The main mechanism of E2 degradation by **LF6** seems to be the formation of E1. Other metabolites could not be detected with the given HPLC-UV method, which may suggest that cleavage of the aromatic ring could have occurred. E1 was not consumed until reaching the maximal concentration (1.94 $mg \cdot L^{-1}$), once that E2 was not detected anymore in the samples (LOD: 0.15 $mg \cdot L^{-1}$) (Fig. 4.3).

OD_{600} measurements were used to determine bacterial growth during biodegradation tests. Growth curves of **LF6** and **LF7** had an apparent pattern of adaptation, logarithmic growth and stability stages. Results showed that bacterial growth occurred efficiently with the presence of greater levels of E2 in the samples, and decreased when the concentration of E2 was scarce. This can be understood as a preference of **LF6** to grow on E2 rather than on E1.

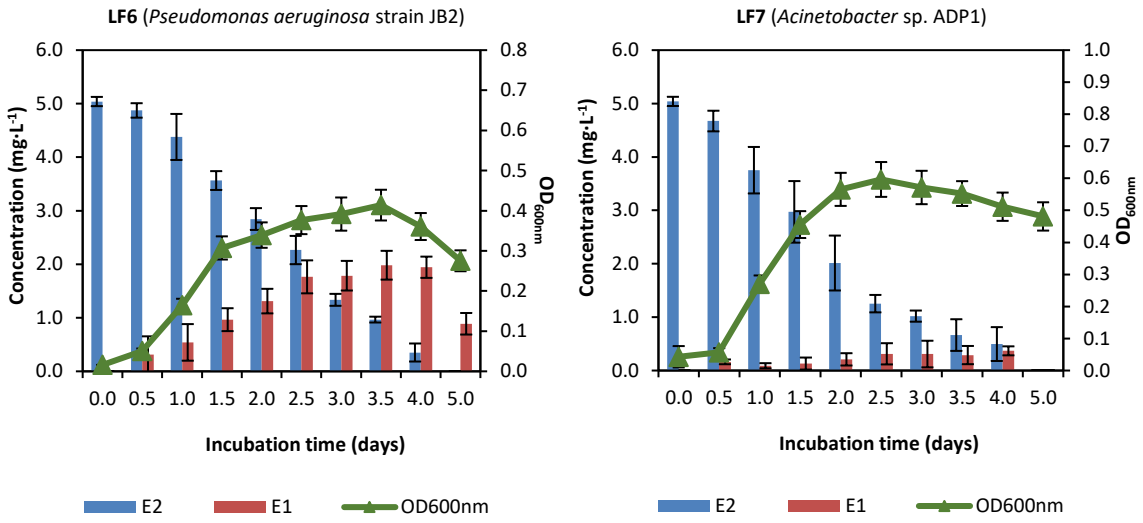

Figure 4.3. E2 degradation (5 mg·L^{-1}) profiles by strains strains isolated from compost, **LF6** and **LF7**, under aerobic conditions. Data shown represent the average values of E2 (blue bars), E1 (red bars) and bacterial OD measured at 600 nm (green triangles), and errors of three independent experiments.

On the other hand, **LF7** achieved the complete removal of E2 within 5 days of incubation, or at least below LOD, with low amounts of bioproduced E1. A maximum of 0.37 mg·L^{-1} of E1 was accumulated after 4 days of incubation, and was not detected anymore (LOD: 0.09 mg·L^{-1}) within one more day of incubation. These results suggest that other main metabolic routes of E2 biotransformation were here involved. OD_{600} measurements showed an efficient bacterial cell growth of **LF7** of in presence of E2.

Conclusions herein attained are comparable to previous results obtained by Pauwels *et al.*, who reported the ability of these strains to degrade both the natural estrogens, E1 and E2, and also E3. In addition, EE2 could also be co-metabolized by **LF6** and **LF7** in presence of the natural estrogens E1, E2 and E3.[29b]

Strains **LF8**-**LF11** were isolated from the estuarine system of Ria de Aveiro, located in the North-West of Portugal, where most likely microorganisms have been exposed to organic pollutants, such as estrogens. In 2010, Sousa and co-workers reported the levels of E1, E2, EE2, and other non-estrogenic EDCs, in effluents from WWTPs located in Ria de Aveiro. E1 levels varied from 0.5 to 85 ng·L^{-1} in the summer survey and between LOD (0.2 ng·L^{-1}) and 43 ng·L^{-1} in winter; E2 levels ranged from LOD (0.2 ng·L^{-1}) to 9.2 ng·L^{-1} in summer and were always below LOD in the winter survey; and EE2 levels were always below LOD (0.2 ng·L^{-1}) for both surveys.[180]

LF8-**LF11** were described by Louvado *et al.* as phenanthrene-degrading bacteria.[190] Phenanthrene is a polycyclic aromatic hydrocarbon composed by three fused benzene

rings, thus relating the chemical skeleton of estrogens, which are composed by three hexagonal and one pentagonal fused rings. However, it is necessary to remark that the chemical structure of phenanthrene is planar and estrogens present non-planar geometry. In addition, the tendency of microbial degradation of E2 suggests that the main mechanism may start in the 17-hydroxyl group, which phenanthrene does not contain in its structure. For these reasons, potential ability of **LF8-LF11** to degrade estrogens was uncertain.

On the other hand, **LF8**-**LF11** (and **LF6**) are biosurfactant producers. Molecular structures of biosurfactants comprise a hydrophilic portion, typically composed by mono-, oligo- or polysaccharides, amino acids or peptides, or phosphate groups, and a hydrophobic portion, which is constituted by fatty acids or fatty alcohols.[204] The fact of that these bacteria produce biosurfactants may be useful for the necessary contact between hydrophobic substances, such as estrogens, and the external bacterial cell wall, for an effective uptake of these substances and their further biotransformation. In addition, for a successful bioremediation, it is necessary that target pollutants are solubilized in the media. Biosurfactants can help releasing estrogens sorbed to soil organic matter by solubilization and emulsification, thus increasing their aqueous concentration, resulting may result again in a higher mass transfer ratio.[205]

Results of E2 degradation in presence of **LF8**-**LF11** are presented in Fig. 4.4. As general conclusion, OD_{600} growth curves of **LF8-LF11** showed apparent patterns of adaptation, logarithmic growth and stability stages.

According to their classification, **LF8** (*Pseudomonas aeruginosa* GIM 32) and **LF6** (*Pseudomonas aeruginosa* strain JB2) are very similar. However, experiments of E2 biodegradation in presence of **LF8** showed slower kinetics of E2 removal, and after 5 days of incubation with **LF8**, 0.33 $mg \cdot L^{-1}$ of E2 remained in the sample (< LOD in presence of **LF6**, under the same conditions). Interestingly, E1 formed with **LF8** was in lower concentrations, reaching its maximum at 0.86 $mg \cdot L^{-1}$ in the fourth day of incubation (1.98 $mg \cdot L^{-1}$ of accumulated E1 at maximum in presence of **LF6**, under the same conditions). Moreover, levels of E1 produced by **LF8** increased and decreased in samples collected consecutively, such as in days 0.5 (0.20 $mg \cdot L^{-1}$) and 1 (0.14 $mg \cdot L^{-1}$), 2.5 (0.68 $mg \cdot L^{-1}$) and 3.0 (0.47 $mg \cdot L^{-1}$), and 4.0 (0.86 $mg \cdot L^{-1}$) and 5.0 (0.77 $mg \cdot L^{-1}$). These results show evidences that **LF8** can, to some extent, metabolize E1. OD_{600} measurements were similar to those obtained with **LF6**, which show a preference of **LF8** to grow on E2, where grows efficiently until reaching its maximum at OD_{600}= 0.53 after three days of incubation, rather than on E1.

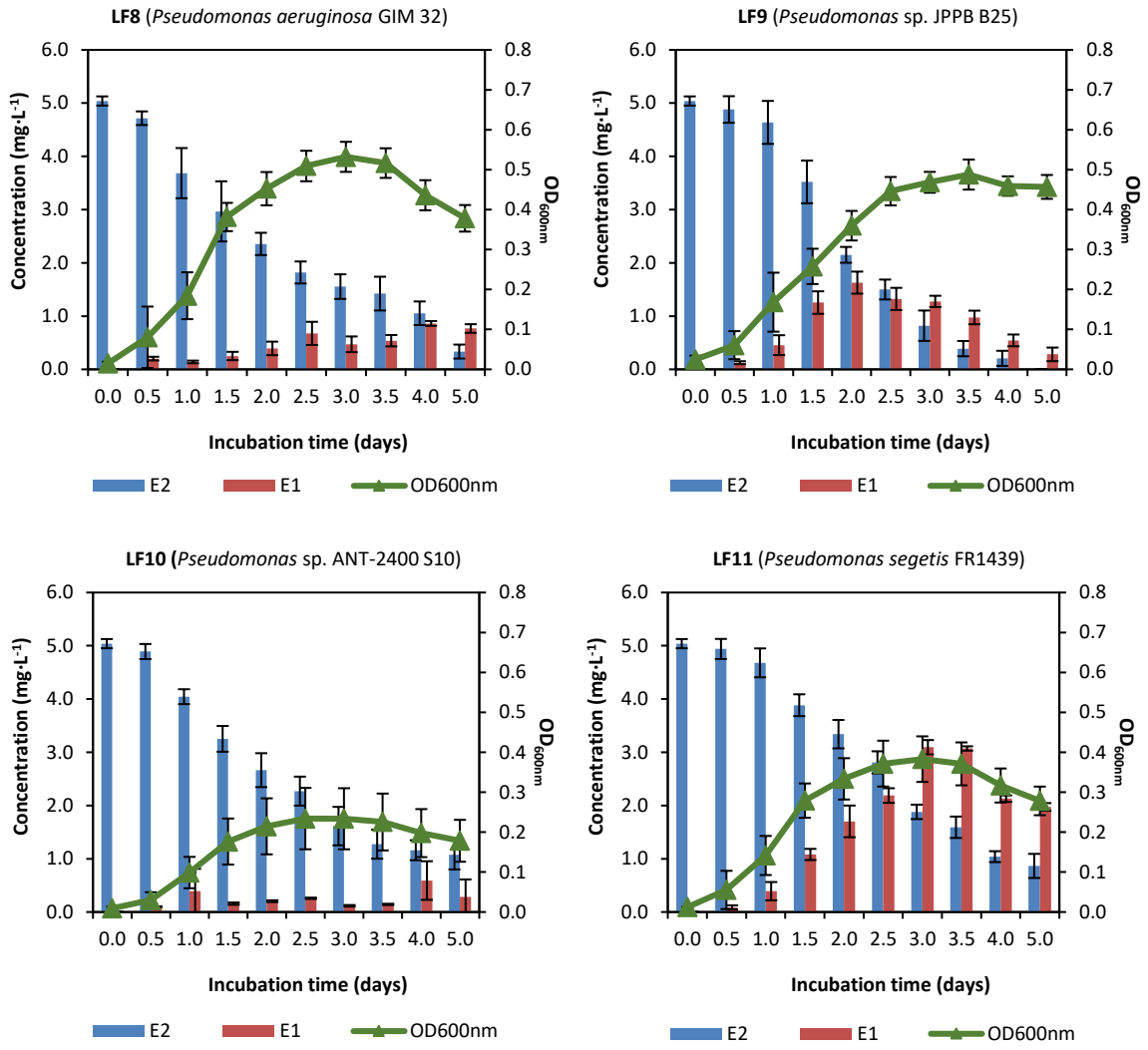

Figure 4.4. E2 degradation profiles by strains isolated from Ria de Aveiro, **LF8**-**LF11**, under aerobic conditions. Data shown represent the average values of E2 (blue bars), E1 (red bars) and bacterial OD measured at 600 nm (green triangles), and errors of three independent experiments.

Comparatively, **LF9** showed better performance in the removal of E2. Within five days of incubation of **LF9** with E2 at 5 mg·L^{-1}, E2 no longer detected. Levels of formed E1 reached their maximum at 1.63 mg·L^{-1} after two days of incubation. E1 could be degraded to certain extent by **LF9** (0.28 mg·L^{-1} remained in the samples after five days of incubation). OD_{600} measurements show an efficient growth of **LF9** under the test conditions.

LF10 was led efficient in E2 biodegradation (1.08 mg·L^{-1} of E2 remained in the samples after the tests). OD_{600} measurements support these results by indicating a slow growth of **LF10**. However, levels of E1 formed were low, achieving its maximum of accumulated E1 at 0.59 mg·L^{-1}. In addition, **LF10** presented to degrade E1.

The removal of E2 by **LF11** was directly accompanied by the formation of E1 during the first 2.5 days of incubation, where the sum of equivalents of E1 and E2 remains constant (18.5 μmol·L^{-1}). Then, levels of E1 started to decrease. In the end of the study, 2.13 mg·L^{-1} of E2 remained and 1.97 mg·L^{-1} of E1 accumulated in the samples.

Bacterial strains **LF1**-**LF5** were isolated from sediments of mud volcanoes of the Gulf of Cadiz, located at ~4500 m water depth,[188] in selective cultures containing phenanthrene as sole carbon source. As **LF8**-**LF11**, these bacteria had also been identified as phenanthrene-degrading bacteria by Louvado *et al*. Prokaryotic organisms isolated from deep sea habitats are known to harbour unique adaptations in response to local abiotic conditions. A particular adaptation is the maintenance of a high enzymatic diversity, particularly those related to xenobiotic compounds degradation.[206] Sediments are considered as sinks for contaminants in environmental waters, particularly for organic pollutants with little to no water solubility. This organic matter in deep sea areas may serve as carbon sources which otherwise would be scarce for heterotrophic bacterial growth. Fig. 4.5 displays an image taken by the NASA; showing the sediment plume along Gulf of Cádiz due to a large load of thick sediment delivered by the Guadalquivir River in 2012. Hazards to water quality and wildlife health have been assessed here through different areas of research.[207] However, levels of estrogens in this area are still not reported.

Figure 4.5. Sediment plume along Gulf of Cádiz. Image taken on 12th November 2012 by NASA's Aqua satellite.[208]

Microorganisms responsible for organic pollutants degradation in deep sea areas are mostly unknown.[209] However, environmental disasters, such as the oil spill into the Gulf of Mexico caused by the Deepwater Horizon in 2010, have stimulated the search for bacteria involved in organics degradation (especially long-chain hydrocarbons and PAHs) in deep waters.[210]

Preliminary studies of E2 degradation with **LF1**-**LF5** under aerobic conditions were conducted by varying NaCl content of the suspension medium from 1% to 3.5% (see section 4.2.4). These results evidenced that an increased NaCl concentration benefited the E2 removal in presence of **LF1**-**LF5**. Samples containing NaCl at 3.5% resulted in faster degradation and higher values of OD_{600} measurements. Therefore, the following studies of estrogen degradation with deep sea isolates were performed using PBS_{mod} containing 5 $mg \cdot L^{-1}$ of E2, with 3.5 % NaCl.

In general, the five strains isolated from deep sea sediments, **LF1-LF5**, could degrade E2 with production of E1 (Fig. 4.6), which suggests again that at least one degradation pathway starts oxidizing the 17-hydroxylgroup of E2. Further transformation of E1 and, in some cases, complete removal of E1 was also observed. OD_{600} measurements showed bacterial viability under the test conditions.

LF1 could use E2 as sole carbon source and completely degrade it within 2.5 days. The concentration of E1, produced by biotransformation of E2, reached a maximum concentration of 1.37 $mg \cdot L^{-1}$ after 12 h of incubation. E1 was also degraded and completely removed from the solution after 5 days. E1 was consumed at a later stage in relation to E2, indicating that it was used as an alternative carbon source. OD_{600} measurements show an efficient growth of **LF1** under the test conditions, consistent with rates of organics removal.

LF2 exhausted E2 within 2.5 days of incubation. In this case, concentrations of produced E1 followed a different trend, reaching a first maximum at 1.89 $mg \cdot L^{-1}$ after 12 h of incubation, and a second maximum at 1.15 $mg \cdot L^{-1}$ after 2.5 days, once E2 was completely cleared. E1 was not detected on the 5^{th} day of the study.

LF3 showed slower kinetics in E2 removal and after 5 days of incubation, 0.19 $mg \cdot L^{-1}$ of E2 accumulated in the samples. E1 was produced in low amounts, having a maximum concentration at 0.62 $mg \cdot L^{-1}$ on the second day of the studies. E1 was not completely removed by **LF3** and finally accumulated 0.39 $mg \cdot L^{-1}$ in the samples. OD_{600} measurements show an efficient viability of **LF3** to grow on E2 and E1.

LF4 displayed a phase of fast E2 biodegradation after 12 h of incubation, and E2 was completely removed after 5 days. However, on the last day of the tests, 0.76 $mg \cdot L^{-1}$ of E1 accumulated in the samples. **LF4** did not show special preference to degrade E1, and when E2 was removed, OD_{600} measurements showed a slowdown in bacterial growth.

LF5 was slower in the degradation of E2, but complete degradation was achieved after 5 days of incubation. **LF5** showed low levels of E1 formation (0.61 $mg \cdot L^{-1}$ on 4^{th} day),

which additionally could be removed from the samples. OD_{600} measurements showed a consistent trend of **LF5** growth under the test conditions.

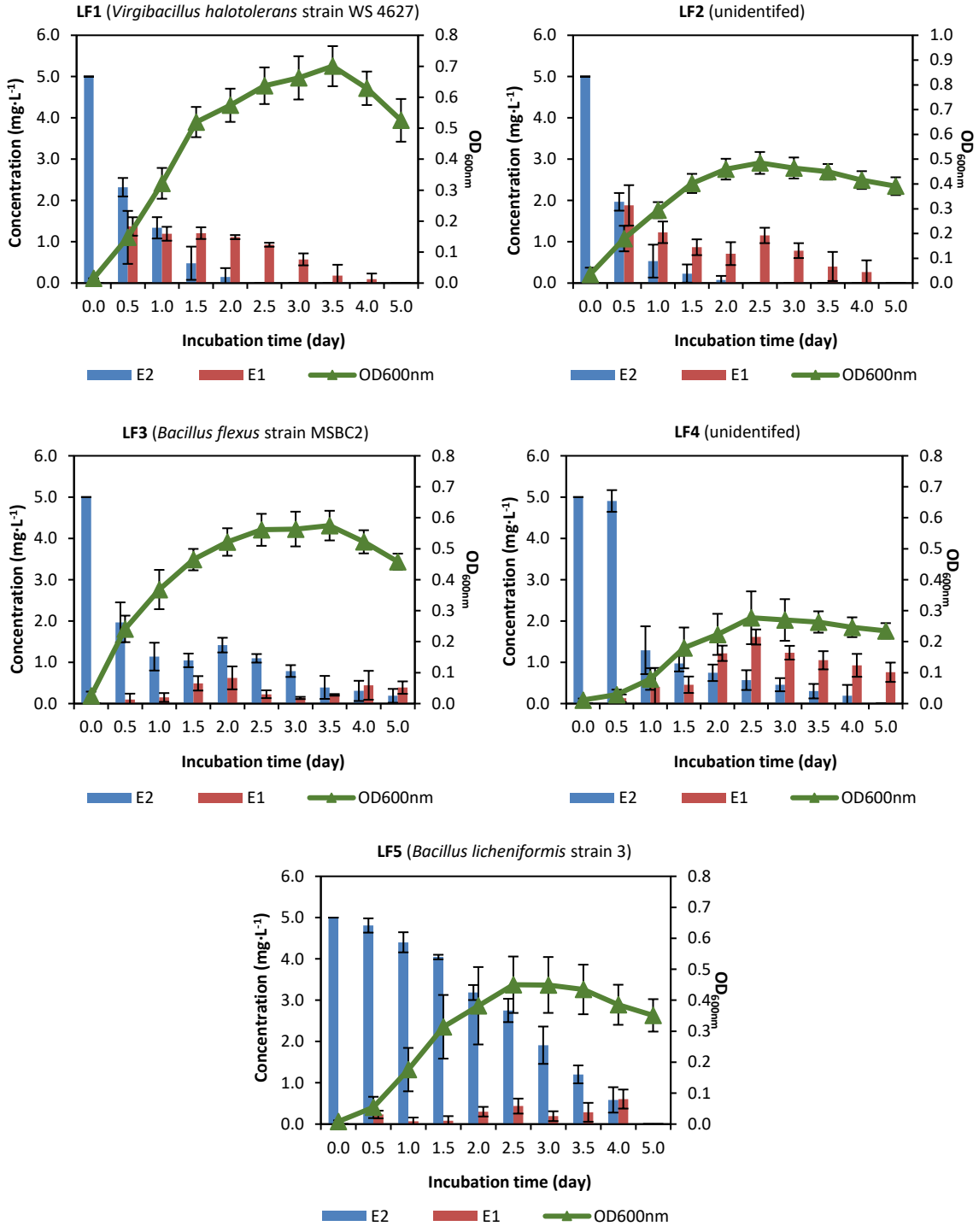

Figure 4.6. E2 degradation profiles by strains isolated from deep sea sediments, **LF1**-**LF5**, under aerobic conditions. Data shown represent the average values of E2 (blue bars), E1 (red bars) and bacterial OD measured at 600 nm (green triangles), and errors of three independent experiments.

Some bacteria capable of degrading E2 fast, completely and without producing toxic products (as E1), have been already reported, such as *Novosphingobium tardaugens*,[107] *Rhodococcus equi* and *Rhodococcus zopfii*.[108] **LF1**, **LF2** and **LF5** exhibited the ability to degrade E2, form E1 as metabolite during E2 transformation, and further degrade E1 completely within the incubation time of these studies. A similar activity was found previously in *Achromobacter xylosoxidans* and *Ralstonia picketii*,[109] *Sphingomonas sp.*[211] and *Novosphingobium tardaugens*.[105] **LF3** and **LF4** could partially degrade the E1 formed during E2 transformation, as found in studies with *Aminobacter sp.*,[105] *Bacillus sp.*[29a] and *Brevundimonas diminuta*.[212] E2 removal rates herein obtain can be compared with results already reported, as the biodegradation of 1 $mg \cdot L^{-1}$ of E2 in 9 h, by *Novosphingobium* sp. JEM-1;[184] the biodegradation of 180 $mg \cdot L^{-1}$ of E2 in 120 h, by *Rhodococcus* sp. ED7;[116] or the biodegradation of 3.3 $mg \cdot L^{-1}$ of E2 in 100 h by *Stenotrophomonas maltophilia* ZL1.[213]

To the best of our knowledge, neither deep sea bacteria have been previously reported as estrogen degraders, nor any of the identified strains (*Virgibacillus halotolerans* strain WS 4627 (**LF1**), *Bacillus flexus* strain MSBC2 (**LF3)** and *Bacillus licheniformis* strain 3 (**LF5**) have been earlier described as estrogen-degrading microorganisms. In contrast to the bacteria isolated from more common environmental conditions, **LF1-LF5** may have advantageous properties for utilization in bioremediation of water bodies subjected to ordinary or extreme conditions, thus making the exploration of these microorganisms more meaningful.

The following sections will focus on estrogen biodegradation with deep sea bacteria so far studied, in particular with **LF1**, **LF3** and **LF5**, since **LF2** and **LF4** remained unidentified. The effects of different sample conditions on the E2 degradation efficiency and cell growth of **LF1**, **LF3** and **LF5** have been studied, as well as the potential to degrade E2 at lower and more environmental significant levels, as well as other estrogens apart from E1 and E2, such as E3 and EE2, and the influence of the presence of other carbon source in the samples in E2 degradation experiments. All the following studies were performed at Bundesanstalt für Materialforschung und -prüfung (BAM), in Berlin (except for section 4.2.10).

4.3.3. Influence of NaCl content and temperature on E2 degradation by LF1, LF3 and LF5

After selection of **LF1**, **LF3** and **LF5** as biodegraders for a more in depth study of E2 biodegradation, the influence of temperature (20-37 ºC) and content of NaCl (1-4%) in these studies was evaluated in samples of 30 mL of PBS_{mod} containing 5 $mg \cdot L^{-1}$ of E2 (Fig. 4.7). Samples were incubated for 5 days. Abiotic control samples were included and showed a stable concentration of E2 within the incubation period (data non-shown).

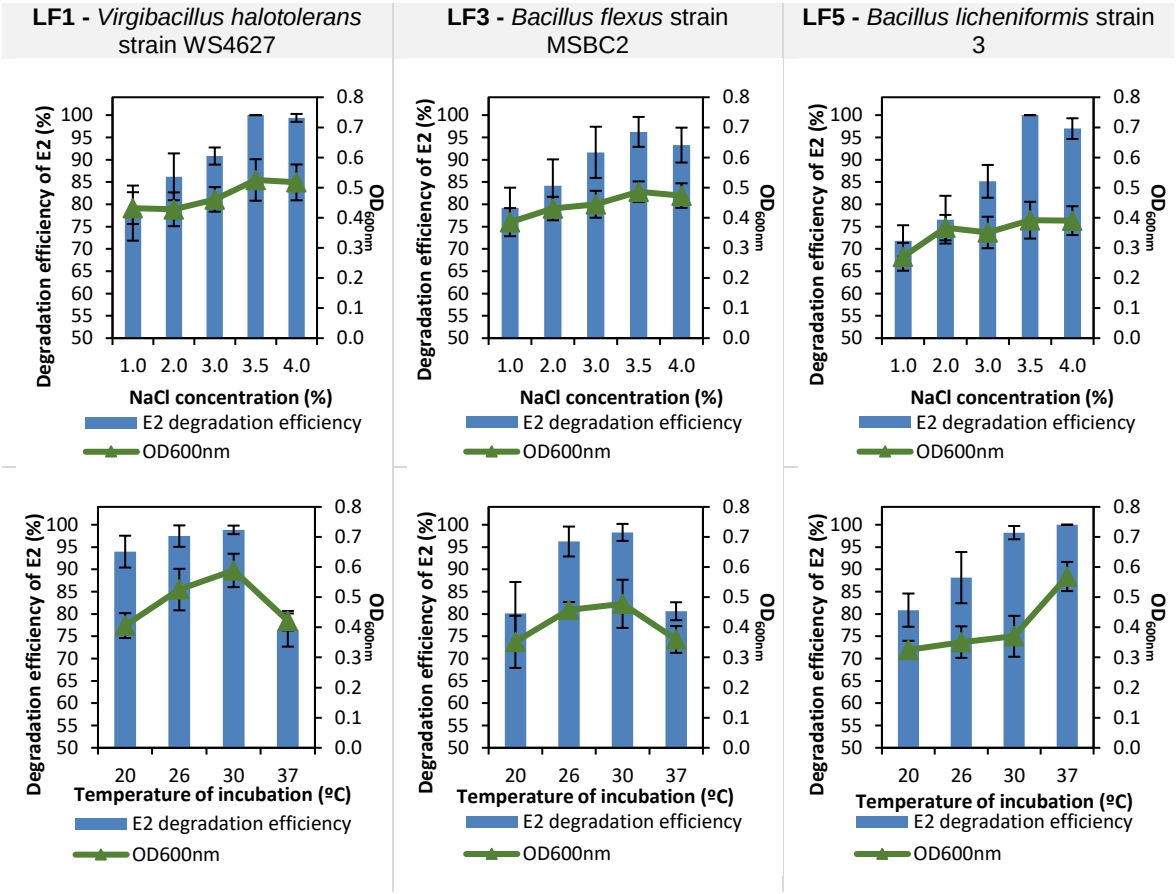

Figure 4.7. Effects of temperature and NaCl content on E2 (5 $mg \cdot L^{-1}$) removal in PBS_{mod} by **LF1**, **LF3** and **LF5** after 5 days of incubation. Data shown represent the average values of E2 (blue bars) and bacterial OD measured at 600 nm (green triangles), and errors of three independent experiments.

To study the influence of NaCl concentration in PBS_{mod}, samples were incubated at 26 ºC, as in the previous tests of E2 degradation. Samples to test the effect of temperature were done in PBS_{mod} containing NaCl at 3.5%.

As an overall conclusion, a temperature of 30 ºC and a content of 3.5% of NaCl were the most suitable conditions to yield more efficient degradation rates with **LF1** and **LF3**, obtaining E2 removal efficiencies yielding 96.2-100% after 5 days of incubation. A temperature of 37 ºC and a content of 3.5% of NaCl yielded complete removal of E2 in presence of **LF5**. OD_{600} measurements were correlated with the degradation efficiency of E2. Data herein optimized were used in following studies to promote E2 degradation efficiency.

4.3.4. Influence of initial concentration of E2 in biodegradation tests with LF1, LF3 and LF5

Previous studies of biodegradation of estrogens with **LF1**-**LF11** were performed using a starting concentration of E2 (5 $mg \cdot L^{-1}$) far higher than those found in WWTPs and natural waters. This allowed an initial screening to identify and make a collection of bacteria able to transform E2 in batch experiments. The ability of **LF1**, **LF3** and **LF5** to degrade E2 under more environmentally relevant concentrations of this compound in water, is an important aspect to investigate in the context of their application for bioremediation purposes. Usually, biodegradation rates of organic compounds increase when rising the initial concentration of the substrate.[214] Therefore, small scale data obtained in batch experiments may not reflect biodegradation rates when bacteria are transferred to practical applications, with lower concentrations of substrates.[181]

Occasionally, with toxic substrates for bacteria, removal rates decrease with increasing concentrations of the target compound. That is the case of chlorinated hydrocarbons.[215] Other consequence of the low concentration of substrate is the change of the biodegradation mechanisms themselves, or even the insufficient amount of carbon source to sustain bacterial growth. In this case, degradation can only occur by co-metabolism.[216]

Tests in this study were performed with initial concentrations of E2 of 5 $mg \cdot L^{-1}$, 1 $mg \cdot L^{-1}$, 100 $\mu g \cdot L^{-1}$ and 2 $\mu g \cdot L^{-1}$ and results are displayed in Fig 4.8.

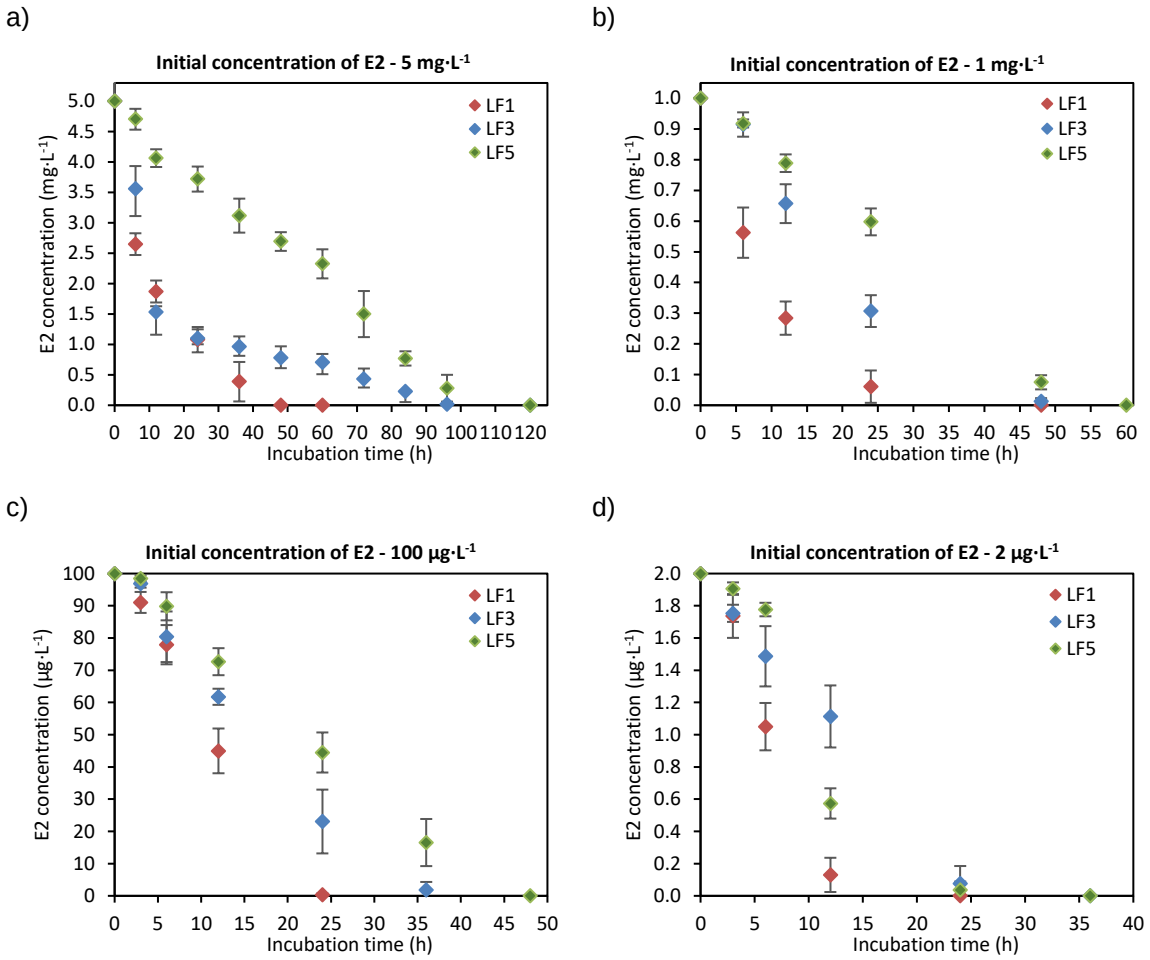

Figure 4.8. E2 degradation profiles by strains **LF1**, **LF3** and **LF5**, under aerobic conditions, with initial E2 concentrations of a) 5 mg·L^{-1}, b) 1 mg·L^{-1}, c) 100 µg·L^{-1} and d) 2 µg·L^{-1}. Data shown represent the average values (red diamonds represent LF1, blue diamonds represent **LF3**, green diamonds represent **LF5**,) and errors of three independent experiments.

Incubation temperature was set up as previously optimized for each strain. Samples containing 5 mg·L^{-1}, 1 mg·L^{-1}and 100 µg·L^{-1} of E2 were prepared in 30 mL of PBS_{mod}. Estrogen quantification in aliquots of samples with 5 mg·L^{-1}and 1 mg·L^{-1} of E2 was done using HPLC-UV. Samples with starting 100 µg·L^{-1} of E2 were monitored by using LC-MS. Samples containing 2 µg·L^{-1} of E2 were prepared in 500 mL of PBS_{mod}. Aliquots (100 mL) were concentrated (x100) by solid phase extraction (SPE) and eluted with 10 mL MeOH. Next, eluates were concentrated to dryness and re-dissolved in 1 mL of MeOH. Aliquots were then analysed by LC-MS for estrogen determination.

OD_{600} measurements done during the tests (data non-shown) were correlated with E2 degradation efficiency, as well as with the initial concentration of E2 as sole carbon source in the samples.

Table 4.4 summarizes the incubation times required by each isolate to completely remove E2 at different initial concentrations. Results of degradation studies of 5 $mg \cdot L^{-1}$ of E2 in presence of **LF1**, **LF3** and **LF5**, with optimized incubation temperatures, showed improved efficiencies than previous tests performed at 26 ºC. **LF1** achieved complete removal of E2 within 48 h of incubation, while **LF3** required 96 h and **LF5**, 120 h. This hierarchy of biodegradation efficiency among strains is maintained with degradation of 1 $mg \cdot L^{-1}$, 100 $\mu g \cdot L^{-1}$ and 2 $\mu g \cdot L^{-1}$ of E2. To completely remove 1 $mg \cdot L^{-1}$ of E2, **LF1** required 48 h, while **LF3** needed 48-60 h and **LF5** 60 h. To degrade 100 $\mu g \cdot L^{-1}$ of E2, **LF1** needed 24 h, **LF3** between 36 and 48 h and **LF5** 48 h. To remove 2 $\mu g \cdot L^{-1}$ of E2, **LF1** took 24 h, **LF3** between 24 and 36 h and **LF5** 36 h.

The indicate that the degradation efficiency is not linearly dependent on the initial concentration of E2. Degradation rate exhibited by **LF1**, **LF3** and **LF5** decreased with lower concentrations of E2. However, the results can be considered as encouraging, since the strains still preserve their ability to degrade E2 at low concentrations.

During these tests, the formation and removal of E1 as transformation product of E2 was observed by LC-MS (data non-shown), as previously detected in E2 degradation studies with the three strains.

Table 4.4. Incubation time (h) required by **LF1**, **LF3** and **LF5** to eliminate 5 $mg \cdot L^{-1}$, 1 $mg \cdot L^{-1}$, 100 $\mu g \cdot L^{-1}$ and 2 $\mu g \cdot L^{-1}$ of E2.

Incubation time (h) required to eliminate E2			
E2 concentration	(LF1 *Virgibacillus halotolerans* strain WS 4627)	LF3 (*Bacillus flexus* strain MSBC2)	LF5 (*Bacillus licheniformis* strain 3)
5 $mg \cdot L^{-1}$	48	96	120
1 $mg \cdot L^{-1}$	48	48-60	60
100 $\mu g \cdot L^{-1}$	24	36-48	48
2 $\mu g \cdot L^{-1}$	24	24-36	36

4.3.5. Simultaneous biodegradation of E1, E2, E3 and EE2 with LF1, LF3 and LF5

Once **LF1**, **LF3** and **LF5** were identified as efficient E2 degraders even at low concentrations, experiments to examine the simultaneous degradation of other relevant

EDCs were performed. For this purpose, **LF1**, **LF3** and **LF5** were individually cultured in 30 mL of

PBS_{mod} contained 100 µg·L^{-1} of each of the natural estrogens, E1, E2 and E3, along with 100 µg·L^{-1} of the artificial estrogen EE2, as sole carbon sources. Samples were incubated for 4 days at 30 ºC (**LF1** and **LF3**) or 37 ºC (**LF5**). Aliquots (500 µL) of samples were taken at different treatment times and were injected in LC-MS for quantification of estrogens. OD measurements at 600 nm were used as descriptor of bacterial growth. Abiotic control samples were also included, and showed insignificant removal of E1, E2, E3 or EE2 (Fig. 4.9), so that any change in the estrogens concentration will be attributed to the ability of the strains to transform them.

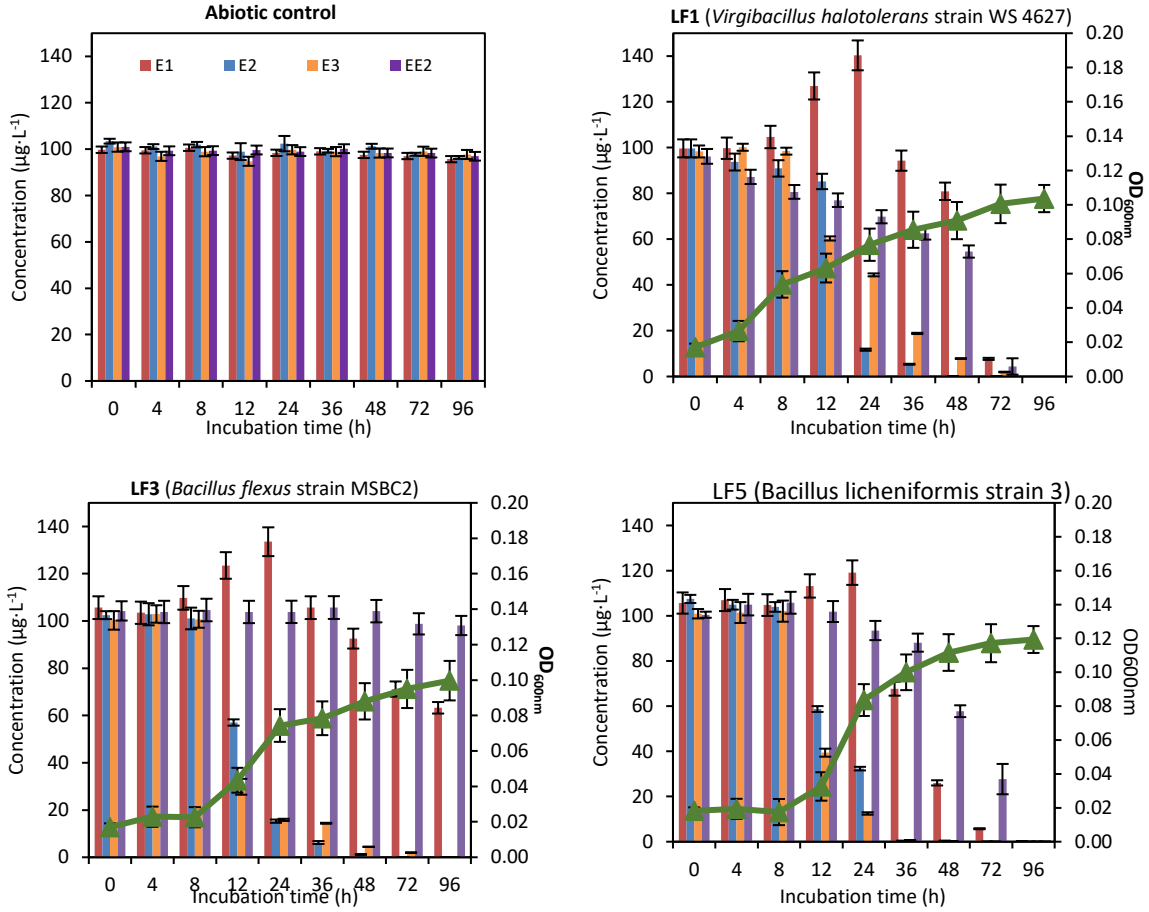

Figure 4.9. E1, E2, E3, EE2 co-degradation (100 µg·L^{-1} each) profiles by strains **LF1**, **LF3** and **LF5**, under aerobic conditions. Data shown represent the average values (blue bars represent E2, red bars represent E1, orange bars represent E3, purple bars represent EE2) and errors of three independent experiments, and bacterial OD measured at 600 nm (green triangles).

Within the first hours of the tests, the three strains accumulated higher amounts of E1 than the initial concentration (100 $\mu g \cdot L^{-1}$), which can be attributed to the oxidation of E2. **LF1** reached a maximal concentration of E1 (140.33 $\mu g \cdot L^{-1}$) after 24 h of incubation. Next E1 measurement, after 36 h of incubation, showed an average concentration of 94.32 $\mu g \cdot L^{-1}$. At this stage, levels of E2 were already low (5.34 $\mu g \cdot L^{-1}$). **LF3** accumulated 133.55 $\mu g \cdot L^{-1}$of E1 after the initial 24 h of incubation. However, E1 was not effectively removed from the sample during the biological treatment, and after 96 h, 63.26 $\mu g \cdot L^{-1}$ of E1 remained in the samples. In contrast, low amounts of E1 were produced in presence of **LF5** (a maximum of 119.12 $\mu g \cdot L^{-1}$ after 24 h of incubation), which in addition were removed during the treatment.

The three strains degraded 100 $\mu g \cdot L^{-1}$ of E3 efficiently: complete degradation occurred after 96 h with **LF1** and **LF3**, and 72 h with **LF5**. Additionally, **LF1** and **LF5** completely degraded 100 $\mu g \cdot L^{-1}$ of EE2 in 96 h. On the other hand, **LF3** did not show evidence of EE2 metabolization.

In comparison with E2 sole degradation (see Table 4.4), in co-degradation, E2 was removed at slower rates by **LF1** (48 h) and **LF3** (72 h). This can be understood as a differential preference of the strains for particular estrogens. However, **LF5** degraded faster 100 $\mu g \cdot L^{-1}$ of E2 in presence of other estrogens/carbon sources, needing only 36 h to completely remove it from the samples.

OD_{600} measurements done during the tests were correlated with estrogen consumption and bacterial growth, displaying for **LF3** and **LF5** patterns of adaptation, logarithmic growth and stability stages.

4.3.6. Biodegradation of E2 by LF1, LF3 and LF5 in presence of other carbon sources

Before testing **LF1**, **LF3** and **LF5** in real wastewaters for remediation purposes, biodegradation studies with 100 $\mu g \cdot L^{-1}$ of E2 were repeated by adding 10 $mg \cdot L^{-1}$ of D-(+) glucose as additional carbon source for bacteria. D-(+) glucose was proposed as alternative substrate for the strains, to assess their preference to grow on E2. From these preliminary results, it can be evaluated if **LF1**, **LF3** and **LF5** would have potential as estrogen degraders in wastewaters, with more complex composition of organic matter, and therefore alternative metabolic pathways for cell growth and sustainment.

Concentration of D-(+) glucose was determined by the phenol/sulfuric acid method, which is an expedite colorimetric assay to quantify total carbohydrates in aqueous samples (Scheme 4.1).[217] D-(+) glucose reacts in the presence of concentrated sulfuric acid to generate 5-hydroxymethylfurfural, which condenses with phenol to form a stable yellow-gold compound that can be measured spectrophotometrically (λ_{max}= 490 nm). This colour can last several hours, and the accuracy of the method is within ±2%.

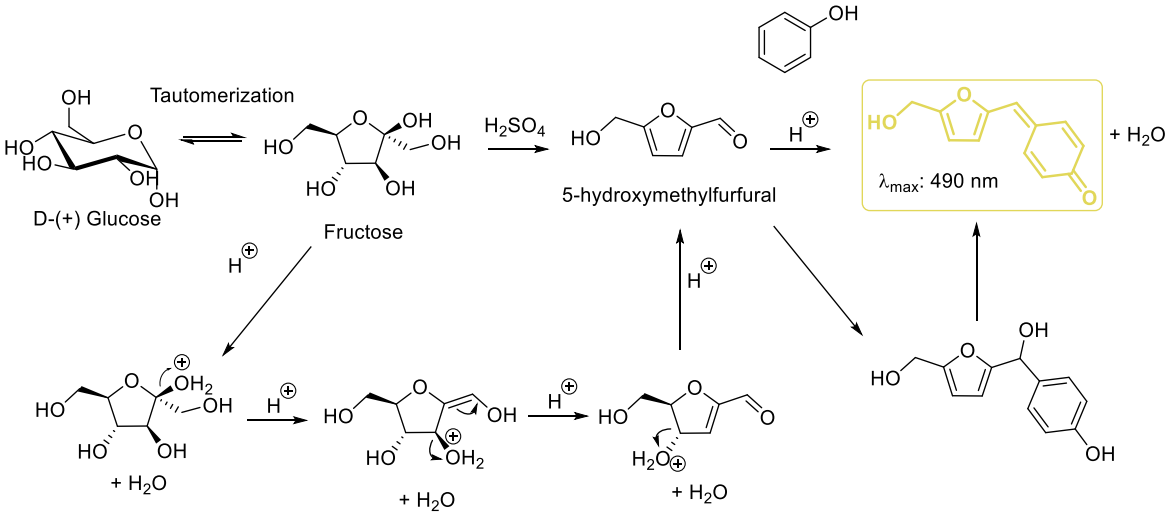

Scheme 4.1

First, standards were prepared in triplicate, in PBS_{mod} solutions containing 0.2, 0.4, 0.6, 0.8, 1.0, 2.0, 4.0, 6.0, 8.0, 10.0 and 12.2 mg·L^{-1} of D-(+) glucose. Then, standards were treated with sulfuric acid and phenol (see section 4.4.13) and absorbance was measured at 490 nm. Results were averaged and displayed in Fig. 4.10. Measurements of absorbance at 490 nm and concentration of D-(+) glucose presented a linear relation, with LOQ= 0.40 mg·L^{-1} and LOD= 0.20 mg·L^{-1}.

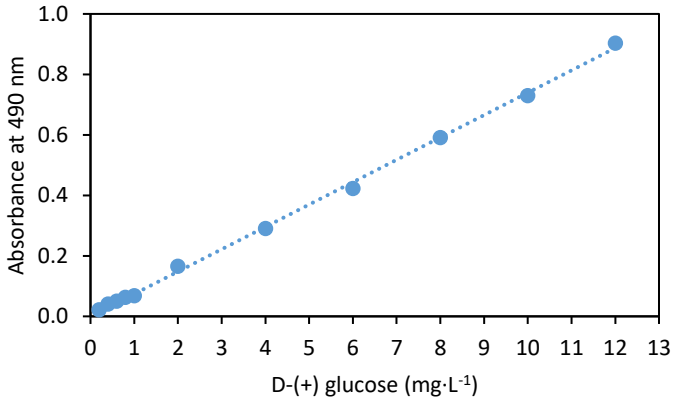

Figure 4.10. D-(+) Glucose calibration curve. Data shown represent the average values and errors of three independent experiments. R^2 = 0.9986.

Results of biodegradation of 100 µg·L^{-1} of E2 by strains **LF1**, **LF3** and **LF5** are presented in Fig. 4.11. Abiotic controls showed stable concentrations of D-(+) glucose, E2 and E1 upon three days of incubation in PBS_{mod}. Strains **LF3** and **LF5** were more efficient in E2 removal in samples containing D-(+) glucose, than in samples with E2 as sole carbon source (Table 4.4). **LF3** and **LF5** degraded 100 µg·L^{-1} of E2 within 36 h of incubation time, and growth (data non-shown) was significantly enhanced by the addition of D-(+) glucose. In this study, **LF1** equally metabolized 100 µg·L^{-1} of E2 either in presence or the absence of D-(+) glucose. **LF1** was also able to degrade D-(+) glucose and could grow efficiently, according to OD_{600nm} measurements (data non-shown).

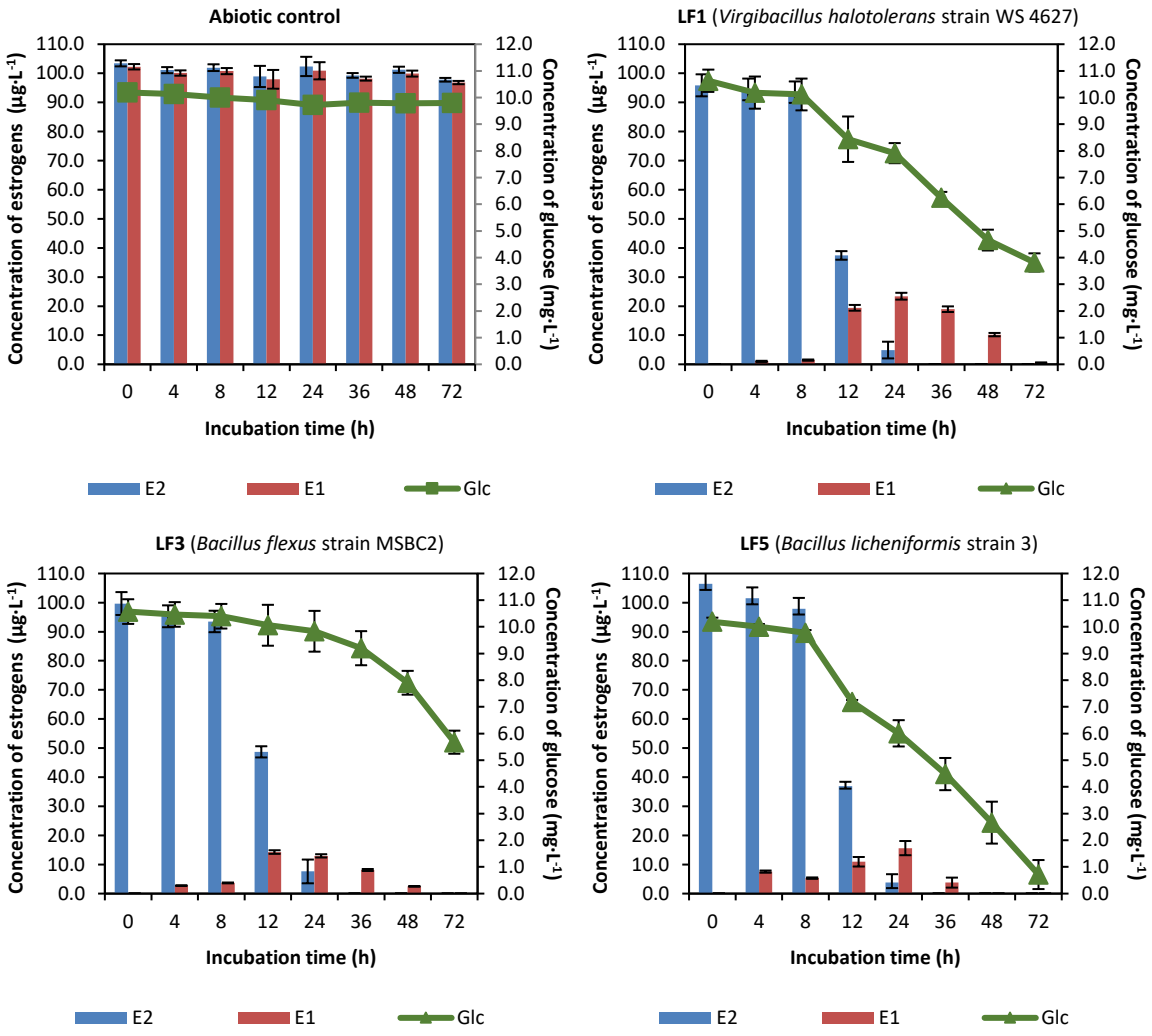

Figure 4.11. E2 degradation (100 µg·L^{-1}) profiles by strains **LF1**, **LF3** and **LF5**, under aerobic conditions, in presence of D-(+) glucose (10 mg·L^{-1}). Data shown represent the average values (blue bars represent E2, red bars represent E1, green triangles represent D-(+) glucose) and errors of three independent experiments.

Once again, production of E1 was detected during the consumption of E2 by the three strains in this study. Maximal concentrations of E1 produced within the tests (23.41 $\mu g \cdot L^{-1}$ by **LF1**, 14.28 $\mu g \cdot L^{-1}$ by **LF3**, 15.63 $\mu g \cdot L^{-1}$ by **LF5**) were fully removed after 3 days of incubation.

Effect of carbon supplementation (biosolids) on biodegradation rates of hydrocarbons was described by Sarkar *et. al* in 2005.[218] Later, enhancement of biodegradation activity of petroleum hydrocarbons in presence of D-(+) glucose was explored by X. Li *et al*.[219] In this study, consumption of petroleum hydrocarbons was accelerated by 200% in presence of D-(+) glucose in saline soil samples, as co-substrate.

4.3.7. Biodegradation of estrogens in real water samples from a WWTP

Wastewater samples were collected from the influent and effluent streams of the Ruhleben sewage treatment plant (STP) (Fig. 4.12), in Berlin, which handles the flows from 1.6 million inhabitants and has a plant capacity of 240000 m^3 per day. In this STP, the water treatment involves screening (removal of large non-biodegradable and floating solids), primary sedimentation, biological phosphorous removal (anaerobic tank), denitrification (anoxic tank), nitrification (aerobic tank) and a clarification process.[220] Samples (3L each sampling from the influent stream, 200 mL each sampling from the effluent stream) were provided by the operating company, Berliner Wasserbetriebe. Then, samples were stored in brown glass bottles at 4 °C and analysed within five days. Sampling was carried out by a flow-proportional automatic sampler over a period of 24 h, on 13/07/2016, 18/07/2016 and 25/07/2016.

a) **b)**

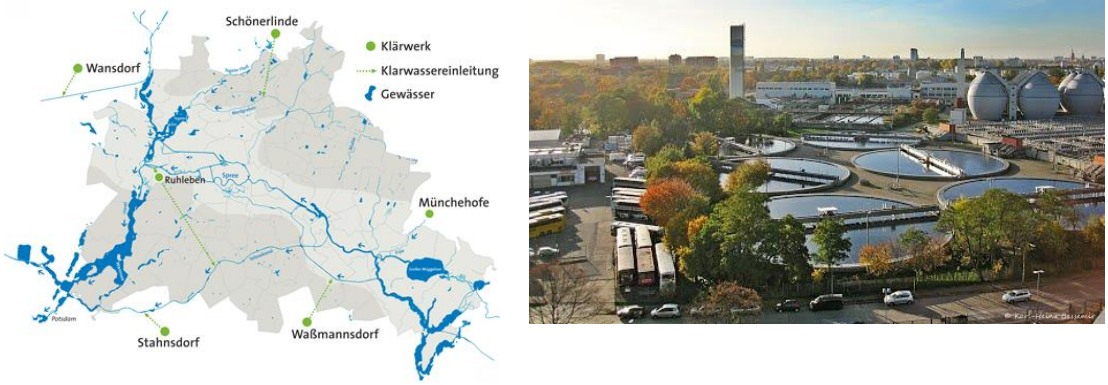

Figure 4.12. a) Map of the Berlin waterways: clear water discharge (Klarwassereinleitung), water bodies (Gewässer) and the locations of the STPs (Klärwerk), and b) picture of the Ruhleben STP.

Fig. 4.13 represents the procedure of the pre-treatment, biological treatment and analysis of the samples used in this study.

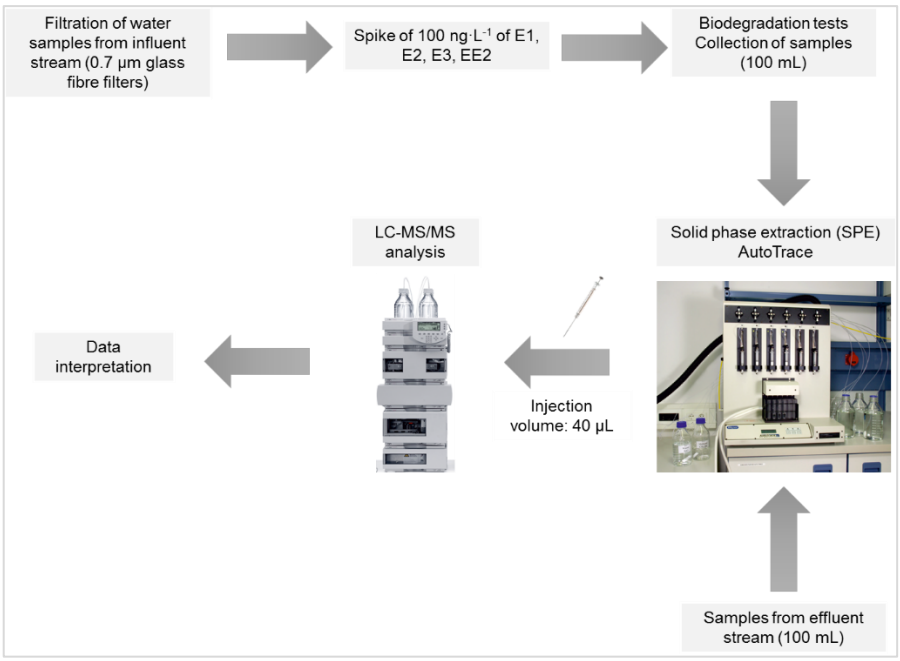

Figure 4.13. Schematic representation of the biodegradation procedure with real water samples collected from WWTP in Ruhleben, Berlin.

First, to simulate the primary treatment of the STP, consisting on the initial screening and sedimentation of solids, water samples from the influent stream were filtrated twice with glass fibre filters of 0.70 µm (Fig. 4.14). Influent aliquots of the filtrated fractions, along with aliquots from the effluent stream (15 mL), were taken to analyse total organic carbon (TOC) after settlement. Results are displayed in Table 4.5, which also shows values of total carbon (TC) and inorganic carbon (IC). Influent samples of the three days presented a TC content between 1889.5 and 2131.0 $mg \cdot L^{-1}$. TC content of effluent samples was between 120.1 and 204.0 $mg \cdot L^{-1}$. These analyses were kindly performed by Dr. Ute Kalbe, from BAM, in Berlin.

Figure 4.14. Water sample of the influent stream of Ruhleben STP before (left) and after (right) filtration.

Table 4.5. Values of TOC, TC and IC of water samples taken from the influent and effluent streams of Ruhleben STP.

Sampling date	TOC	TC	IC	Unit
13/07/2016 Inf.	1790.5	1889.5	99.0	$mg \cdot L^{-1}$
13/07/2016 Eff.	42.3	120.1	77.8	$mg \cdot L^{-1}$
18/07/2016 Inf.	1906.0	1987.9	81.9	$mg \cdot L^{-1}$
18/07/2016 Eff.	97.3	204.2	106.9	$mg \cdot L^{-1}$
25/07/2016 Inf.	2054.5	2131.0	76.5	$mg \cdot L^{-1}$
25/07/2016 Eff.	78.2	144.4	66.2	$mg \cdot L^{-1}$

The LC-ESI-MS method used in this study was previously developed and validated at the Division 1.8 of Environmental Analysis at BAM (Berlin). For more details, see Section 4.4.11. Due to LOQ values of the LC-MS/MS instrument method used to analyse estrogens with this matrix complexity, and since these biodegradation studies were performed to evaluate the potential of **LF1**, **LF3** and **LF5** to remove estrogens in real water samples, each estrogen (E1, E2, E3 and EE2) was spiked at a concentration of 100 $ng \cdot L^{-1}$, which facilitated the monitoring of removal rates of estrogens.

Secondary treatment of wastewaters consists on the removal of dissolved and suspended organic matter, which usually is derived from human and food waste, soaps and detergent. Secondary treatment is typically performed by microorganisms. Samples (500 mL) of real wastewaters were inoculated with **LF1**, **LF3** and **LF5**, and incubated in dark conditions for 4 days, adjusting pH to 7.0 every day. Aliquots (100 mL) were taken at incubation times 0, 1, 2, 3 and 4 day, and were submitted to a solid phase extraction (SPE) procedure, along with non-treated aliquots from the effluent stream (100 mL). SPE was performed automatically with an AutoTrace™ SPE workstation, with Strata™-X cartridges. First, cartridges were washed with 10 mL of MeOH, equilibrated with 10 mL of ultrapure water and followed by loading the respective samples, which previously were diluted to a volume of 1000 mL with 900 mL of ultrapure water. Afterwards, the cartridges were dried and the adsorbates were eluted with 10 mL of MeOH. Eluates were concentrated to dryness and re-dissolved in 1 mL of MeOH. Aliquots (100-fold concentrated) were then analysed by LC-MS/MS for estrogens determination.

By subtracting the previously spiked amount of estrogens (100 $ng \cdot L^{-1}$ of each estrogen), real concentrations in the influent stream were calculated and, with calculated concentrations of estrogens in the effluent stream, removal rates were determined (Table 4.6). The average removal rates of E1 (91%), E2 (87%) and EE2 (82%) are comparable to those already reported by Heberer *et al.* for Ruhleben STP in 2005 (average removal rates:

93% for E1, 93% for E2 and 80% for EE2; E3 was not monitored).[221] The average removal rate of E3 was 93%.

Table 4.6. Concentrations ($ng \cdot L^{-1}$) of E1, E2, E3 and EE2 and removal rates (%) determined in water samples taken from the influent and effluent streams of Ruhleben STP during July, 2016.

Sample	E1	E2	E3	EE2
Influent ($ng \cdot L^{-1}$)	96.2-108.2	32.8-42.7	79.4-94.5	13.3-11.0
Effluent ($ng \cdot L^{-1}$)	4.2-15.6	<LOQ (1.8)-9.1	1.0-11.5	1.0-3.1
Removal rate (%)	86-96	79-94	88-99	72-93

Results of simultaneous biodegradation of E1, E2, E3 and EE2 by **LF1**, **LF3** and **LF5** are summarized in Table 4.7. Due to the turbidity of the samples, OD_{600} could not be monitored in this study. Abiotic samples maintained the initial concentrations of estrogens throughout the study. All tested strains degraded E3 from real wastewaters, being **LF5** the more efficient isolate (49%), followed by **LF1** (47%) and **LF3** (20%). **LF1** and **LF3** presented low degradation rates of E2 (5% and 4%, respectively), and did not show evidence of degrading E1, or EE2. On the other hand, **LF5** also displayed efficient degradation of E1 (22%) and E2 (27%), and a modest degradation of EE2 (10%).

Table 4.7. Concentrations ($ng \cdot L^{-1}$) of E1, E2, E3 and EE2 and removal rates (%) determined simultaneous estrogens degradation by **LF1**, **LF3** and **LF5**, in water samples taken from the influent stream of Ruhleben STP during July, 2016.

Sample	E1		E2		E3		EE2	
	Conc. ($ng \cdot L^{-1}$)	removal rate (%	Conc. ($ng \cdot L^{-1}$)	removal rate (%)	Conc. ($ng \cdot L^{-1}$)	removal rate (%)	Conc. ($ng \cdot L^{-1}$)	removal rate (%)
Abiotic sample	208.5 207.1	0	137.0 133.2	3	188.4 183.3	3	112.3 112.1	0
LF1	230.0 227.1	1	136.6 129.4	5	188.4 100.7	47	112.3 111.3	1
LF3	224.6 225.7	0	133.8 128.4	4	195.5 155.6	20	112.3 112.6	0
LF5	230.0 178.7	22	136.6 100.2	27	188.0 95.4	49	112.8 102.0	10

These results demonstrate the potential of **LF5** to be used as estrogen degrader in wastewater for biorremediation applications, being able to simultaneously remove E1, E2, E3 and EE2. The augmentation of an activated sludge with **LF5** could enhance the

efficiency of removal of EDCs in the effluent streams that discharges into superficial natural waters.

4.3.8. Transformation products in E2 biodegradation with LF5

Studies aimed at looking for transformation products arising from the biodegradation of E2 were performed with samples of PBS_{mod} containing 5 $mg \cdot L^{-1}$ of E2, which were incubated with **LF5**. **Fig. 4.15** shows HPLC chromatograms of E2 removal (retention time 10.46 min) in presence of **LF5** within one and four days of incubation. During this period, E1 (retention time 10.98 min) was produced as major metabolite.

Chromatograms indicate the formation of unknown intermediate products eluting faster than E1 and E2 (retention times between 3.08 and 5.05 min). Due to the elution characteristics of the methodology, these products are more polar than related estrogens. The peak areas of these products decreased, thus suggesting to be cleaved during degradation by **LF5**. According to previous research, different patterns of E2 biodegradation form products with additional hydroxyl groups in the phenol of E2 and E1.[106-108, 222] Kurisu *et al.* described consistent evidences of the transformation of E2 to 4-OH-E2 in presence of *Sphingomonas* sp., where 4-OH-E2 was further degraded *via* meta cleavage.[223] However, the difference in retention times with related E1 and E2 suggest that these products could be smaller molecules arising from the cleavage of E2 and/or E1. Chromatograms also indicate low concentrations of an unknown intermediate product at 13.36 min, which accumulated during the incubation period.

After examination of unknown transformation products in HPLC chromatograms, according to the elution characteristics of the method, and considering some E2 metabolites already reported, six E2 aerobic-degradation pathways in presence of **LF5** were proposed (Fig. 4.16).

.

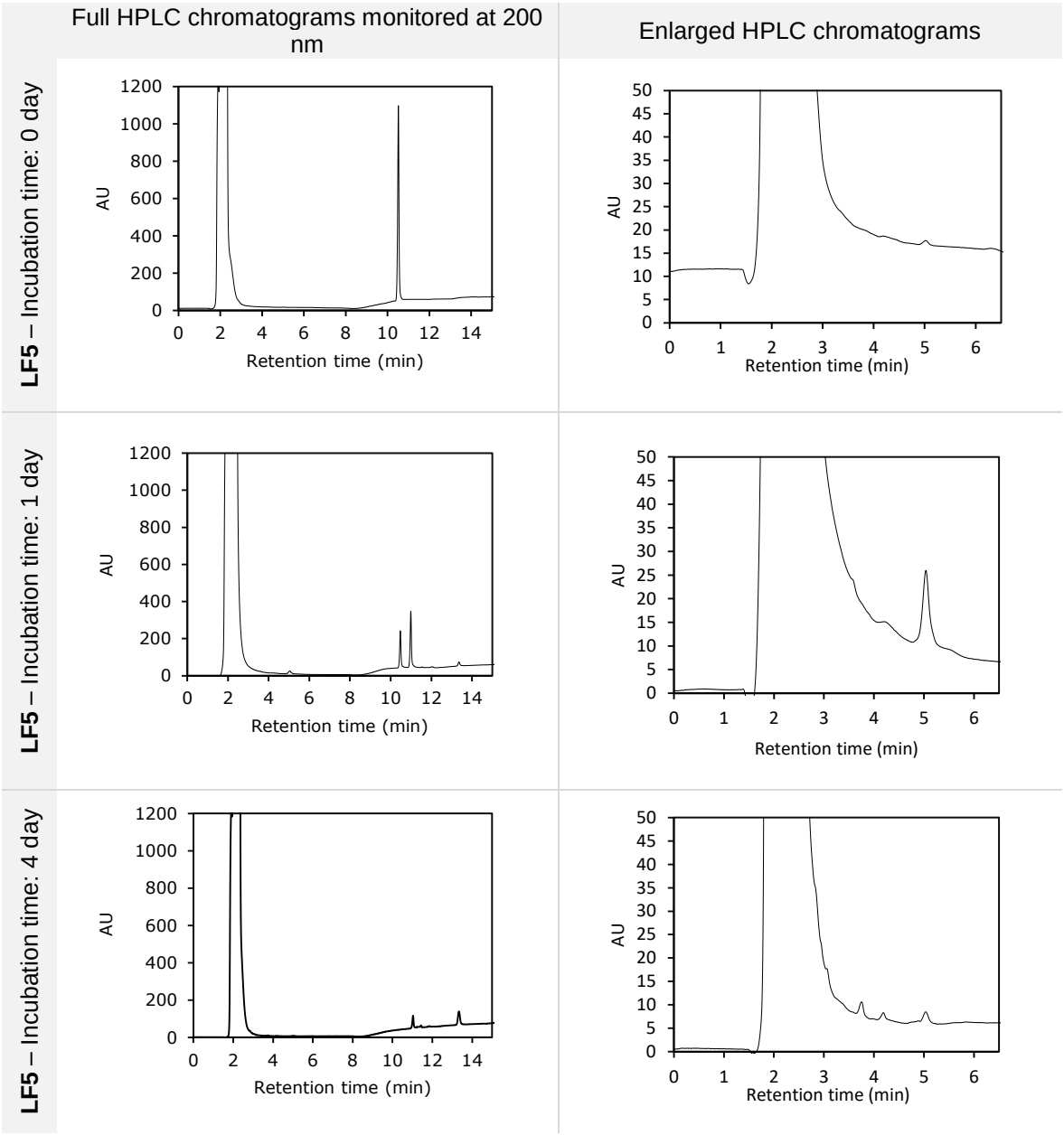

Figure 4.15. Selected HPLC chromatograms corresponding to samples collected from incubation of **LF5** with 5 mg·L^{-1} of E2 after 0, 1 and 4 days. Retention time of E2 is 10.46 min. Retention time of E1 is 10.98 min.

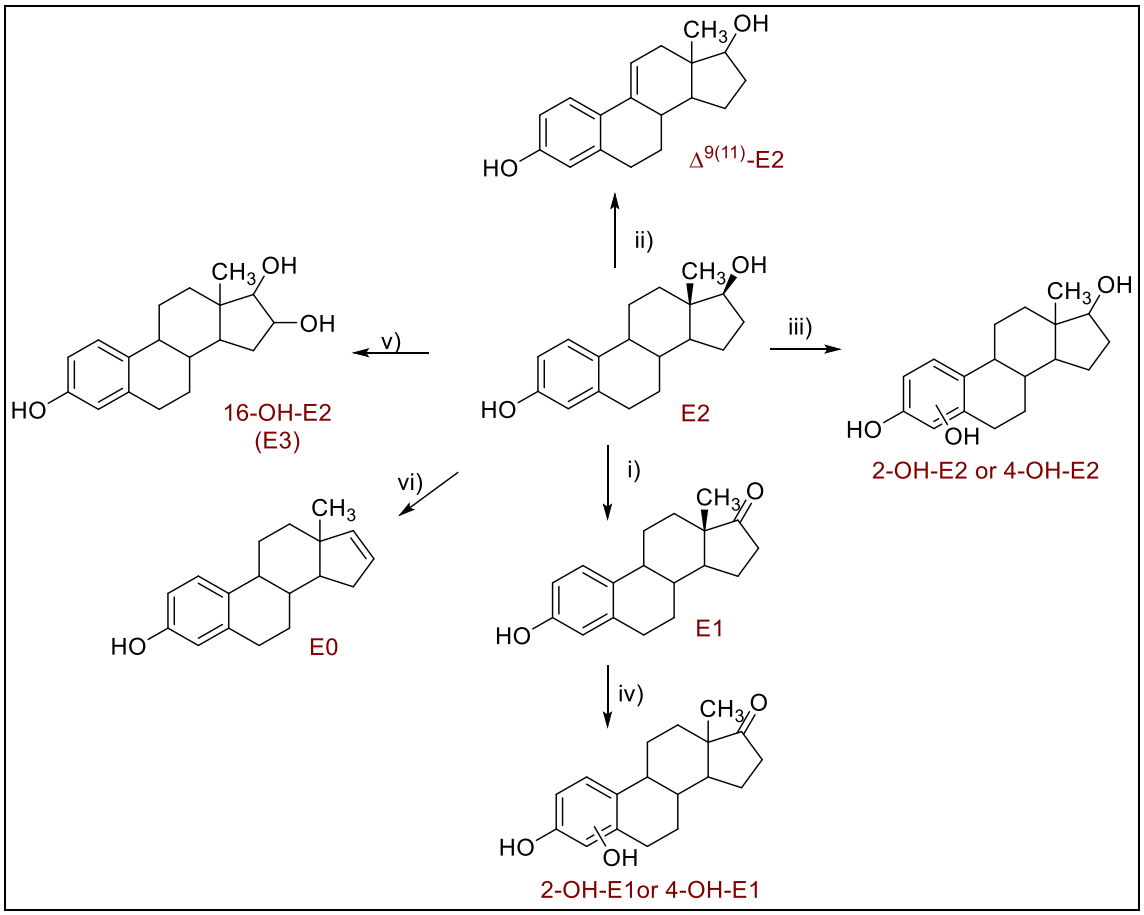

Figure 4.16. Proposed pathways for E2 degradation by **LF5**, under aerobic conditions.

To obtain more detailed information on the structural characteristics of the unknown compounds, samples were re-injected in a LC-MS equipment. It is important to note that retention times in MS chromatograms are slightly shifted: E2 is detected at 10.92 min, E1 is detected at 11.30 min. First, MS spectrum of E2 was identified in the samples. The electrospray ionization of E2 in the negative ion mode resulted in the molecular anion $[M - H]^-$ *m/z* 271.1. The collisional activation of this $[M - H]^-$ resulted in numerous product ions, including *m/z* 143.0, *m/z* 183.0 and *m/z* 239.1 (Fig. 4.17).[224]

Proposed pathway for E2 degradation (i): Dehydrogenation of ring D of E2 at C-17, and formation of E1. This mechanism agrees with observations of biodegradation tests performed in these studies. A typical MRM LC-MS chromatogram of E1 was obtained from the samples at retention time 11.30 min (Fig. 4.18). ESI of E1 in negative mode resulted in the molecular anion $[M - H]^-$ *m/z* 269.1, and its collision resulted in intense peaks corresponding to fragment ions as *m/z* 142.8, *m/z* 144.9 and *m/z* 182.9. Results are in agreement with data already reported.[178]

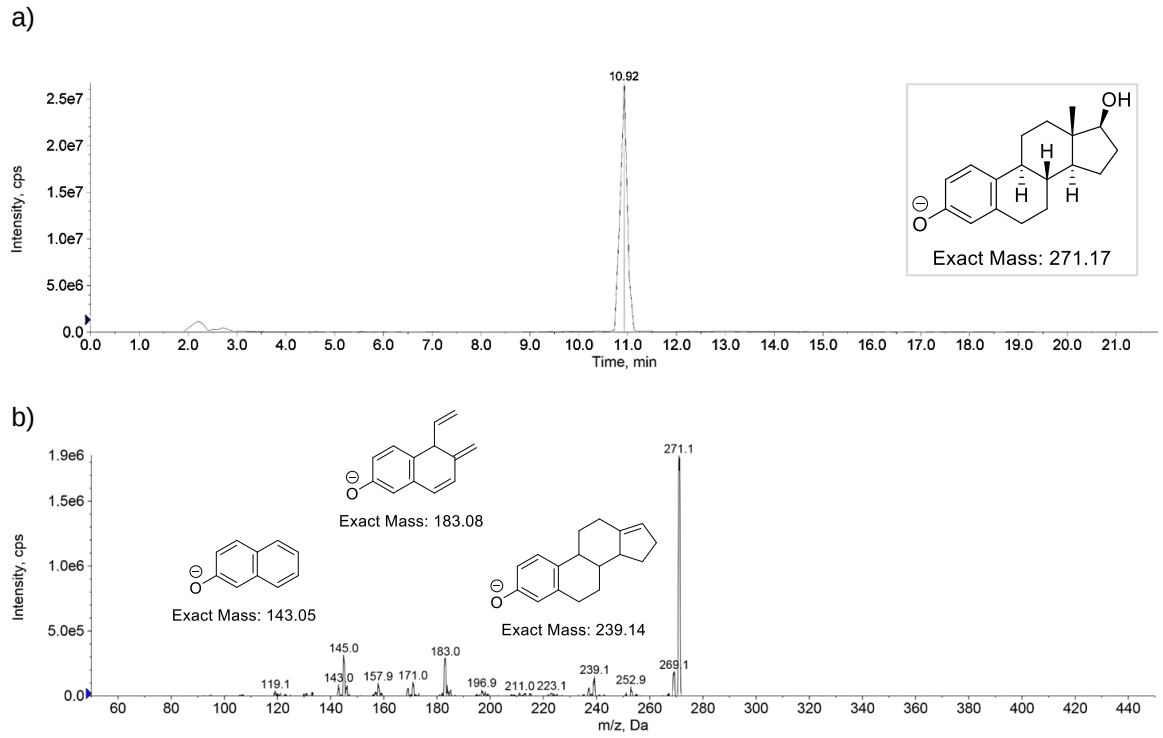

Figure 4.17. a) LC-ESI-MS extracted chromatogram for *m/z* 271,1; b) Product-ion spectra from collisionally activated decompositions of the ESI produced $[M-H]^-$ ion *m/z* 271.17.

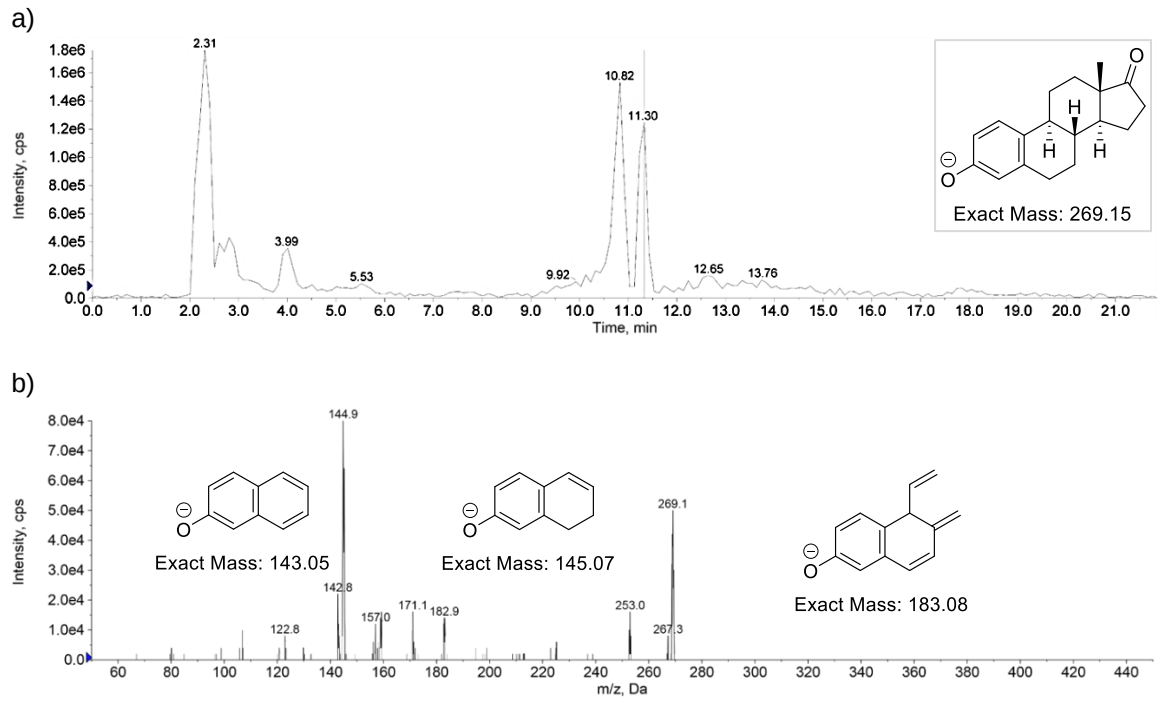

Figure 4.18. a) LC-ESI-MS extracted chromatogram for *m/z* 269,1 and proposed structure; b) Product-ion spectra from collisionally activated decompositions of the ESI produced $[M-H]^-$ ion *m/z* 269.1**.**

Proposed pathway for E2 degradation (ii): Dehydrogenation of E2 at C-9 and C-11, and formation of $\Delta^{9(11)}$-E2. MS extracted chromatogram for *m/z* 269,1 shows a peak eluted at the same retention time of E2 (10.92 min) (Fig 4.19). Collisional activation of this molecular anion $[M - H]^-$ *m/z* 269.15, resulted in intense fragment ions as *m/z* 142.8, *m/z* 157.0, *m/z* 171.0, *m/z* 197.0 and *m/z* 251.3. This unknown product could have been formed from a dehydrogenation of E2 at C-9 and C-11, which may present a similar polarity to E2. Assuming $\Delta^{9(11)}$-E2 as transformation product of E2, *m/z* of fragment ions would coincide well with the fragmentation pathways of $\Delta^{9(11)}$-E2, when compared to its parent, E2. $\Delta^{9(11)}$-E2 was already proposed as intermediate product of E2 by Havlíková *et al.*[225]

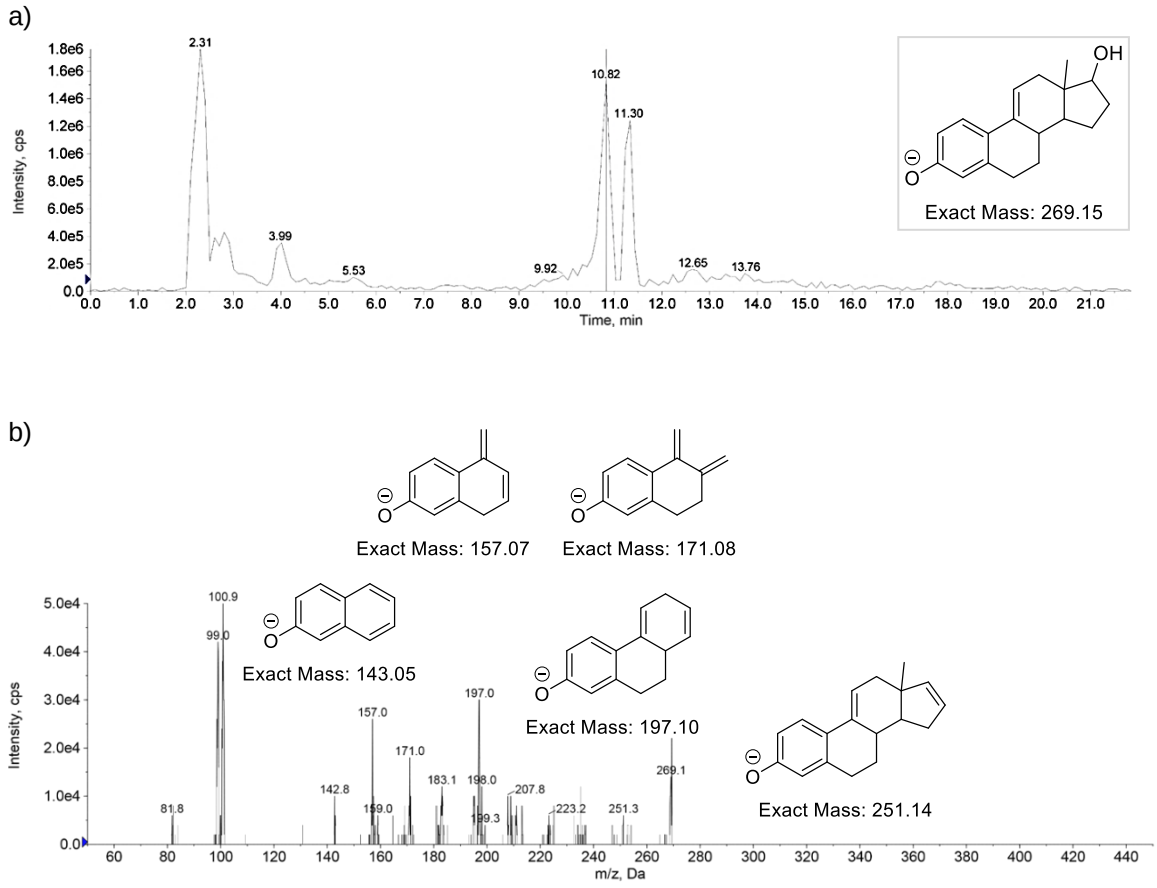

Figure 4. 19. a) LC-ESI-MS extracted chromatogram for *m/z* 269,1 and proposed structure; b) Product-ion spectra from collisionally activated decompositions of the ESI produced $[M-H]^-$ ion *m/z* 269.1**.**

Proposed pathway for E2 degradation (iii): Hydroxylation of E2 at C-2 or C-4, and formation of 2-OH-E2 or 4-OH-E2. Enlargement of HPLC chromatograms showed the formation and disappearance of two peaks centred at 9.98 and 10.06 min, at low concentrations, which could be compounds derived from E2 and E1 (Fig. 4.20a). The more

polar compound, eluted at 9.98 min, could be formed as result of E2 hydroxylation in position C-2 or C-4, according to a previous study by Debrauwer *et al*.[226] LC-ESI-MS extracted chromatogram for *m/z* 287,1, which would correspond to the molecular anion [M - H]⁻ of 2-OH-E2 or 4-OH-E2, coincides well in terms of retention time in MS spectrum (note that from HPLC to LC-MS there is a difference of around 0.5 min in retention time) (Fig. 4.20b). Its collision resulted in intense peaks corresponding to fragment ions as *m/z* 161.0, *m/z* 255.0 and *m/z* 269.0, coinciding with the analogous fragmentation pattern of its parent E2 (Fig. 4.20c).

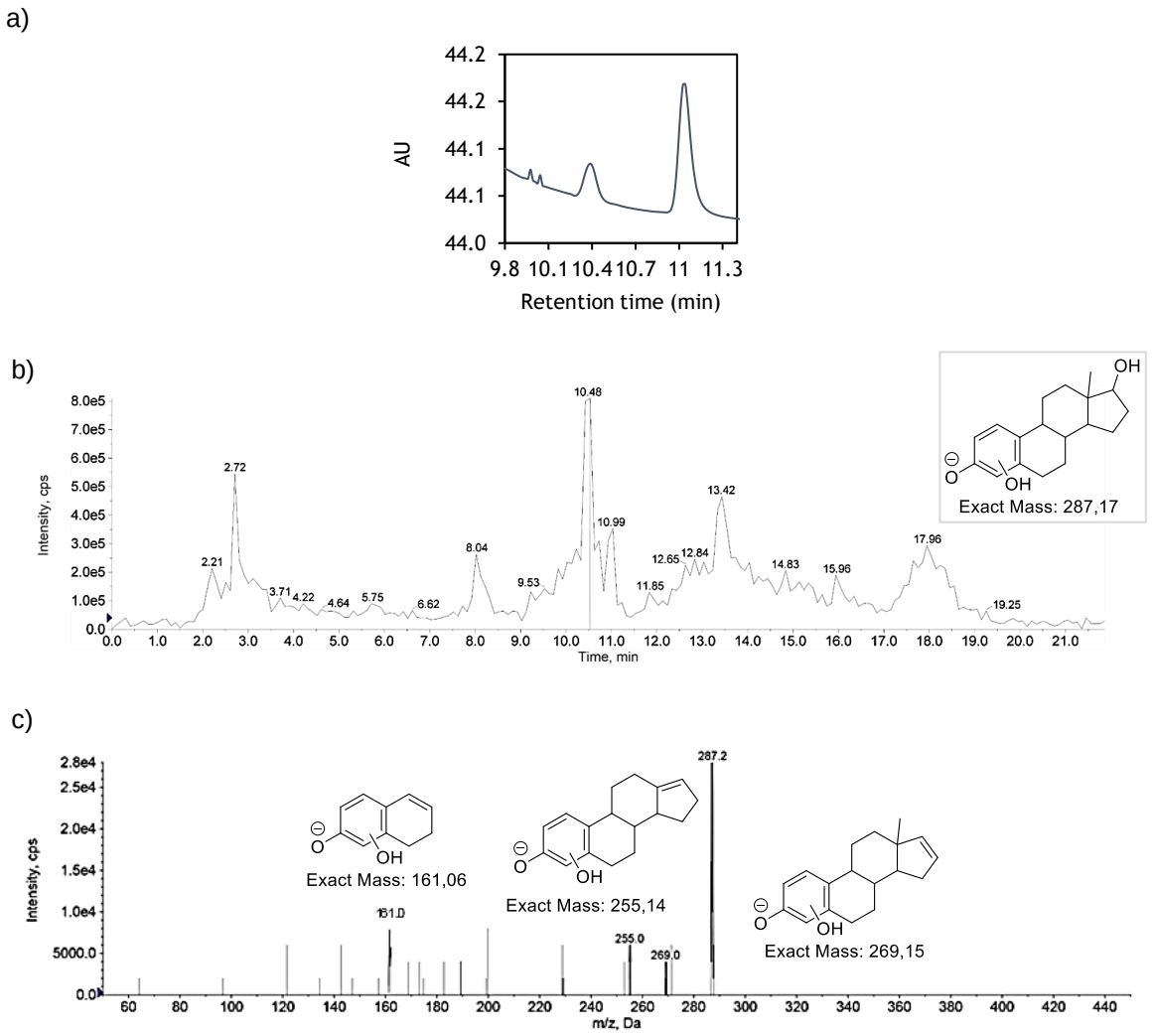

Figure 4.20. a) Enlargement of a HPLC chromatogram corresponding to a sample collected from incubation of **LF5** with 5 mg·L^{-1} of E2 after 4 days; b) LC-ESI-MS extracted chromatogram for *m/z* 287,1 and proposed structure; c) Product-ion spectra from collisionally activated decompositions of the ESI produced [M-H]⁻ ion *m/z* 287.1.

Proposed pathway for E2 degradation (iv): Hydroxylation of E1 at C-2 or C-4, and formation of 2-OH-E1 or 4-OH-E1. The peak found at 10.06 min at low concentrations (Fig. 4.21) could be formed due to the hydroxylation of E1 at C-2 or C-4. Retention time in LC-ESI-MS extracted chromatogram for *m/z* 285,1, which would correspond to the molecular anion $[M - H]^-$ of 2-OH-E1 or 4-OH-E1, coincides well (Fig. 4.21a). Its collision resulted in intense peaks corresponding to fragment ions as *m/z* 161.0, *m/z* 205.0, *m/z* 254.6 and *m/z* 269.0, coinciding with an analogous fragmentation pattern of its parent E2 and the previously proposed structures, 2-OH-E2 or 4-OH-E2 (Fig. 4.20c).

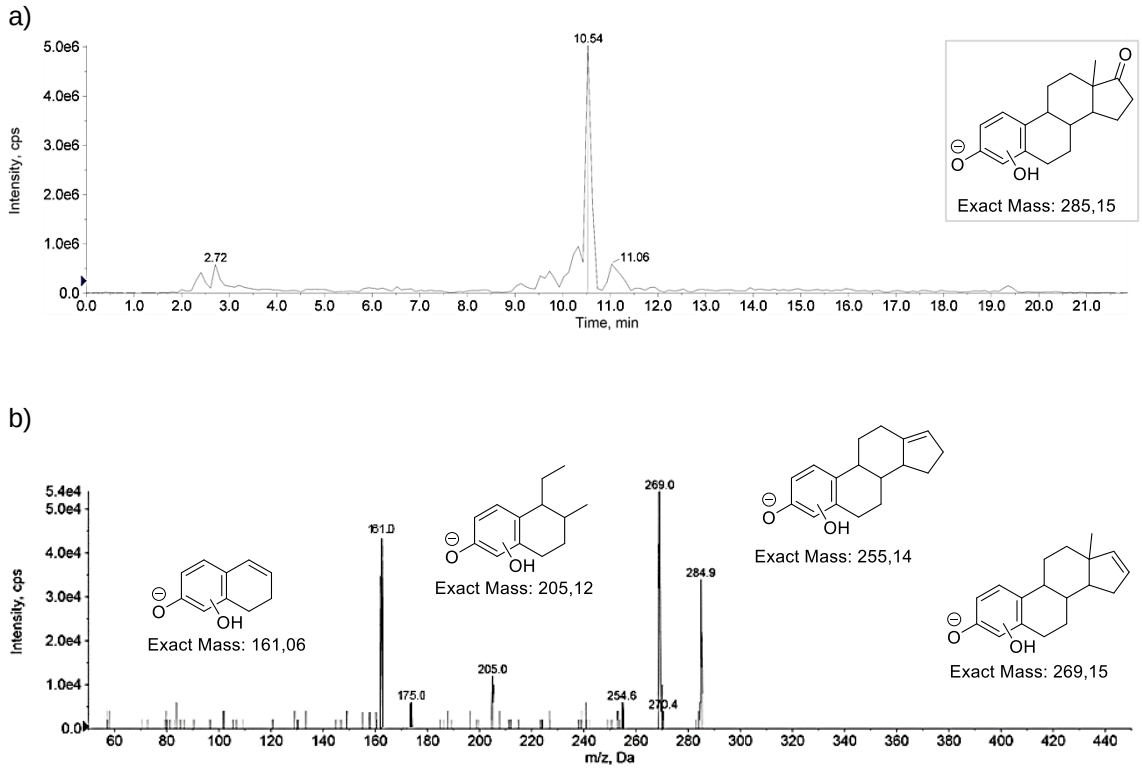

Figure 4.21. a) LC-ESI-MS extracted chromatogram for *m/z* 285,1 and proposed structure; b) Product-ion spectra from collisionally activated decompositions of the ESI produced $[M-H]^-$ ion *m/z* 285.1**.**

Proposed pathway for E2 degradation (v): Hydroxylation of E2 at C-16, and formation of 16-OH-E2. Enlargements of HPLC chromatograms (Fig. 4.15) showed the formation of unknown intermediate products eluting at retention times between 3.08 and 5.05 min. Polarity characteristics of these unknown products suggested the formation of 16-OH-E2, or E3, if stereochemistry is not considered in the proposed structure. E3 was

confirmed after injection of the commercially available estrogen, and product-ion-scan mass spectrum coincide well with reported data (Fig. 4.22**).**[227] The electrospray ionization of E3 in the negative ion mode resulted in the molecular anion $[M - H]^-$ *m/z* 287.2. The collisional activation of this $[M – H]^-$ resulted in two main product ions: *m/z* 253.0 and *m/z* 269.0.

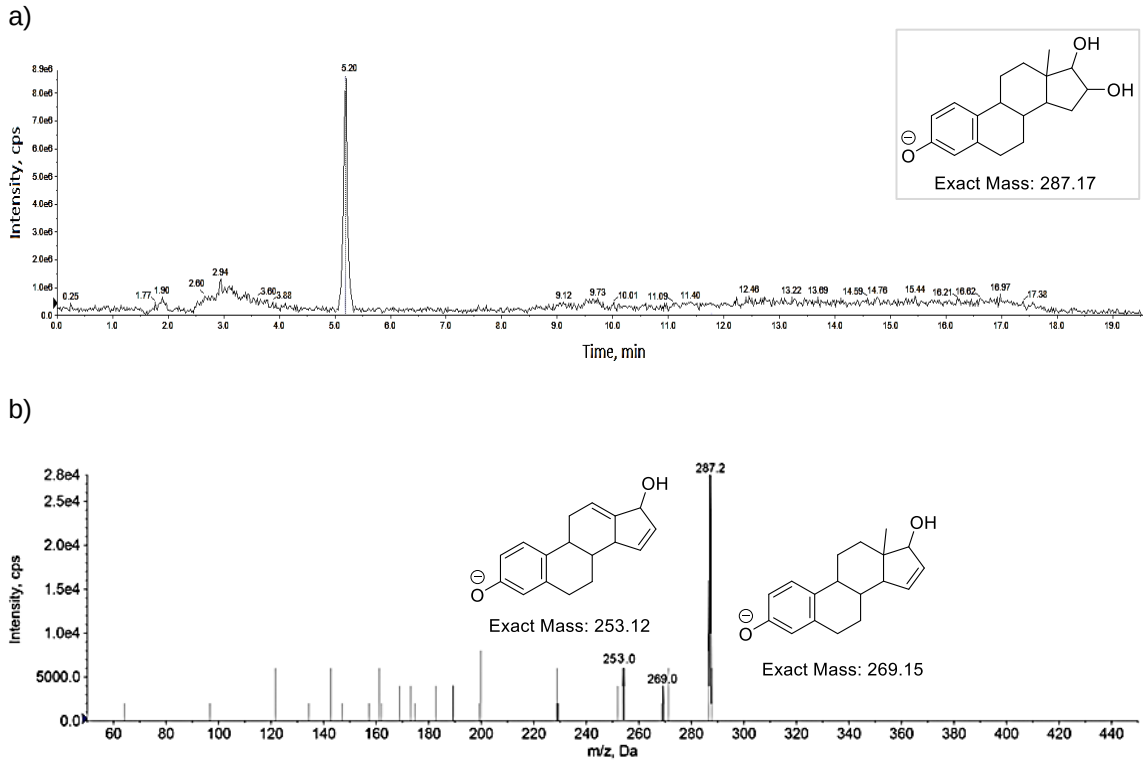

Figure 4.22. a) LC-ESI-MS extracted chromatogram for *m/z* 287.2 and proposed structure; b) Product-ion spectra from collisionally activated decompositions of the ESI produced $[M-H]^-$ ion *m/z* 287.2**.**

Proposed pathway for E2 degradation (vi): Dehydration of ring D of E2 at C-17, and formation of estra-1,3,5(10),16-tetraen-3-ol (E0). Previous HPLC chromatograms (Fig. 4.15) showed the formation in low concentrations of an unknown intermediate product at 13.36 min, which accumulated during the incubation period. The low polarity of this product intermediate product at 13.36 min suggested the dehydration of E2 at C-17, forming E0, as previously reported by Nakai *et al.*[222] However, in the LC-ESI-MS extracted chromatogram for the corresponding molecular anion $[M - H]^-$ of E0, *m/z* 253 was not detected.

As general conclusion, E1 was the main transformation product of E2 by LF5, under aerobic conditions. LF5 is also able to degrade E1. Metabolites detected by LC-MS, $\Delta^{9(11)}$-

E2, 2-OH-E2 or 4-OH-E2, 2-OH-E1 or 4-OH-E1, and E3 (all of them are proposed structures), were detected in low concentrations and were removed from the aqueous samples by **LF5**. The intermediate product detected at 13.36 min in the HPLC chromatogram was not identified and accumulated during the biodegradation test.

4.3.9. E2 degradation under anaerobic conditions with LF1, LF3 and LF5

In aerobic water treatments, organic matter in wastewater is highly converted to sludge, a bulky waste product which represents up to 50% of the operating costs of a WWTP. In contrast, organics in wastewater from anaerobic processes are highly converted to methane, which moreover is a valuable fuel, and very little sludge is produced.[228] Therefore, anaerobic water treatment may make environmental and economic sense.

The aim of this study was to test the capacity for anaerobic degradation of E2 in isolates **LF1**-**LF5**. Oxygen depletion occurs when organic matter is degraded through microbial activity, under limited oxygenation conditions.[229] The biodegradation of E2 has been found in the denitrifying step of WWTPs and in anoxic river sediments, but responsible bacteria and further oxidation products of E1 are in most cases still unknown.[230] In anoxic environments, estrogens may accumulate as recalcitrant compounds. Czajka and Londry tested the anaerobic biodegradation of E2 using cultures of lake water and sediment, having that, under some reducing conditions, reversible interconversion of E2 and E1 was produced.[231]

Due to the slow and long incubation times required in anaerobic biodegradation experiments, oxygen can diffuse through stoppers. Even small amounts of O_2 may allow hydrocarbon activation, thus leading to partly oxygenated products that can be degraded further. Therefore, maintenance of strictly anoxic conditions must be ensured. In this study, resazurin was used as a redox indicator for the presence of oxygen in the media. The abiotic control sample showed that after 90 days of incubation, the analysed content of E2 had diminished in ~0.5 $mg \cdot L^{-1}$ (data not shown).

Bacillus are facultative anaerobes, thus may survive on facultative anaerobic metabolic pathways.[232] In contrast, *Virgibacillus halotolerans* is a strict aerobe. Among the tested isolates, only *Bacillus* **LF5** showed estrogen-degrading anaerobic activity in presence of E2 for 90 days (Fig. 4.23). The degradative capacity was much lower than in aerobic conditions. The lag phase for **LF5** corresponded to *ca.* 25 days of incubation.

Between days 25 and 90, **LF5** could degrade 68% of the starting 5 $mg \cdot L^{-1}$ of E2. As in aerobic E2 biodegradation studies, E1 was produced as major metabolite detected in the samples. However, during 90 days of incubation, consumption of the formed E1 was not observed.

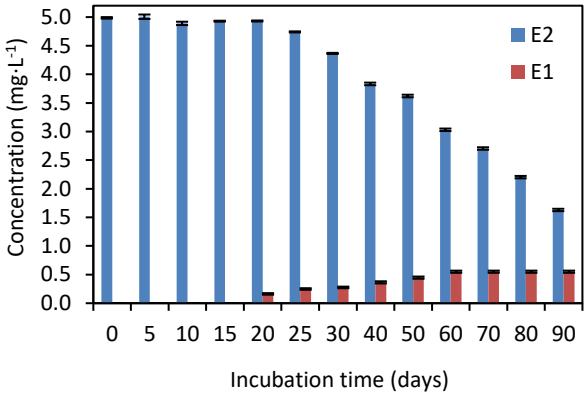

Figure 4.23. Profile of E2 degradation by **LF5** under anaerobic conditions. Values represent the average (squares represent E2, triangles represent E1) and errors bars represent the standard error of duplicates of one experiment.

Usually, anaerobic enrichment cultures show long lag phases of bacterial inactivity which may last months before significant biodegradation of the substrates is initiated.[233] In some cases, many years may be required to optimize conditions in order to achieve significantly rapid rates of biodegradation and those may or may not ever approach the rates of comparable aerobic biodegradation processes.[234] Consequently, anaerobic processes are considered to be more difficult to optimize than aerobic ones. As general conclusion, **LF5** demonstrated its ability to metabolize E2 under anaerobic conditions. However, it is important to note that this study could have not presented the best conditions for the enrichment of all the strains, due to, for instance, lack of specific micronutrients or an optimized incubation temperature, which would improve the anaerobic digestion of E2.

4.4. Conclusions

A set of five Gram-positive bacterial strains isolated from deep sea sediments (**LF1-LF5)** were identified as E2 biodegraders. Analysis of 16S rDNA gene sequences identified three of them as *Virgibacillus halotolerans* (**LF1**), *Bacillus flexus* (**LF3**) and *Bacillus licheniformis* (**LF5**). In addition, four *Pseudomonas* bacterial strains isolated from Ria de Aveiro (**LF9-LF11**) were also recognized as E2-degraders. In this study, E2 did not behave as a persistent compound and could be degraded by all the tested strains under aerobic conditions, resulting in low concentrations of E1 during E2 biotransformation.

LF5 was the most versatile strain, being able to simultaneously remove different estrogens (E1, E2, E3 and EE2) in wastewater from the STP of Ruhleben, in Berlin, with the following removal rates during 4-day experiments: 22.30% for E1 (230.02 $ng \cdot L^{-1}$), 26.63% for E2 (136.61 $ng \cdot L^{-1}$), 49.26 % for E3 (188.02 $ng \cdot L^{-1}$) and 9.56% for EE2 (112.84 $ng \cdot L^{-1}$). In addition, **LF5** showed anaerobic estrogen-degrading activity in presence of E2, and presented E2 removal rates of 68% (5 $mg \cdot L^{-1}$ of E2, 90 days).

Transformation products of E2 in presence of **LF5** under aerobic conditions, were studied using LC-MS, and structures proposed were: E1, $\Delta^{9(11)}$-E2, 2-OH-E2 or 4-OH-E2, 2-OH-E1 or 4-OH-E1, and E3. All of them were removed from the aqueous samples by **LF5**, being E1 the main metabolite.

Within the frame of the Ph.D. objectives, **LF5** has demonstrated to be an appropriate candidate for a future water treatment approach based on the combination of photocatalytic and biodegradation processes. Moreover, for a bioaugmentation approach of water treatment, these results suggest that the incorporation of **LF5** into the bacterial community of an activated sludge of a WWTP could significantly decrease the effects of EDCs in the effluent streams that discharges into superficial natural waters.

4.5. Materials and methods

4.5.1. Materials and equipment

All chemicals and solvents were obtained from commercial sources and were used without further purification steps. Primers U27 and 1492R were purchased from Stabvida. PCR amplifications were performed in a T ProfessionalTrio thermocycler from Analytik-Jena. Visualization of electrophoresis gels was performed in a Chemidrop XRS+ imaging system from Biorad.

4.5.2. Bacterial growth conditions

Strains **LF1** to **LF5** were grown in Luria-Bertani broth (LB) with 0.1 $mg \cdot L^{-1}$ of phenanthrene, for 5 days, at 26 ºC, under orbital stirring, and then streak-plated in a solid M9M medium adapted from Notomista *et al.*: 0.1 $g \cdot L^{-1}$ peptone, 0.1 $g \cdot L^{-1}$ yeast extract, 0.1 $g \cdot L^{-1}$ phenanthrene, 10 $g \cdot L^{-1}$ NaCl, 1 $g \cdot L^{-1}$ NH_4Cl, 150 $mg \cdot L^{-1}$ $MgSO_4 \cdot 7H_2O$, 180 $mg \cdot L^{-1}$ ammonium ferric citrate, 0.05 $mg \cdot L^{-1}$ KH_2PO_4, 0.05 $mg \cdot L^{-1}$ NaH_2PO_4, 15 $\cdot L^{-1}$ agar, and 5 $mL \cdot L^{-1}$ of a micronutrient solution (1 $g \cdot L^{-1}$ $CaCl_2$, 700 $mg \cdot L^{-1}$ $ZnSO_4 \cdot 7H_2O$, 560 $mg \cdot L^{-1}$ $MnSO_4 \cdot H_2O$, 125 $mg \cdot L^{-1}$ $Cu\ SO_4$, 196 $mg \cdot L^{-1}$ $Cu\ SO_4 \cdot 5H_2O$, 140 $mg \cdot L^{-1}$ $Co(NO_3)_2 \cdot 6H_2O$, 114 $mg \cdot L^{-1}$ $CoCl_2 \cdot 6H_2O$, 4 $mg \cdot L^{-1}$ H_3BO_3, 6 $mg \cdot L^{-1}$ $NiSO_4 \cdot 6H_2O$, 12 $mg \cdot L^{-1}$ $Na_2MoO_4 \cdot 2H_2O$). Cultures in solid medium were incubated for 5 days, at 26 ºC.[235]

According to the procedure described by Boon and co-workers, strains **LF6** and **LF7** were grown on tryptic soy broth (TSB), for 16 h, under orbital agitation (130 rpm), at 26ºC, and streak-plated in tryptic soy agar (TSA). Cultures in solid medium were incubated for 4 days, at 26 ºC.[29b]

According to the procedure described by Louvado and co-workers, strains **LF8** to **LF11** were grown for 5 days, under orbital stirring (150 rpm), at 26 ºC in a liquid medium containing 0.1% yeast extract, 0.01% peptone, and either 0.36 g L^{-1} of cetyl trimethylammonium bromide (CTAB), in case of **LF8**, or 20 $g \cdot L^{-1}$ of sodium dodecyl sulfate (SDS), in case of **LF9**, **LF10** and **LF11**. Cultures were then streak-plated in a solid medium with the same composition, with 1.5% agar added. Cultures in solid medium were incubated for 5 days at 26 ºC.[190]

4.5.3. Identification of strains LF1 to LF5

DNA extraction: Extraction of total DNA of bacterial isolates was carried out following the phenol/chloroform extraction procedure[192] using fresh bacterial culture grown in LB for 5 days at 26 °C on a rotary shaker. DNA was placed in 50 µL of TE buffer (10 mM Tris-HCl, 1 mM EDTA, pH 8.0) and stored at -20 °C. To evaluate the extraction procedure, 5 µL of each sample were subjected to electrophoresis on agarose gel 1.5% with GelRed at 80 V for 30 min in TAE buffer (0.04M Tris-acetate, 0.001M EDTA, pH 8.0). The gel was visualized on a ChemiDOC XRS+ imaging system (Biorad).

Identification of isolates: The 16S rDNA gene was amplified by PCR using universal bacterial primers U27 and 1492R.[193] PCR reactions were carried out in 25 µL reaction mixtures containing 1 µL of sample, 1x DreamTaq (ThermoScientific), 0.1 µM of each primer (Stabvida), 0.25 mg of BSA and ultrapure water (ThermoScientific). A negative control containing everything but the sample was included for detecting possible contaminations. PCR conditions were as follows: one initial denaturation step at 94 °C for 5min, followed by 30 cycles of denaturation at 94 for 45 secs, annealing at 56 °C for 45 secs, and extension at 72 °C for 90 sec. The PCR reaction was completed with a step final extension of 72 °C for 10 min. The DNA amplification product was externally sequenced (Stabvida) using the Sanger method.[194] The sequences obtained were classified with the program Naive Bayessian rRNA Classifier (Version 2.0) of RDP (Ribossomal Database Project http://rdp.cme.msu.edu) and compared to existing sequences in GenBank using the software BLAST (Basic Local Alignment Search Tool) (http://www.ncbi.nlm.nih.gov/).

4.5.4. Estrogen degradation tests under aerobic conditions

Degradation experiments were conducted to examine whether isolates were capable of degrading E2 in aerobic conditions. Isolates (**LF1**-**LF11**) were grown in their corresponding solid medium (see section 4.4.4) containing 5 $mg \cdot L^{-1}$ of E2 by adding the appropriate volume of a stock solution of E2 in dimethyl sulfoxide (DMSO) at 1 $g \cdot L^{-1}$. One isolated colony was inoculated in liquid medium (see section 4.4.4) and grown at 26 ºC.

Cells were harvested during the exponential phase of growth (OD_{600} =0.7) from aliquots (2 mL) by centrifugation at 6000 *g* for 7 min. Each cell pellet was washed with PBS_{mod} (1.80 $g \cdot L^{-1}$ NaH_2PO_4, 0.30 $g \cdot L^{-1}$ KH_2PO_4, 0.25 $g \cdot L^{-1}$ KCl, 0.20 $g \cdot L^{-1}$ NH_4Cl, 0.18 $g \cdot L^{-}$

[1] ammonium ferric citrate, 5 mL of micronutrient solution described in section 4.4.4; a higher content of NaCl (35.00 $g \cdot L^{-1}$) was only included in biodegradation tests with strains **LF1**-**LF5**; prepared in MilliQ water; pH 7.4) and then transferred into in 30 mL of PBS_{mod} containing E2 at 5 $mg \cdot L^{-1}$. Samples were incubated in a dark incubator shaker (5 days, at 26 ºC, 150 rpm). An abiotic control sample of 30 mL of PBS_{mod} containing 5 $mg \cdot L^{-1}$ of E2 and 5 $mg \cdot L^{-1}$ of E1, was submitted to the same experimental conditions. Aliquots of the aqueous samples were collected for estrogens determination by HPLC-UV (500 µL) and OD_{600} measurements (100 µL). Three independent experiments were performed and results were averaged.

In order to optimize biodegradation conditions, tests with **LF1**, **LF3** and **LF5** were repeated varying NaCl content in PBS_{mod} (1-4%) and incubation temperature (20-37ºC). All other biodegradation conditions remained the same, as previously described.

4.5.5. Estrogen degradation tests at lower concentrations

Degradation assays with strains **LF1**, **LF3** and **LF5** and E2 concentration of 5 $mg \cdot L^{-1}$ (5 days of incubation), 1 $mg \cdot L^{-1}$ (2.5 days of incubation), 100 $\mu g \cdot L^{-1}$ (2 days of incubation) or 2 $\mu g \cdot L^{-1}$ (1.5 day of incubation) were individually set up. Incubation temperature of tests with **LF1** and **LF3** was 30 ºC, and with **LF5** was 37 ºC.

Samples with starting E2 at 5 $mg \cdot L^{-1}$, 1 $mg \cdot L^{-1}$ and 100 $\mu g \cdot L^{-1}$ were prepared in 30 mL of PBS_{mod}. Sample preparation and biodegradation procedure were done as previously described in section 4.4.6. Abiotic control samples of 30 mL of PBS_{mod} containing 5 $mg \cdot L^{-1}$, 1 $mg \cdot L^{-1}$ or 100 $\mu g \cdot L^{-1}$ of E2 were submitted to the same experimental conditions. Aliquots of the aqueous samples with starting E2 at 5 $mg \cdot L^{-1}$ and 1 $mg \cdot L^{-1}$ were collected for estrogens determination by HPLC-UV (500 µL). Aliquots of the aqueous samples with starting E2 at 100 $\mu g \cdot L^{-1}$ were collected for estrogen determination by LC-MS (500 µL). Aliquots were also taken for OD_{600} measurements (100 µL). Three independent experiments were performed and results were averaged.

Samples with starting E2 at 2 $\mu g \cdot L^{-1}$ were performed for 1 day in 500 mL of PBS_{mod}. Samples preparation and biodegradation procedure were done as previously described in section 4.4.6, but with adapted volume. Abiotic control samples of 500 mL of PBS_{mod} containing 2 $\mu g \cdot L^{-1}$ of E2 were submitted to the same experimental conditions.

Aliquots (100 mL) were collected in brown glass bottles and pre-concentrated by solid-phase extraction (SPE).

SPE was performed automatically with an AutoTrace™ SPE workstation (Dionex, Idstein, Germany). First, Strata™-X cartridges were washed with 10 mL MeOH, equilibrated with 10 mL ultrapure water and followed by loading the respective sample, which previously was diluted to a volume of 1000 mL with 900 mL of ultrapure water. The flow rate for each step was 10 $mL \cdot min^{-1}$. Afterwards, the cartridges were dried by flushing N_2 (20 psi) for 15 min and the adsorbates were eluted with 10 mL MeOH. The eluate was concentrated to dryness and re-dissolved in 1 mL of MeOH. Aliquots were then analysed by LC-MS for estrogens determination.

4.5.6. E1, E2, E3 and EE2 degradation tests

Degradation experiments with **LF1**, **LF3** and **LF5** were individually set up with 30 mL of PBS_{mod} containing E1, E2, E3 and EE2, each at 100 $\mu g \cdot L^{-1}$. Samples were incubated in a dark incubator shaker for 4 days, at 150 rpm, at 30 ºC (**LF1** and **LF3**) or at 37 ºC (**LF5**). Abiotic control samples of 30 mL of PBS_{mod} containing E1, E2, E3 and EE2, each at 100 $\mu g \cdot L^{-1}$, were submitted to the same experimental conditions. Aliquots of the aqueous samples were collected for estrogens determination (500 µL) using LC-MS and OD_{600} measurements (100 µL). Three independent experiments were performed and results were averaged.

4.5.7. Estrogen degradation tests in presence of D-(+) glucose

Degradation experiments with **LF1**, **LF3** and **LF5** were individually set up with 30 mL of PBS_{mod} containing E2 at 100 $\mu g \cdot L^{-1}$ and D-(+) glucose at 100 $mg \cdot L^{-1}$. Samples were incubated in a dark incubator shaker for 3 days, at 150 rpm, at 30 ºC (**LF1** and **LF3**) or at 37 ºC (**LF5**). Abiotic control samples of 30 mL of PBS_{mod} containing E2 and E1 at 100 $\mu g \cdot L^{-1}$ and D-(+) glucose at 100 $mg \cdot L^{-1}$, were submitted to the same experimental conditions. Aliquots of the aqueous samples were collected for estrogens determination (500 µL) using LC-MS, for D-(+) glucose using the phenol/sulfuric acid method (see section 4.4.13) and for bacterial growth monitoring by OD_{600} measurements (100 µL). Three independent experiments were performed and results were averaged.

4.5.8. Estrogen degradation in wastewater

Samples (3L each sampling from the influent stream, 200 mL each sampling from the effluent stream) were provided by the operating company, Berliner Wasserbetriebe. Then, samples were stored in brown glass bottles at 4 °C and analysed within five days. Sampling was carried out by a flow-proportional automatic sampler over a period of 24 h, on the 13/07/2016, 18/07/2016 and 25/07/2016. Water samples from the influent stream were filtrated twice with glass fibre filters of 0.70 µm. Influent aliquots of the filtrated fractions, along with aliquots from the effluent stream (15 mL), were taken to analyse TOC.

Each estrogen (E1, E2, E3 and EE2) was spiked at a concentration of 100 $ng \cdot L^{-1}$ in samples (500 mL) of the influent stream, which were then individually inoculated with **LF1**, **LF3** and **LF5**, and incubated in dark conditions for 4 days, adjusting pH to 7.0 every day. Aliquots (100 mL) were taken at incubation times 0, 1, 2, 3 and 4 day, and were submitted to a solid phase extraction (SPE) procedure, along with non-treated aliquots from the effluent stream (100 mL). SPE was performed automatically with an AutoTrace™ SPE workstation, with Strata™-X cartridges. First, cartridges were washed with 10 mL of MeOH, equilibrated with 10 mL of ultrapure water and followed by loading the respective samples, which previously were diluted to a volume of 1000 mL with 900 mL of ultrapure water. Afterwards, the cartridges were dried and the adsorbates were eluted with 10 mL of MeOH. Eluates were concentrated to dryness and re-dissolved in 1 mL of MeOH. Aliquots (100-fold concentrated) were then analysed by LC-MS/MS for estrogens determination.

4.5.9. Estrogen degradation tests under anaerobic conditions

The bicarbonate buffered mineral salts medium for the E2 degradation tests under anaerobic conditions was prepared as described by Plugge,[236] with minor modifications. The liquid medium contained 0.5 $mg \cdot L^{-1}$ of resazurin (redox indicator), 400 $mg \cdot L^{-1}$ KH_2PO_4, 530 $mg \cdot L^{-1}$ Na_2HPO_4, 300 $mg \cdot L^{-1}$ NH_4Cl, 300 $mg \cdot L^{-1}$ NaCl, 100 $mg \cdot L^{-1}$ $MgCl_2 \cdot 6H_2O$, and 1 mL of each of the trace elements stock solutions I and II and distilled water up to 1 L. The acid trace elements stock solution I contained 50 mM HCl, 1mM H_3BO_3, 63 $mg \cdot L^{-1}$ $MnCl_2$, 951 $mg \cdot L^{-1}$ $FeCl_2$, 65 $mg \cdot L^{-1}$ $CoCl_2$, 13 $mg \cdot L^{-1}$ $NiCl_2$, and 68 $mg \cdot L^{-1}$ $ZnCl_2$. The alkaline trace elements stock solution II contained 400 $mg \cdot L^{-1}$ NaOH, 17 $mg \cdot L^{-1}$ Na_2SeO3, 29 $mg \cdot L^{-1}$ Na_2WO_4, and 21 $mg \cdot L^{-1}$ Na_2MoO_4.

To reduce the medium completely, 50 mL of a sterilized reducing solution containing 800 mg·L^{-1} $NaHCO_3$, 4.8 g·L^{-1} Na_2S·9 H_2O solution, and 500 mg·L^{-1} of cystein·HCl were added to 500 mL of medium. Then, 10 mL of a 500 mg·L^{-1} stock solution of E2 in DMSO was added (5 mg·L^{-1} of E2). Finally, the volume of the medium was made up to 1000 mL with distilled H_2O. After homogenization, the medium was distributed into 50 mL flasks and brought to a full boil for 20 seconds to remove O_2, cooled down under N_2 atmosphere, and autoclaved. The flasks were kept under N_2 atmosphere.

Isolates were previously grown in modified M9M medium containing 5 mg·L^{-1} of E2. One colony of each isolate was then transferred to LB medium and grown aerobically at 26 ºC. Cells were harvested from aliquots (2 mL) by centrifugation at 6000 *g* for 7 min. The pellet was then washed in PBS, resuspended in 500 µL of PBS and purged under N_2. The cell suspension was taken with a syringe and transferred to the flasks containing the E2 at 5 mg·L^{-1}, prepared from a stock solution of E2 in DMSO at 1 g·L^{-1}. The cultures were incubated at room temperature (20-25 ºC) for 90 days in dark conditions. An abiotic control sample of 30 mL of PBS containing 5 mg·L^{-1} of E2 was submitted to the same experimental conditions. Aliquots (500 µL) of the aqueous samples were collected for estrogens determination. One independent experiment was performed.

4.5.10. Quantification of estrogens with HPLC-UV

Aliquots (500 µL) of the aqueous samples collected at different times during the biodegradation processes were taken and bacterial cells were separated from the culture medium by centrifugation at 6000 *g*. Estrogens in the supernatant were extracted with ethyl acetate and then quantified by high performance liquid chromatography with UV detector (HPLC-UV). Aliquots (20 µL) were injected without any more sample preparation, into a HPLC column with UV detection at 200 nm. Separation was achieved on a Kinetex XB-C18 core/shell column (150 mm *x* 3 mm, 2.6 µm). A binary gradient consisting of (A) water and (B) methanol, was used under the following conditions: 20% B, isocratic for 3 min, linear increase to 95% B within 5 min, kept at 95% B for 4 min, return to the initial conditions 20% B within 2 min, and kept for 8 min. Samples were analysed in duplicate to ensure their values.

To optimize the HPLC conditions in order to determine the efficiency of the method, standards of mixtures of the estrogens E1 and E2 were analysed. The elution conditions

used to separate the compounds gave a good resolution. The limits of detection (LOD) for each estrogen were determined according with the equations bellow:

$y = a + b\,x$

$LOD = Y_B + 3S_B$

$Y_B = a;\ S_B = S_{y/x}$

Where LOD is the value of *y* at the limit of detection, and $S_{y/x}$ is the standard deviation in the *y*-direction. The instrumental LOD obtained were 0.15 mg L^{-1} for E2, 0.09 mg L^{-1} for E1. The correlation coefficients of the calibration lines were higher than 0.999.

4.5.11. Quantification of estrogens and evaluation of metabolites with LC-MS

Bacterial cells were separated from the culture medium by centrifugation at 6000 *g*. Estrogens and metabolites in the supernatant were extracted with ethyl acetate and then analysed by using LC-MS using an Agilent 1260 Infinity LC system (Agilent Technologies Waldbronn, Germany) with a binary pump, degasser, autosampler, column heater and UV-detector coupled to a Triple Quad™ 6500 MS (AB Sciex, Darmstadt, Germany). A Kinetex C18 precolumn (Phenomenex, Aschaffenburg, Germany) and a Kinetex XB-C18 core/shell column (150 mm *x* 3 mm, 2.6 µm) were used. 10 µL of the samples were injected. The column oven temperature was set to 40 °C, the flow rate was kept at 300 µL/min. A binary gradient consisting of (A) water and (B) acetonitrile containing 0.00025% (v/v) ammonia, was used under the following conditions: 30% B, isocratic for 2 min, linear increase to 95% B within 5 min, kept at 95% B for 4 min, return to the initial conditions 30% B within 2 min, and kept for 8 min. The mass spectrometer was operated with an electrospray ionization source in negative ion mode. Parameters used to produce fragment ions in selected reaction monitoring mode (SRM) are given in Table 4.8.

For quantification of estrogens in water samples, calibrators with standard concentrations of 0, 0.01, 0.05, 0.1, 1, 5, 10, 25, 50, 100 and 120 µg·L^{-1} of E1 (LOQ: 4.3 ng·L^{-1}), or E2 (LOQ: 5.4 ng·L^{-1}), or E3 (LOQ: 4.8 ng·L^{-1}) or EE2 (LOQ: 5.63 ng·L^{-1}) were used.

Table 4. 8. Retention times, precursor ions, product ions, and MRM conditions used in LC-ESI-MS measurement.

Substance	E1	E2	E3	EE2
Retention time [min]	11.51	11.02	5.39	10.70
Precursor ion [m/z]	269.2	271.2	287.2	295.2
Cone voltage	55	63	55	55
Collision energy	48	48	50	48
Product ion 1 [*m/z*]	145.1	145.1	183.1	145.1
Collision energy	70	50	48	70
Product ion 2 [*m/z*]	143.1	183.1	145.1	143.1

4.5.12. Quantification of D-(+) glucose

Consumption of D-(+) glucose was estimated colorimetrically by using the phenol-sulfuric acid method for determination of sugars and related substances of Dubois (1956).[237]

- Preparation of standards and calibration

Standards of D-(+) glucose were prepared as solutions of PBS_{mod} containing 0.2, 0.4, 0.6, 0.8, 1.0, 2.0, 4.0, 6.0, 8.0, 10.0 and 12.0 $mg \cdot L^{-1}$ of D-(+) glucose. Then, 150 µl of a 5% (w/v) phenol solution were added to each tube. Tubes were briefly mixed in vortex and rapidly, 750 µL of concentrated sulfuric acid were added to each tube. After 10 minutes, tubes were mixed again in vortex and then were left 30 min at room temperature while the colour developed. Solutions from each tube were transferred to 1.0-ml (1-cm path length) glass cuvette. Using the spectrophotometer, measurements of the absorbance of each tube at 490 nm were done. Results were averaged and plotted in a standard curve of calibration.

- Determination of D-(+) glucose in samples

Three aliquots (150 µL) of each aqueous sample were collected at different times during the biodegradation process. Bacterial cells were separated from the culture medium by centrifugation at 6000 *g*. Then, liquid fractions were transferred into new Pyrex test tubes, and 150 µl of a 5% (w/v) phenol solution were added to each tube. Tubes were briefly mixed in vortex and, rapidly, 750 µL of concentrated sulfuric acid were added to each tube. After 10 minutes, tubes were mixed again in vortex and then were left 30 min at room temperature

while the colour developed. Absorbance of each was read and the amount of D-(+) glucose was determined by reference the standard curve.

4.5.13. Growth related degradation

To monitor cell growth related to estrogen biodegradation, aliquots (100 µL) of the aqueous samples collected at different times during the biodegradation process were taken and bacterial growth was determined photometrically (Thermo Genesys 10S) at 600 nm against medium as a reference (OD_{600}).

4.5.14. Statistical analysis

Statistical analysis was performed by using SPSS 15.0 for Windows (SPSS Inc, USA). The significance of E2 degradation was assessed by two-way univariate analysis of variance (ANOVA) model with Bonferroni post-hoc test. A value of $p < 0.05$ was considered significant.

CHAPTER 5

WATER TREATMENT BY COMBINATION OF PHOTOCATALYTIC AND BIOLOGICAL PROCESSES

Summary

With focus on sustainable applications of photocatalysis in wastewater treatment, some factors to be considered are the use of sunlight as energy source, the recovery and recyclability of the catalyst and the possibility of combining the photo-treatment with a biodegradation process. Typically, photocatalysis represent an efficient way to simultaneously remove different types compounds present in water. However, full mineralization of organic pollutants using photocatalysis under sunlight may imply high costs associated with the amount of photocatalyst needed and extended treatment times. To reduce its use to some extent, a second step of biodegradation treatment can be added. For a successful approach, the biodegradability of the organic compounds present in the partially treated water must be evaluated.

*The present study explores the potential of the previously described hybrid photomaterial, **NP^{+}-$TPPF_{17}(SGlc)_3$**, in more practical applications, and its use in combination with the bacterial strain Bacillus licheniformis (**LF5**) to degrade 17β-estradiol and its intermediate products in water.*

5.1 Introduction

Photocatalysis is an efficient treatment for the removal of a wide range of organic pollutants in wastewaters, including hydrocarbons, chlorinated aromatic hydrocarbons, chlorinated phenols, and many pesticides.[118] However, operating costs related to energy consumption (especially in typical advanced oxidation process (AOP) treatments, when UV light is applied) and/or high concentrations of photocatalyst are important drawbacks. In addition, when the oxidation intermediates formed during the photo-treatment are more resistant to their complete chemical degradation, their mineralization is usually expensive.[120]

Combination of AOPs and biological systems may offer advantages in effectiveness of pollutant removal rates and operating costs for wastewater treatment. When AOPs are used as pre-treatments, a complete mineralization of the organic pollutants is not necessary, being more relevant to transform them into biodegradable intermediate compounds, subsequently to be followed by a biological process. Most studies of AOPs as pre-treatment of wastewaters for their biological processing consider the oxidant dose used. The issue of using high concentrations of photocatalyst is not only related to increased operating costs, but also to serious damages to microorganisms.[238] However, low concentrations of photocatalyst could result in an inadequate pre-treatment of wastewaters.

The effectiveness of AOPs has been proved for the pre-treatment of different types of wastewaters, including industrial ones.[239] Wastewaters that usually are successfully treated by combination of AOPs and biological processes are the ones containing bio- or photo-resistant compounds, as well as those containing toxic pollutants, which affect cell viability of microorganisms.[240]

This work studies the use of a heterogeneous photocatalyst, which can be easily recovered after its use, in the pre-treatment of organic pollutants in wastewaters, with focus on 17β-estradiol (E2). In this way, the dose of photocatalyst used will not affect the bacterial viability in the next step and the photocatalyst will be reused in further treatments. The photocatalyst used during the pre-treatment in this study is **NP^{+}-$TPPF_{17}(SGlc)_3$**, since its ability to generate $^1O_2$ and radicals at high rates, as well as its photostability and efficiency under white light (see Chapter 3), make it an ideal candidate. Biodegradability of intermediate products arising from E2 photodegradation will be studied for its biological processing by *Bacillus licheniformis* (**LF5**). In this study, **LF5** was selected due to its

great versatility to simultaneously remove different estrogens (E1, E2, E3 and EE2) in relevant concentrations found in wastewaters (see Chapter 4).

5.2 Results and discussion

NP^+-$TPPF_{17}(SGlc)_3$ was selected as photocatalyst, or photosensitizer (PS), as oxidizing agent in the pre-treatment of wastewaters (Fig. 5.1). The preparation, characterization and properties of this PS can be consulted in Chapters 2 and 3. Prior to its use in the pre-treatment, to explore the potential of **NP^+-$TPPF_{17}(SGlc)_3$** in real applications, some additional features were studied, such as its pore size distribution, photostability under UVA radiation, performance and stability during recycling tests, and ability to degrade different organic pollutants in wastewaters.

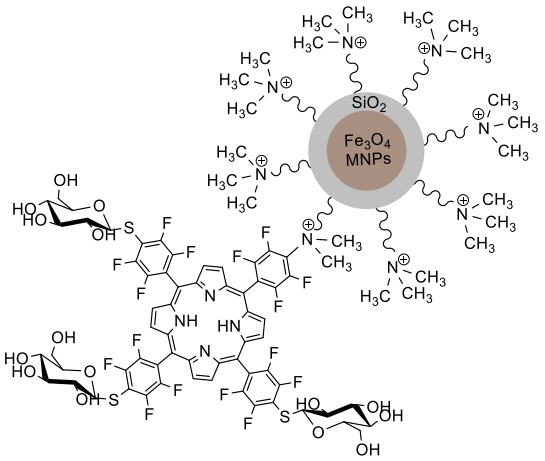

Figure 5. 1. Structural representation of **NP^+-$TPPF_{17}(SGlc)_3$**.

5.2.1 Nitrogen adsorption-desorption isotherm and pore size distribution of NP^+-$TPPF_{17}(SGlc)_3$

Previous studies demonstrated the capability of these type of hybrid materials to adsorb E2 onto its silica outer shell. Water samples containing 5 $mg \cdot L^{-1}$ of E2 and 10 µM of a NP-PS showed adsorption capacities of 12.4-24.2% of E2 onto the NPs after 60 min (see Chapter 2). In this work, concentration of hybrid materials, NP-PS or NP^+-PS, always refers to the amount of PS in the material. Adsorption is a surface-based process and refers to the spontaneous concentration of a dissolved substance from a gas, liquid, or dissolved

solid onto a solid surface, by a finite time.[241] Adsorption rate of a substance depends on its chemical properties, such as its solubility in water, and medium conditions, such as pH. Upon completion of the photodegradation treatment, the rinse solvent of washing processes of the photocatalysts showed that the E2 adsorbed had been degraded during the tests. Considering these results, pore size distribution of **NP$^+$-TPPF$_{17}$(SGlc)$_3$** surface was studied.

These measurements were kindly performed by Carsten Prinst and Annett Zimathies, from the Division 1.3 of Structure Analysis of BAM, in Berlin. According to IUPAC, the nitrogen adsorption/desorption isotherms of **NP$^+$-TPPF$_{17}$(SGlc)$_3$**, which are displayed in Fig. 5.2a, are of type IV and therefore, **NP$^+$-TPPF$_{17}$(SGlc)$_3$** is a mesoporous material.[242] Curves show an apparent hysteresis loop at a relative pressure (P/P_0) between 0.5 and 1.0.

a) b)

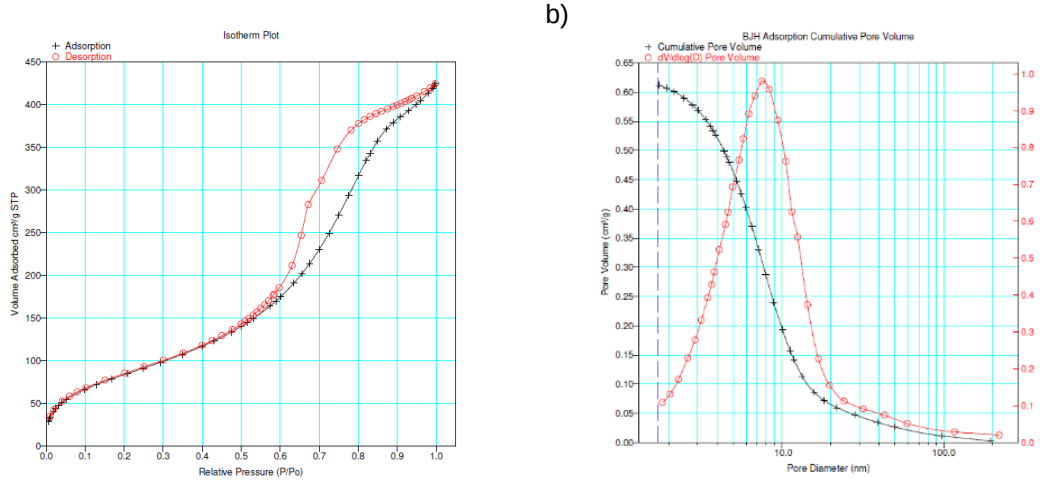

Figure 5. 2. a) N_2 isothermal adsorption-desorption curves with **NP$^+$-TPPF$_{17}$(SGlc)$_3$**; b) pore size distribution **of NP$^+$-TPPF$_{17}$(SGlc)$_3$** (BJH adsorption cumulative pore volume).

The Barrett, Joyner, and Halenda (BJH) method is a pore size distribution determination method based on the N_2 adsorption/desorption isotherm data measured at 77 K on mesoporous materials. It uses the modified Kelvin equation to relate the amount of adsorbate removed from the pores of the material, as the relative pressure (P/P_0) is decreased from a high to low value, to the size of the pores.[243] The plot of pore size distribution determined by the BJH method shows a pore size distribution between 1.8 and 24.2 nm, with predominant pore widths of 5-8 nm (Fig. 5.2b).

The Brunauer-Emmett-Teller equation (BET) determines the specific surface area of solids, and is based on the isothermal formation of adsorbed multilayers as a function of relative pressure (P/P_0). This equation is mostly widely applied to N_2 adsorption at 77 K, measured in manometric sorption instruments.[244] According to BET theory, specific surface area of **NP$^+$-TPPF$_{17}$(SGlc)$_3$** is above 300 $m^2 \cdot g^{-1}$, which is in agreement with previous results

of Fe_3O_4@SiO_2 NPs (272.5 $m^2 \cdot g^{-1}$).[245] The theoretical specific surface area of non-coated magnetite NPs is 77–96 $m^2 \cdot g^{-1}$, under the assumption that the primary particles are spherical, contain no internal porosity, have a mean diameter of 12–15 nm (according to TEM images) and have a density of 5.2 g cm^{-3}. The increased specific surface of **NP^+-$TPPF_{17}(SGlc)_3$** is therefore attributed to the silica shell, which may provide a favourable space for the adsorption of pollutants onto the nanomaterial.

5.2.2 Photostability studies of NP^+-$TPPF_{17}(SGlc)_3$ under UVA radiation

UV radiation is divided into wavelength ranges identified as: UVA (315-400 nm), UVB (280-315 nm) and UVC (100-280 nm). UV constitutes about 10% of the total light output of the Sun. However, UVC radiation and around 90% of UVB is absorbed by ozone, water vapour, oxygen and carbon dioxide, when sunlight passes through the atmosphere. UV radiation reaching the surface of the Earth is basically formed by UVA, with a small component of UVB (around 5% in the equator).[246]

With focus on future applications of **NP^+-$TPPF_{17}(SGlc)_3$** in sunlight-assisted water treatment, photostability studies of the material in water suspensions were conducted under UVA light (Fig. 5.3a and b). Photostability studies were performed by exposing aqueous suspensions of **NP^+-$TPPF_{17}(SGlc)_3$** at 1 µM, under UVA light, at room temperature, with vigorous magnetic stirring, for 6 h. At fixed intervals of time, visible absorption spectra of the samples were recorded. The intensity of the Soret and Q bands of **NP^+-$TPPF_{17}(SGlc)_3$** showed that suspensions were stable upon 6 h of radiation (Fig. 5.3c). Absorption spectra of control samples kept in dark conditions showed the same behaviour (data non-shown). These results, along with the ones of photostability studies under white light (see Chapter 3), suggest the viability of **NP^+-$TPPF_{17}(SGlc)_3$** to be used under sunlight.

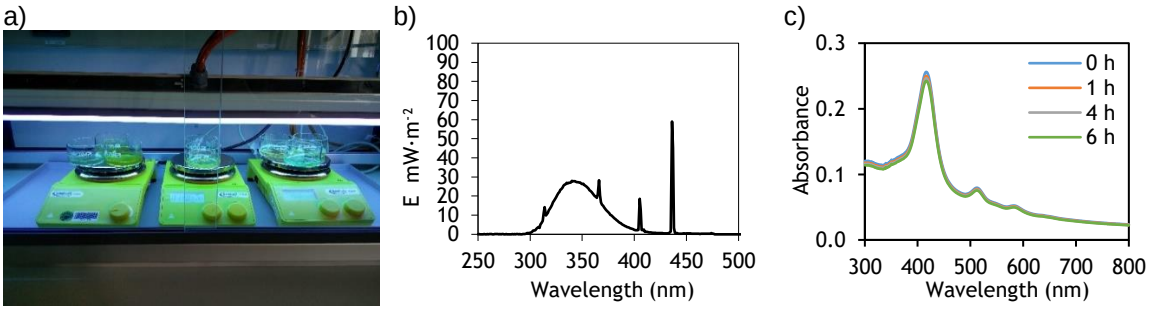

Figure 5. 3. a) Set-up of the photostability studies of **NP^+-$TPPF_{17}(SGlc)_3$** under UVA radiation; b) emission spectrum of the UVA lamp used; c) absorption spectra of **NP^+-$TPPF_{17}(SGlc)_3$** suspensions in water upon different times of irradiation with UVA light.

Additionally, samples of **NP$^+$-TPPF$_{17}$(SGlc)$_3$** in suspension were taken upon different irradiation times with UVA light, dried and submitted to XRD analysis (Fig. 5.4). Powder XRD pattern of **NP$^+$-TPPF$_{17}$(SGlc)$_3$** after 6 h of irradiation contained peaks of magnetite, centred at *ca.* 30.1, 35.5, 43.1, 57.1 and 62.7º 2θ. Hump between 17 and 26º belongs to the amorphous silica shell, and apparently preserves the same shape and intensity among samples of different irradiation times. In the view of these results, it can be concluded that neither the outer silica shell, or the magnetite nucleus of **NP$^+$-TPPF$_{17}$(SGlc)$_3$**, were affected by the phototreatment.

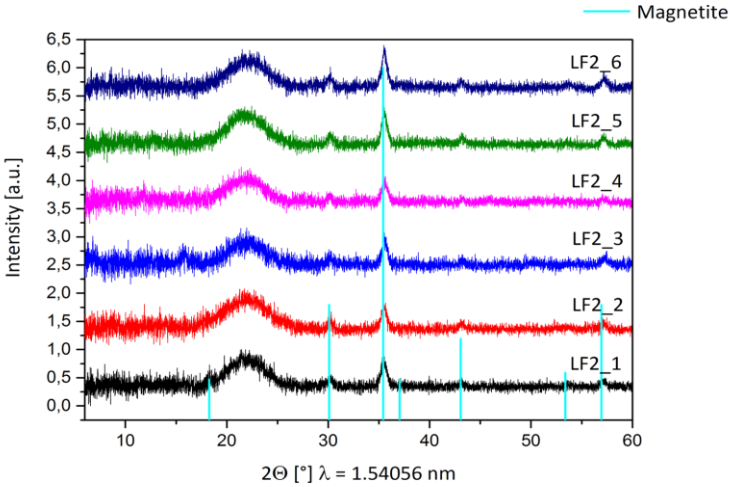

Code	UVA irradiation time
LF2_6	6 h
LF2_5	4 h
LF2_4	3 h
LF2_3	2 h
LF2_2	1 h
LF2_1	0 h

Figure 5. 4. XRD spectra of magnetite (light blue line) and **NP$^+$-TPPF$_{17}$(SGlc)$_3$** before (black line) and after different exposure times of UVA irradiation (red, blue, pink, green and dark blue lines, corresponding to 1-6 h).

5.2.3 Photocatalytic performance of NP$^+$-TPPF$_{17}$(SGlc)$_3$ in recycling studies of E2 photodegradation

As previously explored with neutral hybrid materials (Chapter 2), photodegradation studies of 5 mg·L^{-1} of E2 in presence of **NP$^+$-TPPF$_{17}$(SGlc)$_3$** at 10 μM, under white light irradiation (4 mW·cm^{-2}) were performed. Isotherms of adsorption/desorption of E2 onto the cationic nanomaterial, **NP$^+$-TPPF$_{17}$(SGlc)$_3$**, showed increased amounts of E2 (25.3% of starting E2) compared to its neutral precursor, **NP-TPPF$_{17}$(SGlc)$_3$** (12.4% of starting E2). The reduction of the average aggregate size of **NP$^+$-TPPF$_{17}$(SGlc)$_3$** increases the ratio between area and volume, which may benefit the adsorption of E2 onto the surface of the NPs.

Prior results with **NP-TPPF$_{17}$(SGlc)$_3$** showed a removal activity of around 85% of the starting E2 after 8 h of irradiation. As expected, **NP$^+$-TPPF$_{17}$(SGlc)$_3$** presented more efficient removal activities of E2, since it has already demonstrated to generate $^1O_2$ at higher rates than its corresponding neutral hybrid material. **NP$^+$-TPPF$_{17}$(SGlc)$_3$** degrades 5 mg·L^{-1} of E2 (100% of the starting E2) after 6 h of irradiation.

Catalyst recovery and reuse are important features for sustainable processes. **NP$^+$-TPPF$_{17}$(SGlc)$_3$** was separated and reused without significant loss of catalytic activity for additional five cycles (Fig. 5.5). For subsequent uses in E2 photodegradation, **NP$^+$-TPPF$_{17}$(SGlc)$_3$** was recovered by centrifugation and the supernatant was removed. Then, **NP$^+$-TPPF$_{17}$(SGlc)$_3$** was cleaned by rinsing in ethanol and water and reused in further experiments under the same conditions. After six runs, efficiency of photocatalytic activity of **NP$^+$-TPPF$_{17}$(SGlc)$_3$** decreased an average percentage of 3.58%. HPLC analysis of rinse solvent of washing processes did not detect E2, thus revealing that E2 adsorbed onto **NP$^+$-TPPF$_{17}$(SGlc)$_3$** was degraded.

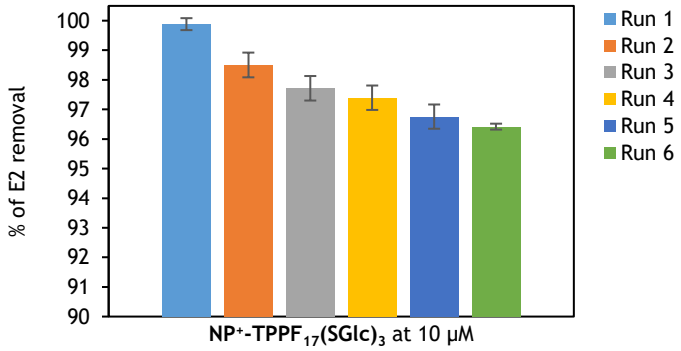

Figure 5. 5. Reuse of **NP$^+$-TPPF$_{17}$(SGlc)$_3$** after recovering and washing processes, in the photodegradation of 5 mg·L^{-1} of E2 for 6 h, under white light (4 mW·cm^{-2}). Results represent the average values of three independent studies, bars represent standard deviations.

5.2.4 Photodegradation of pharmaceuticals in real water samples of a WWTP influent in presence of NP$^+$-TPPF$_{17}$(SGlc)$_3$

To evaluate a more realistic potential of **NP$^+$-TPPF$_{17}$(SGlc)$_3$** as photocatalyst in water treatment applications, studies of the simultaneous photodegradation of different organic pollutants in real wastewater samples were performed. Environmentally relevant analytes chosen were E1, E2, E3, EE2, carbamazepine (CBZ), cetirizine dihydrochloride (CET) and sulfamethoxazole (SMX). Chemical structures of CBZ, CET and SMX are

represented in Table 5.1. For additional information of estrogenic compounds, see Chapter 1.

Table 5. 1. Chemical structures of the environmentally relevant analytes: CBZ, CET, SMX.

Compound	Formula	M.W.	CAS	Molecular structure
Carbamezepine (CBZ)	$C_{15}H_{12}N_2O$	236.27	298-46-4	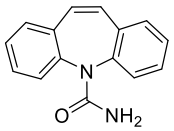
Cetirizine dihydrochloride (CET)	$C_{21}H_{25}ClN_2O_3{\cdot}2HCl$	461.81	83881-52-1	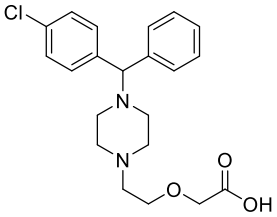
Sulfamethoxazole (SMX)	$C_{10}H_{11}N_3O_3S$	253.28	723-46-6	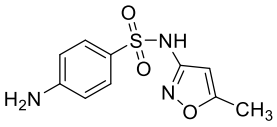

Pharmaceuticals and their metabolites are usually released into environmental waters at trace levels (from ng L^{-1} to $\mu g{\cdot}L^{-1}$) through conventional wastewater treatment plants (WWTPs).[247] CBZ is an antiepileptic drug widely used in the treatment of trigeminal neuralgia, grand mal seizures and psychiatric disorders, such as bipolar disorder or borderline personality disorder.[248] Due to its extensive use and persistence in WWTPs (up to 1.20 µg L^{-1} in effluent streams),[249] CBZ usually enters surface waters, causing negative effects on the health status of aquatic organisms.[249-250] CBZ is often used as a marker for wastewater input into surface and groundwater.[251]

SMX is a bacteriostatic antibiotic, mostly prescribed to treat urinary infections, bronchitis, and prostatitis. Removal rates of SMX in WWTPs depends on the type of wastewater treatment and varies from 7.5% to 88%.[252] Levels of SMX in different WWTPs range from 8 to 3180 $ng{\cdot}L^{-1}$ in influent streams,[252] and from 243 to 2000 $ng{\cdot}L^{-1}$ in effluent streams.[252b, 253] SMX has been also detected in surface waters (8 ng L^{-1}).[254] The prevalence of substances as SMX in the water cycle supports the antibiotic resistance development.[255]

CET is an antihistamine drug used for the treatment of allergic reactions.[256] CET is usually detected in effluents of WWTPs and environmental waters: in concentrations of up to 510 ng L^{-1} in wastewater effluents in Germany,[257] up to 9 ng L^{-1} in river water in

Finland,[258] and up to 6 and 13 ng L^{-1} in the San Francisco Bay and the Baltic Sea (German coast line), respectively.[259]

Studies of visible-light assisted photodegradation of target organic pollutants (E1, E2, E3, EE2, CBZ, CET, SMX) with **NP^{+}-$TPPF_{17}(SGlc)_3$** were performed in wastewaters from the influent stream of the Ruhleben sewage treatment plant (STP). The reason of sampling in the influent stream and not after an intermediate treatment was just due to the availability of samples provided by the operating company, Berliner Wasserbetriebe. Then, samples were stored in brown glass bottles at 4 °C and analysed within three days. Sampling was carried out by a flow-proportional automatic sampler over a period of 24 h, and were taken on the dates 01/08/2016, 08/08/2016 and 15/08/2016.

Prior to photocatalysis procedure, samples were analysed to determine the level of each analyte (Table 5.2), and then each compound was spiked to achieve a final concentration of 1.9 - 2.2 $\mu g \cdot L^{-1}$. TOC values were also determined for the samples after settlement, which ranged from 1902.3 to 2136.2 $mg \cdot L^{-1}$. (Table 5.3).

Table 5. 2. Concentrations ($ng \cdot L^{-1}$) of E1, E2, E3, EE2, CBZ, CET and SMX determined in water samples taken from the influent stream of Ruhleben STP during August, 2016.

Sampling date	E1	E2	E3	EE2	CBZ	CET	SMX
01/08/2016	99.6	20.1	78.7	9.6	256.9	110.1	1125.6
08/08/2016	123.2	41.2	93.8	16.9	312.6	156.8	2156.3
15/08/2016	106.5	23.6	75.4	15.0	115.2	94.0	1987.5

Table 5. 3. Values of TOC, TC and IC of water samples taken from the influent stream of Ruhleben STP.

Sampling date	TOC	TC	IC	Unit
01/08/2016	1922.4	2001.0	78.6	$mg \cdot L^{-1}$
08/08/2016	2136.2	2217.9	81.7	$mg \cdot L^{-1}$
15/08/2016	1902.3	1994.6	92.3	$mg \cdot L^{-1}$

The photocatalytic activity of **NP^{+}-$TPPF_{17}(SGlc)_3$** (20 µM) in 500 mL of wastewater samples from the influent of the Ruhleben STP, was evaluated in the photodegradation of E1, E2, E3, EE2, CBZ, CET, SMX under white light irradiation (4 $mW \cdot cm^{-2}$), in batch mode, using cylindrical glasses of 1000 mL. Light control samples were included in each irradiation experiment, containing the analytes at the same concentration, without **NP^{+}-$TPPF_{17}(SGlc)_3$**, and submitted to the same irradiation conditions as the samples. Aliquots (100 mL) were

taken at irradiation times 0, 8, 24 and 48 h, and submitted to a solid phase extraction (SPE) procedure. Aliquots (100-fold concentrated) were then analysed by LC-MS/MS for analytes determination.

Light control samples showed that concentrations of all the analytes remained rather stable after 48 h of irradiation: E1 at 98%, E2 at 94%, E3 at 92%, EE2 at 89%, CET at 93%, SMX at 93%, CBZ at 91% (Fig. 5.6). After 48 h of irradiation, **NP^+-$TPPF_{17}(SGlc)_3$** at 20 µM could degrade all the starting estrogen compounds and CET. However, CBZ and SMX remained at 0.2 and 0.5 $\mu g \cdot L^{-1}$.

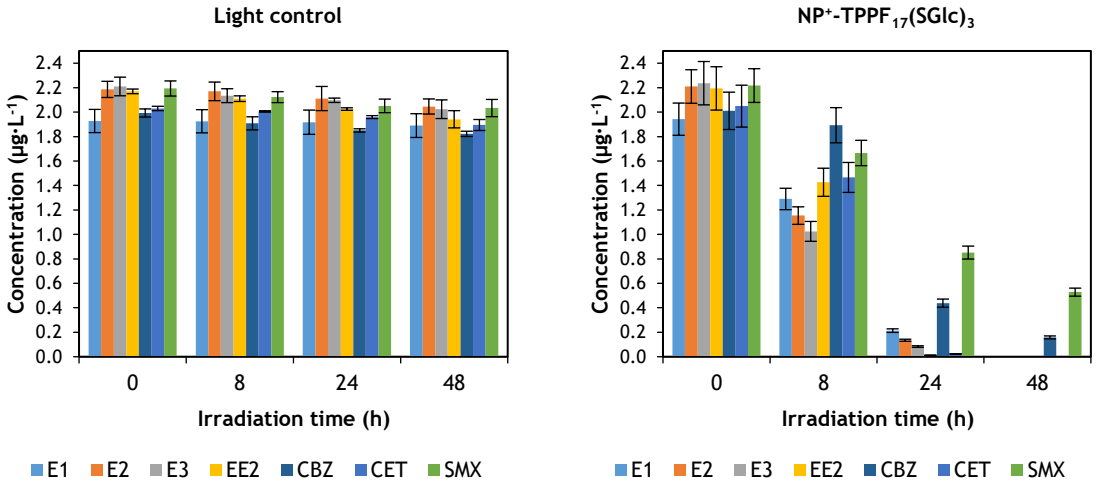

Figure 5. 6. Photodegradation of pharmaceuticals in real water samples of a WWTP influent in presence of **NP^+-$TPPF_{17}(SGlc)_3$** at 20 µM.

Previous studies reported that direct photolysis is an important mechanism to eliminate SMX from natural surface waters, although degradation rates are lower than in distilled water. However, indirect photolysis does not contribute to its overall photolytic fate. In contrast, it was found that indirect photodegradation is relevant for the removal of CBZ, although at low rates, being more persistent than other pharmaceuticals.[260]

Aliquots of the treated samples were taken to analyse their TOC content. Compared to non-treated samples, these measurements did not show great changes of TOC, most probably due to TOC values, which are in the range of $mg \cdot L^{-1}$, and/or the complete mineralization of the degraded compounds did not occur.

As a general conclusion. these results show the efficiency of $^1O_2$ and radicals *in situ* generated to degrade different types of compounds, and enhance the versatility of **NP^+-$TPPF_{17}(SGlc)_3$** in practical applications for water treatment purposes.

5.2.5 17β-Estradiol removal by combination of photocatalytic and biological processes with NP^+-$TPPF_{17}(SGl)_3$ and *Bacillus licheniformis* (LF5)

Samples were prepared in 30 mL of PBS_{mod} containing 10 $mg \cdot L^{-1}$ of E2 (by adding the adequate volume from a stock solution in DMSO at 500 $mg \cdot L^{-1}$) and **NP^+-$TPPF_{17}(SGlc)_3$** at 10 μM, and were submitted to a partial photodegradation treatment using white light irradiation ($4mW \cdot cm^{-2}$) for 4 h. Then, **NP^+-$TPPF_{17}(SGlc)_3$** was removed from the samples by centrifugation. Afterwards, samples were treated by a biodegradation process with the addition of **LF5**.

During the photo-treatment, aliquots were taken to quantify E2 and study intermediate products using LC-ESI-MS. After 1 h of irradiation, *ca.* 5.3 $mg \cdot L^{-1}$ of E2 (53 %) remained in solution, along with the adsorbed fraction onto the NPs (undetermined) and the photoproducts. E2 was not detected in the samples after 4 h of irradiation. HPLC chromatograms recorded at different irradiation times showed the appearance of two major transformation products at 6.51 and 7.26 min, which were removed from the samples after 4 h of treatment, and two peaks of lower intensity, at 5.34 and 9.71 min, which accumulated in the samples (Fig. 5.7). Due to the elution characteristics of the method, these products are more polar than related estrogens, and it is expected that they had been formed from the oxidation with ROS, *in situ* generated by the presence of **NP^+-$TPPF_{17}(SGlc)_3$**, under irradiation. The two persistent intermediates were studied by LC-ESI-MS (Fig. 5.8).

MS spectrum of E2 was previously presented (Fig. 4.18). The electrospray ionization of E2 in the negative ion mode resulted in the molecular anion $[M - H]^-$ *m/z* 271.1, and the collisional activation of this $[M - H]^-$ resulted in numerous product ions, including *m/z* 143.0, *m/z* 183.0 and *m/z* 239.1.

MS extracted chromatogram for *m/z* 287.17 corresponds to the peak eluted at 5.34 min (Fig. 5.8a). Collisional activation of this molecular anion, $[M - H]^-$ *m/z* 287.17, resulted in intense fragment ions as *m/z* 121.0, *m/z* 135.0 and *m/z* 269.0. This unknown product, designated as 6-OH-E2, could have been formed from the oxidation of E2 at C-6 with hydroxyl radicals, which would agree with previous findings.[261]

MS extracted chromatogram for *m/z* 253.10 corresponds to the peak eluted at 9.71 min (Fig. 5.8b)**.** Collisional activation of this molecular anion resulted in intense fragment ions as *m/z* 121.0, *m/z* 135.0 and *m/z* 269.0. Those photodegradation products of E2

already described in the literature do not fit the structural characteristics found in the MS spectrum of this unknown intermediate, whose proposed structure would match the fragment ions presented and is also included in Fig. 5.8b.

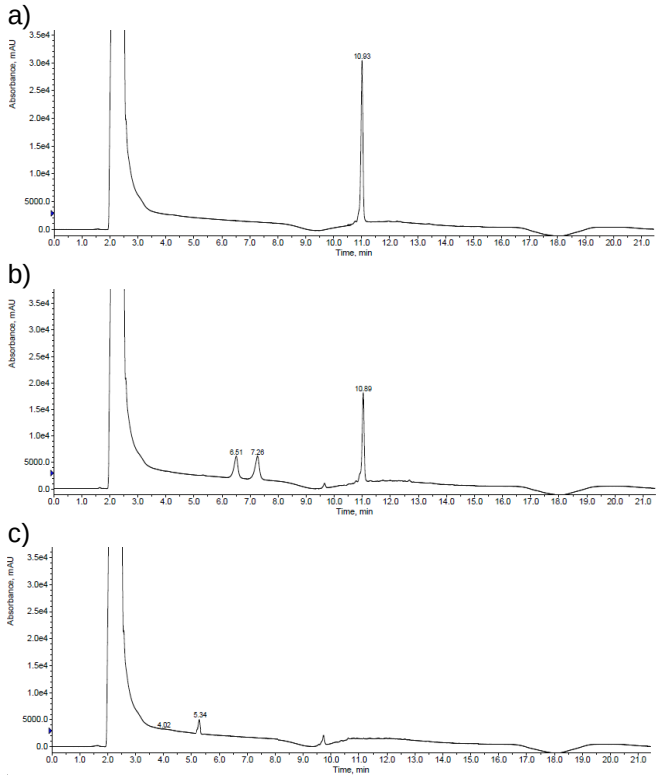

Figure 5. 7. Selected HPLC chromatograms corresponding to samples collected from photodegradation of 10 mg·L^{-1} of E2 with **NP^{+}-TPPF$_{17}$(SGlc)$_3$** at 10 µM after 0, 1 and 4 hours under white light (4 mW·cm^{-2}). Retention time of E2 is 10.93 min.

After 4 h of phototreatment and removal by centrifugation of **NP^{+}-TPPF$_{17}$(SGlc)$_3$**, **LF5** was added and the samples were incubated in dark conditions for 3 days, at 30 ºC. Within this incubation time, aliquots were taken and analysed by LC-ESI-MS to study the persistence of the intermediate products. By the end of the study, the proposed product, 6-OH-E2, was fully removed from the samples. This proposed chemical structure remains to some E2 metabolites, such as 2-OH-E2 or 4-OH-E2, which have been already reported as intermediate products of microbial degradation, and which are also typically metabolized by the strains.[226] 2-OH-E2 and 4-OH-E2 were also detected during E2 degradation by **LF5** (see Chapter 4), and were further removed from the samples. In contrast, intermediate eluted at 9.71 min remained in the samples after incubation period, suggesting that **LF5** does not provide adequate metabolic routes for its uptake and conversion.

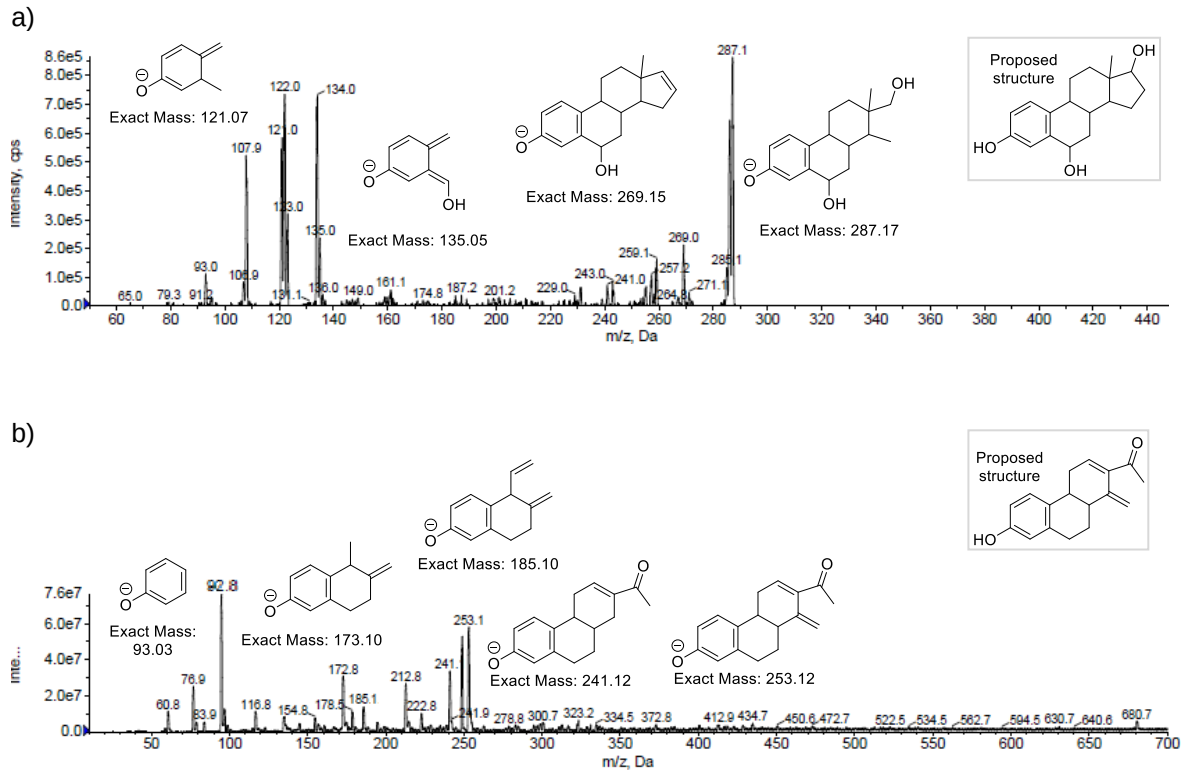

Figure 5. 8. Product-ion spectra from collisionally activated decompositions of the ESI produced $[M-H]^-$ ions: a) *m/z* 287.17, extracted at 5.34 min; and b) *m/z* 253.10, extracted at 9.71 min.

5.3 Conclusions

This study has explored the potential of **NP^+-$TPPF_{17}(SGlc)_3$** to be applied in more realistic conditions, for a sustainable water treatment approach. To reduce energetic consumption to certain extent, sunlight can be applied as light source in photo-treatment for the removal of organic pollutants. **NP^+-$TPPF_{17}(SGlc)_3$** has shown to be photostable under white and UVA light, the larger component of UV light present in solar radiation that reaches Earth's surface. Both absorption and XRD spectra of **NP^+-$TPPF_{17}(SGlc)_3$** presented stable patterns after its irradiation.

In relation to **NP-$TPPF_{17}(SGlc)_3$**, **NP^+-$TPPF_{17}(SGlc)_3$** presented an increased adsorption capability of E2 onto its mesoporous surface, which may benefit the degradation of organic pollutants, and higher removal rates of E2 in water samples. In addition, recovery and recyclability of **NP^+-$TPPF_{17}(SGlc)_3$** showed that the photocatalyst can be used for at least six cycles without suffering an important decay in its efficiency.

The use of **NP^+-$TPPF_{17}(SGlc)_3$** in real wastewaters demonstrated its ability to simultaneously degrade different organic pollutants of great concern in environmental waters, such as E1, E2, E3, EE2, CBZ, CET and SMX.

Two persistent photoproducts arising from the degradation of E2 with **NP^+-$TPPF_{17}(SGlc)_3$** were proposed, obtaining that one of them, 6-OH-E2, could be degraded in a second step of the water treatment, by the addition of the bacterial strain *Bacillus licheniformis* (**LF5**). This fact suggests that the combination of photo- and biodegradation treatments with **NP^+-$TPPF_{17}(SGlc)_3$** and **LF5** could be feasible, thus benefiting from the efficiency of the photocatalyst, but reducing the costs with the addition of the bioremediation step.

5.4 Materials and methods

5.4.1 Materials and equipment

X-ray diffraction (XRD) patterns were obtained on a Shimadzu LabX XRD-6000 X-ray diffractometer with Cu Kα radiation (λ = 1.54178 Å). A scan speed of 3.00 $min^{-1}$was applied to record the pattern in the 2θ range of 20º–70º.

The nitrogen adsorption and desorption isotherms and the Brunauer–Emmett–Teller (BET) tests were performed with a Micromeritics ASAP 2020^{TM} Physisorption system (Norcross, USA) at 77 K. Interparticle space distribution was determined by the Barrett–Joyner–Halenda (BJH) method. Before analysis, the samples were degassed for 4 h at 105 ºC under vacuum.

Homemade UVA lamp used in photostability tests was built at the Division of Environmental Analysis, in BAM. Its emission spectrum is in Fig. 5.3b.

5.4.2 Photostability studies of NP^{+}-$TPPF_{17}(SGlc)_3$ under UVA radiation

Photostability of **NP^{+}-$TPPF_{17}(SGlc)_3$** was evaluated by exposing aqueous suspensions at 1 µM, under UVA irradiation, at room temperature, with vigorous magnetic stirring, for 6 h. At fixed intervals of time, visible absorption spectra of the samples were recorded. To evaluate the stability of **NP^{+}-$TPPF_{17}(SGlc)_3$** in water, a procedure similar to that described above but in dark conditions was performed.

5.4.3 Photocatalytic performance of NP^{+}-$TPPF_{17}(SGlc)_3$ in recycling studies of E2 photodegradation

Photodegradation studies in batch were performed using 100 mL cylindrical glasses. The photocatalytic activity of **NP^{+}-$TPPF_{17}(SGlc)_3$** (10.0 µM) was evaluated in the degradation of 50 mL of aqueous samples containing 5 $mg \cdot L^{-1}$ of E2 under visible light irradiation (4 $mW \cdot cm^{-2}$). The stock solution of E2 was prepared at 1.84 mM (500 $mg \cdot L^{-1}$) in DMSO. Preparation of samples consisted in dispersing appropriate volumes of stock

solutions of **NP^+-$TPPF_{17}(SGlc)_3$** and E2 in water until the desired concentration. Two control samples were included in each irradiation experiment: a light control containing 5 $mg \cdot L^{-1}$ of E2, without PS, and submitted to the same irradiation conditions as the samples, and a dark control containing 5 $mg \cdot L^{-1}$ of E2 and **NP^+-$TPPF_{17}(SGlc)_3$** (10.0 µM), but kept in dark conditions. To estimate the reproducibility of the experimental results, photodegradation experiments were carried out in triplicate, showing in the graphs the average value corresponding for each experimental condition.

After one photodegradation experiment (1 cycle), samples containing **NP^+-$TPPF_{17}(SGlc)_3$** were transferred into polystyrene tubes and the materials were collected at the bottom by centrifugation. Supernatant in each tube was removed and **NP^+-$TPPF_{17}(SGlc)_3$** was washed with ethanol and water and reused in further photocatalytic cycles.

5.4.4 Photodegradation of pharmaceuticals in real water samples of a WWTP influent in presence of NP^+-$TPPF_{17}(SGlc)_3$

Influent samples from the Ruhleben WWTP were collected by Berliner Wasserbetriebe on the 01/08/2016, 07/08/2016 and 15/08/2016. The samples were collected in brown glass bottles, filtered through a folded filter (0.70 µm) on the day of sampling and stored at 4 °C. The filtered samples were treated within three days. Samples (500 mL) were analysed by LC-MS/MS to determine the level of each analyte (E1, E2, E3, EE2, CBZ, CET and SMX), and then each compound was spiked to achieve a final concentration of 1.9 - 2.2 $\mu g \cdot L^{-1}$. Samples were treated in batch mode, using cylindrical glasses of 1000 mL, with **NP^+-$TPPF_{17}(SGlc)_3$** (20 µM), under white light irradiation (4 $mW \cdot cm^{-2}$) and kept under vigorous magnetic stirring for 48 h. Light control samples were included in each irradiation experiment, containing the analytes at the same concentration, without **NP^+-$TPPF_{17}(SGlc)_3$**, and submitted to the same irradiation conditions as the samples. Aliquots (100 mL) were taken at irradiation times 0, 8, 24 and 48 h, and submitted to a solid phase extraction SPE procedure (see section 4.4.10). Aliquots (100-fold concentrated) were then analysed by LC-MS/MS for analytes determination.

To estimate the reproducibility of the experimental results, photodegradation experiments were carried out twice, showing in the graphs the average value corresponding for each experimental condition.

3.3.1 Combined water treatment approach

Samples were prepared in 30 mL of PBS_{mod} (1.80 g·L^{-1} NaH_2PO_4, 0.30 g·L^{-1} KH_2PO_4, 0.25 g·L^{-1} KCl, 35.00 g·L^{-1} NaCl, 0.20 g·L^{-1} NH_4Cl, 0.18 g·L^{-1} ammonium ferric citrate, 5 mL of micronutrient solution described in section 4.4.4; prepared in MilliQ water; pH 7.4), containing 10 mg·L^{-1} of E2. **NP^+-$TPPF_{17}$(SGlc)$_3$** (10 µM) was added and samples were submitted to a partial photodegradation treatment for 4 h, under white light irradiation (4 mW·cm^{-2}). At the end of the treatment, **NP^+-$TPPF_{17}$(SGlc)$_3$** was separated by centrifugation.

Biodegradation of the transformation photoproducts with **LF5** was carried out by the addition of the bacteria to the samples already treated with **NP^+-$TPPF_{17}$(SGlc)$_3$**. For this, **LF5** was harvested during the exponential phase of growth (OD_{600} =0.7) from aliquots (2 mL) by centrifugation at 6000 *g* for 7 min. The cell pellet was washed with PBS_{mod} and then transferred into the samples already treated with **NP^+-$TPPF_{17}$(SGlc)$_3$**. Samples were incubated in a dark incubator shaker (3 days, at 30 ºC, 150 rpm). An abiotic control sample was submitted to the same experimental conditions. Aliquots of the aqueous samples were collected for intermediates evaluation by LC-ESI-MS (500 µL).

For additional details about the PS used, **NP^+-$TPPF_{17}$(SGlc)$_3$**, see Chapters 2 and 3. For additional details about **LF5**, see Chapter 4.

5.4.5 Quantification of organic pollutants and evaluation of metabolites with LC-MS

An Agilent 1260 Infinity LC system with a binary pump, degasser, autosampler, column heater and UV-detector was used. Chromatographic separation was achieved on a Kinetex XB-C18, 2.6 mm, 150 mm *x* 3 mm (Phenomenex, Aschaffenburg, Germany) analytical LC column with a UHPLC C18, 3 mm (Phenomenex) column guard. The quantification was performed by an ABSciex 6500 Triple™ mass spectrometer.

- Determination of E1, E2, E3, EE2

  See section 4.4.13.

- Determination of CBZ, CET, SMX

The mobile phases were ultrapure water with 10 mM NH_4Ac and 0.1% (v/v) acetic acid (A) and MeOH with 10 mM NH_4Ac and 0.1% (v/v) acetic acid (B). The flow rate was

350 µL/min and the column heater temperature was 50 °C. An elution gradient was applied, starting with 80% A, held for 3 min. Afterwards A was decreased to 5% within 5 min and held constant for the next 4 min, increased back to 80% A within 2 min and held for the next 8 min to re-equilibrate the column. The injection volume was 10 µL. Parameters used to produce fragment ions in selected reaction monitoring mode (SRM) like declustering potentials (DP), collision cell exit potentials (CXP) and collision energies (CE) are given in Table 5.4.

Table 5. 4. Summary of the selected reaction monitoring (SRM) transitions for CBZ, CET, SMX and the deuterated internal standard and some useful tandem mass spectrometry parameters: declustering potential (DP), collision energy (CE), collision cell exit potential (CXP).

Compound	SRM transition	DP (V)	CE (V)	CXP (V)
SMX	254 → 92 (quantifier)	11	35	12
	254 → 108 (1st qualifier)	11	31	14
	254 → 156 (2nd qualifier)	11	27	12
SMX-d_4	258 → 96 (quantifier)	11	35	12
	258 → 112 (1st qualifier)	11	31	14
	258 → 160 (2nd qualifier)	11	27	12
CBZ	237 → 194 (quantifier)	11	30	14
	237 → 179 (qualifier)	11	50	12
CBZ-d_2	239 → 196 (quantifier)	11	30	11
	239 → 181 (qualifier)	11	50	11
CET	389 → 201 (quantifier)	11	28	14
	389 → 166 (qualifier)	11	60	14
CET-d_8	397 → 201 (quantifier)	11	28	14

The electrospray ionization source (ESI) was operated in the positive ionization mode. The parameters used for ionization were a temperature of 550 °C, 5000 V ion spray voltage, an entrance potential (EP) of 10 V, a curtain gas with 35 psi, a nebulizer gas (GS1) with 50 psi, a turbo gas (GS2) with 70 psi and a collision gas with 10 psi. Analysts version 1.6.2 software was used to control the instrument, acquire data and evaluate the results.

For quantification of CBZ, CET and SMX, water samples calibrators with standard concentrations of 0, 5, 10, 25, 50, 100, 200 and 300 $\mu g \cdot L^{-1}$ were used. Treated samples were measured with 100-fold pre-concentration. SPE procedure is described in Section 4.5.8.

CHAPTER 6

GENERAL CONCLUSIONS AND FUTURE PERSPECTIVES

GENERAL CONCLUSIONS AND FUTURE PERSPECTIVES

This Ph.D. thesis has focused on the development of sustainable alternatives for water treatment. Particular attention has been paid to prepare and evaluate versatile photocatalysts for the degradation of organic pollutants in water, with special interest in 17β-estradiol (E2), which was selected as model of organic pollutant due to the hazardous effects of its presence in environmental waters. The design of heterogeneous hybrid materials, based on magnetite nanoparticles decorated with porphyrins or phthalocyanines, succeeded in taking advantage from the nanostructured magnetic support and the photosensitizing effect of the dyes. Photodegradation studies in continuous flow mode showed increased removal rates of E2. This mode benefits from the photocatalytic properties of the hybrid materials in water treatment applications, thus promoting homogeneous dispersions in the medium, which enhance their photophysical features.

Future perspectives of this work could include the evaluation of photocatalysts in flow mode under improved and more realistic conditions, such as the effect of the addition of oxidants as H_2O_2, the temperature applied, fitting of the channels diameter in which water flows, or processing of real wastewaters. An especially relevant application of this approach would include the use of sunlight, thus minimizing the energetic requirements of the treatment.

The aforementioned photocatalysts can be used for water remediation purposes against pathogenic microorganisms, after minor modifications of their structures. Cationization of the nanoparticles' shell allows the interaction with Gram-positive and Gram-negative bacterial cell wall. After the incubation of the photocatalyst with bacteria, the irradiation with light of appropriate wavelengths causes the photodynamic inactivation of the cells. In this work, it was highlighted the importance of the size distribution of the nanoparticles, as well as the nature of the dye used of the hybrid materials. A deeper understanding of these characteristics would improve the photosensitizing performance of the antimicrobial materials.

Another matter to explore could be the use of these versatile photocatalysts in water treatment with simultaneous removal of organic pollutants and pathogen inactivation.

The screening of bacterial strains able to metabolize target organic pollutants in water allows a future design of a water treatment approach with improved efficiency and reduced energetic needs, based on the coupling of a partial phototreament to produce biodegradable water, which can be treated by microorganisms. This combination benefits

from the efficiency of the photocatalyst and reduces the costs with the addition of the bioremediation step. This work has focused on the biodegradation of estrogens, with relevant results using the bacterial strain *Bacillus licheniformis* (**LF5**), previously isolated from deep sea sediments in the Gulf of Cádiz (Spain). **LF5** displayed great versatility, being able to remove different estrogens in relevant concentrations ($\mu g \cdot L^{-1}$) in wastewaters. Future work could involve the incorporation of **LF5** into the bacterial community of an activated sludge of a WWTP, to evaluate if its presence improves the estrogens removal and decreases the hazardous effects that imply their discharge into superficial natural waters.

Finally, one photocatalyst prepared within the frame of this work, **NP^+-$TPPF_{17}(SGlc)_3$**, was evaluated under UVA light, the larger component of UV light present in solar radiation that reaches the Earth's surface. **NP^+-$TPPF_{17}(SGlc)_3$** presented high photostability, which suggest its future use under natural sunlight. In addition, **NP^+-$TPPF_{17}(SGlc)_3$** demonstrated ability to simultaneously degrade different types of organic pollutants present in wastewaters, as well as an efficient recyclability in six successive cycles.

Two persistent intermediates of the degradation of E2 with **NP^+-$TPPF_{17}(SGlc)_3$** were detected by LC-ESI-MS. One of them, 6-OH-E2, could be degraded in a second step of the water treatment, by the addition of **LF5**. Forthcoming investigations could explore this combined approach in more realistic conditions of wastewater treatments, using sunlight as irradiation source. For this, photostability and photocatalytic performance of **NP^+-$TPPF_{17}(SGlc)_3$** under typical fluence rates of irradiation during all seasons of the year must be evaluated.

REFERENCES

1. *Study on enhancing the endocrine disrupter priority list with a focus on low production volume chemicals*; European Commission: rec.europa.eu/environment/endocrine/documents/final_report_2007.pdf, 2007.

2. Ali, I.; Asim, M.; Khan, T.A., Low cost adsorbents for the removal of organic pollutants from wastewater. *J. Environ. Manage.*, **2012**, *113*, 170-183.

3. Redshaw, C.H.; Cooke, M.P.; Talbot, H.M.; McGrath, S.; Rowland, S.J., Low biodegradability of fluoxetine HCl, diazepam and their human metabolites in sewage sludge-amended soil. *J. Soil. Sediment.*, **2008**, *8*, 217-230.

4. (a) Hignite, C.; Azarnoff, D.L., Drugs and drug metabolites as environmental contaminants - chlorophenoxyisobutyrate and salicylic-acid in sewage water effluent. *Life Sci.* , **1977**, *20*, 337-341; (b) Stumm-Zollinger, E.; Fair, G.M., Biodegradation of steroid hormones. *J. Water Pollut. Control Fed.*, **1965**, *37*, 1506-1510.

5. (a) Purdom, C.E.; Hardiman, P.A.; Bye, V.V.J.; Eno, N.C.; Tyler, C.R.; Sumpter, J.P., Estrogenic effects of effluents from sewage treatment works. *J. Chem. Ecol.*, **1994**, *8*, 275-285; (b) Desbrow, C.; Routledge, E.J.; Brighty, G.C.; Sumpter, J.P.; Waldock, M., Identification of estrogenic chemicals in STW effluent. 1. Chemical fractionation and in vitro biological screening. *Environ. Sci. Technol.*, **1998**, *32*, 1549-1558.

6. Halling-Sørensen, B.; Nors Nielsen, S.; Lanzky, P.F.; Ingerslev, F.; Holten Lützhoft, H.C.; Jørgensen, S.E., Occurrence, fate and effects of pharmaceutical substances in the environment - a review. *Chemosphere*, **1998**, *36*, 357-393.

7. Gaw, S.; Thomas, K.V.; Hutchinson, T.H., Sources, impacts and trends of pharmaceuticals in the marine and coastal environment. *Phil. Trans. R. Soc. B*, **2014**, *369*.

8. Plant, K.A.; Voulvoulis, N.; Vala Ragnarsdottir, K., *Pollutants, Human Health and the Environment: A Risk Based Approach*. Wiley-Blackwell: Chichester, 2012.

9. Calamari, D.; Zuccato, E.; Castiglioni, S.; Bagnati, R.; Fanelli, R., Strategic survey of therapeutic drugs in the rivers Po and Lambro in northern Italy. *Environ. Sci. Technol.*, **2003**, *37*, 1241-1248.

10. Ternes, T.A., Occurrence of drugs in German sewage treatment plants and rivers. *Water Res.*, **1998**, *32*, 3245-3260.

11. Kuspis, D.A.; Krenzelok, E.P., What happens to expired medications? A survey of community medication disposal. *Vet. Hum. Toxicol.*, **1996**, *38*, 48-49.

12. *Global assessment of the state-of-the-science of endocrine disruptors*. World Health Organization: 2002.

13. *Community strategy for endocrine disrupters - A range of substances suspected of interfering with the hormone systems of humans and wildlife* European Commission: Brussels, 1999; p 6.

14. Kime, D.E., *Endocrine Disruption in Fish*. Springer Science & Business Media: Norwell, 1998.

15. Campbell, N.A.; Reece, J.B.; Mitchell, L.G., *Biology*. 5th ed.; Addison Wesley Longman: Menlo Park, CA, 1999.

16. Johnson, A.C.; Williams, R.J., A model to estimate influent and effluent concentrations of estradiol, estrone and ethinylestradiol at sewage treatment works. *Environ. Sci. Technol.*, **2004**, *38*, 3649-3658.

17. (a) Caliman, F.A.; Gavrilescu, M., Pharmaceuticals, personal care products and endocrine disrupting agents in the environment: A review. *CLEAN*, **2009**, *37*, 277-303; (b) Caserta, D., Maranghi, L., Mantovani, A., Marci, R., Maranghi, F., Moscarini, M., Impact of endocrine disruptor chemicals in gynaecology. *Hum. Reprod. Update*, **2008**, *14*, 59-72; (c) Goldman, J.M., Laws, S. C., Balchak, S. K., Cooper, R. L., Kavlock, R. J., Endocrine Disrupting chemicals: prepubertal exposures and effects on sexual maturation and thyroid activity in the female rat. A focus on the EDSTAC recommendations. *Crit. Rev. Toxicol.*, **2000**, *30*, 135-196; (d) Matozzo, V., Gagné, F., Marin, M. G., Ricciardi, F., Blaise, C. , Vitellogenin as a biomarker of exposure to estrogenic compounds in aquatic invertebrates: a review. *Environ. Int.*, **2008**, *34*, 531-545; (e) Conroy, O., Sáez, A. E., Quanrud, D., Ela, W., Arnold, R. G., Changes in estrogen/ anti-estrogen activities in ponded secondary effluent. *Sci. Total Environ.*, **2007**, *382*, 311-323; (f) Stoker, T.E., Laws, S. C., Guidici, D. L., Cooper, R. L., The effect of atrazine on puberty in male wistar rats: an evaluation in the protocol for the assessment of pubertal development and thyroid function. *Toxicol. Sci.*, **2000**, *58*, 50-59.

18. Combalbert, S., Hernandez-Raquet, G., Occurrence, fate, and biodegradation of estrogens in sewage and manure. *Appl. Microbiol. Biotechnol.*, **2010**, *86*, 1671-1692.

19. Lai, K.M., Scrimshaw, M. D., Lester, J. N., Biotransformation and bioconcentration of steroid estrogens by Chlorella vulgaris. *Appl. Environ. Microbiol.*, **2002**, *68*, 859-864.

20. Dray, J.; Dray, F.; Tiller, F.; A., U., Hydrolysis of urine metabolites of different steroid hormones by β-glucuronidase of Escherichia coli. *Ann. Inst. Pasteur*, **1972**, *123*, 853-857.

21. Ying, G.-G.; Kookana, R.S.; Ru, Y.-J., Occurrence and fate of hormone steroids in the environment. *Environ. Int.*, **2002**, *28*, 545-551.

22. (a) Abe, I., Adsorption properties of endocrine disruptors onto activated carbon. *J. Water Waste* **1991**, *41*, 43-47; (b) Iwasaki, S.; Fukuhara, T.; Abe, I.; Yanagi, J.; Mouri, M.; Y., I., Adsorption of alkylphenols onto microporous carbons prepared from coconut shell. *Synth. Met.*, **2001**, *125*, 207-211.

23. Zhang, Y.P.; Zhou, J.L., Removal of estrone and 17β-estradiol from water by adsorption. *Water Res.*, **2005**, *39*, 3991-4003.

24. (a) Silva, C.P.; Otero, M.; Esteves, V.I., Processes for the elimination of estrogenic steroid hormones from water: A review. *Environ. Pollut.*, **2012**, *165*, 38-58; (b) Chang, S.; Wait, D.T.; Schafer, A.I.; Fane, A.G., Adsorption of trace steroid estrogens to hydrophobic hollow fibre membranes. *Desalination*, **2002**, *146*, 381-386; (c) Cartinella, J.L.; Cath, T.Y.; Flynn, M.T.; Meller, G.C.; Hunter, K.W.; Childress, A.E., Removal of natural steroid hormones from wastewater using membrane contactor processes. *Environ. Sci. Technol.*, **2006**, *40*, 7381-7386.

25. Comeau, Y.; Henze, M., *Wastewater concentrations. Biological Wastewater Treatment*. IWA Publishing: London, UK, 2008.

26. Shi, J., Fujisawa, S., Nakai, S., Hosomi, M., Biodegradation of natural and synthetic estrogens by nitrifying activated sludge and ammonia-oxidizing bacterium Nitrosomonas europaea. *Water Res.*, **2004**, *38*, 2323-2330.

27. Joutey, N.T.; Bahafid, W.; Sayel, H.; El Ghachtouli, N., *Biodegradation - Life of Science*. InTech: 2013.

28. Leitão, A.L., Potential of Penicillium Species in the Bioremediation Field. *Int. J. Environ. Res. Public Health.*, **2009**, *6*, 1393-1417.

29. (a) Jiang, L., Yang, J., Chen, J., Isolation and characteristics of 17β-estradiol-degrading Bacillus spp. strains from activated sludge. *Biodegradation*, **2010**, *21*, 729-736; (b) Pauwels, B.; Wille, K.; Noppe, H.; DeBrabander, H.; Van de Wiele, T.; Verstraete, W.; Boon, N., 17α-ethinylestradiol cometabolism bybacteria degrading estrone, 17β-estradiol and estriol. *Biodegradation*, **2008**, *19*, 683-693.

30. Dubroca, J.; Collignon, N.; Brault, A.; Hernandez-Raquet, G.; Patureau, D.; Mougin, C., Fate of 17b-estradiol in terrestrial model ecosystems amended with contaminated composted biosolids. *Environ. Chem. Lett.*, **2009**, *7*, 369-373.

31. Ternes, T.A., Kreckel, P., Mueller, J., Behaviour and occurrence of estrogens in municipal sewage treatment plants-II. Aerobic batch experiments with activated sludge. *Sci. Total Environ.*, **1999**, *225*, 91-99.

32. Chowdhury, R.R.; Charpentier, P.A.; Ray, M.B., Photodegradation of 17β-estradiol in aquatic solution under solar irradiation: Kinetics and influencing water parameters. *J. Photochem. Photobiol. A*, **2011**, *219*, 67-75.

33. Glaze, W.H.; Kang, J.W.; Chapin, D.H., The chemistry of water treatment processes involving ozone, hydrogen peroxide, and ultraviolet radiation. *Ozone Sci. Eng.*, **1987**, *9*, 335-352.

34. Olle, I.; Malato, S.; Sánchez-Pérez, J.A., Combination of advanced oxidation processes and biological treatments for wastewater decontamination - A review. *Sci. Total Environ.*, **2011**, *409*, 4141-4166.

35. (a) Waki, K.; Zhao, J.; Horikoshi, S.; Watanabe, N.; Hidaka, H., Photooxidation mechanism of nitrogen-containing compounds at TiO_2/H_2O interface: an experimental and theoretical examination of hydrazine derivatives. *Chemosphere*, **2000**, *41*, 337-343; (b) Lányi, K.; Dinya, Z., Photodegradation study of some triazine-type herbicides. *Microchem. J.*, **2003**, *75*, 1-14; (c) Warner, S.D.; Farant, J.; Butler, I.S., Photochemical degradation of selected nitropolycyclic aromatic hydrocarbons in solution and adsorbed to solid particles. *Chemosphere*, **2004**, *54*, 1207-1215.

36. (a) Vargas, E.; Vargas, R.; Núñez, O., A TiO_2 surface modified with copper(II) phthalocyanine-tetrasulfonic acid tetrasodium salt as a catalyst during photoinduced dichlorvos mineralization by visible solar light *Appl. Catal., B.*, **2014**, *156-157*, 8-14; (b) Huang, Z.; Zheng, B.; Zhu, S.; Yao, Y.; Ye, Y.; Lu, W.; Chen, W., Photocatalytic activity of phthalocyanine-sensitized TiO_2–SiO_2 microparticles irradiated by visible light. *Mater. Sci. Semicond. Process.*, **2014**, *25*, 148-152; (c) Ajmal, A.; Majeed, I.; Malik, R.N.; Idriss, H.; Nadeem, M.A., Principles and mechanisms of photocatalytic dye degradation on TiO_2 based photocatalysts: a comparative overview. *RSC Adv.*, **2014**, *4*, 37003-37026.

37. Ma, Y.; Wang, X.; Jia, Y.; Chen, X.; Han, H.; Li, C., Titanium Dioxide-Based Nanomaterials for Photocatalytic Fuel Generations. *Chem. Rev.*, **2014**, *114*, 9987−10043.

38. Thandu, M.; Comuzzi, C.; Goi, D., Phototreatment of water by organic photosensitizers and comparison with inorganic semiconductors. *Int. J. Photoenergy*, **2015**, *2015*, 1-22.

39. Challis, J.K.; Hanson, M.L.; Friesen, K.J.; Wong, C.S., A critical assessment of the photodegradation of pharmaceuticals in aquatic environments: defining our current understanding and identifying knowledge gaps. *Env. Sci. Process. Impact.*, **2014**, *16*, 672-696.

40. Ohko, Y.; Iuchi, K.-I.; Niwa, C.; Tatsuma, T.; Nakashima, T.; Iguchi, T.; Kubota, Y.; Fujishima, A., 17 beta-estradiol degradation by TiO_2 photocatalysis as a means of reducing estrogenic activity. *Environ. Sci. Technol.*, **2002**, *19*, 4175-4181.

41. Koutantou, V.; Kostadima, M.; Chatzisymeon, E.; Frontistis, Z.; Binas, V.; Venieri, D.; Mantzavinos, D., Solar photocatalytic decomposition of estrogens over immobilized zinc oxide. *Catal. Today*, **2013**, *209*, 66-73.

42. Schweitze, C.; Schmidt, R., Physical mechanisms of generation and deactivation of singlet oxygen. *Chem. Rev.*, **2003**, *103*, 1685-1757.

43. Barata, J.F.B., Zamarrón, A., Neves, M. G. P. M. S., Faustino, M. A. F., Tomé, A. C., Cavaleiro, J. A. S., Röder, B., Juarranz, A., Sanz-Rodríguez, F., Photodynamic effects induced by meso-tris(pentafluorophenyl)corrole and its cyclodextrin conjugates on cytoskeletal components of HeLa cells. *Eur. J. Med. Chem.*, **2015**, *92*, 135-144.

44. Rocha, D.M.; Venkatramaiah, N.; Gomes, M.C.; Almeida, A.; Faustino, M.A.; Almeida Paz, F.A.; Cunha, Â.; Tomé, J.P., Photodynamic inactivation of Escherichia coli with cationic ammonium Zn(II) phthalocyanines. *Photochem. Photobiol. Sci.*, **2015**, *14*, 1872-1879.

45. Xu, J., Wu J., Zong, C., Ju, H., Yan, F., Manganese porphyrin-dsDNA complex: a mimicking enzyme for highly efficient bioanalysis. *Anal Chem.*, **2013**, *85*, 3374-3379.

46. Rodrigues, J.M.M.; Farinha, A.S.F.; Muteto, P.V.; Woranovicz-Barreira, S.M.; Almeida Paz, F.A.; Neves, M.G.P.M.S.; Cavaleiro, J.A.S.; Tome, A.C.; Gomes, M.T.S.R.; Sessler, J.L.; Tome, J.P.C., New porphyrin derivatives for phosphate anion sensing in both organic and aqueous media. *Chem. Commun.*, **2014**, *50*, 1359-1361.

47. Gottfried, J.M., Surface chemistry of porphyrins and phthalocyanines. *Surf. Sci. Rep.*, **2015**, *70*, 259-379.

48. Ebrahimian, A.; Zanjanchi, M.A.; Noei, H.; Arvand, M.; Wang, Y., TiO_2 nanoparticles containing sulphonated cobalt phthalocyanine: Preparation, characterization and photocatalytic performance. *J. Environ. Chem. Eng.*, **2014**, *2*, 484-494.

49. Lourenço, L.M.O.; Resende, J.; Iglesias, B.A.; Castro, K.; Nakagaki, S.; Lima, M.J.; da Cunha, A.F.; Neves, M.G.P.M.S.; Cavaleiro, J.A.S.; Tomé, J.P.C., Synthesis, characterization and electrochemical properties of meso-thiocarboxylate-substituted porphyrin derivatives. *J. Porphyrins Phthalocyanines*, **2014**, *18*, 967-974.

50. Tanaka, S., Hanada, T., Ono, K., Watanabe, K., Yoshino, K., Hiromitsu, I., Improvement of power conversion efficiency of phthalocyanine/C60 heterojunction solar cells by inserting a lithium phthalocyanine layer at the indium-tin oxide/phthalocyanine interface. *Appl. Phys. Lett.*, **2010**, *97*, 253306.

51. Gürol, İ.; Durmuş, M.; Ahsen, V., Photophysical and photochemical properties of fluorinated and nonfluorinated *n*-propanol-substituted zinc phthalocyanines. *Eur. J. Inorg. Chem.*, **2010**, *2010*, 1220–1230.

52. Wöhrle, D.; Suvorova, O.; Gerdes, R.; Bartels, O.; Lapok, L.; Baziakina, N.; Makarov, S.; Slodek, A., Efficient oxidations and photooxidations with molecular oxygen using metal phthalocyanines as catalysts and photocatalysts. *J. Porphyrins Phthalocyanines*, **2004**, *08*, 1020-1041.

53. DeRosa, M.C.; Crutchley, R.J., Photosensitized singlet oxygen and its applications. *Coord. Chem. Rev.*, **2002**, *233–234*, 351-371.

54. Dolphin, D., *The Porphyrins*. Academic Press: New York, 1978; Vol. 1.

55. Ortfi, E.; Bredas, J.L., Electronic structure of metal-free phthalocyanine: A valence effective Hamiltonian theoretical study. *J. Chem. Phys.*, **1988**, *89*, 1009-1016.

56. Senge, M.O.; Fazekas, M.; Notaras, E.G.A.; Blau, W.J.; Zawadzka, M.; Locos, O.B.; Ni Mhuircheartaigh, E.M., Nonlinear Optical Properties of Porphyrins. *Adv. Mat.*, **2007**, *19*, 2737–2774.

57. Claessens, C.G.; Hahn, U.; Torres, T., Phthalocyanines: From Outstanding Electronic Properties to Emerging Applications. *Chem. Rec.*, **2008**, *8*, 75-97.

58. DeRosa, M.C.; Crutchley, R.J., Photosensitized singlet oxygen and its applications. *Coord. Chem. Rev.*, **2002**, *233*, 351-371.

59. Jiang, J., *Functional phthalocyanine molecular materials*. Springer: Heidelberg, 2010; Vol. 135, p 51.

60. Baker, K.S.; Smith, R.C., *The Role of Solar Radiation in Marine Ecosystems*. Plenum Press: New York, 1982.

61. Smith, K.M., *Porphyrins and Metalloporphyrins*. Company: Amsterdam, 1975.

62. Gouterman, M., *The Porphyrins*. Academic Press: New York, 1978; Vol. III.

63. Fischer, H.; Klarer, J.L., *Ann. Chem.* , **1929**, *98*, 468-.

64. Rothemund, P., A New porphyrin synthesis. The synthesis of porphin. *J. Am. Chem Soc.*, **1936**, *58*, 625-627.

65. Ball, R.H.; Dorough, G.D.; Calvin, M., A further study of the porphine-like products of the reaction of benzaldehyde and pyrrole. *J. Am. Chem. Soc.*, **1946**, *68*, 2278-2281.

66. Adler , A.D.; Longo, F.R.; Finarelli, J.D.; Goldmacher, J.; Assour, J.; Korsakoff, L., A simplified synthesis for meso-tetraphenylporphine. *J. Org. Chem.*, **1967**, *32*, 476-476.

67. Lindsey, L.S.; Schreiman, I.C.; Hsu, H.C.; Kearney, P.C.; Marquerattaz, A.M., Rothemund and Adler-Longo reactions revisited: synthesis of tetraphenylporphyrins under equilibrium conditions. *J. Org. Chem.*, **1987**, *52*, 827-836.

68. Gonsalves, A.M.A.R.; Varejão, J.M.T.B.; Pereira, M.M., Some new aspects related to the synthesis of meso-substituted porphyrins. *J. Heterocyclic Chem.*, **1991**, *28*, 635-640.

69. Linstead, R.P., *J. Chem. Soc.*, **1934**, 1022-1027.

70. Sharman, W.M.; van Lier, J.E., *The Porphyrin Handbook* Academic Press: New York, 2003; Vol. 15.

71. Durmuş, M.; Yaman, H.; Göl, C.; Ahsen, V.; Nyokong, T., Water-soluble quaternized mercaptopyridine-substituted zinc-phthalocyanines: Synthesis, photophysical, photochemical and bovine serum albumin binding properties. *Dyes Pigm.*, **2011**, *91*, 153-163.

72. Sorokin, A.B., Phthalocyanine Metal Complexes in Catalysis. *J. Am. Chem. Soc.*, **2013**, *113*, 8152-8191.

73. Sakamoto, K.; Ohno-Okumura, E., Syntheses and Functional Properties of Phthalocyanines. *Materials*, **2009**, *2*, 1127-1179.

74. Sastre, A.; Torres, T.; Hanack, M., Synthesis of Novel Unsymmetrical Monoaminated Phthalocyanines *Tetrahedron Lett.*, **1995**, *36*, 8501-8504.

75. Wiihrle, D.; Schnurpfeil , G.; Knothe, G., Efficient Synthesis of Phthalocyanines and Related Macrocyclic Compounds in the Presence of Organic Bases. *Dyes Pigm.*, **1992**, *18*, 91-102.

76. Leznoff, C.C.; Hu, M.; Nolan, K.J.M., The synthesis of phthalocyanines at room temperature *Chem. Commun.*, **1996**, 1245-1246.

77. Shaabani, A.; Maleki-Moghaddam, R.; Maleki, A.; Rezayan, A.H., Microwave assisted synthesis of metal-free phthalocyanine and metallophthalocyanines. *Dyes Pigm.*, **2007**, *74*, 279-282.

78. Cook, M.J.; McMurdo, J.; Miles, D.A.; Poynter, R.H., Monolayer behaviour and Langmuir–Blodgett film properties of some amphiphilic phthalocyanines: factors influencing molecular organisation within the film assembly. *J. Mater. Chem.*, **1994**, *4*, 1205-1213.

79. (a) Weber, J.H.; Busch, D.H., Complexes Derived from Strong Field Ligands. XIX. Magnetic Properties of Transition Metal Derivatives of 4,4',4'',4'''-Tetrasulfophthalocyanine. *Inorg. Chem.*, **1965**, *4*, 469-471; (b) Rodrigues, S.E.; Machado, A.E.H.; Berardi, M.; Ito, A.S.; Almeida, L.M.; Santana, M.J.; Liao, L.M.; Barbosa Neto, N.M.; Gonçalves, P.J., Investigation of protonation effects on the electronic and structural properties of halogenated sulfonated porphyrins. *J. Mol. Struct.*, **2015**, *1084*, 284-293.

80. (a) Lourenço, L.M.O.; Resende, J.; Iglesias, B.A.; Castro, K.; Nakagaki, S.; Lima, M.J.; da Cunha, A.F.; Neves, M.G.P.M.S.; Cavaleiro, J.A.S.; Tomé, J.P.C., Synthesis, characterization and electrochemical properties of meso-thiocarboxylate-substituted porphyrin derivatives. *JPP*, **2014**, *18*, 967-974; (b) Shaposhnikov, G.P.; Maizlish, V.E.; Kulinich, V.P., Carboxy-substituted Phthalocyanine Metal Complexes. *Russ. J. Gen. Chem.*, **2005**, *75*, 1553-1562.

81. Král, V.; Rusin, O.; Charvátová, J.; Anzenbacher, J.P.; Fogl, J., Porphyrin phosphonates: novel anionic receptors for saccharide recognition. *Tetrahedron Lett.*, **2000**, *41*, 10147-10151.

82. Ren, L.; Zhang, A.; Huang, J.; Wang, P.; Weng, X.; Zhang, L.; Liang, F.; Tan, Z.; Zhou, X., Quaternary ammonium zinc phthalocyanine: inhibiting telomerase by stabilizing G quadruplexes and inducing G-quadruplex structure transition and formation. *Chembiochem.* , **2007**, *8*, 775-780.

83. Oliveira, A.; Almeida, A.; Carvalho, C.M.B.; Tomé, J.P.C.; Faustino, M.A.F.; Neves, M.G.P.M.S.; Tomé, A.C.; Cavaleiro, J.A.S.; Cunha, A., Porphyrin derivatives as photosensitizers for the inactivation of Bacillus cereus endospores. *J. Appl. Microbiol.*, **2009**, *106*, 1986–1995.

84. Tanielian, C.; Wolff, C.; Esch, M., Singlet oxygen production in water: aggregation and charge-transfer effects. *J. Phys. Chem.*, **1996**, *100*, 6555-6560.

85. Singh, S.; Aggarwal, A.; Thompson, S.; Tomé, J.P.C.; Zhu, X.; Samaroo, D.; Vinodu, M.; Gao, R.; Drain, C.M., Synthesis and Photophysical Properties of Thioglycosylated Chlorins, Isobacteriochlorins, and Bacteriochlorins for Bioimaging and Diagnostics. *Bioconjugate Chem.*, **2010**, *21*, 2136-2146.

86. Aggarwal, A., Singh, S., Zhang, Y., Anthes, M., Samaroo, D., Gao, R., Drain, C. M., Synthesis and photophysics of an octathioglycosylated zinc(II) phthalocyanine. *Tetrahedron Lett.*, **2011**, *52*, 5456-5459.

87. Soares, A.R.; Tomé, J.P.; Neves, M.G.; Tomé, A.C.; Cavaleiro, J.A.; Torres, T., Synthesis of water-soluble phthalocyanines bearing four or eight D-galactose units. *Carbohydr. Res.*, **2009**, *4*, 507-510.

88. Guo, Z., Chen B, Mu J, Zhang M, Zhang P, Zhang Z, Wang J, Zhang X, Sun Y, Shao C, Liu Y, Iron phthalocyanine/TiO_2 nanofiber heterostructures with enhanced visible photocatalytic activity assisted with H_2O_2. *J. Hazard. Mater.*, **2012**, *219-220*, 156-163.

89. Pepe, E.; Abbas, O.; Rebufa, C.; Simon, M.; Lacombe, S.; Julliard, M., Supported photosensitizers for the visible light activation of phenols towards oxygen. *J. Photochem. Photobiol. A Chem.*, **2005**, *170*, 143-149.

90. Agboola, B.; Ozoemena, K.I.; Nyokong, T., Comparative efficiency of immobilized non-transition metal phthalocyanine photosensitizers for the visible light transformation of chlorophenols. *J. Mol. Catal. A: Chem.*, **2006**, *248*, 84-92.

91. Govan, L.; Gun´ko, Y.K., Recent Advances in the Application of Magnetic Nanoparticles as a Support for Homogeneous Catalysts. *J. Nanomater.*, **2014**, *4*, 222-241.

92. Modisha P, N.T., Antunes E, Photodegradation of Orange-G using zinc octacarboxyphthalocyaninesupported on Fe_3O_4 nanoparticles. *J. Mol. Catal. A: Chem.*, **2013**, *380*, 131-138.

93. Carvalho, C.M.B.; Alves, E.; Costa, L.; Tomé, J.P.C.; Faustino, M.A.F.; Neves, M.G.P.M.S.; Tomé, A.C.; Cavaleiro, J.A.S.; Almeida, A.; Cunha, A.; Lin, Z.; Rocha, J., Functional Cationic Nanomagnet-Porphyrin Hybrids for the Photoinactivation of Microorganisms. *ACS Nano*, **2010**, *4*, 7134-7140.

94. Alves, E.; Rodrigues, J.M.M.; Faustino, M.A.F.; Neves, M.G.P.M.S.; Cavaleiro, J.A.S.; Lin, Z.; Cunha, Â.; Nadais, M.H.; Tomé, J.P.C.; Almeida, A., A new insight on nanomagnet–porphyrin hybrids for photodynamic inactivation of microorganisms. *Dyes Pigmen.*, **2014**, *110*, 80-88.

95. Ogunbayo, T.B.; Nyokong, T., Phototransformation of 4-nitrophenol using Pd phthalocyanines supported on single walled carbon nanotubes. *J. Mol. Catal. A: Chem.*, **2011**, *337*, 68-76.

96. Adams, G.O.; Fufeyin, P.T.; Okoro, S.E.; Ehinomen, I., Bioremediation, Biostimulation and Bioaugmention: A Review. *Int. J. Environ. Bioremed. Biodegrad.*, **2015**, *3*, 28-39.

97. Rockne, K.J.; Reddy, K.R., Bioremediation of contaminated sites. In *International e-Conference on Modern Trends in Foundation Engineering: Geotechnical Challenges and Solutions*, Indian Institute of Technology: Madras, India, 2003; pp 1-22.

98. Riser-Roberts, E., *Remediation of petroleum contaminated soils: biological, physical, and chemical processes*. CRC-Press LLC: Boca Raton, 1998.

99. Fass , R.; Flashner, Y.; Reuveny, S., *Novel Approachesfor Bioremediation of Organic Pollution*. Plenum Publishers: New York, 1999.

100. Das, N.; Chandran, P., Microbial Degradation of Petroleum Hydrocarbon Contaminants: An Overview. *Biotechnol. Res. Int.*, **2011**, *2011*, 1-13.

101. Foght, J.M.; Westlake, D.W.S.; Johnson, W.M.; Ridgway, H.F., Environmental gasoline-utilizing isolates and clinical isolates of Pseudomonas aeruginosa are taxonomically indistinguishable by chemotaxonomic and molecular techniques. *Microbiology*, **1996**, *142*, 2333-2340.

102. Atlas, R.M., *Petroleum Effects in the Arctic Environment*. Elsevier: London, UK, 1985.

103. Chaillan, F.; Chaîneau, C.H.; Point, V.; Saliot, A.; Oudot, J., Factors inhibiting bioremediation of soil contaminated with weathered oils and drill cuttings. *Environ. Pollut.*, **2006**, *144*, 255-265.

104. Fritsche, W.; Hofrichter, M., Aerobic Degradation by Microorganisms. In *Biotechnology*, Wiley-VCH Verlag GmbH: 2008; pp 144-167.

105. Yu, C.P., Roh, H., Chu, K. H., 17ß-Estradiol-Degrading Bacteria Isolated from Activated Sludge. *Environ. Sci. Technol.*, **2007**, *41*, 486-492.

106. Yu, C.P.; Deeb, A.A.; Chu, K.H., Microbial degradation of steroidal estrogens. *Chemosphere*, **2013**, *91*, 1225-1235.

107. Fujii, K., Kikuchi, S., Satomi, M., Ushio-Sata, N., Morita, N., Degradation of 17α-estradiol by a gram-negative bacterium isolated from activated sludge in a sewage treatment plant in Tokyo, Japan. *Appl. Environ. Microbiol.*, **2002**, *68*, 2057-2060.

108. Yoshimoto, T., Nagai, F., Fujimoto, J., Watanabe, K.; Mizukoshi, H., Makino, T., Kimura, K., Saino, H., Sawada, H., Omura, H., Degradation of estrogens by Rhodococcus zopfii and Rhodococcus equi isolates from activated sludge in wastewater treatment plants. *Appl. Environ. Microbiol.*, **2004**, *70*, 5283-5289.

109. Weber, S., Leuschner, P., Kampfer, P., Dott, W., Hollender, J., Degradation of estradiolandethinyl estradiol by activated sludge and by a defined mixed culture. *Appl. Environ. Microbiol.*, **2005**, *67*, 106-112.

110. Zhang, T.; Xiong, G.; Maser, E., Characterization of the steroid degrading bacterium S19-1 from the Baltic Sea at Kiel, Germany. *Chem. Biol. Interact.*, **2011**, *191*, 83-88.

111. Sang, Y.; Xiong, G.; Maser, E., Identification of a new steroid degrading bacterial strain H5 from the Baltic Sea and isolation of two estradiol inducible genes. *J. Steroid Biochem. Mol. Biol.*, **2012**, *129*, 22-30.

112. Fahrbach, M.; Kuever, J.; Meinke, R.; Kämpfer, P.; Hollender, J., Denitratisoma oestradiolicum gen. Nov. Sp. Nov., a 17β-oestradiol-degrading, denitrifying betaproteobacterium. *Int. J. Syst. Evol. Microbiol.*, **2006**, *56*, 1547-1552.

113. Geize, R.; Dijkhuizen, L., Harnessing the catabolic diversity of Rhodococci for environmental and biotechnological applications. *Ecol. Ind. Microbiol.*, **2004**, *7*, 255-261.

114. Coombe, R.G., Tsong, Y. Y., Hamilton, P. B., Sih, C. J., Mechanisms of steroid oxidation by microorganisms: oxidative cleavage of estrone. *J. Biol. Chem.*, **1966**, *241*, 1587-1595.

115. Ren, H.; Ji, S.; Ahmad, N.; Wang, D.; Cui, C., Degradation characteristics and metabolic pathway of 17α-ethinylestradiol by Sphingobacterium sp. JCR5. *Chemosphere*, **2007**, *66*, 340-346.

116. Kurisu, F.; Ogura, M.; Saitoh, S.; Yamazoe, A.; Yagi, O., Degradation of natural estrogen and identification of the metabolites produced by soil isolates of Rhodococcus sp. and Sphingomonas sp. *J. Biosci. Bioeng.*, **2010**, *109*, 576-582.

117. Lee, H.B., Liu, D., Degradation of 17b-estradiol and its metabolites by sewage bacteria. *Water Air Soil Pollut.*, **2002**, *134*, 353-368.

118. Chatterjee, D.; Dasgupta, S., Visible light induced photocatalytic degradation of organic pollutants. *J. Photochem. Photobiol. C: Photochem. Rev.*, **2005**, *6*, 186-205.

119. (a) Muñoz, R.; Guieysee, B., Algal–bacterial processes for the treatment of hazardous contaminants: a review. *Water Res.*, **2006**, *40*, 2799-2815; (b) Lapertot, M.; Pulgarín, C.; Fernández-Ibañez, P.; Maldonado, M.I.; Pérez-Estrada, L.; Oller, I.; Gernjak, W.; Malato, S., Enhancing biodegradability of priority substances (pesticides) by solar photo-Fenton. **2006**, *40*, 1086-1094.

120. Muñoz, I.; Rieradevall, J.; Torrades, F.; Peral, J.; Doménech, X., Environmental assessment of different solar driven advanced oxidation processes. *Sol. Energy*, **2005**, *79*, 369-375.

121. Oller, I.; Malato, S.; Sánchez-Pérez, J.A., Combination of Advanced Oxidation Processes and biological treatments for wastewater decontamination—A review. *Sci. Total Environ.*, **2011**, *409*, 4141-4166.

122. Zapata, A.; Malato, S.; Sánchez-Pérez, J.A.; Oller, I.; Maldonado, M.I., Scale-up strategy for a combined solar photo-Fenton/biological system for remediation of pesticide-contaminated water. *Catal. Today*, **2010**, *151*, 100-106.

123. Cesaro, A.; Naddeo, V.; Belgiorno, V., Wastewater Treatment by Combination of Advanced Oxidation Processes and Conventional Biological Systems. *J. Bioremed. Biodeg.*, **2013**, *4*, 1-8.

124. Ohko, Y.; Iuchi, K.; Niwa, C.; Tatsuma, T.; Nakashima, Y.; Iguchi, T.; Kubota, Y.; Fujishima, A., 17 beta-estradiol degradation by TiO_2 photocatalysis as a means of reducing estrogenic activity. *Environ. Sci. Technol.*, **2002**, *19*, 4175-4181.

125. (a) Knowles, J.P.; Elliott, L.D.; Booker-Milburn, K.I., Flow photochemistry: Old light through new windows. *Beilstein J. Org. Chem.*, **2012**, *8*, 2025-2052; (b) Moghaddam, M.M.; Pieber, B.; Glasnov, T.; Kappe, C.O., Immobilized Iron Oxide Nanoparticles as Stable and Reusable Catalysts for Hydrazine-Mediated Nitro Reductions in Continuous Flow. *ChemSusChem*, **2014**, *7*, 3122-3131.

126. Silva, S.; Pereira, P.M.R.; Silva, P.; Almeida Paz, F.A.; Faustino, M.A.F.; Cavaleiro, J.A.S.; Tomé, J.P.C., Porphyrin and phthalocyanine glycodendritic conjugates: synthesis, photophysical and photochemical properties. *Chem. Commun.*, **2012**, *48*, 3608-3610.

127. Ricchelli, F., Photophysical properties of porphyrins in biological membranes. *J. Photochem. Photobiol. B.*, **1995**, *29*, 109-118.

128. Singh, S.; Aggarwal, A.; Bhupathiraju, N.; Arianna, G.; Tiwari, K.; Drain, C.M., Glycosylated Porphyrins, Phthalocyanines, and Other Porphyrinoids for Diagnostics and Therapeutics. *Chem. Rev.*, **2015**, *115*, 10261-10306.

129. Rothemund, P., A New Porphyrin Synthesis. The Synthesis of Porphin[1]. *J. Am. Chem. Soc.*, **1936**, *58*, 625-627.

130. Gonsalves, A.M.d.A.R.; Varejão, J.M.T.B.; Pereira, M.M., Some new aspects related to the synthesis of meso-substituted porphyrins. *J. Heterocyclic Chem.*, **1991**, *28*, 635-640.

131. Chen, X.; Hui, L.; Foster, D.A.; Drain, C.M., Efficient synthesis and photodynamic activity of porphyrin-saccharide conjugates: targeting and incapacitating cancer cells. *Biochemistry*, **2004**, *43*, 10918-10929.

132. Tang, J.; Chen, J.-J.; Jing, J.; Chen, J.-Z.; Lv, H.; Yu, Y.; Xu, P.; Zhang, J.-L., b-Lactonization of fluorinated porphyrin enhances LDL binding affinity, cellular uptake with selective intracellular localization. *Chem. Sci.*, **2014**, *5*, 558-566.

133. Chen, X., Hui, L., Foster D. A., Drain, C. M., Efficient synthesis and photodynamic activity of porphyrin-saccharide conjugates: targeting and incapacitating cancer cells. *Biochemistry*, **2004**, *43*, 10918-10929.

134. van Leeuwen, M.; Beeby, A.; Fernandes, I.; Ashworth, S.H., The photochemistry and photophysics of a series of alpha octa(alkyl-substituted) silicon, zinc and palladium phthalocyanines. *Photochem. Photobiol. Sci.*, **2014**, *13*, 62-69.

135. Guinier, A., *X-ray Diffraction*. Freeman: San Francisco, 1963.

136. Han, S.K.; Bilski, P.; Karriker, B.; Sik, R.H.; Chignell, C.F., Oxidation of flame retardant tetrabromobisphenol A by singlet oxygen. *Environ. Sci. Technol.*, **2008**, *42*, 166-172.

137. Smith, B.A.; Teel, A.L.; Watts, R.J., Identification of the reactive oxygen species responsible for carbon tetrachloride degradation in modified Fenton's systems. *Environ. Sci. Technol.*, **2004**, *38*, 5465-5469.

138. Xiong, Z.G.; Xu, Y.M.; Zhu, L.Z.; Zhao, J.C., Photosensitized oxidation of substituted phenols on aluminum phthalocyanine-intercalated organoclay. *Env. Sci. Technol.*, **2005**, *69*, 651-657.

139. Zhang, Y., Zhou, J. L., Ning, B., Photodegradation of estrone and 17b-estradiol in water. *Water Res.*, **2007**, *41*, 19- 26.

140. Hurwitz, A.R.; Liu, S.T., Determination of aqueous solubility and pKa values of estrogens. *J. Pharm. Sci.*, **1977**, *66*, 624-627.

141. Shareef, A.; Angove, M.J.; Wells, J.D.; Johnson, B.B., Aqueous Solubilities of Estrone, 17β-Estradiol, 17α-Ethynylestradiol, and Bisphenol A. *J. Chem. Eng. Data*, **2006**, *51*, 879-881.

142. Bancirova, M., Sodium azide as a specific quencher of singlet oxygen during chemiluminescent detection by luminol and Cypridina luciferin analogues. *Luminescence*, **2011**, *26*, 685-688.

143. Costa, L.; Carvalho, C.M.B.; Faustino, M.A.F.; Neves, M.G.P.M.S.; Tome, J.P.C.; Tome, A.C.; Cavaleiro, J.A.S.; Cunha, A.; Almeida, A., Sewage bacteriophage inactivation by cationic porphyrins: influence of light parameters. *Photochem. Photobiol. Sci.*, **2010**, *9*, 1126-1133.

144. Mor, S.M.; Griffiths, J.K., Water-Related Diseases in the Developing World A2 - Nriagu, J.O. In *Encyclopedia of Environmental Health*, Elsevier: Burlington, 2011; pp 741-753.

145. Cabral, J.P.S., Water Microbiology. Bacterial Pathogens and Water. *Int. J. Environ. Res. Public Health.*, **2010**, *7*, 3657-3703.

146. Gleick, P.H. *Dirty Water: Estimated Deaths from Water-Related Disease 2000-2020*; Pacific Institute for Studies in Development, Environment, and Security: 2002; pp 1-12.

147. Griffiths, J.K., Waterborne Diseases A2 - Quah, Stella R. In *International Encyclopedia of Public Health (Second Edition)*, Academic Press: Oxford, 2017; pp 388-401.

148. Meireles, A.; Giaouris, E.; Simões, M., Alternative disinfection methods to chlorine for use in the fresh-cut industry. *Food Res. Int.*, **2016**, *82*, 71-85.

149. Robert Jones, M.D.; Brandon Wills, D.O.; Christopher Kang, M.D., Chlorine Gas: An Evolving Hazardous Material Threat and Unconventional Weapon. *West. J. Emerg. Med.*, **2010**, *11*, 151-156.

150. Xi, C.; Zhang, Y.; Marrs, C.F.; Ye, W.; Simon, C.; Foxman, B.; Nriagu, J., Prevalence of Antibiotic Resistance in Drinking Water Treatment and Distribution Systems. *Appl. Environ. Microbiol.*, **2009**, *75*, 5714-5718.

151. Krasner, S.W.; Weinberg, H.S.; Richardson, S.D.; Pastor, S.J.; Chinn, R.; Sclimenti, M.J.; Onstad, G.D.; Thruston, A.D., Occurrence of a New Generation of Disinfection Byproducts. *Environ. Sci. Technol.*, **2006**, *40*, 7175-7185.

152. (a) Sperandio, F.F.; Huang, Y.-Y.; Hamblin, M.R., Antimicrobial Photodynamic Therapy to Kill Gram-negative Bacteria. *Recent Pat. Antiinfect. Drug Discov.*, **2013**, *8*, 108-120; (b) Yin, R.; Dai, T.; Avci, P.; Jorge, A.E.S.; de Melo, W.C.M.A.; Vecchio, D.; Huang, Y.-Y.; Gupta, A.; Hamblin, M.R., Light based anti-infectives: ultraviolet C irradiation, photodynamic therapy, blue light, and beyond. *Curr. Opin. Pharmacol.*, **2013**, *13*, 731-762; (c) Jori, G.; Magaraggia, M.; Fabris, C.; Soncin, M.; Camerin, M.; Tallandin, L.; Coppellotti, O.; Guidolin, L., Photodynamic inactivation of microbial pathogens: disinfection of water and prevention of water-borne diseases. *J. Environ. Pathol. Toxicol. Oncol.*, **2011**, *30*, 261-271; (d) Winter, S.; Tortik, N.; Kubin, A.; Krammer, B.; Plaetzer, K., Back to the roots: photodynamic inactivation of bacteria based on water-soluble curcumin bound to polyvinylpyrrolidone as a photosensitizer. *Photochem. Photobiol. Sci.*, **2013**, *12*, 1795-1802.

153. (a) Bertoloni, G.; Lauro, F.M.; Cortella, G.; Merchat, M., Photosensitizing activity of hematoporphyrin on Staphylococcus aureus cells. *Biochim. Biophys. Acta, Gen. Subj.*, **2000**, *1475*, 169-174; (b) Kassab, K.; Amor, T.B.; Jori, G.; Coppellotti, O., Photosensitization of Colpoda inflata cysts by meso-substituted cationic porphyrins. *Photochem. Photobiol. Sci.*, **2002**, *1*, 560-564; (c) Alves, E.; Faustino, M.A.F.; Neves, M.G.P.M.S.; Cunha, Â.; Nadais, H.; Almeida, A., Potential applications of porphyrins in photodynamic inactivation beyond the medical scope. *J. Photochem. Photobiol. C*, **2015**, *22*, 34-57.

154. Lourenco, L.; Sousa, A.; Gomes, M.C.; Faustino, M.A.F.; Almeida, A.; Silva, A.; Neves, G.; Cavaleiro, J.A.S.; Cunha, A.; Tome, J., Inverted methoxypyridinium phthalocyanines for PDI of pathogenic bacteria. *Photochem. Photobiol. Sci.*, **2015**.

155. Alves, E.; Costa, L.; Carvalho, C.M.B.; Tomé, J.P.C.; Faustino, M.A.; Neves, M.G.; Tomé, A.C.; Cavaleiro, J.A.S.; Cunha, Â.; Almeida, A., Charge effect on the photoinactivation of Gram-negative and Gram-positive bacteria by cationic meso-substituted porphyrins. *BMC Microbiol.*, **2009**, *9*, 70-70.

156. (a) Yogo, T.; Urano, Y.; Ishitsuka, Y.; Maniwa, F.; Nagano, T., Highly Efficient and Photostable Photosensitizer Based on BODIPY Chromophore. *J. Am. Chem. Soc.*, **2005**, *127*, 12162-12163; (b) Bonnett, R.; Martínez, G., Photobleaching of sensitisers used in photodynamic therapy. *Tetrahedron*, **2001**, *57*, 9513-9547.

157. DiMagno, S.G.; Biffinger, J.C.; Sun, H., Fluorinated Porphyrins and Corroles: Synthesis, Electrochemistry, and Applications. In *Fluorine in Heterocyclic Chemistry Volume 1: 5-Membered Heterocycles and Macrocycles*, Nenajdenko, V., Ed. Springer International Publishing: Cham, 2014; pp 589-620.

158. Singh, S.; Aggarwal, A.; Bhupathiraju, N.V.S.D.K.; Arianna, G.; Tiwari, K.; Drain, C.M., Glycosylated Porphyrins, Phthalocyanines, and Other Porphyrinoids for Diagnostics and Therapeutics. *Chem. Rev.*, **2015**, *115*, 10261-10306.

159. Fernández, L.; Esteves, V.I.; Cunha, Â.; Schneider, R.J.; Tomé, J.P.C., Photodegradation of organic pollutants in water by immobilized porphyrins and phthalocyanines. *Journal of Porphyrins and Phthalocyanines*, **2016**, *20*, 150-166.

160. Thandu, M.; Comuzzi, C.; Goi, D., Phototreatment of Water by Organic Photosensitizers and Comparison with Inorganic Semiconductors. *Int. J. Photoenergy*, **2015**, *2015*, 22.

161. Mannucci, S.; Ghin, L.; Conti, G.; Tambalo, S.; Lascialfari, A.; Orlando, T.; Benati, D.; Bernardi, P.; Betterle, N.; Bassi, R.; Marzola, P.; Sbarbati, A., Magnetic Nanoparticles from Magnetospirillum gryphiswaldense Increase the Efficacy of Thermotherapy in a Model of Colon Carcinoma. *PLOS ONE*, **2014**, *9*, e108959.

162. Silhavy, T.J.; Kahne, D.; Walker, S., The Bacterial Cell Envelope. *Cold Spring Harb. Perspect. Biol.*, **2010**, *2*, 1-16.

163. (a) Lukšiene, Ž., New Approach to Inactivation of Harmful and Pathogenic Microorganisms by Photosensitization. *Food Technol. Biotechnol.*, **2005**, *43*, 411-418; (b) Preuss, A.; Zeugner, L.; Hackbarth, S.; Faustino, M.A.; Neves, M.G.; Cavaleiro, J.A.; Roeder, B., Photoinactivation of Escherichia coli (SURE2) without intracellular uptake of the photosensitizer. *J. Appl. Microbiol.*, **2013**, *114*, 36-43.

164. Nitzan, Y.; Gutterman, M.; Malik, Z.; Ehrenberg, B., Inactivation of gram-negative bacteria by photosensitized porphyrins,. *Photochem. Photobiol.*, **1992**, *55*, 89-96.

165. Caminos, D.A.; Spesia, M.B.; Durantini, E.N., Photodynamic inactivation of Escherichia coli by novel meso-substituted porphyrins by 4-(3-N,N,N-trimethylammoniumpropoxy) phenyl and 4-(trifluoromethyl) phenyl groups. *Photochem. Photobiol. Sci.*, **2006**, *5*, 56-65.

166. Dosselli, R.; Ruiz-González, R.; Moret, F.; Agnolon, V.; Compagnin, C.; Mognato, M.; Sella, V.; Agut, M.; Nonell, S.; Gobbo, M.; Reddi, E., Synthesis, Spectroscopic, and

Photophysical Characterization and Photosensitizing Activity toward Prokaryotic and Eukaryotic Cells of Porphyrin-Magainin and -Buforin Conjugates. *J. Med. Chem.*, **2014**, *57*, 1403-1415.

167. Natarajan, A.; Srienc, F., Dynamics of Glucose Uptake by Single Escherichia coli Cells. *Metab. Eng.*, **1999**, *1*, 320-333.

168. (a) Huo, S.; Jiang, Y.; Gupta, A.; Jiang, Z.; Landis, R.F.; Hou, S.; Liang, X.-J.; Rotello, V.M., Fully Zwitterionic Nanoparticle Antimicrobial Agents through Tuning of Core Size and Ligand Structure. *ACS Nano*, **2016**, *10*, 8732-8737; (b) Carpenter, A.W.; Slomberg, D.L.; Rao, K.S.; Schoenfisch, M.H., Influence of Scaffold Size on Bactericidal Activity of Nitric Oxide Releasing Silica Nanoparticles. *ACS nano*, **2011**, *5*, 7235-7244.

169. Alves, E.; Carvalho, C.M.B.; Tomé, J.P.C.; Faustino, M.A.F.; Neves, M.G.P.M.S.; Tomé, A.C.; Almeida, A., Photodynamic inactivation of recombinant bioluminescent Escherichia coli by cationic porphyrins under artificial and solar irradiation. *J. Ind. Microbiol. Biotechnol.*, **2008**, *35*, 1447-1454.

170. Kusk, K.O.; Krüger, T.; Long, M.; Taxvig, C.; Lykkesfeldt, A.E.; Frederiksen, H.; Andersson, A.-M.; Andersen, H.R.; Hansen, K.M.S.; Nellemann, C.; Bonefeld-Jørgensen, E.C., Endocrine potency of wastewater: Contents of endocrine disrupting chemicals and effects measured by in vivo and in vitro assays. *Environ. Toxicol. Chem.*, **2011**, *30*, 413-426.

171. (a) Andersen, H.R., Hansen, M., Kjolholt, J., Stuer-Lauridsen, F., Ternes, T., Halling-Sorensen, Assessment of the importance of sorption for steroid estrogens removal during activated sludge treatment. *Chemosphere*, **2005**, *61*, 139-146; (b) Muller, M., . Rabenoelina, F., Balaguer, P., Patureau, D., Lemenach, K., Budzinski, H., Barcelo, D., De Alda, M. L., Kuster, M., Delgenes, J. P., Hernandez-Raquet, G., Chemical and biological analysis of endocrine disrupting hormones and estrogenic activity in an advanced sewage treatment plant. *Environ. Toxicol. Chem.*, **2008**, *27*, 1649-1658; (c) Braga, O., Smythe, G. A., Schafer, A. I., Feltz, A. J., Steroid estrogens in primary and tertiary wastewater treatment plants. *Water Sci. Technol.*, **2005**, *52*, 273-278.

172. D'Ascenzo, G., Di Corcia, A., Gentili, A., Mancini, R., Mastropasqua, R., Nazzari, M., Samperi, R., Fate of natural estrogen conjugates in municipal sewage transport and treatment facilities. *Sci. Total Environ.*, **2003**, *302*, 199-209.

173. Petrovic, M.; Eljarrat, E.; Lopez de Alda, M.J.; Barceló, D., Endocrine disrupting compounds and other emerging contaminants in the environment: A survey on new monitoring strategies and occurrence data. *Anal. Bioanal. Chem.*, **2004**, *378*, 549-562.

174. MCargouet, M.; Perdiz, D.; Mouatassim-Souali, A.; Tamisier-Karolak, S.; Levi, Y., Assessment of river contamination by estrogenic compounds in Paris area (France). *Sci. Total Environ.*, **2004**, *324*, 55-66.

175. Ternes, T.A.; Stumpf, M.; Mueller, J.F.; Haberer, K.; R.-D., W.; Servos, M., Behavior and occurrence of estrogens in municipal sewage treatment plants - I. Investigations in Germany, Canada and Brazil. *Sci. Total Environ.*, **1999**, *225*, 81-90.

176. Belfroid, A.C.; Van der Horst, A.; Vethaak, A.D.; Schafer, A.J.; Rijs, G.B.J.; Wegener, J.; Cofino, W.P., Analysis and occurrence of estrogenic hormones and their glucuronides in surface water and wastewater in Netherlands. *Sci. Total Environ.*, **1999**, *225*, 101-108.

177. Xiao, X.-Y.; McCalley, D.V.; Mcevoy, J., Analysis of estrogens in river water and effluents using solid-phase extraction and gas chromatographynegative chemical ionization mass spectrometry of the pentafluorobenzoyl derivates. *J. Chromatogr. A*, **2001**, *923*, 195-204.

178. Baronti, C.; Curini, R.; D'Ascenzo, G.; Di Corcia, A.; Gentili, A.; Samperi, R., Monitoring natural and synthetic estrogens at activated sludge sewage treatment plants and in receiving river water. *Environ. Sci. Technol.*, **2000**, *34*, 5059-5066.

179. Petrovic, M.; Solé, M.; López de Alda, M.J.; Barceló, D., Endocrine disruptors in sewage treatment plants, receiving river waters, and sediments: integration of chemical analysis and biological effects on feral carp. *Environ. Toxicol. Chem.*, **2002**, *21*, 2146-2156.

180. Sousa, A.; Schönenberger, R.; Jonkers, N.; Suter, M.J.-F.; Tanabe, S.; Barroso, C.M., Chemical and Biological Characterization of Estrogenicity in Effluents from WWTPs in Ria de Aveiro (NW Portugal). *Arch. Environ. Contam. Toxicol.*, **2010**, *58*, 1-8.

181. Xu, N.; Johnson, A.C.; Jürgens, M.D.; Llewellyn, N.R.; Hankins, N.P.; Darton, R.C., Estrogen Concentration Affects its Biodegradation Rate in Activated Sludge. *Environ. Toxicol. Chem.*, **2009**, *28*, 2263-2270.

182. (a) Antonopoulou, M.; Evgenidou, E.; Lambropoulou, D.; Konstantinou, I., A review on advanced oxidation processes for the removal of taste and odor compounds from aqueous media. *Water Res.*, **2014**, *53*, 215-234; (b) Liu, Z.-h.; Kanjo, Y.; Mizutani, S.,

Removal mechanisms for endocrine disrupting compounds (EDCs) in wastewater treatment — physical means, biodegradation, and chemical advanced oxidation: A review. *Sci. Total Environ.*, **2009**, *407*, 731-748.

183. Whidbey, C.M.; Daumit, K.E.; Nguyen, T.-H.; Ashworth, D.D.; Davis, J.C.C.; Latch, D.E., Photochemical induced changes of in vitro estrogenic activity of steroid hormones. *Water Res.*, **2012**, *46*, 5287-5296.

184. Hashimoto, T., Onda, K., Morita, T., Luxmy, B., Tada, K., Miya, A., Murakami, T., Contribution of the Estrogen-Degrading Bacterium Novosphingobium sp. Strain JEM-1 to Estrogen Removal in Wastewater Treatment. *J. Environ. Eng.*, **2010**, *136*, 890-896.

185. (a) Kurisu, F., Ogura, M., Saitoh, S., Yamazoe, A., Yagi, O., Degradation of natural estrogen and identification of the metabolites produced by soil isolates of Rhodococcus sp. and Sphingomonas sp. *J. Biosci. Bioeng.*, **2010**, *109*, 576-582; (b) Ke, J.X., Zhuang, W. Q., Gin, K. Y. H., Reinhard, M., Hoon, L. T., Tay, J. H. , Characterization of estrogen-degrading bacteria isolated from an artificial sandy aquifer with ultrafiltered secondary effluent as the medium. *Appl. Microbiol. Biotechnol.*, **2007**, *75*, 1163-1171.

186. Hensen, C.; Scholz, F.; Nuzzo, M.; Valadares, V.; Gràcia, E.; Terrinha, P.; Liebetrau, V.; Kaul, N.; Silva, S.; Martínez-Loriente, S.; Bartolome, R.; Piñero, E.; Magalhães, V.H.; Schmidt, M.; Weise, S.M.; Cunha, M.; Hilario, A.; Perea, H.; Rovelli, L.; Lackschewitz, K., Strike-slip faults mediate the rise of crustal-derived fluids and mud volcanism in the deep sea. *Geology*, **2015**, *43*, 339-342.

187. Margesin, R.; Schinner, F., Biodegradation and bioremediation of hydrocarbons in extreme environments. *Appl. Microbiol. Biotechnol.*, **2001**, *56*, 650-663.

188. Cunha, T.A.; Matias, L.M.; Terrinha, P.; Negredo, A.M.; Rosas, F.; Fernandes, R.M.S.; Pinheiro, L.M., Neotectonics of the SW Iberia margin, Gulf of Cadiz and Alboran Sea: a reassessment including recent structural, seismic and geodetic data. *Geophys. J. Int.*, **2012**, *188*, 850-872.

189. Allen, E.E.; Bartlett, D.H., *Piezophiles: microbial adaptation to the deep-sea environment*. Eolss Publishers Co Ltd: Oxford, 2004; Vol. III.

190. Louvado, A., Coelho, F. J. R. C., Domingues, P., Santos, A. L., Gomes, N. C. M., Almeida, A., Cunha, A., Isolation of Surfactant-Resistant Pseudomonads from the Estuarine Surface Microlayer. *J. Microbiol. Biotechnol.*, **2012**, *22*, 283-291.

191. (a) Tapilatu, Y.; Acquaviva, M.; Guigue, C.; Miralles, G.; Bertrand, J.C.; Cuny, P., Isolation of alkane-degrading bacteria from deep-sea Mediterranean sediments. *Lett. Appl. Microbiol.*, **2010**, *50*, 234-236; (b) Park, Y.D.; Yi, H.; Baik, K.S.; Seong, C.N.; Bae, K.S.; Moon, E.Y.; Chun, J., Pseudomonas segetis sp. nov., isolated from soil. *Int. J. Syst. Evol. Microbiol.*, **2006**, *56*, 2593-2595.

192. Wallace, D., Large- and Small-Scale Phenol Extractions. *Methods Enzymol.*, **1987**, *152*, 33-41.

193. Yamamoto, S.; Harayama, S., PCR Amplification and Direct Sequencing of gyrB Genes with Universal Primers and Their Application to the Detection and Taxonomic Analysis of Pseudomonas putida strains. *Appl. Environ. Microbiol.*, **1995**, *61*, 1104-1109.

194. Sanger, F.; Nicklen, S.; Coulson, A.R., DNA sequencing with chain-terminating inhibitors. *Proc. Natl. Acad. Sci. U.S.A.*, **1977**, *74*, 5463-5467.

195. Seiler, H.; Wenning, M., Virgibacillus halotolerans sp. nov., isolated from a dairy product. *Int. J. Syst. Evol. Microbiol.*, **2013**, *63*, 3358-3363.

196. Meenakshisundaram, M.; Bharathiraja, C., Isolation and Molecular Identification of Hydrocarbon Degrading Bacteria from Oil Contaminated Soils from Tamilnadu Indian *J. App. Res.*, **2014**, *7*, 39-42.

197. Li, P.; Aflakpui, F.W.K.; Yu, H.; Luo, L.; Lin, W.T., Characterization of activity and microbial diversity of typical types of Daqu for traditional Chinese vinegar. *Ann Microbiol*, **2015**, 1-9.

198. Beveridge, T.J., Use of the Gram stain in microbiology. *Biotech. Histochem.*, **2001**, *76*, 111-118.

199. Lado, B.H.; Yousef, A.E., Alternative food-preservation technologies: efficacy and mechanisms. *Microb. Infect.*, **2002**, *4*, 433-440.

200. Alamri, S.A., Biodegradation of microcystin-RR by Bacillus flexus isolated from a Saudi freshwater lake. *Saudi J. Biol. Sci.*, **2012**, *19*, 435-440.

201. Trivedi, N.; Gupta, V.; Kumar, M.; Kumari, P.; C.R.K.Reddy; Jha, B., An alkali-halotolerant cellulase from Bacillus flexus isolated from green seaweed Ulva lactuca. *Carbohyd. Polym.*, **2011**, *83*, 891-897.

202. Parvathi, A.; Krishna, K.; Jose, J.; Joseph, N.; Nair, S., Biochemical and molecular characterization of Bacillus pumilus isolated from coastal environment in Cochin, India. *Braz. J. Microbiol.*, **2009**, *40*, 269-275.

203. (a) Peng, Q.Z.; Chen, J.; Zhang, Y.Q.; Chen, Q.H.; Peng, D.J.; Cui, X.L.; Li, W.J.; Chen, Y.G., Virgibacillus zhanjiangensis sp. nov., a marine bacterium isolated from sea water. *Antonie Van Leeuwenhoek*, **2009**, *96*, 645-652; (b) Yoon, J.H.; Kang, S.J.; Jung, Y.T.; Lee, K.C.; Oh, H.W.; Oh, T.K., Virgibacillus byunsanensis sp. nov., isolated from a marine solar saltern. *Int. J. Syst. Evol. Microbiol.*, **2010**, *60*, 291-295; (c) Zhang, D.Z.; Schumann, P.; Wu, J.; França, L.; Neuner, K.; Margesin, R., Virgibacillus flavescens sp. nov., isolated from marine sediment. *Int. J. Syst. Evol. Microbiol.*, **2016**, *66*, 1138-1143.

204. Lang, S., Biological amphiphiles (microbial biosurfactants). *Curr. Opin. Colloid Inter. Sci.*, **2002**, *7*, 12-20.

205. Pacwa-Płociniczak, M.; Płaza, G.A.; Piotrowska-Seget, Z.; Cameotra, S.S., Environmental Applications of Biosurfactants: Recent Advances. *Int. J. Mol. Sci.*, **2011**, *12*, 633-654.

206. Louvado, A.; Gomes, N.C.M.; Simões, M.M.Q.; Almeida, A.; Cleary, D.F.R.; Cunha, A., Polycyclic aromatic hydrocarbons in deep sea sediments: Microbe–pollutant interactions in a remote environment. *Sci. Total Environ.*, **2015**, *526*, 312-328.

207. (a) Usero, J.A.; Rosado, D.; Usero, J.; Morillo, J., Environmental quality in sediments of Cadiz and Algeciras Bays based on a weight of evidence approach (southern Spanish coast). *Marine Poll. Bull.*, **2016**, *110*, 65-74; (b) Barón, E.; Giménez, J.; Verborgh, P.; Gauffier, P.; De Stephanis, R.; Eljarrat, E.; Barceló, D., Bioaccumulation and biomagnification of classical flame retardants, related halogenated natural compounds and alternative flame retardants in three delphinids from Southern European waters. *Environ. Pollut.*, **2015**, *203*, 107-115.

208. Schmaltz, J. Sediment Plume Along The Coast Of Spain. https://visibleearth.nasa.gov/view.php?id=79677 (accessed 2017-04-10).

209. Deming, J.W., Deep ocean environmental biotechnology. *Curr. Opin. Biotechnol.*, **1998**, *9*, 283-287.

210. (a) Hazen, T.C.; Dubinsky, E.A.; DeSantis, T.Z.; Andersen, G.L.; Piceno, Y.M.; Singh, N.; Jansson, J.K.; Probst, A.; Borglin, S.E.; Fortney, J.L.; Stringfellow, W.T.; Bill, M.; Conrad, M.E.; Tom, L.M.; Chavarria, K.L.; Alusi, T.R.; Lamendella, R.; Joyner, D.C.; Spier, C.; Baelum, J.; Auer, M.; Zemla, M.L.; Chakraborty, R.; Sonnenthal, E.L.; D'haeseleer, P.; Holman, H.-Y.N.; Osman, S.; Lu, Z.; Van Nostrand, J.D.; Deng, Y.; Zhou, J.; Mason, O.U., Deep-Sea Oil Plume Enriches Indigenous Oil-Degrading Bacteria. *Science*, **2010**, *330*, 204-208; (b) Yuan, J.; Lai, Q.; Sun, F.; Zheng, T.; Shao, Z., The diversity of PAH-degrading

bacteria in a deep-sea water column above the Southwest Indian Ridge. *Front. Microbiol.*, **2015**, *6*, 853.

211. Roh, H.; Chu, K.-H., A 17β-Estradiol-utilizing Bacterium, Sphingomonas Strain KC8: Part I - Characterization and Abundance in Wastewater Treatment Plants. *Environ. Sci. Technol.*, **2010**, *44*, 4943-4950.

212. Muller, M.; Patureau, D.; Godon, J.J.; Delgenès, J.P.; Hernandez-Raquet, G., Molecular and kinetic characterization of mixed cultures degrading natural and synthetic estrogens. *Appl. Microbiol. Biotechnol.*, **2010**, *85*, 691-701.

213. Li, Z.; Nandakumar, R.; Madayiputhiya, N.; Li, X., Proteomic Analysis of 17β-Estradiol Degradation by Stenotrophomonas maltophilia. *Environ. Sci. Technol.*, **2012**, *46*, 5947-5955.

214. (a) Wang, Y.-S.; Subba-Rao, R.V.; Alexander, M., Effect of Substrate Concentration and Organic and Inorganic Compounds on the Occurrence and Rate of Mineralization and Cometabolism. *Appl. Environ. Microbiol.*, **1984**, *47*, 1195-1200; (b) Torång, L.; Nyholm, N.; Albrechtsen, H.J., Shifts in biodegradation kinetics of the herbicides MCPP and 2,4-D at low concentrations in aerobic aquifer materials. *Environ. Sci. Technol.*, **2003**, *37*, 3095-3103.

215. Mu, D.Y.; Scow, K.M., Effect of trichloroethylene (TCE) and toluene concentrations on TCE and toluene biodegradation and the population density of TCE and toluene degraders in soil. *Environ. Microbiol.*, **1994**, *60*, 2661-2665.

216. Clara, M.; Kreuzinger, N.; Strenn, B.; Gans, O.; Kroiss, H., The solids retention time: A suitable design parameter to evaluate the capacity of wastewater treatment plants to remove micropollutants. *Water Res.*, **2005**, *39*, 97-106.

217. Nielsen, S.S., Phenol-Sulfuric Acid Method for Total Carbohydrates. In *Food Analysis Laboratory Manual*, Nielsen, S. S., Ed. Springer US: Boston, MA, 2010; pp 47-53.

218. Sarkar, D.; Ferguson, M.; Datta, R.; Birnbaum, S., Bioremediation of petroleum hydrocarbons in contaminated soils: comparison of biosolids addition, carbon supplementation, and monitored natural attenuation. *Environ. Pollut.*, **2005**, *136*, 187-195.

219. Li, X.; Wang, X.; Wan, L.; Zhang, Y.; Li, N.; Li, D.; Zhou, Q., Enhanced biodegradation of aged petroleum hydrocarbons in soils by glucose addition in microbial fuel cells. *J. Chem. Technol. Biotechnol.*, **2016**, *91*, 267-275.

220. Streicher, J.; Ruhl, A.S.; Gnirß, R.; Jekel, M., Where to dose powdered activated carbon in a wastewater treatment plant for organic micro-pollutant removal. *Chemosphere*, **2016**, *156*, 88-94.

221. Zuehlke, S.; Duennbier, U.; Heberer, T., Determination of estrogenic steroids in surface water and wastewater by liquid chromatography–electrospray tandem mass spectrometry. *Journal of Separation Science*, **2005**, *28*, 52-58.

222. Shi, J.; Fujisawa, S.; Nakai, S.; Hosomi, M., Biodegradation of natural and synthetic estrogens by nitrifying activated sludge and ammonia-oxidizing bacterium Nitrosomonas europaea. *Water Res.*, **2004**, *38*, 2323-2330.

223. Kurisu, F.; Ogura, M.; Saitoh, S.; Yamazoe, A.; Yagi, O., Degradation of natural estrogen and identification of the metabolites produced by soil isolates of Rhodococcus sp. and Sphingomonas sp. *J. Biosci. Bioeng.*, **2010**, *109*, 576-582.

224. Wooding, K.M.; Barkley, R.M.; Hankin, J.A.; Johnson, C.A.; Bradford, A.P.; Santoro, N.; Murphy, R.C., Mechanism of Formation of the Major Estradiol Product Ions Following Collisional Activation of the Molecular Anion in a Tandem Quadrupole Mass Spectrometer. *J. Am. Soc. Mass. Spectrom.*, **2013**, *24*, 1451-1455.

225. Havlíková, L.; Nováková, L.; Matysová, L.; Šícha, J.; Solich, P., Determination of estradiol and its degradation products by liquid chromatography. *J. Chromatogr. A*, **2006**, *1119*, 216-223.

226. Rathahao, E.; Hillenweck, A.; Paris, A.; Debrauwer, L., Investigation of the in vitro metabolism of 17b-estradiol by LC-MS/MS using ESI and APC. *Analusis*, **2000**, *28*, 273-279.

227. Chun, S.; Lee, J.; Geyer, R.; White, D.C., Comparison of Three Extraction Methods for 17 β -Estradiol in Sand, Bentonite, and Organic-Rich Silt Loam. *J. Environ. Sci. Health B*, **2005**, *40*, 731-740.

228. Appels, L.; Baeyens, J.; Degrève, J.; Dewil, R., Principles and potential of the anaerobic digestion of waste-activated sludge. *Prog. Energy Combust. Sci.*, **2008**, *34*, 755-781.

229. García, J.L.; Uhía, I.; García, E.; Galán, B., *Bacterial Degradation of Cholesterol and Other Contaminant Steroids*. Caister Academic Press: Ioannina, 2011.

230. (a) Andersen, H.R.; Siegrist, H.; Halling-Sørensen, B.; Ternes, T., Fate of estrogens in a municipal sewage treatment plant. *Environ. Sci. Technol.*, **2003**, *37*, 4021-4026; (b)

Joss, A.; Andersen, H.; T., T.; Richle, P.R.; Siegrist, H., Removal of estrogens in municipal wastewater treatment under aerobic and anaerobic conditions: consequences for plant optimization. *Environ. Sci. Technol.*, **2004**, *38*, 3047-3055.

231. Czajka, C.P.; Londry, K.L., Anaerobic biotransformation of estrogens. *Sci. Total Environ.*, **2006**, *367*, 932-941.

232. Hogg, S., *Essential Microbiology*. second ed.; John Wiley & Sons: New York, 2013.

233. (a) O'Flaherty, V.; Lens, P.; Leahy, B.; Colleran, E., Long-term competition between sulphate-reducing and methane-producing bacteria during full-scale anaerobic treatment of citric acid production wastewater. *Water Res.*, **1998**, *32*, 815-825; (b) Rinzema, A.; Boone, M.; Knippenberg, K.; Lettinga, G., Bactericidal Effect of Long Chain Fatty Acids in Anaerobic Digestion. *Water Environ. Res.*, **1994**, *66*, 40-49; (c) Angelidaki, I.; Ahring, B.K., Effects of free long-chain fatty acids on thermophilic anaerobic digestion. *Appl. Microbiol. Biotechnol.*, **1992**, *37*, 808-812.

234. Leadbetter, J.R., *Environmental microbiology*. Elsevier: Amsterdam, 2007; Vol. 397.

235. Notomista, E.; Pennacchio, F.; Cafaro, V.; Smaldone, G.; Izzo, V.; Troncone, L.; Varcamonti, M.; Di Donato, A., The Marine Isolate Novosphingobium sp PP1Y Shows Specific Adaptation to Use the Aromatic Fraction of Fuels as the Sole Carbon and Energy Source. *Microbial Ecology*, **2011**, *61*, 582-594.

236. Plugge, C.M., Anoxic media design, preparation, and considerations. *Methods Enzymol.*, **2005**, *397*, 3-16.

237. DuBois, M.; Gilles, K.A.; Hamilton, J.K.; Rebers, P.A.; Smith, F., Colorimetric Method for Determination of Sugars and Related Substance. *Anal. Chem.*, **1956**, *28*, 350-356.

238. (a) Carberry, J.B.; Benzing, T.M., Peroxide preoxidation of recalcitrant toxic waste to enhance biodegradation. *Water Sci. Technol.*, **1991**, *23*, 367-376; (b) Barton, D.A.; Drake, E.P., Biotreatability of blow heat condensates with and without hydrogen peroxide pretreatment. *Water Sci. Technol.*, **1994**, *29*, 229-238.

239. Mantzavinos, D.; Psillakis, E., Enhancement of biodegradability of industrial wastewaters by chemical oxidation pre-treatment. *J. Chem. Technol. Biotechnol.*, **2004**, *79*, 431-454.

240. Scott, J.P.; Ollis, D.F., Integration of chemical and biological oxidation processes for water treatment: review and recommendations. *Environ. Prog.*, **1995**, *14*, 88-103.

241. McNaught, A.D.; Wilkinson, A., Compendium of Chemical Terminology, Gold Book. In *Pure and Applied Chemistry*, 2nd ed.; Blackwell Scientific Publications: Oxford, 1997.

242. (a) Alothman, Z.A., A Review: Fundamental Aspects of Silicate Mesoporous Materials. *Materials*, **2012**, *5*, 2874-2902; (b) Rouquerol, J.; Avnir, D.; Fairbridge, C.W.; Everett, D.H.; Haynes, J.M.; Pernicone, N.; Ramsay, J.D.F.; Sing, K.S.W.; Unger, K.K., Recommendations for the characterization of porous solids (Technical Report). In *Pure and Applied Chemistry*, 1994; Vol. 66, p 1739.

243. Villarroel-Rocha, J.; Barrera, D.; Sapag, K., Introducing a self-consistent test and the corresponding modification in the Barrett, Joyner and Halenda method for pore-size determination. *Microp. Mesopor. Mat.*, **2014**, *200*, 68-78.

244. Rouquerol, F.; Rouquerol, J.; Sing, K., *Adsorption by Powders and Porous Solids*. Academic Press: London, 1999.

245. Karimi Pasandideh, E.; Kakavandi, B.; Nasseri, S.; Mahvi, A.H.; Nabizadeh, R.; Esrafili, A.; Rezaei Kalantary, R., Silica-coated magnetite nanoparticles core-shell spheres (Fe_3O_4@SiO_2) for natural organic matter removal. *J. Environ. Health Sci. Eng.*, **2016**, *14*, 21.

246. WHO | Ultraviolet radiation and health. http://www.who.int/uv/uv_and_health/en/#.WRWPcDGyA-k.mendeley&title=Ultraviolet (accessed 2017-05-12).

247. Gómez, M.J.; Martínez Bueno, M.J.; Lacorte, S.; Fernández-Alba, A.R.; Agüera, A., Pilot survey monitoring pharmaceuticals and related compounds in a sewage treatment plant located on the Mediterranean coast. *Chemosphere*, **2007**, *66*, 993-1002.

248. Bedada, S.K.; Nearati, P., Effect of Resveratrol on the Pharmacokinetics of Carbamazepine in Healthy Human Volunteers. *Phytother. Res.*, **2015**, *29*, 701-706.

249. Ferrari, B.; Paxéus, N.; Lo Giudice, R.; Pollio, A.; Garric, J., Ecotoxicological impact of pharmaceuticals found in treated wastewaters: study of carbamazepine, clofibric acid, and diclofenac. *Ecotoxicol. Environ. Saf.*, **2003**, *55*, 359-370.

250. Almeida, A.; Calisto, V.; Esteves, V.I.; Schneider, R.J.; Soares, A.M.; Figueira, E.; Freitas, R., Presence of the pharmaceutical drug carbamazepine in coastal systems: effects on bivalves. *Aquat Toxicol.*, **2014**, *156*, 74-87.

251. (a) Kahle, M.; Buerge, I.J.; Müller, M.D.; Poiger, T., Hydrophilic anthropogenic markers for quantification of wastewater contamination in ground-and surface waters.

Environ. Toxicol. Chem., **2009**, *28*, 2528-2536; (b) Dickenson, E.R.; Snyder, S.A.; Sedlak, D.L.; Drewes, J.E., Indicator compounds for assessment of wastewater effluent contributions to flow and water quality. *Water Res.*, **2011**, *45*, 1199-1212.

252. (a) Yan, Q.; Gao, X.; Chen, Y.P.; Peng, X.Y.; Zhang, Y.X.; Gan, X.M.; Zi, C.F.; Guo, J.S., Occurrence, fate and ecotoxicological assessment of pharmaceutically active compounds in wastewater and sludge from wastewater treatment plants in Chongqing, the Three Gorges Reservoir Area. *Sci. Total Environ.*, **2014**, *470-471*, 618-630; (b) Le-Minh, N.; Stuetz, R.M.; Khan, S.J., Determination of six sulfonamide antibiotics, two metabolites and trimethoprim in wastewater by isotope dilution liquid chromatography/tandem mass spectrometry. *Talanta*, **2012**, *89*, 407-416.

253. Miao, X.S.; Bishay, F.; Chen, M.; Metcalfe, C.D., Occurrence of antimicrobials in the final effluents of wastewater treatment plants in Canada. *Environ. Sci. Technol.*, **2004**, *38*, 3533-3541.

254. Kasprzyk-Hordern, B.; Dinsdale, R.M.; Guwy, A.J., The removal of pharmaceuticals, personal care products, endocrine disruptors and illicit drugs during wastewater treatment and its impact on the quality of receiving waters. *Water Res.*, **2009**, *43*, 363-380.

255. García-Aljaro, C.; Riera-Heredia, J.; Blanch, A.R., Antimicrobial resistance and presence of the SXT mobile element in Vibrio spp. isolated from aquaculture facilities. *New Microbiol.*, **2014**, *37*, 339-346.

256. Borowska, E.; Bourgin, M.; Hollender, J.; Kienle, C.; McArdell, C.S.; von Gunten, U., Oxidation of cetirizine, fexofenadine and hydrochlorothiazide during ozonation: Kinetics and formation of transformation products. *Water Res.*, **2016**, *94*, 350-362.

257. Bahlmann, A.; Carvalho, J.J.; Weller, M.G.; Panne, U.; Schneider, R.J., Immunoassays as high-throughput tools: Monitoring spatial and temporal variations of carbamazepine, caffeine and cetirizine in surface and wastewaters. *Chemosphere*, **2012**, *89*, 1278-1286.

258. Kosonen, J.; Kronberg, L., The occurrence of antihistamines in sewage waters and in recipient rivers. *Environ. Sci. Pollut.*, **2009**, *16*, 555-564.

259. Nödler, K.; Voutsa, D.; Licha, T., Polar organic micropollutants in the coastal environment of different marine systems. *Marine Pollut. Bull.*, **2014**, *85*, 50-59.

260. Lam, M.W.; Mabury, S.A., Photodegradation of the pharmaceuticals atorvastatin, carbamazepine, levofloxacin, and sulfamethoxazole in natural waters. *Aquat. Sci.*, **2005**, *67*, 177-188.

261. Mazellier, P.; Méité, L.; De Laat, J., Photodegradation of the steroid hormones 17β-estradiol (E2) and 17α-ethinylestradiol (EE2) in dilute aqueous solution. *Chemosphere*, **2008**, *73*, 1216-1223.